

Gadi Rothenberg

WILEY-VCH

Catalysis

Concepts and Green Applications



Gadi Rothenberg

Catalysis

Gadi Rothenberg

Catalysis

Concepts and Green Applications



**WILEY-
VCH**

WILEY-VCH Verlag GmbH & Co. KGaA

The Author

Dr. Gadi Rothenberg

Van't Hoff Institute for Molecular Sciences,
University of Amsterdam, The Netherlands
www.science.uva.nl/~gadi

Cover picture

Ada Rothenberg, Tel Aviv, Israel,
<http://www.adarothenberg.com>

All books published by Wiley-VCH are carefully produced. Nevertheless, authors, editors, and publisher do not warrant the information contained in these books, including this book, to be free of errors. Readers are advised to keep in mind that statements, data, illustrations, procedural details or other items may inadvertently be inaccurate.

Library of Congress Card No.: applied for

British Library Cataloguing-in-Publication Data

A catalogue record for this book is available from the British Library.

Bibliographic information published by the Deutsche Nationalbibliothek

Die Deutsche Nationalbibliothek lists this publication in the Deutsche Nationalbibliografie; detailed bibliographic data are available in the Internet at <<http://dnb.d-nb.de>>.

© 2008 WILEY-VCH Verlag GmbH & Co. KGaA, Weinheim

All rights reserved (including those of translation into other languages). No part of this book may be reproduced in any form – by photoprinting, microfilm, or any other means – nor transmitted or translated into a machine language without written permission from the publishers. Registered names, trademarks, etc. used in this book, even when not specifically marked as such, are not to be considered unprotected by law.

Typesetting Thomson Digital, Noida, India

Printing Strauss GmbH, Mörlenbach

Binding Litges & Dopf Buchbinderei GmbH, Heppenheim

Printed in the Federal Republic of Germany

Printed on acid-free paper

ISBN: 978-3-527-31824-7

I never write *metropolis* for seven cents, because I can get the same price for *city*.

Mark Twain

Contents

Preface XIII

1	Introduction	1
1.1	Green Chemistry and Sustainable Development	1
1.1.1	What is “Green Chemistry”?	2
1.1.2	Quantifying Environmental Impact: Efficiency, <i>E</i> -factors, and Atom Economy	4
1.1.3	Just How “Green” is this Process?	6
1.1.4	Product and Process Life-Cycle Assessment (LCA)	9
1.2	What is Catalysis and Why is it Important?	10
1.2.1	Homogeneous Catalysis, Heterogeneous Catalysis, and Biocatalysis	12
1.2.2	Replacing Stoichiometric Reactions with Catalytic Cycles	19
1.2.3	Industrial Example: The BHC Ibuprofen Process	22
1.3	Tools in Catalysis Research	23
1.3.1	Catalyst Synthesis and Testing Tools	24
1.3.2	Catalyst Characterization Tools	26
1.3.3	Tools for Modeling/Mechanistic Studies	28
1.4	Further Reading	29
1.5	Exercises	31
	References	35
2	The Basics of Catalysis	39
2.1	Catalysis is a Kinetic Phenomenon	39
2.1.1	Reaction Rates, Reaction Orders, Rate Equations, and Rate-Determining Steps	40
2.1.1.1	The Reaction Order	42
2.1.1.2	The Rate-Determining Step	43
2.1.2	The Reaction Profile and the Reaction Coordinate	44
2.1.3	Zero-Order, First-Order, and Second-Order Kinetics	46

2.1.3.1	Zero-Order Rate Equations	46
2.1.3.2	First-Order Rate Equations	47
2.1.3.3	Second-Order Rate Equations	48
2.1.4	Langmuir–Hinshelwood Kinetics	49
2.1.5	The Steady-State Approximation	52
2.1.6	Michaelis–Menten Kinetics	54
2.1.7	Consecutive and Parallel First-Order Reactions	56
2.1.8	Pre-Equilibrium, “Catalyst Reservoirs,” and Catalyst Precursors	58
2.2	Practical Approaches in Kinetic Studies	60
2.2.1	Initial Reaction Rates and Concentration Effects	61
2.2.1.1	Concentration Effects	62
2.2.2	Creating Pseudo Order Conditions	62
2.2.3	What You See versus What You Get	63
2.2.4	Learning from Stoichiometric Experiments	64
2.3	An Overview of Some Basic Concepts in Catalysis	64
2.3.1	Catalyst/Substrate Interactions and Sabatier’s Principle	65
2.3.2	Catalyst Deactivation, Sintering, and Thermal Degradation	66
2.3.2.1	Catalyst Deactivation	66
2.3.2.2	Catalyst Sintering and Thermal Degradation	66
2.3.3	Catalyst Inhibition	68
2.3.3.1	Catalyst Poisoning	69
2.4	Exercises	69
	References	73
3	Homogeneous Catalysis	77
3.1	Metal Complex Catalysis in the Liquid Phase	77
3.1.1	Elementary Steps in Homogeneous Catalysis	78
3.1.1.1	Ligand Exchange: Dissociation and Coordination	79
3.1.1.2	Oxidative Addition	81
3.1.1.3	Reductive Elimination	83
3.1.1.4	Insertion and Migration	84
3.1.1.5	De-insertion and β -Elimination	85
3.1.1.6	Nucleophilic Attack on a Coordinated Substrate	85
3.1.1.7	Other Reaction Types	86
3.1.2	Structure/Activity Relationships in Homogeneous Catalysis	88
3.1.2.1	Steric Effects: Ligand Size, Flexibility, and Symmetry	88
3.1.2.2	Electronic Effects of Ligands, Substrates, and Solvents	92
3.1.3	Asymmetric Homogeneous Catalysis	93
3.1.4	Industrial Examples	96
3.1.4.1	The Shell Higher Olefins Process (SHOP)	97
3.1.4.2	The Wacker Oxidation Process	99
3.1.4.3	The Du Pont Synthesis of Adiponitrile	100
3.1.4.4	The Ciba–Geigy Metolachlor Process	102
3.2	Homogeneous Catalysis without Metals	104

3.2.1	Classic Acid/Base Catalysis	104
3.2.2	Organocatalysis	105
3.3	Scaling up Homogeneous Reactions: Pros and Cons	108
3.3.1	Catalyst Recovery and Recycling	108
3.3.2	Hybrid Catalysts: Bridging the Homogeneous/Heterogeneous Gap	110
3.4	“Click Chemistry” and Homogeneous Catalysis	111
3.5	Exercises	113
	References	117
4	Heterogeneous Catalysis	127
4.1	Classic Gas/Solid Systems	129
4.1.1	The Concept of the Active Site	131
4.1.2	Model Catalyst Systems	132
4.1.3	Real Catalysts: Promoters, Modifiers, and Poisons	134
4.1.4	Preparation of Solid Catalysts: Black Magic Revealed	135
4.1.4.1	High-Temperature Fusion and Alloy Leaching	137
4.1.4.2	Slurry Precipitation and Co-precipitation	138
4.1.4.3	Impregnation of Porous Supports	139
4.1.4.4	Hydrothermal Synthesis	139
4.1.4.5	Drying, Calcination, Activation, and Forming	141
4.1.5	Selecting the Right Support	143
4.1.6	Catalyst Characterization	146
4.1.6.1	Traditional Surface Characterization Methods	146
4.1.6.2	Temperature-Programmed Techniques	149
4.1.6.3	Spectroscopy and Microscopy	149
4.1.7	The Catalytic Converter: an Example from Everyday Life	154
4.1.8	Surface Organometallic Chemistry	156
4.2	Liquid/Solid and Liquid/Liquid Catalytic Systems	158
4.2.1	Aqueous Biphasic Catalysis	159
4.2.2	Fluorous Biphasic Catalysis	161
4.2.3	Biphasic Catalysis Using Ionic Liquids	163
4.2.4	Phase-Transfer Catalysis	164
4.3	Advanced Process Solutions Using Heterogeneous Catalysis	165
4.3.1	The BP AVADA Ethyl Acetate Process	166
4.3.2	The ABB Lummus/Albemarle AlkyClean Process	168
4.3.3	The IFP and Yellowdiesel Processes for Biodiesel Production	168
4.3.4	The ABB Lummus/UOP SMART Process	172
4.4	Exercises	173
	References	177
5	Biocatalysis	189
5.1	The Basics of Enzymatic Catalysis	190
5.1.1	Terms and Definitions – The Bio Dialect	191
5.1.2	Active Sites and Substrate Binding Models	194

5.1.3	Intramolecular Reactions and Proximity Effects	195
5.1.4	Common Mechanisms in Enzymatic Catalysis	197
5.2	Applications of Enzyme Catalysis	199
5.2.1	Whole-Cell Systems versus Isolated Enzymes	200
5.2.2	Immobilized Enzymes: Bona Fide Heterogeneous Catalysis	202
5.2.2.1	Binding Enzymes to Solid Supports	202
5.2.2.2	Trapping Enzymes in Polymers or Sol/Gel Matrices	203
5.2.2.3	Cross-Linking of Enzymes	204
5.2.3	Replacing “Conventional Routes” with Biocatalysis	205
5.2.4	Combining “Bio” and “Conventional” Catalysis	207
5.3	Developing New Biocatalysts: Better than Nature’s Best	210
5.3.1	Prospecting Natural Diversity	210
5.3.2	Rational Design	211
5.3.3	Directed Evolution	211
5.4	Nonenzymatic Biocatalysts	213
5.4.1	Catalytic Antibodies (Abzymes)	213
5.4.2	Catalytic RNA (Ribozymes)	214
5.5	Industrial Examples	215
5.5.1	High-Fructose Corn Syrup: 11 Million Tons per Year	215
5.5.2	The Mitsubishi Rayon Acrylamide Process	217
5.5.3	The BMS Paclitaxel Process	218
5.5.4	The Tosoh/DSM Aspartame Process	220
5.6	Exercises	221
	References	224
6	Computer Applications in Catalysis Research	231
6.1	Computers as Research Tools in Catalysis	231
6.2	Modeling of Catalysts and Catalytic Cycles	233
6.2.1	A Short Overview of Modeling Methods	233
6.2.2	Simplified Model Systems versus Real Reactions	236
6.2.3	Modeling Large Catalyst Systems Using Classical Mechanics	236
6.2.4	In-Depth Reaction Modeling Using Quantum Mechanics	238
6.3	Predictive Modeling and Rational Catalyst Design	240
6.3.1	Catalysts, Descriptors, and Figures of Merit	241
6.3.2	Three-Dimensional (3D) Descriptors	242
6.3.2.1	Comparative Molecular Field Analysis (CoMFA)	243
6.3.2.2	The Ligand Repulsive Energy Method	244
6.3.3	Two-Dimensional (2D) Descriptors	245
6.3.4	Generating Virtual Catalyst Libraries in Space A	248
6.3.5	Understanding Catalyst Diversity	250
6.3.6	Virtual Catalyst Screening: Connecting Spaces A, B, and C	253
6.3.7	Predictive Modeling in Heterogeneous Catalysis	255
6.3.8	Predictive Modeling in Biocatalysis	256
6.4	An Overview of Data-Mining Methods in Catalysis	257
6.4.1	Principal Components Analysis (PCA)	259

6.4.2	Partial Least-Squares (PLS) Regression	260
6.4.3	Artificial Neural Networks (ANNs)	262
6.4.4	Classification Trees	264
6.4.5	Model Validation: Separating Knowledge from Garbage	264
6.4.5.1	Cross-Validation and Bootstrapping	265
6.4.5.2	Mixing the Dependent Variables (γ -Randomizing)	266
6.4.5.3	Defining the Model Domain	266
6.5	Exercises	266
	References	268

Index	275
--------------	-----

Preface

This textbook covers the basics of catalysis from a “green chemistry” perspective. Its main message is that heterogeneous catalysis, homogeneous catalysis, and biocatalysis are all one discipline, so you need to understand only once how catalysis works. The book is divided in three sections. Chapters 1 and 2 introduce and explain the fundamentals of sustainable chemistry, catalysis, and reaction kinetics. Chapters 3, 4 and 5 show how these principles are applied in homogeneous, heterogeneous, and biocatalysis, respectively. Finally, Chapter 6 gives an overview of the exciting and fast-growing field of computer applications in catalysis research, with a special section on predictive modeling.

I have written this book for senior undergraduate students, as well as graduate researchers. Thus, each chapter includes detailed literature references, as well as exercises that embed the knowledge in a practical context. I assume that you have some background in chemistry/chemical engineering, life sciences, or earth/environmental sciences. To help you master the catalysis jargon, key terms in catalysis are printed in **bold** and defined the first time they appear in the text. They are also included in the index.

The website accompanying this book, www.catalysisbook.org, features additional teaching material (exercises, answers, and lecture slides). It also contains a searchable list of all the references, each with its corresponding digital object identifier (DOI) hyperlink. Access to this website is free of charge.

The bulk of the references are original papers and review articles in peer-reviewed journals. I cite reviews and books when introducing a subject, and articles when discussing specific examples. Chapter 1 also contains a “Further Reading” list of recommended books on related specialized subjects.

I thank my wife Live for her constant support throughout the writing of this book, and my colleagues Jurriaan Beckers, Hans Boelens, Kees Elsevier, Anil Gaikwad, Jos Hageman, Klaas Hellingwerf, Huub Hoefsloot, Christopher Lowe, Marjo Mittelmeijer-Hazeleger, Dorette Tromp, Ron Wever, and Gooitzen Zwanenburg for their constructive and insightful comments. Thanks also to my sister Ada, who drew the cover picture, and to the Wiley-VCH editors Axel Eberhard, Joe Richmond, Gudrun Walter, and Waltraud Wüst for their encouraging and professional attitude.

As you will see, catalysis is one of the most exciting and fun subjects in chemistry. Hopefully you will share some of my enthusiasm and fascination after reading this book.

Amsterdam, December 2007

Gadi Rothenberg

1

Introduction

This chapter outlines the principles of green chemistry, and explains the connection between catalysis and sustainable development. It covers the concepts of environmental impact, atom economy, and life-cycle analysis, with hands-on examples. Then it introduces the reader to heterogeneous catalysis, homogeneous catalysis, and biocatalysis, explaining what catalysis is and why it is important. The last two sections give an overview of the tools used in catalysis research, and a list of recommended books on specialized subjects in catalysis.

1.1

Green Chemistry and Sustainable Development

In the 20th century, chemistry changed our lives. It has shaped our modern technological society by supplying us with energy, medicines, crop protection, foodstuffs, and new materials worldwide. Unfortunately, even though chemistry is the science with the highest impact on our everyday lives, chemicals and the chemical industry have a poor public image. This is partly due to misconceptions and media scares, but there is also a valid reason: the traditional chemical industry, certainly until the 1980s, was a hazardous and polluting one. It generated stoichiometric amounts of waste, causing much pollution of both air and water. A number of major chemical accidents have reinforced this image in recent decades [1,2]. The most infamous are the Bhopal catastrophe in 1984, where 3000 people were killed and more than 40 000 injured [1], and the grounding of the *Exxon Valdez* [3] in the Prince William Sound in Alaska in 1989, that still affects the marine ecosystem nearly 20 years later [4].

Apart from the immediate health and environmental hazards, there is also the problem of resource management. The chemical industry during the past 200 years drew heavily on resources. Today, the escalating costs of petrochemicals, and the increasing energy and raw material demands in Asia's emerging markets, are forcing a change. Two popular terms associated with this change are **sustainability**, or

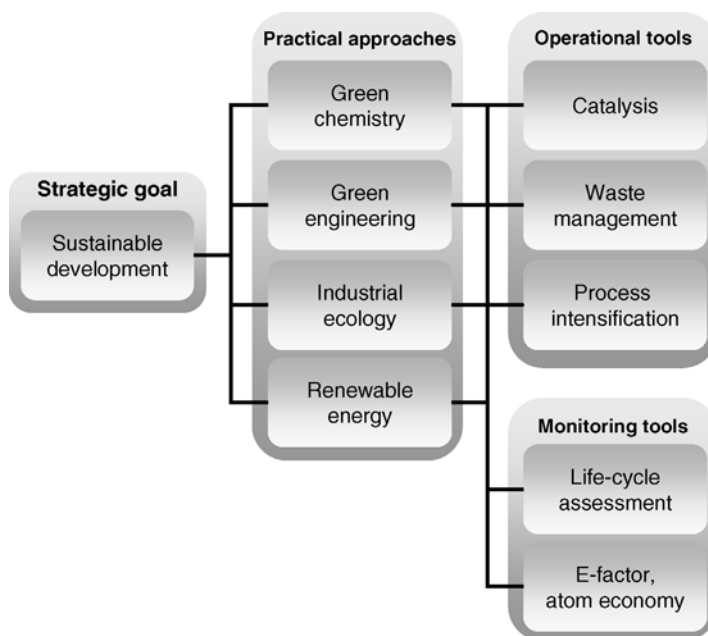


Figure 1.1 The strategic goal of sustainable development relies on practical approaches such as green chemistry, industrial ecology, and green engineering. These approaches use various operational tools (e.g., catalysis), and monitoring tools (e.g., life-cycle assessment).

sustainable development. A sustainable society is one that “meets the needs of the current generation without sacrificing the ability to meet the needs of future generations.” Sustainable development is a strategic goal. It can be reached using various approaches, and this is where green chemistry comes in. Figure 1.1 shows the relationship between the strategic goals, the practical approaches, and the operational and monitoring tools. Thus, green chemistry is just one step (albeit an important one) along the road to sustainability.

1.1.1

What is “Green Chemistry”?

In the 1990s, the concept of “green chemistry” was initiated in both the US and Europe, and has since been adopted widely by the chemical industry [5]. Green chemistry deals with designing chemical products and processes that generate and use fewer (or preferably no) hazardous substances. By applying the **principles of green chemistry**, companies embrace cleaner and more efficient technologies, with an *a priori* commitment to a cleaner and healthier environment. The green chemistry message is simple: “Seek prevention, not cure.” In 1998, Anastas and Warner formulated the following 12 principles of green chemistry [6,7] (I have rephrased these in the active voice, in keeping with the spirit of this book):

- Prevent waste instead of treating it.
- Design atom-efficient synthetic methods.
- Choose synthetic routes using nontoxic compounds where possible.
- Design new products that preserve functionality while reducing toxicity.
- Minimize the use of auxiliary reagents and solvents.
- Design processes with minimal energy requirements.
- Preferably use renewable raw materials.
- Avoid unnecessary derivatization.
- Replace stoichiometric reagents with catalytic cycles.
- Design new products with biodegradable capabilities.
- Develop real-time and on-line process analysis and monitoring methods.
- Choose feedstocks and design processes that minimize the chance of accidents.

Green chemistry offers an alternative to the traditional environmental protection agenda, mainly because it deals with avoiding hazards, rather than treating and solving exposure problems. Three forces drive the green chemistry initiative [8]: Government legislation, societal pressure, and economic benefit (Figure 1.2). The new 800-page EU Directive on the registration, evaluation, and assessment of chemicals (**REACH**) [9] is changing the chemical industry across Europe. Similar regulations are expected worldwide in the coming decade. But legislation is just one of the drivers. Societal pressure is also important: the public favors industrial green chemistry initiatives, as they lead to safer and eco-friendly products and processes.

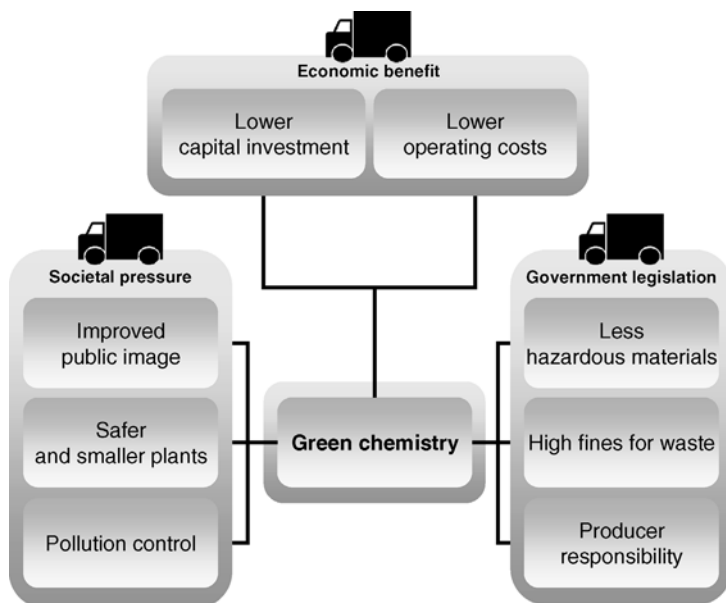


Figure 1.2 Green chemistry initiatives are driven by government legislation, societal pressure, and economic benefits.

This creates goodwill for the company, something that is difficult to quantify but undoubtedly important.

The third driver is *bona fide* economic benefit. Applying the principles of green chemistry decreases both capital investment and operating costs. If you use less (or no) solvent, and replace stoichiometric reagents with catalytic cycles, your reactor space–time yields go up. Similarly, processes running at ambient temperatures are less energy-intensive. This means doing the same work using smaller and safer equipment. Eliminating waste also eliminates the need for waste treatment and disposal. Replacing toxic reagents with benign ones saves on safety costs during transportation and storage. Thus, more and more companies are adopting green chemistry because it simply improves their bottom-line performance.

1.1.2

Quantifying Environmental Impact: Efficiency, E-factors, and Atom Economy

Everyone agrees that green chemistry and “green manufacture” are good things. The websites and pamphlets of all the major chemical companies emphasize their concern for the environment. They all say that their processes and products are “efficient,” “green,” and “environmentally friendly.” But how should we compare these processes? How should we judge such claims?

First, let us define some key terms. One method for quantifying a reaction’s efficiency is by examining the **reactant conversion**, the **product selectivity**, and the **product yield** over time. The reactant conversion is the fraction of reactant molecules that have transformed to product molecules (regardless of which product it is). The selectivity to product **P** is the fraction (or percentage) of the converted reactant that has turned into this specific product **P**. The yield of **P** is simply conversion \times selectivity. High conversions in short time spans mean smaller and safer reactors. Similarly, high selectivity means less waste, and simpler and cheaper separation units. Thus, conversion, selectivity, and yield are all measures of the **reaction efficiency**.

In addition, there are specific rulers for measuring the “greenness” or “ecofriendliness” of processes and products. One such measure is the **E-factor**, introduced by Roger Sheldon in 1994 [10,11]. A reaction’s *E*-factor is the quotient $\text{kg}_{\text{waste}}/\text{kg}_{\text{product}}$ (here “waste” is everything formed in the reaction except the desired product). The waste can be gases such as CO_2 or NO_x , water, common inorganic salts (e.g., NaCl , Na_2SO_4 , or $(\text{NH}_4)_2\text{SO}_4$), heavy metal salts, and/or organic compounds. Table 1.1 compares the production tonnage and *E*-factors of various industrial sectors. Note that the petrochemicals and the bulk chemicals sectors are the least polluting. This is surprising, as we are used to thinking of such chemicals as pollutants. In fact, *E*-factors increase substantially when going from bulk chemicals to fine chemicals and specialties. This is partly because fine-chemicals production often involves multistep syntheses, and partly because stoichiometric reagents are more often used for producing fine chemicals and pharmaceuticals.

Table 1.1 Annual production and *E*-factors in the chemical industry.

Industrial sector	Production/ton y ⁻¹	<i>E</i> -factor
Petrochemicals	10 ⁶ –10 ⁸	<0.1
Bulk chemicals	10 ⁴ –10 ⁶	1–5
Fine chemicals	10 ² –10 ⁴	5–50
Specialities/pharmaceuticals	10–10 ³	20–100

The concept of **atom economy**, introduced by Barry Trost in 1991, is similar to that of the *E*-factor [12]. Here one considers how many and which atoms of the reactants are incorporated into the products. With these two concepts, we can evaluate chemical reactions to get a quantitative result.

As an example, let us consider the stoichiometric oxidation of diphenylmethanol to benzophenone, one of the most commonly used photosensitizers in photochemistry (Figure 1.3). We will evaluate this reaction using the measures of product yield, product selectivity, *E*-factor, and atom economy. In this reaction, three equivalents of diphenylmethanol react with two equivalents of chromium trioxide and three equivalents of sulfuric acid, giving three equivalents of benzophenone. First, let us see how the reaction measures with respect to product yield and selectivity. Assume that this is an ideal chemical reaction which goes to completion, so one obtains 100% yield of the product, benzophenone. If no other (organic) by-product is obtained, the product selectivity is also 100%. This is all well and good, and indeed for many years this has been the way that chemical processes were evaluated, both in academia and in the (fine-) chemical industry.

However, examining the *E*-factor for this reaction, we see that for every three moles of benzophenone we produce one mole of chromium sulfate and six moles of water. The molecular weight of benzophenone is 182.2 g mol⁻¹, so every kilogram of benzophenone contains 5.48 moles of benzophenone. This means that for every kilogram of benzophenone we generate 5.48/3 = 1.83 moles (or 0.717 kg) of

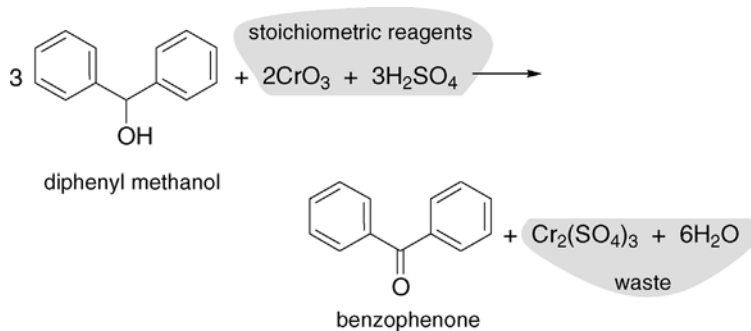
**Figure 1.3** Oxidation of diphenylmethanol to benzophenone using chromium trioxide and sulfuric acid.

Table 1.2 Hazard quotient (*Q*) values for some common chemical by-products.

Compound	<i>Q</i> -value	Compound	<i>Q</i> -value
Nitrogen gas	zero	acids	medium
Carbon dioxide	low	bases	medium
Water	low	heavy-metal salts	high
NaCl	low	CFC gases	high
Nonmetal salts	medium	persistent materials	high

chromium sulfate and 10.98 moles (or 0.197 kg) of water. The overall *E*-factor is therefore given by Eq. (1.1).

$$E\text{-factor} = \frac{\text{kg}_{\text{waste}}}{\text{kg}_{\text{product}}} = \frac{0.717 + 0.197}{1} = 0.914 \quad (1.1)$$

Nearly a whole kilogram of waste for every kilogram of product! Remember, this is for the ideal case of 100% yield and 100% selectivity. In real life, the *E*-factor is usually much higher, because product yields are less than 100% and the reagents are often used in excess. Furthermore, in many cases one needs to neutralize acid or base side-products, so the overall waste amounts are even higher.

The *E*-factor and atom economy can be used for comparing reaction alternatives, but we should remember that there are different types of “waste”. The reaction example above has two by-products: chromium sulfate and water. Obviously, water is “good waste”, while chromium sulfate is “bad waste”, so evaluating a synthetic protocol on the basis of only the amount of waste produced is insufficient. To solve this problem, Sheldon put forward the concept of the **environmental quotient** (EQ) [10]. By multiplying the *E*-factor by *Q*, an arbitrarily assigned hazard quotient, this measure takes both the amount and the nature of the waste into account. Table 1.2 shows some possible *Q*-values for different by-products. Assigning absolute *Q*-values to waste streams is difficult, because cases differ according to location and type of waste. Nevertheless, the EQ gives a better measure of the environmental impact of a process than the *E*-factor or the atom economy alone.

1.1.3

Just How “Green” is this Process?

Some processes and products seem more eco-friendly than others. Often this is because we see only part of the process. An overall environmental impact analysis should take into account not only the chemical reactions, but also the hazards and consequences of acquiring and transporting the raw materials. Additionally, it should factor in the overall energy demand. A reaction can have 100% atom economy, yet still be problematic because of hazardous reagents. Adding Br₂, HF, or HCN to a double bond, for example, is “clean” from the atom economy perspective, but storing

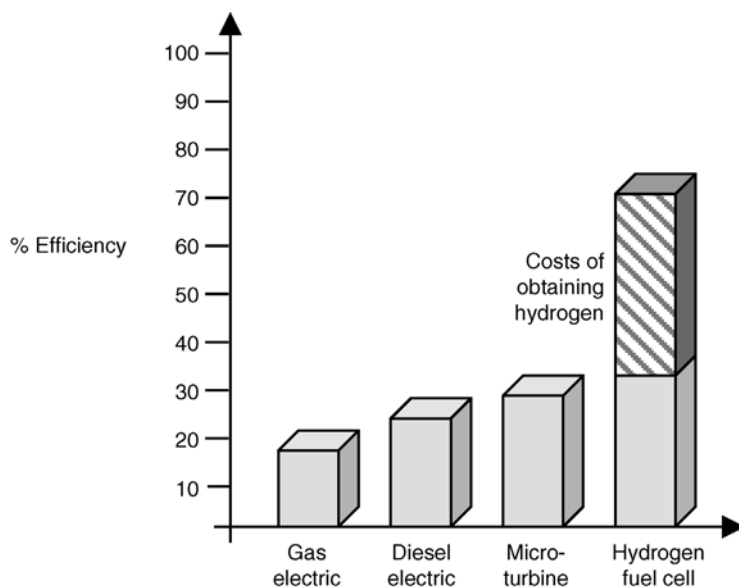


Figure 1.4 Relative efficiency of various engine types. The column on the right also shows the estimated “hidden costs” of obtaining hydrogen in the case of fuel cells.

and/or transporting these highly toxic reagents is problematic. To understand this better, let us look at two examples: hydrogen-powered fuel cells and oxidation of propene to propene oxide.

Hydrogen-powered fuel cells are a “hot topic.” In principle, such fuel cells can provide us with energy, while at the same time reducing emissions. They are highly efficient and, because they burn hydrogen, the only by-product is water, or “good waste.” Moreover, because fuel cells require high-purity hydrogen, the resulting water waste is also pure [13]. Figure 1.4 compares the efficiency of a hydrogen-powered fuel cell with those of various gas-powered and diesel-powered energy sources. Adding this high efficiency to the environmental benefits (no emission of CO_2 , NO_x , SO_x , or hydrocarbon particulates), it seems that fuel cells are the ideal source of power. But there is a catch: Where does the hydrogen come from? There is no natural source of pure hydrogen on Earth. It must be manufactured from fossil fuels, biomass, or water. This manufacture costs time, capital, and energy. Then the hydrogen must be transported and stored. This also requires dedicated infrastructure. All these factors must be taken into account when evaluating the overall efficiency of fuel cells. Further, hydrogen manufacture generates waste. This waste should also be taken into account when calculating the overall environmental impact of fuel cells compared to conventional energy sources.

Propene oxide is an important bulk chemical, used for making propylene glycol (**propane-1,2-diol**), polyethers, glycerol (**propane-1,2,3-triol**), and other products. Currently there is no catalytic process for oxidizing propene directly to propene oxide using molecular oxygen. The classic manufacturing route goes via chlorohydrin

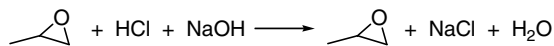
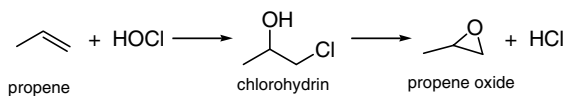


Figure 1.5 Traditional route to propene oxide. Note how the choice of HOCl as reagent adds another step and another reagent (NaOH) to the process.

(Figure 1.5). The HCl by-product is neutralized with caustic soda or lime. Although this process is wasteful and polluting, it still accounts for 40% of the global manufacture of propene oxide.

There are several alternatives to the polluting chlorohydrin route. One is the styrene monomer propene oxide (SMPO) process, used by Shell and Lyondell (Figure 1.6a) [14]. It is less polluting, but couples the epoxide production to that of styrene, a huge-volume product. Thus, this route depends heavily on the styrene market price. Another alternative, the ARCO/Oxirane process, uses a molybdenum

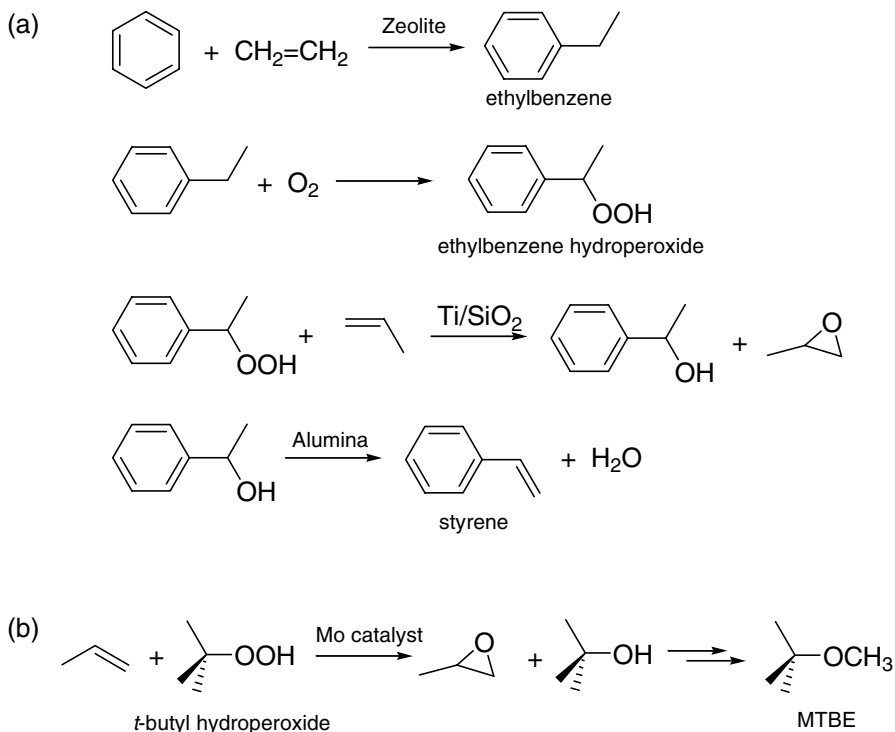


Figure 1.6 a SMPO process; b the catalytic oxidation of propene with *tert*-butyl hydroperoxide in the presence of a molybdenum-oxo complex.

catalyst, and couples the epoxidation of propene to isobutene oxidation (Figure 1.6b). The *t*-butanol that this generates as a by-product is then used as a gasoline additive and a starting material for making methyl *t*-butyl ether (MTBE). The disadvantages here are that Mo is a toxic heavy metal, and MTBE use is being phased out in the US and Europe.

In theory, one can also use N_2O as an epoxidation agent, with supported iron catalysts or homogeneous polyoxometallate Mn/Zn catalysts [15]. N_2O already contains an activated oxygen atom, and the only by-product is harmless molecular nitrogen. Furthermore, N_2O itself is a greenhouse gas, so reacting it with propene to give a valuable product seems like an ideal solution. However, the fact that N_2O is a greenhouse gas does not mean that it is generally available. This solution, like the hydrogen process above, depends on raw material availability.

1.1.4

Product and Process Life-Cycle Assessment (LCA)

The examples above show that we must take into account the overall environmental impact of chemical processes for an unbiased comparison. One tool that helps us evaluate the environmental impact of a chemical product or process is **life-cycle assessment** (LCA). The main advantage of LCA is that it gives an overall view. This includes raw-material extraction and acquisition, chemical reactions, processing, manufacture, packaging, transportation, distribution, consumer use, and end-of-life management [16]. LCA has four main stages: (1) defining the assessment scope and boundaries; (2) quantifying energy and materials flows (inventory analysis); (3) impact analysis, determining the effects on the environment and human health; and (4) improvement analysis, which can include methods such as green chemistry and green engineering, and environmental design [17]. Figure 1.7 shows the four stages in life-cycle assessment. Note that LCA is not limited to chemistry. It is applied in diverse areas, from assessment of roof types [18] to groundwater remediation technologies [19].

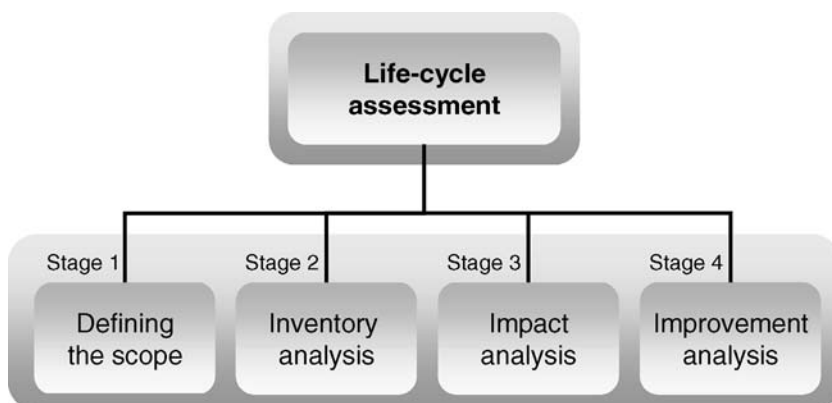


Figure 1.7 The four stages in life-cycle assessment.

The first step in LCA is defining the scope and goal of the study [20]. In this stage, functional units are defined, so that products can be compared on the basis of the functions they fulfill, rather than by their amount. For example, a milk bottle that is collected, cleaned, and reused 20 times fulfills the same function as 20 disposable milk cartons. Defining the scope of the study and its goal within your sphere of influence is useful, because then you can actually carry out the recommendations once the assessment is completed. The second step is making an inventory of all the environmental interventions, such as emissions to air and water, and the acquisition of raw materials. This is done using mass- and energy-balances. The interventions are then clustered by type, and totaled for all the processes. Such inventory tables can contain over 100 entries, e.g., the total emission of lead, SO_2 , or hydrocarbon particulates. The third step is impact analysis. First, impact categories are classified. These usually pertain to common environmental threats, such as global warming, acid rain, or ozone depletion. The environmental interventions from step 2 are then translated into scores in each impact category. These scores are used for calculating an overall environmental impact profile for the original product or process. This is often the most problematic step, because quantifying the environmental impact of a process is complex and subjective. Finally, the results are interpreted and an improvement analysis tries to pinpoint the process elements that can be changed by using a different technology or a different design. This is where we apply the tools of green chemistry and green engineering.

1.2

What is Catalysis and Why is it Important?

In the previous section we saw that one of the key objectives of green chemistry is waste minimization. Moreover, we learned that a sustainable process is one that optimizes the use of resources, while still leaving sufficient resources for future generations. Catalysis is an important tool in both cases. In fact, as far as chemistry is concerned, catalysis is the key to sustainability [21].

A catalyst is a substance that facilitates a chemical reaction. For an outside observer, it seems that the catalyst “makes the reaction go faster.” As we shall see in Chapter 2, this is an oversimplification. In most cases, the catalyst in fact opens a different, faster reaction pathway. However, at this stage we will use the following general definition.

- A catalyst is something that makes a reaction go faster, without being consumed in the process.

Because the catalyst is not consumed in the process, each catalyst molecule can participate in many consecutive cycles, so we need only a small amount of catalyst relative to the substrate. The substrate/catalyst ratio reflects the catalyst's efficiency, which is measured as turnover number or turnover frequency (see below).

There are many different types of catalysts (Figure 1.8). They range from the proton, H^+ , through Lewis acids, organometallic complexes, organic and inorganic polymers, all the way to enzymes. To simplify things, we divide catalysis into three

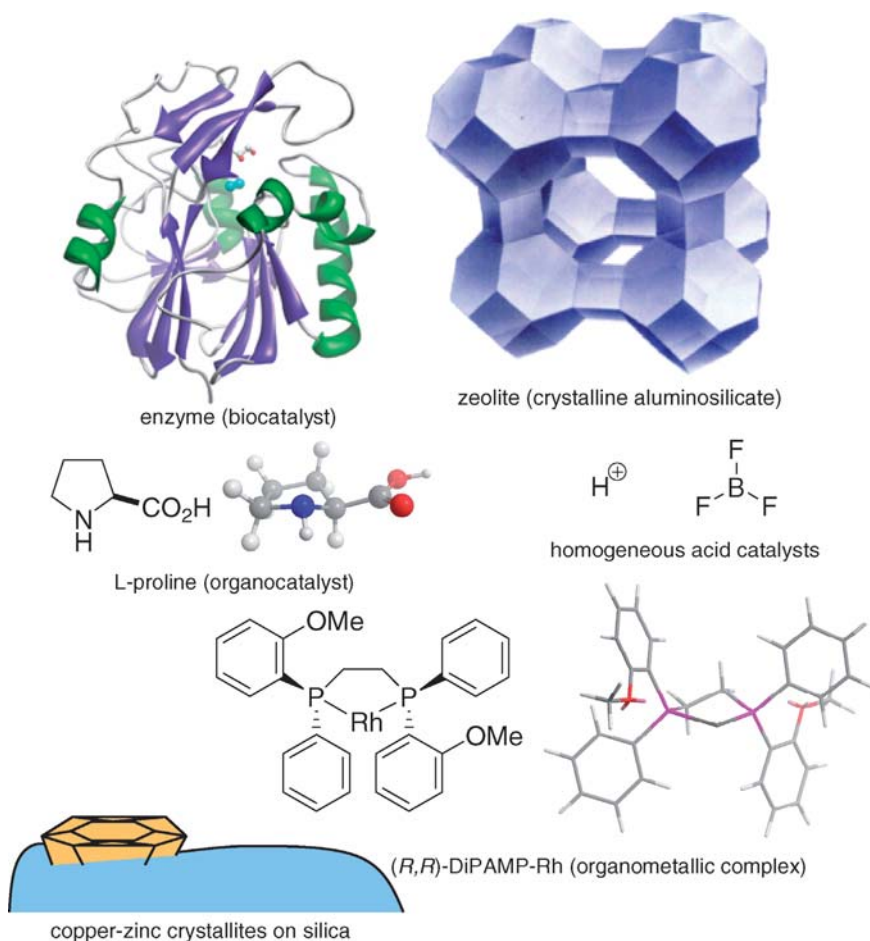


Figure 1.8 Different types of catalysts.

categories: homogeneous catalysis, heterogeneous catalysis, and biocatalysis. Although the catalysts and the process conditions in each category can be very different, the principles of catalysis are the same. Once you understand these principles, you can apply them in all three categories.

The catalyst **turnover number (TON)** and the **turnover frequency (TOF)** are two important quantities used for comparing catalyst efficiency. Their definitions, however, vary slightly among the three catalysis fields. In homogeneous catalysis, the TON is the number of cycles that a catalyst can run through before it deactivates, i.e., the number of **A** molecules that one molecule of catalyst can convert (or “turn over”) into **B** molecules. The TOF is simply TON/time, i.e., the number of **A** molecules that one molecule of catalyst can convert into **B** molecules in one second, minute, or hour. In heterogeneous catalysis, TON and TOF are often defined per active site, or per gram catalyst. This is because one does not know exactly how many

“catalyst molecules” there are on the surface. In biocatalysis, the TON and TOF are defined by the rate measured when all the enzyme molecules are complexed with a reactant, divided by the total enzyme concentration.

- **CAUTION!** Chemists can have different meanings for TON and TOF. To minimize misunderstandings, always include the units of these values when discussing catalytic activity.

The main advantages of catalysis is that you get the desired product faster, using fewer resources and generating less waste. The catalyst opens a selective route to the desired product. There are various kinds of product selectivity. Chemical selectivity, or **chemoselectivity**, denotes a situation where two different chemical reactions can occur, giving two different products. Similarly, **regioselectivity** occurs when the same chemical reaction in different regions of the molecule leads to different products. When a reaction gives two (or more) diastereomers, the selectivity to each of these is called **diastereoselectivity**. In the special case when two products are mirror-image diastereomers, or enantiomers, we talk about **enantioselectivity**. Figure 1.9 shows examples of the various product selectivity types.

1.2.1

Homogeneous Catalysis, Heterogeneous Catalysis, and Biocatalysis

In **homogeneous catalysis**, the catalyst is in the same phase as the reactants and products. Here we will concentrate on homogeneous catalysis in the liquid phase. In the classic case, the reactant (also called the substrate) molecules and the catalyst are reacted in a solvent. For example, the transesterification of fatty acid triglycerides with methanol (Figure 1.10) is catalyzed by hydroxide (OH^-) ions. This is an important process for making fatty acid methyl esters which are then used as biodiesel.

Notice that in Figure 1.10 I have written the “ OH^- ” above the reaction arrow, rather than on the same line as the reactants and products. This notation reminds us that the catalyst, although it participates in the reaction, remains unchanged when the reaction is completed. This does not mean that the catalyst does not change *during* the reaction. A catalytic reaction is made up of several steps. These form a cyclic process, called a **catalytic cycle**. Although the catalyst can (and often does) change during the catalytic cycle, it returns to its original form at the “end” of the cycle. Typical TONs for this reaction are ~ 1000 , so each OH^- anion catalyzes many consecutive cycles.

The easiest way to illustrate this is using an example. Figure 1.11a shows the classic catalytic cycle for the Pd-catalyzed cross-coupling between an alkene and an aryl halide. This reaction, discovered independently by Heck and Mizoroki in 1968, is known as the Heck reaction [22]. Since its discovery it has become ubiquitous in organic chemistry, and is used today in several fine-chemical processes [23]. We see that the catalyst goes through at least six different structures (these are called the **catalytic intermediates**). Each of these is “the catalyst” as much as any other. The point is, however, that at the end of the cycle the original catalyst is regenerated and is ready to catalyze the coupling reaction of two new substrate molecules. Figure 1.11b shows

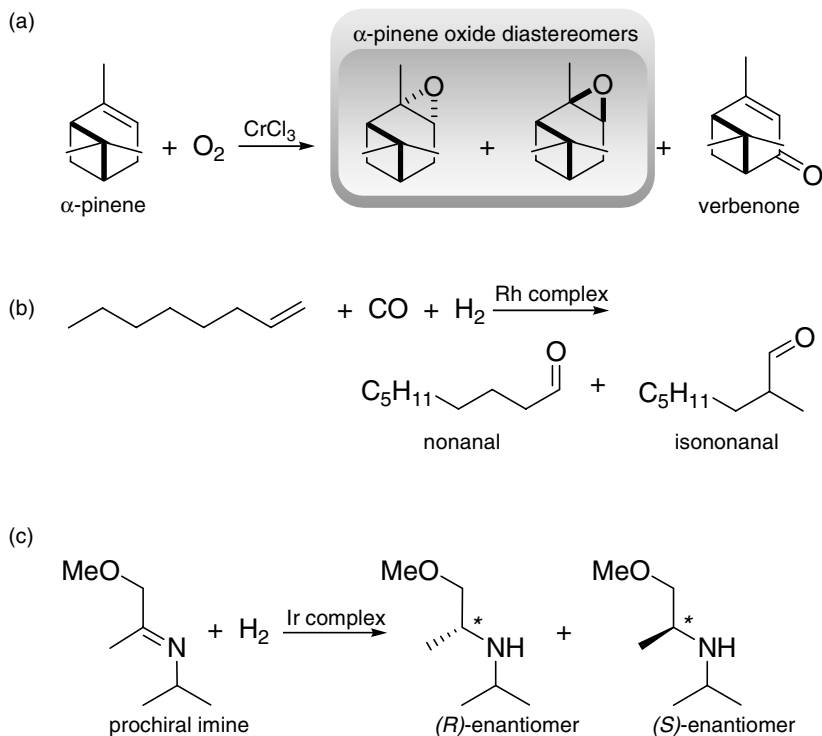


Figure 1.9 Examples of **a** chemoselectivity and diastereoselectivity in the oxidation of α -pinene, **b** regioselectivity in the hydroformylation of 1-octene, and **c** enantioselectivity in the hydrogenation of the prochiral isopropyl(2-methoxyisopropyl) imine (* indicates the asymmetric carbon atoms).

a “black box” version of the same catalytic cycle. This is what we actually observe: the substrates (aryl halide and alkene) enter the reactor and the products and by-products leave it. The catalyst remains in the reactor and, for all practical purposes, remains unchanged.

Many homogeneous catalysts are based on a (transition) metal atom that is stabilized by a **ligand**. The ligand is usually an organic molecule that attaches to the metal atom. By changing this ligand, one can change the catalyst's properties.

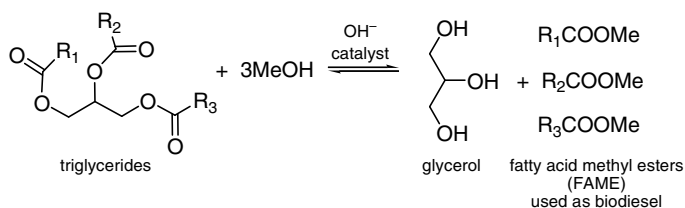


Figure 1.10 Base-catalyzed transesterification of triglycerides.

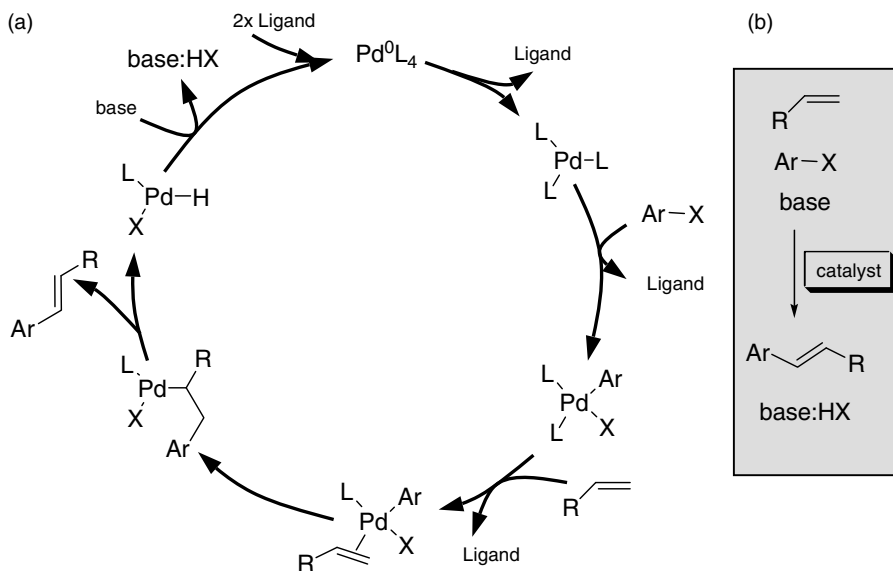


Figure 1.11 Proposed catalytic cycle for the Heck reaction, showing **a** the various catalytic intermediates and **b** the “black box” version. Some Pd catalysts exhibit TONs and TOFs of over 100 000 in this reaction.

Selecting the right metal and the right ligand can improve the catalyst’s activity, selectivity, and stability. In some cases, it also allows the use of renewable feedstocks and reagents, an important aspect of green chemistry. One such example is the alternating copolymerization of limonene oxide and CO₂, catalyzed by a β-diiminato–zinc acetate complex (Figure 1.12). CO₂ is an important raw material – it is abundant,

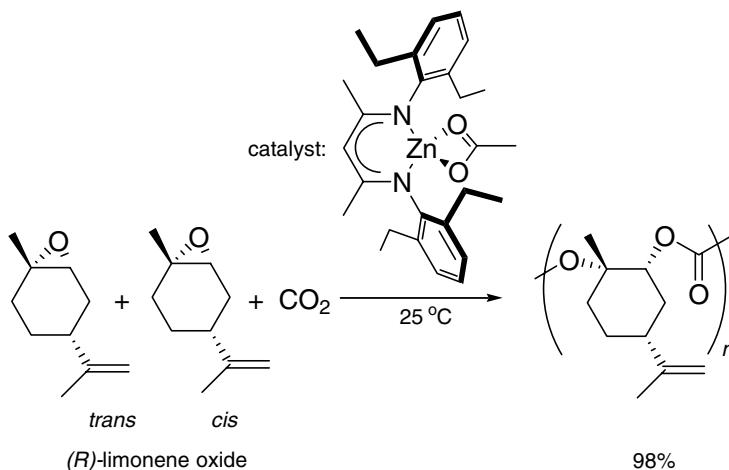


Figure 1.12 Copolymerization of limonene oxide and CO₂ in the presence of β-diiminato–zinc acetate complex.

inexpensive, and nontoxic. Likewise, limonene oxide is easily obtained from limonene, which is the most common terpene in citrus peel oil and has a world production of $>150 \times 10^3$ tpa (tons per annum). Its abundance, low cost, and structural similarity to cyclohexene oxide make (*R*)-limonene oxide an excellent choice as a biorenewable epoxide monomer for copolymerization with CO_2 . By optimizing the steric and electronic parameters of the ligand, Byrne et al. succeeded in copolymerizing limonene oxide and CO_2 , obtaining polymers with a mass of 9.3 kg mol^{-1} and 98% *trans* configuration [24].

Heterogeneous catalysis covers all the cases where the catalyst and the substrate are in different phases. However, when chemists speak about heterogeneous catalysis, they usually refer to a system where the catalyst is a solid and the reactants are (most often) gases or liquids. In fact, the solid/gas combination is so common that some books and journals refer to it as “classic” heterogeneous catalysis or even simply as “catalysis”. This has historical origins: most “classic” heterogeneous catalysis was developed in the petrochemicals and bulk-chemicals industry. Due to reactivity and process size considerations, these industries favor continuous processes at high temperatures. This meant that working with solid catalysts and gaseous reactants was often the best, and often the only, option. One important advantage of heterogeneous catalysis is the ease of catalyst separation. In gas/solid systems the catalyst is easily separated and cleaned, and in liquid/solid systems it can be simply filtered.

Once again, reactants enter the catalytic cycle and products leave, while the catalyst changes during the cycle but regains its original form at the end of the cycle. A simple example of gas/solid heterogeneous catalysis is the hydrogenation of propene to propane. In this reaction, a hydrogen molecule is added to the propene double bond in the presence of a group VIII metal catalyst (Ni, Pd, or Pt). The catalytic cycle (Figure 1.13) involves several steps. First, a propene molecule is adsorbed on the catalyst surface. The carbon–carbon π -bond breaks and bonds with the surface are created. Meanwhile, H_2 molecules are also adsorbed on the catalyst. The H–H bond then breaks, and the H atoms move across the metal surface. Eventually, an H atom diffuses close to one of the bonded C atoms. The C–metal bond is then replaced by a C–H bond. When this happens at the other C atom also, the connection with the surface breaks and the new propane molecule diffuses back into the gas phase.

Note that each of these simple **elementary reactions** is reversible, and so the entire catalytic cycle is also reversible. This is known as the principle of **microscopic reversibility**. Consequently, if platinum is a good hydrogenation catalyst, then it must also be a good dehydrogenation catalyst. In fact, as we will see later, catalysts change only the reaction rate, not the equilibrium. Every catalyst catalyzes both the “forward” and the “reverse” reactions in the same proportions. In the above example, the reverse reaction is actually more interesting for industry, because propene is a valuable monomer for making poly(propylene) and other polymers.

Olefin hydrogenation by heterogeneous catalysis has an interesting history. In 1927, two manufacturers in Oss (the Netherlands) bought the rights to a French patent for hydrogenating the double bonds in vegetable oil using a Ni catalyst. This

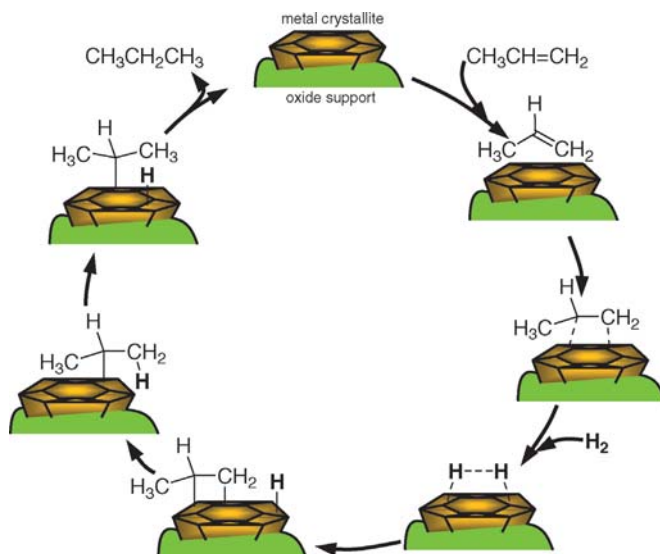


Figure 1.13 Hydrogenation of propene to propane in the presence of a supported metal catalyst (the reverse arrows are omitted for clarity).

yielded a fatty substance – a vegetable-based margarine. They named their joint venture the *Margarine Unie*. Later, they teamed up with two English margarine manufacturers, the Lever brothers, and formed Unilever. In 2007, the company is worth over €37 billion (\$50 billion).

Not all heterogeneous catalysis occurs on metal surfaces. **Zeolites**, for example, are excellent solid acid catalysts. These are porous crystalline structures of metal oxides, often made from silicon, titanium, aluminum, and oxygen. By substituting cations in the zeolite framework, one can create Brønsted and/or Lewis acid sites. As we shall see in Chapters 2 and 4, zeolites are widely used in industry for enriching gasoline octane numbers via gas/solid catalysis. Nevertheless, they can also catalyze liquid/solid reactions, as in the example of geraniol cyclization [25] by zeolite Y (Figure 1.14a–b; see Chapter 4 for a discussion of zeolite types). Geraniol and its corresponding cyclic derivatives are important intermediates in the flavor and fragrance industry [26]. The suggested reaction mechanism involves both carbocation formation, via protonation of the double bond at a Brønsted acid site [27], and complexation of the hydroxy group with a Lewis acid site.

Biocatalysis is a rather special case, somewhere between homogeneous and heterogeneous catalysis. In most cases, the biocatalyst is an enzyme – a complex protein that catalyzes the reactions in living cells. Enzymes are extremely efficient catalysts. An enzyme typically completes 1000 catalytic cycles in one second. Compared to this, conventional homogeneous and heterogeneous catalysts are slow and inefficient (100–10 000 cycles per hour). Speed, however, is not the only advantage: enzymes specialize in converting one specific reactant into another

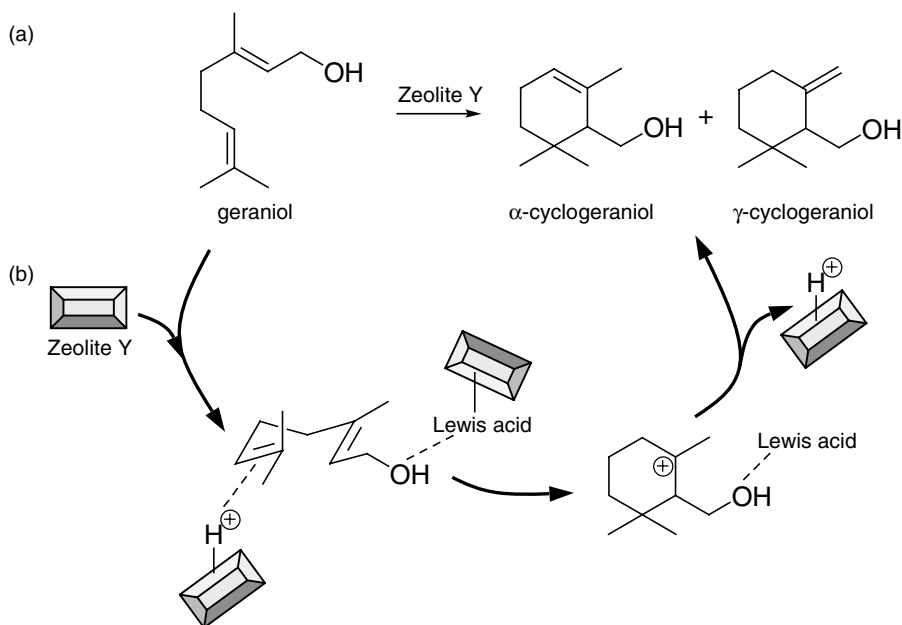


Figure 1.14 **a** Equation for the cyclization of geraniol, and **b** possible mechanism in the presence of zeolite Y, a solid acid catalyst that has both Brønsted and Lewis acid sites.

specific product. This specificity even includes chiral centres, so an enzyme will catalyze the reaction of one substrate enantiomer, but not of the other. Such enantiospecific reactions are extremely important in the pharmaceutical and food industries, because often only one enantiomer has the desired activity. This is the case for many drugs, food additives, flavorings, and fragrances.

Further advantages of biocatalysis over “chemical catalysis” include shorter synthesis routes and milder reaction conditions. Enzymatic reactions are not confined to *in vivo* systems – many enzymes are also available as isolated compounds which catalyze reactions in water and even in organic solvents [28]. Despite these advantages, the activity and stability of most wild-type enzymes do not meet the demands of industrial processes. Fortunately, modern protein engineering methods can be used to change enzyme properties and optimize desired characteristics. In Chapter 5 we will outline these optimization methods, including site-directed mutagenesis and **directed evolution**.

Although biocatalysis is the “new kid on the block,” more and more companies are using enzymes for chemical manufacture. One reason for this is that biocatalysts give sustainable alternatives to chemical manufacture, and not just for making chiral products. The synthesis of acrylamide via an enzyme-catalyzed water addition to acrylonitrile (2-propenenitrile) is a classic example (Figure 1.15). It uses the *Rhodococcus* enzyme nitrile hydratase. Commercialized in 1985 by Nitto Chemicals in

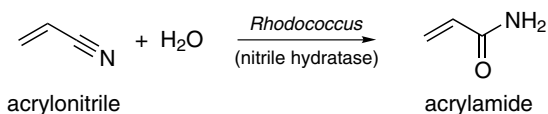


Figure 1.15 The biocatalytic synthesis of acrylamide from acrylonitrile is performed in Japan on a scale of ~10 000 tons per year. The bacterial cells are immobilized in a poly(acrylamide) gel, and the process is run at pH 8.0–8.5 in semi-batch mode, keeping the substrate concentration below 3%.

Japan, this process replaced an acid-catalyzed process, and also avoided the acrylic acid by-product [29]. Biocatalytic acrylamide processes are now running at 50 000 tpa worldwide.

Recent advances in genetic engineering are bringing forth new and exciting possibilities for biocatalysis. One example is the synthesis of important bulk industrial chemicals from renewable feedstocks. Adipic acid, for example, is a key monomer for making nylon 6.6. The world production of adipic acid is 2.2 million tons per annum. Practically all of this is produced from benzene, via cyclohexane and cyclohexanol/hexanone (Figure 1.16, left). Although the process itself is quite efficient, it has three main drawbacks: First, it relies on petroleum, a nonrenewable fossil fuel, as a raw material. Second, it uses benzene, a known carcinogen. Third, it requires high pressures of hydrogen and oxygen, and uses concentrated HNO_3 in the intermediate oxidation step, generating N_2O as a by-product.

In 2002, Frost and co-workers successfully constructed a mutated *Escherichia coli* bacterium that can convert D-glucose to *cis,cis*-muconic acid, which is then easily hydrogenated to adipic acid (Figure 1.16, right) [30]. The biosynthetic route is certainly more complex than the conventional synthesis: it has nine steps, and uses eight different enzymes. But the first eight steps are carried out inside the *E. coli* cell, at 37 °C and ambient pressure. The bacterium simply eats D-glucose, and produces *cis,cis*-muconic acid. Moreover, D-glucose is a cheap (€230, or \$300, per ton) and renewable raw material. Switching from benzene to glucose gives a process that is inherently safer and more sustainable. A similar approach was used to convert D-glucose to hydroquinone, an important intermediate in the synthesis of antioxidants and polymerization inhibitors [31].

Will such biocatalytic processes really replace the traditional chemical manufacturing routes? Yes, but it will take time. Although petroleum prices are increasing, there is still no shortage of benzene for chemical production (>90% of the worldwide petroleum demand ends up as transportation fuel; chemicals production accounts only for ~7%). The bulk-chemical industry is very conservative, and enzymes are expensive compared to conventional catalysts. Nevertheless, biotechnology, and with it biocatalysis, are progressing rapidly. Twenty years ago, such a *tour de force* of genetic engineering could only be found in the science fiction section. Now it is almost commonplace research. Designed metabolic biosynthesis is here, and it is here to stay.

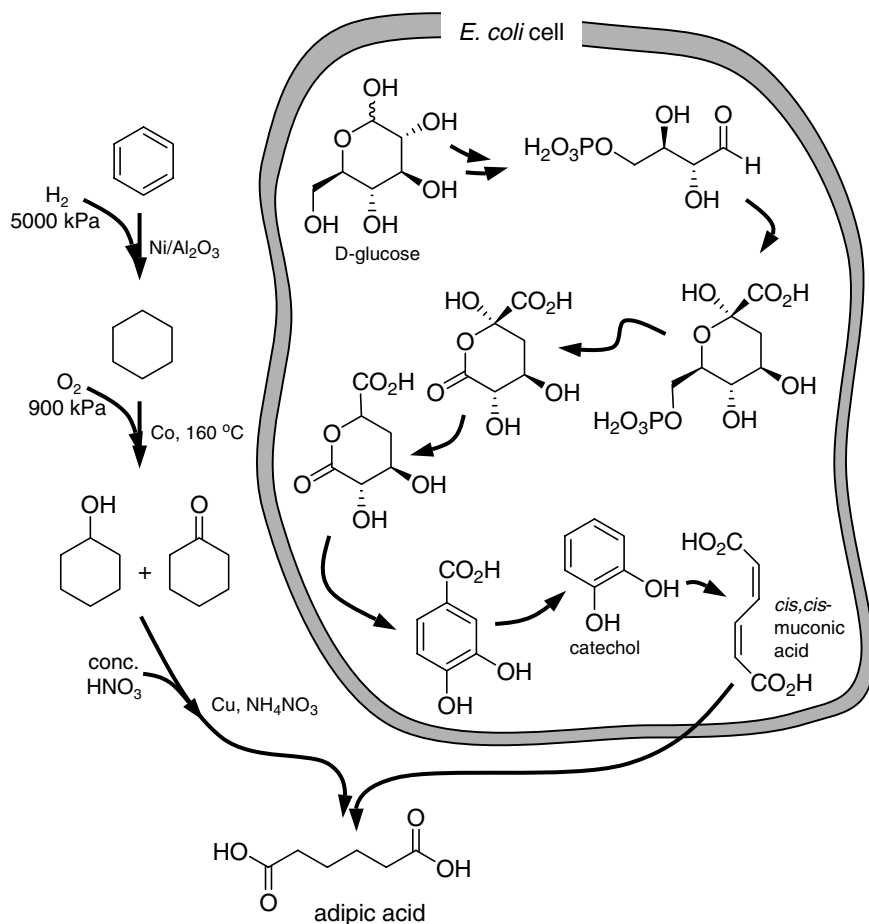


Figure 1.16 The classic Du Pont route to adipic acid (*left*) and Frost's biosynthetic route using a genetically modified *E. coli* cell (*right*; the enzymes and the reagents are omitted for clarity).

1.2.2

Replacing Stoichiometric Reactions with Catalytic Cycles

As we saw in the previous sections, atom economy is an important concept in green chemistry. Preferably, every atom that you put into a process should come out as product. Classic organic synthesis protocols often use stoichiometric reagents. Many of these reagents are polluting, and contain many atoms that are not incorporated in the products and must be disposed of. This is not only bad for the environment, but also very costly – you pay twice: once for buying the additional reagents, and once for disposing of the waste.

A classic example is the homocoupling of aryl iodides in the presence of copper, known as the **Ullmann reaction** (Figure 1.17). This reaction gives symmetric biaryls,

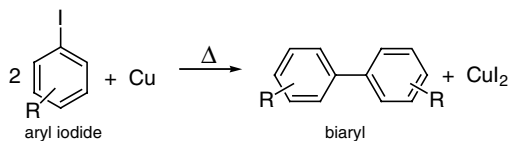
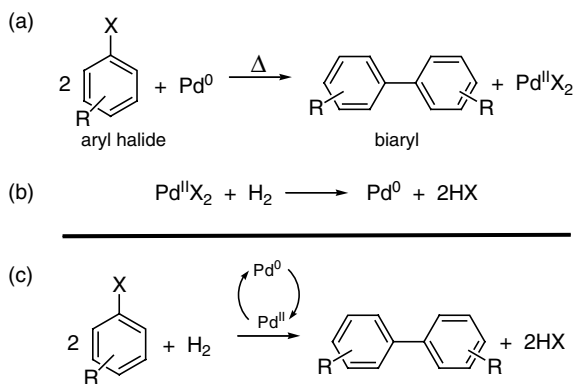


Figure 1.17 The classic Ullmann reaction for coupling aryl iodides by reaction with copper metal at high temperatures.

which are key building blocks for various agrochemical and pharmaceutical products. Although the Ullmann reaction is over 100 years old, it is still used in industry today. The problem is that it consumes stoichiometric copper and generates large amounts of waste. The reaction works best with iodoaryls, which increases the waste problem. This is because chemicals react by their molarity, but are quantified (and bought and sold) by their mass. One ton of iodobenzene contains 620 kg of “iodo” and only 380 kg of “benzene.” Thus, two-thirds of the reactant (PhI) and all of the reagent (Cu) come out as chemical waste.

Using the principles of green chemistry, let us first see if we can replace the stoichiometric reagent (copper) with a catalytic cycle. The iodine atoms are not part of the product. They act as leaving groups, ultimately generating two $\text{C}_6\text{H}_5\cdot$ radicals that couple to give biphenyl. The copper metal reduces the iodine atoms, giving Cu^{2+} and 2I^- . The same stoichiometric reaction can be brought about by using palladium instead of copper (Figure 1.18a). This does not look so useful, because Pd is much more expensive than Cu. However, the advantage of Pd is that it is easily reduced back from Pd^{2+} to Pd^0 . This reduction can happen, for example, using



where $\text{X} = \text{Cl}, \text{Br}, \text{I}$

Figure 1.18 Combination of two stoichiometric reactions: **a** the reductive coupling of halobenzene with Pd^0 and **b** the reduction of Pd^{II} with hydrogen gas creates **c** a catalytic cycle where the Pd catalyst shuttles between the Pd^0 and Pd^{II} species.

hydrogen gas [32], giving Pd^0 and 2H^+ (Figure 1.18b). If we then combine these two reactions, we get the catalytic cycle shown in (Figure 1.18c). This is a very simple representation of the catalytic cycle, but it demonstrates the principle: iodobenzene and hydrogen go in, and biphenyl and HI come out, while the Pd catalyst remains in the cycle and shuttles between Pd^{2+} and Pd^0 . Usefully, this catalytic cycle also works with bromo- and chloroarenes, improving the *E*-factor of the reaction and the atom economy.

Can we improve the atom economy even further, and avoid using any halide? The “greenest solution” for making biphenyl, $\text{C}_{12}\text{H}_{10}$, is to use no leaving group, starting from 12 C atoms and 10 H atoms. This can be done (in theory) by coupling benzene, C_6H_6 , with benzyne, C_6H_4 (Figure 1.19a). Although this route gives 100% atom economy on paper, generating benzyne is very difficult. More practically, the smallest leaving group that is easily available is a hydrogen atom, obtained by, e.g., oxidative coupling of two benzene molecules to form biphenyl (Figure 1.19b). This reaction can be effected by using stoichiometric amounts of PdCl_2 in acetic acid as solvent [33], or by using a Pd catalyst and regenerating it with air as the oxidant, giving water as the only by-product (an additional homogeneous $\text{Co}(\text{OAc})_2$ catalyst is used for activating the oxygen in solution) [34]. Although the actual catalytic cycle involves many steps and intermediates, the principle is simple: benzene and oxygen go in, and biphenyl and water come out. Currently, the highest yields reported for this system are $\sim 80\%$.

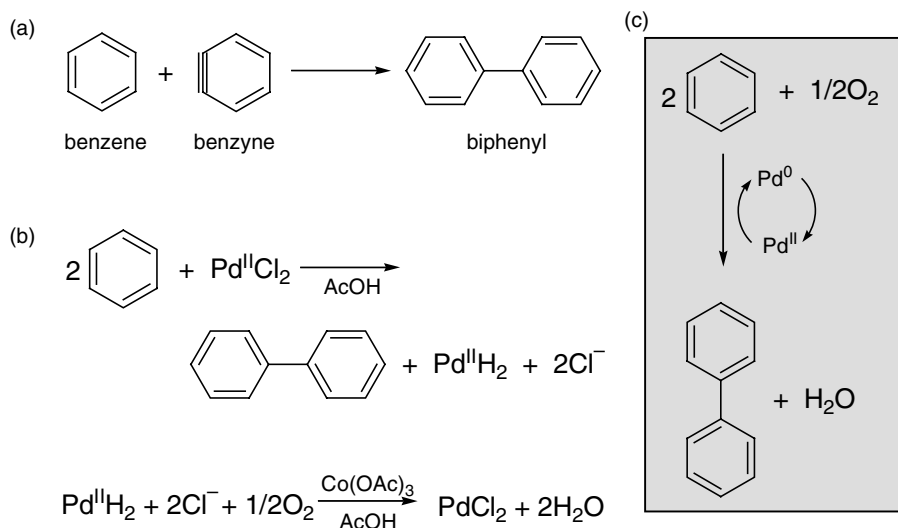


Figure 1.19 a Theoretical waste-free route to biphenyl starting from benzene and benzyne; b oxidative coupling of two benzene molecules with stoichiometric $\text{Pd}^{\text{II}}\text{Cl}_2$ and regeneration of Pd^{II} with molecular oxygen; c the resulting catalytic cycle for oxidative coupling.

Another interesting alternative combines catalysis and electrochemistry [35]. In the reductive coupling cycle of two bromobenzene molecules to biphenyl, the Pd catalyst provides just two electrons. This reaction can be performed in an electrochemical cell, where the electrons are supplied from an outside source [36]. We thus see that catalysis gives us a variety of green alternatives to the classic stoichiometric process. There are no hard and fast rules as to which route to choose – it all depends on the reaction conditions, and on the chemicals available.

1.2.3

Industrial Example: The BHC Ibuprofen Process

In 1992, BASF opened a 35 000 tons per year ibuprofen production plant in Bishop, Texas. This plant was the result of the elegant green chemistry route developed by the BHC consortium. The clean synthesis of ibuprofen is an excellent example of how combining catalysis and green chemistry can yield both commercial success and environmental benefits. Ibuprofen is a nonsteroidal, anti-inflammatory painkiller. It is a popular over-the-counter drug against headache, toothache, and muscular pains. You may know it better as Advil™, Motrin®, or Nurofen.

Ibuprofen, like many other drugs, is a fairly simple compound. It was first patented by Boots in 1962. The original production route consisted of six steps, starting from 2-methylpropylbenzene and acetic anhydride. Each of these steps involved stoichiometric reagents (Figure 1.20a–b). The overall atom economy of the process was only 40%. This means that more than half of the materials that entered the process were thrown away as waste. For example, note the addition of hydroxylamine, NH_2OH , in step 4: This group is used to create the imine **5**, which is then converted to the cyano derivative **6** and finally oxidized to give the carboxylic acid product **7**. Effectively, what happens is that the hydroxylamine is first added to the molecule and then removed. This type of “roundabout synthesis” is precisely what green chemistry tries to avoid.

When the patent rights on ibuprofen expired, Boots teamed with the Hoechst Celanese Corporation and formed the BHC consortium, developing a new process for making ibuprofen. They started from the same raw materials, but replaced the stoichiometric six-step process with a three-step catalytic one (Figure 1.20b). The overall atom economy of this new process was 77%, with acetic acid as the only by-product. The consortium also developed methods for recovering and recycling the acetic acid, increasing the atom utilization to 99%, and creating an essentially waste-free synthesis. Using anhydrous HF as both catalyst and solvent offers important advantages in reaction selectivity and waste reduction, as the new route has also eliminated the large volumes of aqueous salt waste associated with ibuprofen manufacture.

The BHC ibuprofen process is an innovative, efficient technology that has revolutionized bulk pharmaceutical manufacture. The process provides an elegant solution to a prevalent problem encountered in bulk pharmaceutical synthesis: It avoids the large quantities of solvents and waste (especially aqueous salt waste

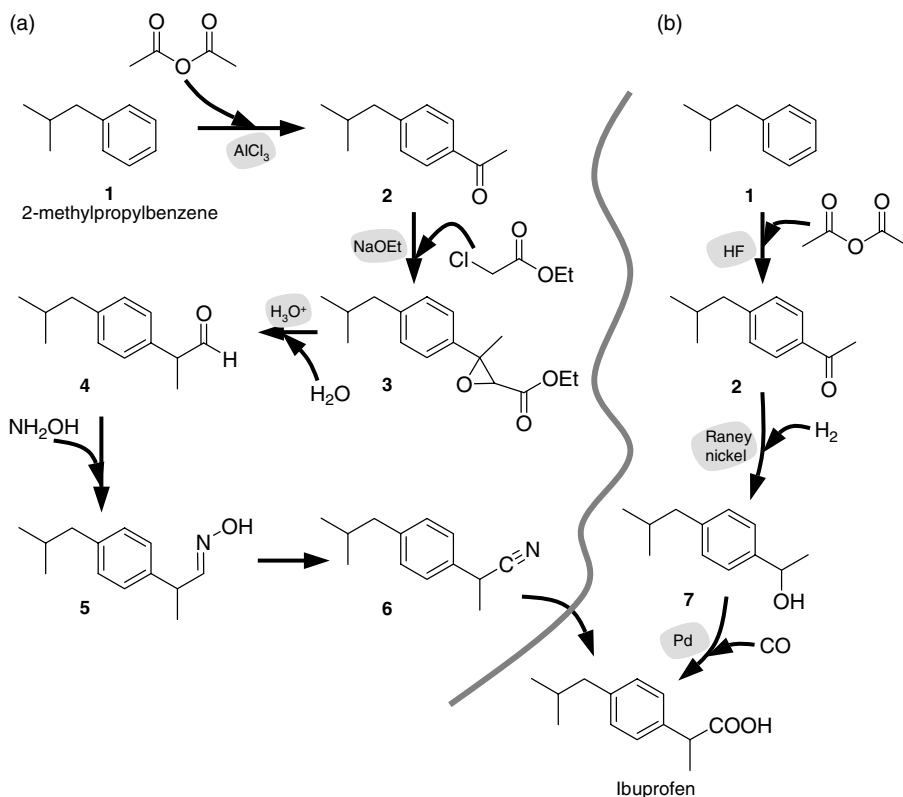


Figure 1.20 Synthesis of ibuprofen: **a** the six-step Boots route; **b** the three-step BHC route. In each case, the catalysts are highlighted in gray.

streams) associated with traditional stoichiometric reagent usage. The anhydrous HF catalyst is recovered and recycled with efficiency greater than 99.9%. No other solvent is needed in the process, simplifying product recovery and minimizing emissions. The new ibuprofen process became a model for environmental excellence in chemical technology, and BHC received the Kirkpatrick Achievement Award for “outstanding advances in chemical engineering technology” in 1993, and the US Presidential Green Chemistry Award in 1997.

1.3 Tools in Catalysis Research

Catalysis plays an integral role in many chemical reactions, all the way from petrochemistry to pharmaceutical chemistry. Because catalysis covers such a wide area, researchers use a variety of tools. These can be roughly divided into three

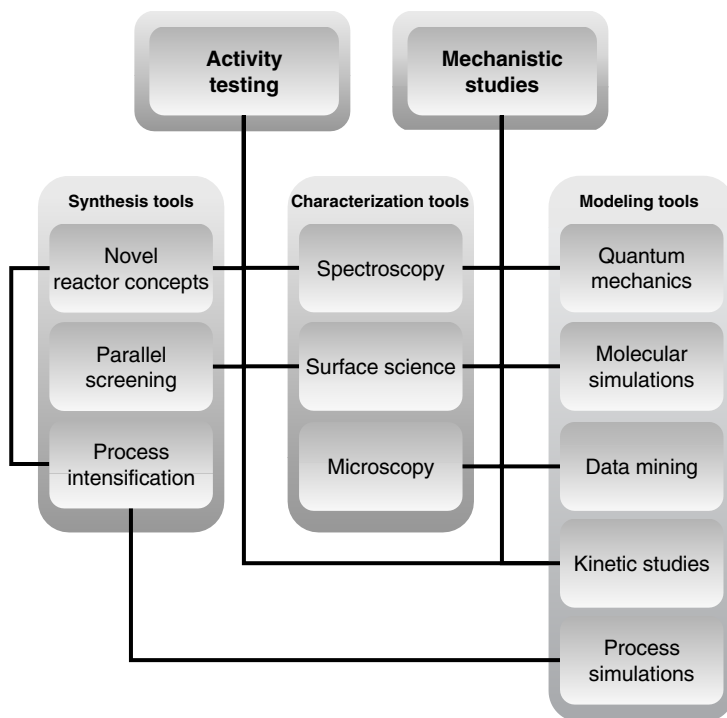


Figure 1.21 Block diagram of the various tools used in catalysis research.

groups: synthesis and testing tools, characterization tools, and modeling/mechanistic studies tools (see Figure 1.21).

1.3.1

Catalyst Synthesis and Testing Tools

The reactors used in organic and organometallic chemistry research did not change much from the 1850s to the 1990s. The chemical industry is a conservative one, so the majority of liquid-phase reactions still take place in batch reactors in one form or another, while most gas-phase reactions are carried out in flow reactors. Nevertheless, recent developments in reactor design and process intensification are now changing the picture [37].

Traditionally, research in catalyst discovery and optimization followed a cyclic workflow of synthesis, characterization, activity testing, and mechanistic studies. Because carrying out reactions was considered costly and labor-intensive, chemists favored working on a few model compounds, learning as much as possible from each reaction. The 1990s saw a paradigm shift, with the entry of parallel screening and high-throughput experimentation in catalysis research. This was pioneered by Alejandro Zaffaroni and Peter Schultz, who founded the company Symyx in

1994. Symyx adapted the concepts of miniaturization and parallel synthesis, used in pharmaceutical and biomedical research, to catalysis and materials science [38]. The main advantages were higher efficiency, and the ability to carry out reactions using smaller amounts of reactant and quantities of catalyst. This was especially important for homogeneous catalysis, where ligand cost and availability are often a problem. Diphosphine ligands, for example, typically cost €75–€370 (\$100–\$500) per gram, while 1 g of Rh costs €120 (\$160) and 1 g of Pt “only” about €24 (\$32). Moreover, performing many experiments in parallel can improve data quality, as repeating experiments is easier, and systematic errors can be minimized. Similar advantages were obtained by “one-pot” reaction systems, where multiple substrates and catalysts were tested simultaneously [39]. Although these new tools were initially viewed with skepticism by the chemical industry, they are used today by most companies that develop catalysts and catalytic processes.

Most of the parallel reactors on the market today are basically arrays of scaled-down batch reactors. There are also several novel concepts for high-throughput catalyst screening based on new microreactor technology [40]. One such example is the mixed-pulse reactor developed by Claude de Bellefon in 2000, which enables the fast sequential screening of catalysts in liquid/liquid and gas/liquid systems [41]. Here, two liquid carriers flow continuously through a micromixer which is connected to a plug-flow reactor. The two carriers can be mutually miscible (e.g., pentane and cyclohexane) or immiscible (e.g., heptane and water). The first carrier contains the substrates, while the second contains the catalyst. Pulses of the two carriers are injected simultaneously. They mix perfectly in the micromixer, with a residence time of less than 10 ms. This creates a “reaction pulse” which then moves through the reactor and can be analyzed by standard gas chromatography (GC) or high-performance liquid chromatography (HPLC) at the reactor outlet. Using this approach, one can test truly minute amounts of catalyst, without sacrificing the high accuracy and precision of chromatographic analysis. This system can also be adapted to high-throughput screening using spectroscopy (Figure 1.22). This involves adding a third valve that injects air bubbles before and after each pulse, and sending the pulses through a spectrophotometric flow cell.

Parallel synthesis and testing of heterogeneous catalysts for gas/solid reactions has also seen a number of ingenious developments, especially in the preparation and screening of catalyst libraries. Masking, sputtering, and lithographic techniques were applied for depositing arrays of metal catalyst precursors on ceramic or silicon wafers. Subsequent oxidation (or reduction) of these wafers gave solid catalyst libraries (mixed metal alloys or mixed metal oxides, depending on the treatment), wherein both the composition and the position of each catalyst was well defined [42]. Today, libraries of hundreds, even thousands, of catalysts are prepared in this way, using very small amounts of metal precursors.

In 1996, Willson and co-workers reported the first parallel screening of such a library using infrared (IR) thermography, using a grid of alumina pellets [43]. By taking infrared photos of the catalyst array through a sapphire window, and measuring the ignition temperature, they tested the catalytic activity for hydrogen oxidation. Two years later, Maier and co-workers refined this concept, screening 50

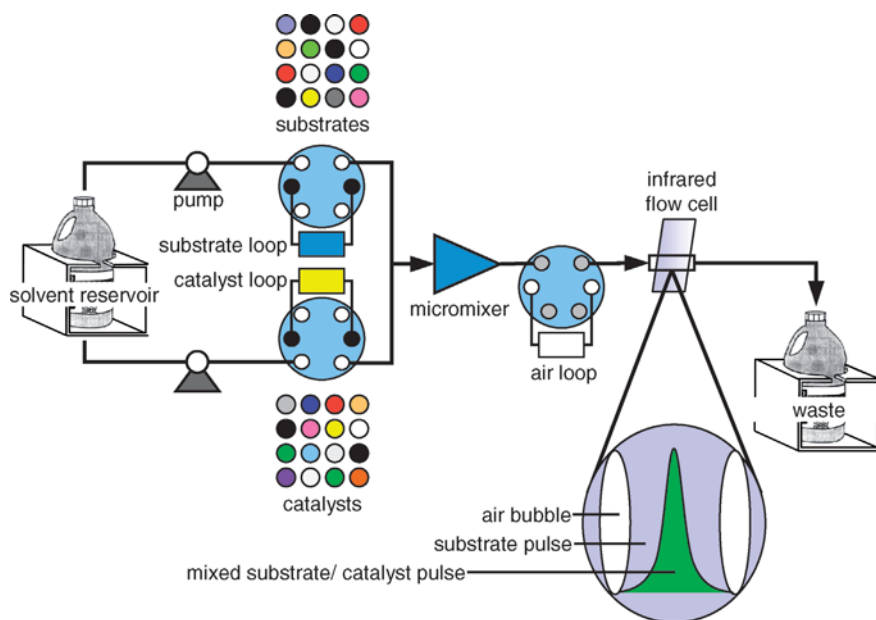


Figure 1.22 Schematic of the sequential pulse injection system developed by de Bellefon, adapted for high-throughput screening using on-line spectroscopy.

catalysts simultaneously and using only 200 μg of catalyst per sample [44]. Higher camera sensitivity enabled the screening of less exothermic reactions, such as the hydrogenation of hexyne at 100 $^{\circ}\text{C}$ and the oxidation of isooctane and toluene at 350 $^{\circ}\text{C}$.

The main advantage of the grid approach is that the catalyst position is well defined. This is easy to do with solid catalysts, but not with homogeneous ones in solution. One way of solving this problem is to attach the homogeneous catalysts to a solid support, such as polymer beads [45] peptide scaffolds [46], or inorganic monoliths [47].

The resulting supported catalysts are heterogeneous, but still similar to their homogeneous analogues. Such solid-phase synthesis is common in pharmaceutical chemistry, where it is often used in combination with split/pool synthesis. In 1998, Taylor and Morken combined solid-phase bead supports with IR thermography, for synthesizing and screening large libraries of supported homogeneous catalysts using the split/pool approach [48].

1.3.2

Catalyst Characterization Tools

Catalysis is still very much a “black box” discipline, and catalyst characterization tools help us look inside this box. Characterization is done on several levels: On the first, the

macroscopic level (the reactor level), engineers search for the optimal formulation and operating conditions of the catalytic process. The second, the mesoscopic level, includes surface analysis and temperature-programmed techniques (in heterogeneous catalysis), as well as kinetic studies, with the aim of finding composition/activity and structure/activity relationships. Finally, on the microscopic (or, more accurately, the nanoscopic) level, chemists and physicists probe catalyst molecules, clusters, and atoms, trying to understand the fundamental steps that make up the catalytic cycle. A discussion of catalyst formulation on the macroscopic level is outside the scope of this book – the reader is referred to specialized texts on industrial catalysis [49]. We will cover the subject of kinetic studies in Chapter 2, and give further specific examples from homogeneous, heterogeneous, and biocatalysis in Chapters 3, 4 and 5 respectively. In heterogeneous catalysis, much information on the mesoscopic level is gained using classic surface-science techniques for measuring surface area, porosity, and particle size distribution. Chapter 4 gives an overview of these methods.

The last two decades have witnessed rapid developments in catalyst characterization on the microscopic level, especially in the area of spectroscopy and imaging of solids [50]. Instruments for transmission electron microscopy (TEM) and scanning electron microscopy (SEM) are now almost commonplace. They can resolve images to within a few nanometers. High-resolution atomic force microscopes are also available which can resolve rows of atoms and single-crystal facets. Using such tools, chemists can “see” the catalyst surface, and sometimes follow the reactions in real time. Other techniques such as Raman spectroscopy, solid-state nuclear magnetic resonance (SS-NMR), and diffuse reflectance ultraviolet spectroscopy (DRIFTS) also give important information regarding the active sites on the surface [51]. Similar spectroscopic techniques are also used in homogeneous catalysis and biocatalysis.

One way of circumventing the high complexity of catalytic systems is by analyzing isolated samples of catalyst precursors or intermediates. The advantage of this *ex situ* approach is that one works with simplified systems, under well-defined conditions (e.g., polished crystals under ultra-high vacuum, or diluted solutions of pure analytes). *Ex situ* characterization can give important information on the catalyst structure, from which one can deduce key structure/activity relationships, and learn about the reaction mechanism. The disadvantage is that the analysis conditions differ from the real reaction conditions. Typical gas/solid catalysis is performed at high temperatures and pressures, not in ultra-high vacuum. Similarly, liquid-phase homogeneous catalysis takes place in solutions and mixtures of numerous species, and enzymes work inside living cells which contain a plethora of compounds, not with “pure analytes.” This difference in pressure, composition, and temperature between the analysis conditions and the real reaction conditions is known as “the gap.” Bridging this gap is an important challenge in catalysis research [52,53].

Alternatively, one can characterize the catalytic intermediates *in situ*, under conditions that are closer to the real reaction conditions. Recent advances in high-pressure IR and NMR equipment, for example, enable the measurement of spectra at up to 200 bar and 150 °C, similar to the reaction conditions in high-pressure autoclaves [54]. In some cases, one can combine the characterization with activity/selectivity analysis, examining the catalyst in real-time operation. This

simultaneous catalyst characterization and activity analysis is known as *operando* spectroscopy, a term coined by Miguel Banares in the 1990s [55]. *In situ* and *operando* characterization studies are increasingly popular, as more and more chemists concede the advantages of studying catalytic processes under realistic conditions.

1.3.3

Tools for Modeling/Mechanistic Studies

The meteoric rise in computer power (and meteoritic decline in hardware prices) has opened exciting avenues for computer modeling in all branches of science. Today, computer models are used in three main areas of catalysis research: modeling of reaction pathways and catalytic cycles, modeling of process kinetics and reaction performance, and computing structure/activity relationships on various levels. The models cover a wide range of approaches and system types.

Quantum mechanics calculations are used for solving the wavefunction equations of catalytic systems, giving a detailed picture of the reaction dynamics on the molecular scale. Two decades ago, such *ab initio* computations were so expensive that they were limited to very simple systems. Now, algorithms based on density-functional theory (DFT) enable the modeling of complex reactions in all three catalysis fields. In heterogeneous catalysis and biocatalysis, where the size of the system prohibits costly computations, hybrid methods are used. For example, one can model the active site of an enzyme using high-level computations, and the rest of the enzyme using low-level methods. Importantly, such models are not limited to energy minima (i.e., reactants, catalytic intermediates and products). They can also be used for computing the structures of the hypothetical activated complexes associated with transition states. Thus, computer modeling can provide a picture of the elusive transition states, which can never be observed directly by experiment (because by definition, transition states have a zero lifetime). In this way, one can model the reaction pathways, and the corresponding reaction kinetics in detail, gaining insight into the various elementary steps in the catalytic cycle.

Classical molecular simulations are used for modeling large systems, such as solid surfaces, enzymes, or large numbers of solvent molecules. In these simulations, the electronic interactions are averaged out using a classical potential, and the dynamics of the system are modeled by solving Newtonian equations. The computational cost here depends on the size of the system and on the level of detail. For example, a butane molecule, C_4H_{10} , can be modeled as a collection of 14 atoms (all-atom model), or as a chain with four links (coarse-grained model), or as one particle. In this way, one can tune the system size and the degree of detail to the requirements of the problem at hand.

Another important modeling aspect is the simulation of catalytic process parameters and reactor configurations. Such models are typically associated with process engineering, and involve computational fluid dynamics and heat- and mass-transfer calculations. They are essential in the process planning and scale-up. However, as this book deals primarily with the chemical aspects of catalysis, the reader is referred to the literature on industrial catalysis and process simulations for further information [49,56].

The third type of modeling deals with catalyst descriptors, structure/activity and structure/property relationships [57,58]. There are various levels of catalyst descriptors, ranging from very simple ones based on composition parameters (in heterogeneous catalysis) or connectivity matrices (in homogeneous catalysis) to ones based on high-level quantum computations and thermodynamic calculations. Like other modeling methods, descriptor models are often used for explaining the behavior of catalytic systems. Following the advances in drug discovery, however, predictive descriptor modeling is emerging as an exciting new field in catalysis research [59]. By combining the data from high-throughput experimentation with statistical analysis and descriptor models, you can predict the properties and performance of new catalysts [60,61]. Chapter 6 explains the basics of predictive modeling and *in silico* catalyst screening.

1.4 Further Reading

There are several books available in the field of catalysis. Here are the important ones, with a short synopsis of my thoughts about each book. All the books listed below were in print and commercially available in August 2007.

Homogeneous Catalysis, S. Bhaduri and D. Mukesh, Wiley-Interscience: 2000, 239 pp., ISBN 0-471-37221-8. This introductory textbook emphasizes the practical side, with a chapter dedicated to chemical engineering basics and process unit operations. The authors cover several examples of industrial homogeneous catalysis processes. Although the book is aimed at graduate students, it contains relatively few references to the primary literature. Each chapter is accompanied by a good selection of review questions and problems.

Homogeneous Catalysis, P.W.N.M. van Leeuwen, Kluwer Academic: 2004, 407 pp., ISBN 1-4020-1999-8. This is an advanced textbook aimed at graduate students with prior knowledge in synthetic, inorganic, and physical-organic chemistry. It gives a comprehensive overview on metal–ligand complexes, especially phosphorus ligands. All the subjects are clearly presented, with many useful references. The author explains ligand effects and the elementary steps in homogeneous catalysis with good examples which also include important process aspects of hydroformylation, hydrogenation, polymerization, and a variety of Rh- and Pd-catalyzed reactions.

The Organometallic Chemistry of the Transition Metals, R. H. Crabtree, Wiley-Interscience: 2005 (4th edn.), 546 pp., ISBN 0-471-66256-9. This is the best graduate-level textbook in organometallic chemistry. It is clear and well written, covering all of the fundamental reactions of organometallic complexes, plus some applications. Each chapter also contains exercises and up-to-date references.

Applied Homogeneous Catalysis with Organometallic Compounds, B. Cornils and W. A. Herrmann, Eds., VCH: 1996, 1246 pp. in two volumes, ISBN 3-527-29286-1. Although it is over 10 years old, this large collection of essays covers many important applications of organometallic homogeneous catalysis. Some chapters are written from an industrial perspective, discussing scale-up and process challenges also.

Concepts of Modern Catalysis and Kinetics, I. Chokendorff and J. W. Niemantsverdriet, Wiley-VCH: 2003, 452 pp., ISBN 3-527-30574-2. This specialized book deals only with classic gas/solid heterogeneous catalysis. It contains excellent technical explanations and has a strong mathematical and physical approach, which makes for rather heavy reading. It covers many surface reaction mechanisms and catalyst characterization techniques.

Principles and Practice of Heterogeneous Catalysis, J. M. Thomas and W. J. Thomas, Wiley-VCH: 1996, 688 pp., ISBN 978-3-527-29239-4. A comprehensive textbook on classic heterogeneous catalysis which covers catalyst preparation and characterization methods. It also includes a chapter on solid-state chemistry and surface chemistry, and a chapter on process engineering.

Spectroscopy in Catalysis, J. W. Niemantsverdriet, VCH: 1995, 288 pp., ISBN 3-527-28726-4. This is an excellent book on heterogeneous catalysis characterization. It is highly specialized, and aimed at advanced graduate students and researchers. It covers only classic gas/solid heterogeneous catalysis, but if you want to specialize in characterizing solid catalysts, this is the book for you.

Catalysis: An Integrated Approach, R. A. van Santen, P. W. N. M. van Leeuwen, J. A. Moulijn, and B. A. Averill, Eds., Elsevier: 1999, 582 pp., ISSN 0167-2991 (Vol. 123 in the *Studies in Surface Science and Catalysis* series). This is one of the few books that cover all categories of catalysis. It is written by 25 different authors, and like many other such collections, this is both a blessing and a curse. The advantage is that each chapter is written by specialists who are discussing research subjects dear to their hearts. The disadvantage is that the overall result is somewhat disjointed.

Handbook of Green Chemistry and Technology, J. H. Clark and D. J. Macquarrie, Eds., Blackwell Publishing: 2002, 540 pp., ISBN 0-632-05715-7. This collection of 22 review essays covers all the important areas of green chemistry, including environmental impact and life-cycle analysis, waste minimization, catalysts and their industrial applications, new synthesis methods, clean energy, and novel solvent systems. The chapters are well referenced and contain pertinent examples and case studies.

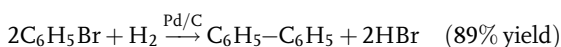
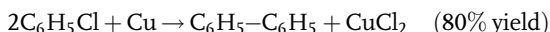
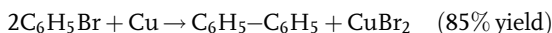
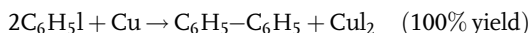
Green Chemistry and Catalysis, R. A. Sheldon, I. W. C. E. Arends, and U. Hanefeld, Wiley-VCH: 2007, 433 pp., ISBN 3-527-30715-9. An up-to-date advanced reference book, containing a collection of chapters on green chemistry applications in academia and industry. The subjects are ordered by reaction (oxidations, reductions, etc.) and are well presented.

An Introduction to Enzyme and Coenzyme Chemistry, T. Bugg, Blackwell Science: 1997, 247 pp., ISBN 0-86542-793-3 (paperback). This is a superb undergraduate/postgraduate textbook about enzymes. It is well written and illustrated, with interesting examples and well-thought-out exercises.

Biocatalysis, A. S. Bommarius and B. R. Riebel, Wiley-VCH: 2004, 611 pp., ISBN 3-527-30344-8. This is a comprehensive advanced textbook covering all aspects of biocatalysis. There are many good examples with references. It is a serious book, definitely not light reading, but one to have on the shelf if you are going to work in biocatalysis.

1.5 Exercises

- Examine the list of the 12 principles of green chemistry shown at the beginning of this chapter. Which of these principles relate to the concepts of atom economy, the *E*-factor, and the environmental quotient *Q*?
- (a) Calculate the *E*-factors and estimate the *Q*-values for the following three Ullmann reactions using stoichiometric copper, as well as for the catalytic alternative using 5 wt.% Pd/C and hydrogen gas.



- Compare the *E*-factors and *Q*-values for these four situations, and discuss the pros and cons of replacing the stoichiometric protocol with a catalytic cycle.
 - If using 100 mg of catalyst gives 98% conversion after 40 min, what are the TON and TOF of this catalyst?
- The most important (and also the most expensive) grapefruit aroma compound is the bicyclic terpene nootkatone. It is manufactured by oxidation of valencene, which is extracted from Valencia oranges. Figure 1.23 shows two routes for this oxidation, a stoichiometric reaction using chromium trioxide, and a catalytic alternative using sodium hypochlorite (bleach) in the presence of 1 mol% osmium tetroxide catalyst.
- Calculate the *E*-factors and atom economy values for both options.
 - Given that both CrO_3 and OsO_4 are equally toxic, estimate the *Q*-values in both cases, and explain which option you favor and why.

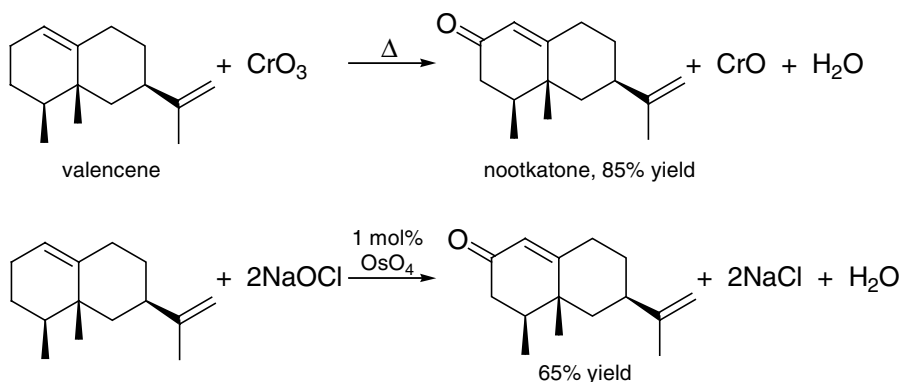


Figure 1.23 Alternative synthesis routes from valencene to nootkatone.

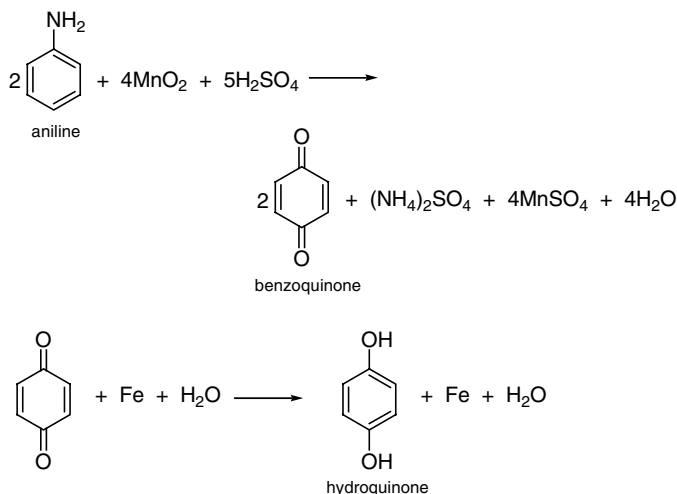


Figure 1.24 The classic synthesis route to hydroquinone starting from aniline.

4. The classic synthesis of hydroquinone starts with aniline, and uses stoichiometric MnO_2 , sulfuric acid, and iron (Figure 1.24).
 - (a) Calculate the atom economy for this process.
 - (b) Aniline itself is made by nitration of benzene to nitrobenzene, followed by hydrogenation. Using the principles of green chemistry, draw a scheme for a new process for making hydroquinone, starting directly from benzene (feel free to invent any catalysts you need).
 - (c) Search on the Internet for information on the Upjohn hydroquinone process, and compare that with your synthesis route. What are the advantages of the Upjohn process and of your synthesis compared to the classic route? Are there any disadvantages?

5. Fluorescent light bulbs contain mercury, which is released into the environment when the bulbs are disposed of in landfills [62]. Incandescent (regular) light bulbs contain no mercury, and so disposal is not a problem. However, regular bulbs use more electricity than fluorescent ones, which means burning more coal at the power station, and burning coal also releases mercury into the environment. A typical fluorescent bulb consumes 11 W h^{-1} and burns for 5000 h, while a typical incandescent one consumes 75 W h^{-1} and burns for 1000 h.
 - (a) Construct two life-cycle charts, one for fluorescent light bulbs and one for incandescent light bulbs.
 - (b) Assuming that coal contains typically 20 ppm mercury impurities, which type of light bulb is better, fluorescent or incandescent, for the environment?

6. A typical 1 L glass bottle for storing milk or juice weighs $\sim 400 \text{ g}$, while a 1 L tetra pak carton weighs only 35 g. This implies a big difference in raw material and transportation costs. Glass bottles, however, are often washed, reused, and

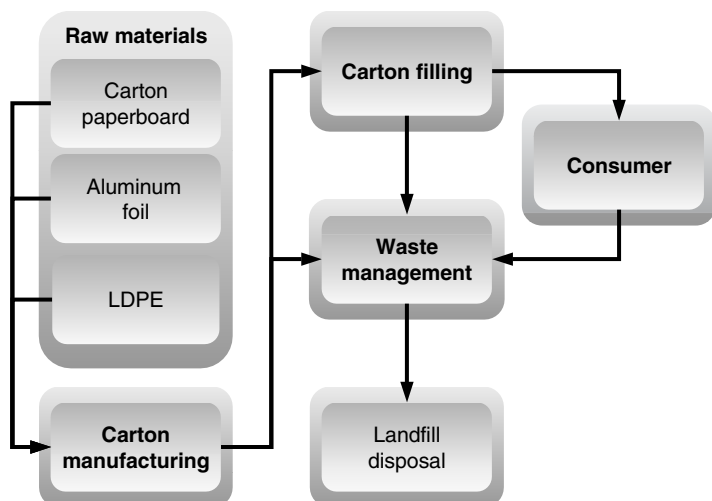
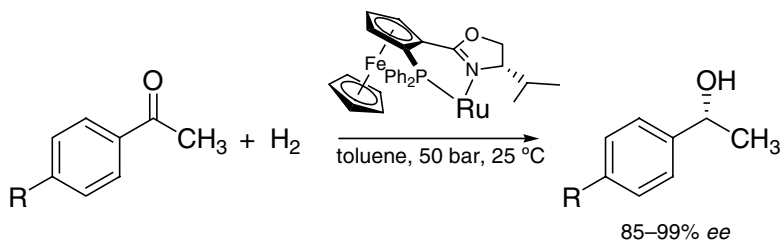


Figure 1.25 Life-cycle flow diagram for milk cartons.

eventually recycled, while cartons are disposed of in landfills (tetra paks are hard to recycle because they contain thin layers of low-density poly(ethylene) and aluminum, and because their collection is costly; the only municipality that currently recycles them is Sao Paolo, in Brazil). Figure 1.25 shows the life-cycle flow diagram for tetra-pak cartons.

- (a) Draw an analogous diagram for glass bottles, and consider the energy input and transport costs associated with 1000 L milk in cartons compared to 1000 L milk in bottles.
 - (b) Compare the prices of 1 L milk in glass bottles and cartons in your local supermarket. Which packaging method is more sustainable?
7. The asymmetric hydrogenation of aryl ketones is an important step in the synthesis of many pharmaceutical intermediates. Blaser and co-workers showed that Ru complexes with Fe–cyclopentadienyl “sandwich complexes” are good catalysts for this reaction [63]. Figure 1.26 shows the different substrates tested, along with the time, conversion, and substrate/catalyst ratio. Using these data, calculate the catalyst TON and TOF in each case.
 8. Monosodium glutamate (MSG) is a common food additive with a “meaty” flavor, used commercially for nearly 100 years. It was originally produced in Japan by extracting glutamic acid (2-aminopentanedioic acid) from wheat flour, and marketed under the trade name Ajinomoto (*Aji no moto* means “the origin of flavor” in Japanese) [64]. After WWII and the discovery of hydroformylation, the Ajinomoto company replaced the extraction with a continuous chemical process, starting from acrylonitrile, CO, and H₂ (see Figure 1.27).
 - (a) Calculate the overall atom economy and *E*-factor for the glutamic acid synthesis.



R-	substrate:catalyst	time, h	conversion, %
Cl-	50,000	78	99
CH ₃ O-	20,000	1	92
F-	500	1	100

Figure 1.26 Catalytic hydrogenation of various aryl ketones and the corresponding kinetic data.

- (b) Recalculate these values, assuming that the ammonia by-product is recycled with 80% yield back to ammonium cyanide. Does this recycling of ammonia make a big change?
- (c) Today, glutamic acid is produced by large-scale batch fermentation in 200 000 L reactors, starting from sugar, oxygen, and ammonia and using *Corynebacterium*

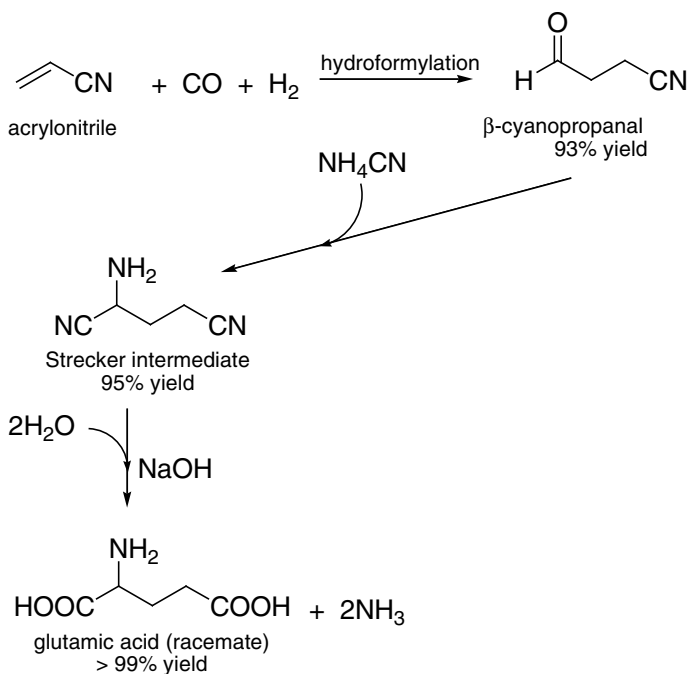


Figure 1.27 Three-step chemical synthesis of glutamic acid, starting from acrylonitrile.

glutamicum bacteria. This process gives ~60% conversion, with a final glutamic acid concentration of $\sim 100 \text{ g L}^{-1}$. List two possible disadvantages of the fermentation route compared to the chemical synthesis route.

- Jack Daniel's "Old No. 7" whiskey has been produced in Lynchburg, Tennessee, using the same recipe and methods since 1866. The production involves cooking and fermenting the corn mash, distillation, filtration over charcoal, and aging in oak barrels. All these steps are done in-house, including making the filter charcoal from locally grown sugar maple trees (unfortunately, Lynchburg is classified as a "dry county," so you will not be served any whiskey if you visit the distillery). Search the Internet for information and draw a life-cycle diagram for the whiskey-making process, indicating the on-site stages (also called the "foreground system") and the outside resources and effects (the "background system").

References

- de Souza Porto, M.F. and de Freitas, C.M. (1996) Major chemical accidents in industrializing countries: the socio-political amplification of risk. *Risk Anal.*, **16**, 19.
- Gunster, D.G., Bonnevie, N.L., Gillis, C.A. and Wenning, R.J. (1993) Assessment of chemical loadings to Newark Bay, New Jersey from petroleum and hazardous chemical accidents occurring from 1986 to 1991. *Ecotoxicol. Environ. Safety*, **25**, 202.
- Maki, A.W. (1991) The Exxon Valdez oil spill: initial environmental impact assessment. *Environ. Sci. Technol.*, **25**, 24.
- Peterson, C.H., Rice, S.D., Short, J.W., Esler, D., Bodkin, J.L., Ballachey, B.E. and Irons, D.B. (2003) Long-term ecosystem response to the Exxon Valdez oil spill. *Science*, **302**, 2082.
- Clark, J.H. (2006) Green chemistry: today (and tomorrow). *Green Chem.*, **8**, 17.
- Anastas, P.T. and Warner, J. (2000) *Green Chemistry: Theory and Practice*, Oxford University Press, ISBN 0-19-850698-8.
- Anastas, P.T. and Kirchoff, M.M. (2002) Origins, current status, and future challenges of green chemistry. *Acc. Chem. Res.*, **35**, 686.
- Clark, J.H. and Smith, P. (2005) Basic principles of Green Chemistry. *Innov. Pharmaceut. Technol.*, 94.
- Regulation (EC) No. 1907/2006 of the European Parliament and of the Council. (2006) *Official J. Eur. Union*, L **396**, 1–849.
- Sheldon, R.A. (1994) Consider the environmental quotient. *Chemtech*, **24**, 38.
- Sheldon, R.A. (1997) Catalysis: the key to waste minimization. *J. Chem. Technol. Biotechnol.*, **68**, 381.
- Trost, B.M. (1991) The atom economy – a search for synthetic efficiency. *Science*, **254**, 1471.
- Carrette, L., Friedrich, K.A. and Stimming, U. (2000) Fuel cells: principles, types, fuels, and applications. *ChemPhysChem*, **1**, 163.
- Buijink, J.K.F., van Vlaanderen, J.J.M., Crocker, M. and Niele, F.G.M. (2004) Propylene epoxidation over titanium-on-silica catalyst – the heart of the SMPO process. *Catalysis Today*, **93–95**, 199.
- Ben-Daniel, R., Weiner, L. and Neumann, R. (2002) Activation of nitrous oxide and selective epoxidation of alkenes catalyzed by the manganese-substituted polyoxometalate, $[\text{Mn}^{\text{III}}]_2\text{ZnW}$

- (Zn₂W₉O₃₄)₂]¹⁰⁻. *J. Am. Chem. Soc.*, **124**, 8788.
- 16 Lankey, R.L. and Anastas, P.T. (2002) Life-cycle approaches for assessing green chemistry technologies. *Ind. Eng. Chem. Res.*, **41**, 4498.
 - 17 McDonough, W., Braungart, M., Anastas, P.T. and Zimmerman, J.B. (2003) Applying the principle of green engineering to cradle-to-cradle design. *Environ. Sci. Technol.*, **37**, 434.
 - 18 Saiz, S., Kennedy, C., Bass, B. and Pressnail, K. (2006) Comparative life cycle assessment of standard and green roofs. *Environ. Sci. Technol.*, **40**, 4312.
 - 19 Bayer, P. and Finkel, M. (2006) Life cycle assessment of active and passive groundwater remediation technologies. *J. Contam. Hydrol.*, **83**, 171.
 - 20 Tukker, A. (2002) Life-cycle assessment and the precautionary principle. *Environ. Sci. Technol.*, **36**, 70.
 - 21 Sheldon, R.A. (2000) Atom efficiency and catalysis in organic synthesis. *Pure Appl. Chem.*, **72**, 1233.
 - 22 Beletskaya, I.P. and Cheprakov, A.V. (2000) The Heck reaction as a sharpening stone of palladium catalysis. *Chem. Rev.*, **100**, 3009.
 - 23 de Vries, J.G. (2001) The Heck reaction in the production of fine chemicals. *Can. J. Chem.*, **79**, 1086.
 - 24 Byrne, C.M., Allen, S.D., Lobkovsky, E.B. and Coates, G.W. (2004) Alternating copolymerization of limonene oxide and carbon dioxide. *J. Am. Chem. Soc.*, **126**, 404.
 - 25 Yu, W., Bian, F., Gao, Y., Yang, L. and Liu, Z.-L. (2006) Y-zeolite-catalyzed cyclizations of terpenols. *Adv. Synth. Catal.*, **348**, 59.
 - 26 Clark, G.S.I.V. (1998) An aroma chemical profile. *Geraniol, Perfum. Flavorist*, **23**, 19.
 - 27 Vlad, P.F. (1993) Superacidic cyclization of terpenoids. *Pure Appl. Chem.*, **65**, 1329.
 - 28 Castro, G.R. and Knubovets, T. (2003) Homogeneous biocatalysis in organic solvents and water-organic mixtures. *Crit. Rev. Biotechnol.*, **23**, 195.
 - 29 Yamada, H. and Kobayashi, M. (1996) Nitrile hydratase and its application to industrial production of acrylamide. *Biosci. Biotechnol. Biochem.*, **60**, 1391.
 - 30 Niu, W., Draths, K.M. and Frost, J.W. (2002) Benzene-free synthesis of adipic acid. *Biotechnol. Prog.*, **18**, 201.
 - 31 Ran, N.Q., Knop, D.R., Draths, K.M. and Frost, J.W. (2001) Benzene-free synthesis of hydroquinone. *J. Am. Chem. Soc.*, **123**, 927.
 - 32 Mukhopadhyay, S., Rothenberg, G., Wiener, H. and Sasson, Y. (1999) Palladium-catalyzed aryl-aryl coupling in water using molecular hydrogen: kinetics and process optimization of a solid-liquid-gas system. *Tetrahedron*, **55**, 14, 763.
 - 33 Van Helden, R. and Verberg, G. (1965) The oxidative coupling of aromatic compounds with palladium salts. *Rec. Trav. Chim. Pays-Bas*, **84**, 1263.
 - 34 Mukhopadhyay, S., Rothenberg, G., Lando, G., Agbaria, K., Kazanci, M. and Sasson, Y. (2001) Air oxidation of benzene to biphenyl – a dual catalytic approach. *Adv. Synth. Catal.*, **343**, 455.
 - 35 Kweon, D., Jang, Y. and Kim, H. (2003) Organic electrochemical synthesis utilizing Mg electrodes. 1. Facile reductive coupling reactions of aromatic halides. *Bull. Kor. Chem. Soc.*, **24**, 1049.
 - 36 Durán Pachón, L., Elsevier, C.J. and Rothenberg, G. (2006) Electroreductive palladium-catalysed Ullmann reactions in ionic liquids: scope and mechanism. *Adv. Synth. Catal.*, **348**, 1705.
 - 37 Jachuck, R. (2002) Process intensification for responsive processing. *Chem. Eng. Res. Design*, **80**, 233.
 - 38 Jandeleit, B., Schaefer, D.J., Powers, T.S., Turner, H.W. and Weinberg, W.H. (1999) Combinatorial materials science and catalysis. *Angew. Chem. Int. Ed.*, **38**, 2495.
 - 39 Satyanarayana, T. and Kagan, H.B. (2005) The multi-substrate screening of asymmetric catalysts. *Adv. Synth. Catal.*, **347**, 737.

- 40 Jähnisch, K., Hessel, V., Löwe, H. and Baerns, M. (2004) Chemistry in microstructured reactors. *Angew. Chem. Int. Ed.*, **43**, 406.
- 41 de Bellefon, C., Tanchoux, N., Caravieilhès, S., Grenouillet, P. and Hessel, V. (2000) Microreactors for dynamic high throughput screening of fluid/liquid molecular catalysis. *Angew. Chem. Int. Ed.*, **39**, 3442.
- 42 Senkan, S. (2001) Combinatorial heterogeneous catalysis – a new path in an old field. *Angew. Chem. Int. Ed.*, **40**, 312.
- 43 Moates, F.C., Somani, M., Annamalai, J., Richardson, J.T., Luss, D. and Willson, R.C. (1996) Infrared thermographic screening of combinatorial libraries of heterogeneous catalysts. *Ind. Eng. Chem. Res.*, **35**, 4801.
- 44 Holzwarth, A. and Maier, W.F. (2000) Catalytic phenomena in combinatorial libraries of heterogeneous catalysts: detection of activation and deactivation by emissivity-corrected IR thermography. *Platinum Met. Rev.*, **44**, 16.
- 45 Menger, F.M., Eliseev, A.V. and Migulin, V.A. (1995) Phosphatase catalysis developed via combinatorial organic chemistry. *J. Org. Chem.*, **60**, 6666.
- 46 Shimizu, K.D., Snapper, M.L. and Hoveyda, A.H. (1998) High-throughput strategies for the discovery of catalysts. *Chem. Eur. J.*, **4**, 1885.
- 47 Kingsbury, J.S., Garber, S.B., Giftos, J.M., Gray, B.L., Okamoto, M.M., Farrer, R.A., Fourkas, J.T. and Hoveyda, A.H. (2001) Immobilization of olefin metathesis catalysts on monolithic sol-gel: practical, efficient, and easily recyclable catalysts for organic and combinatorial synthesis. *Angew. Chem. Int. Ed.*, **40**, 4251.
- 48 Taylor, S.J. and Morken, J.P. (1998) Thermographic selection of effective catalysts from an encoded polymer-bound library. *Science*, **280**, 267.
- 49 Hagen, J. (2006) *Industrial Catalysis: A Practical Approach*, Wiley-VCH, Weinheim, 978-3-527-31144-6.
- 50 Niemantsverdriet, J.W. (1995) *Spectroscopy in Catalysis*, VCH, Weinheim, ISBN 3-527-28726-4.
- 51 Wachs, I.E. (2005) Recent conceptual advances in the catalysis science of mixed metal oxide catalytic materials. *Catalysis Today*, **100**, 79.
- 52 Stoltze, P. and Nørskov, J.K. (1985) Bridging the “pressure gap” between ultrahigh-vacuum surface physics and high-pressure catalysis. *Phys. Rev. Lett.*, **55**, 2502.
- 53 Freund, H.J., Kuhlenbeck, H., Libuda, J., Rupprechter, G., Baumer, M., Hamann, H. (2001) Bridging the pressure and materials gaps between catalysis and surface science: clean and modified oxide surfaces. *Top. Catal.*, **15**, 201.
- 54 Elsevier, C.J. (1994) NMR at elevated gas pressures and its application to homogeneous catalysis. *J. Mol. Catal.*, **92**, 285.
- 55 Weckhuysen, B.M. (2002) Snapshots of a working catalyst: possibilities and limitations of *in situ* spectroscopy in the field of heterogeneous catalysis. *Chem. Commun.*, 97.
- 56 Dimian, A.C. (2003) *Integrated Design and Simulation of Chemical Processes*, Elsevier, Amsterdam, ISBN 0444829962.
- 57 Burello, E. and Rothenberg, G. (2006) *In silico* design in homogeneous catalysis using descriptor modelling. *Int. J. Mol. Sci.*, **7**, 375.
- 58 Corma, A., Serra, J.M., Serna, P. and Moliner, M. (2005) Integrating high-throughput characterization into combinatorial heterogeneous catalysis: unsupervised construction of quantitative structure/property relationship models. *J. Catal.*, **232**, 335.
- 59 Burello, E., Farrusseng, D. and Rothenberg, G. (2004) Combinatorial explosion in homogeneous catalysis: screening 60 000 cross-coupling reactions. *Adv. Synth. Catal.*, **346**, 1844.
- 60 Klanner, C., Farrusseng, D., Baumes, L., Lengliz, M., Mirodatos, C. and Schüth, F. (2004) The development of descriptors for

solids: teaching “catalytic intuition” to a computer. *Angew. Chem. Int. Ed.*, **43**, 5347.

- 61** Rothenberg, G., Hageman, J.A., Clerc, F., Frühauf, H.-W. and Westerhuis, J.A. (2006) How to find the best homogeneous catalyst. *Chem. Ind. (CRC Press) Catal. Org. React.*, **115**, 261.
- 62** Aucott, M., McLinden, M. and Winka, M. (2003) Release of mercury from broken fluorescent bulbs. *J. Air Waste Manag. Assoc.*, **53**, 143.
- 63** Naud, F., Malan, C., Spindler, F., Rugeberg, C., Schmidt, A.T. and Blaser, H.-U. (2006) Ru–(phosphine-oxazoline) complexes as effective, industrially viable catalysts for the enantioselective hydrogenation of aryl ketones. *Adv. Synth. Catal.*, **348**, 47.
- 64** Ault, A. (2004) The monosodium glutamate story: the commercial production of MSG and other amino acids. *J. Chem. Educ.*, **81**, 347.

2

The Basics of Catalysis

2.1

Catalysis is a Kinetic Phenomenon

Catalysis deals with changes on the route to equilibrium. It is about reaction kinetics, not thermodynamics. This is a really important point: catalysts do not and cannot change the thermodynamic equilibrium. Imagine that you are crossing a mountain range on your way from **A** to **B** (Figure 2.1). You start at point **A**, and after walking for some hours you reach point **B**. The “reaction thermodynamics” describe your elevation at your starting point and your destination. Conversely, the “reaction kinetics” depend on which pathway you have taken. This chapter gives a general background to kinetics of catalytic reactions, starting from (almost) scratch. It explains the physical chemistry principles and the basics of chemical kinetics from a practical viewpoint. For a more mathematical overview of reaction kinetics, see textbooks on physical chemistry [1] or chemical engineering [2,3].

As I have outlined in Chapter 1, catalytic processes are performed in two main types of reactors: batch reactors for small- and medium-scale processes (producing speciality chemicals, fine chemicals and pharmaceuticals), and continuous-flow reactors for large-scale processes (producing and treating bulk chemicals). There is also a “hybrid” option, the continuous stirred-tank reactor (CSTR) [4]. This distinction is important for kinetics because the concentrations in batch processes change over time, but those in continuous processes do not. The latter situation is known as “steady state” and we will see some examples of it later in this chapter. I have chosen to focus on batch reactors for two reasons: First, it is easier to grasp the concepts of batch reaction kinetics, because they fit our intuitive “common sense.” Things change over time as you stir chemicals in a pot, just as they do when you cook dinner at home. Second, the mathematics is simpler. Having said that, I will also mention here some important kinetic schemes that pertain to continuous reactors. If you are specifically interested in the kinetics of continuous processes, there are several comprehensive texts on the subject [2,3].

Let us begin by defining some key terms. For a given reaction $\mathbf{A} \rightarrow \mathbf{B}$, the **conversion** of **A** (denoted with a Greek letter *chi*, $\chi_{\mathbf{A}}$) is the number of molecules of **A** that have reacted up to time t . Similarly, the **yield** (there is no common symbol

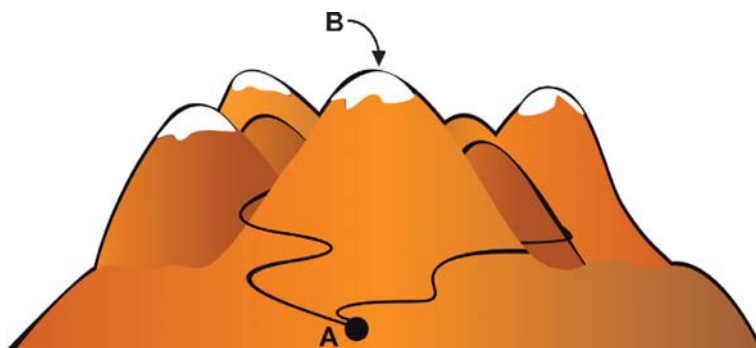


Figure 2.1 Catalysis deals with the transition between reactants and products. It does not affect the overall reaction thermodynamics.

for yield) is the number of molecules of **B** that have been produced up to time t . Conversion and yield are often expressed as fractions or percentages of $[A]_0$, the initial concentration of **A**.

Two important quantities which are used for comparing catalyst efficiency, the catalyst **turnover number (TON)** and the **turnover frequency (TOF)**, are crucial for work in catalysis. I am therefore repeating the definitions given in Chapter 1; however, these definitions vary slightly among the three catalysis fields. In homogeneous catalysis, the TON is the number of cycles that a catalyst can run through before it deactivates, i.e., the number of **A** molecules that one molecule of catalyst can convert (or “turn over”) into **B** molecules. The TOF is simply TON/time, i.e., the number of **A** molecules that one molecule of catalyst can convert into **B** molecules in one second, minute, or hour. In heterogeneous catalysis, TON and TOF are often defined per active site, or per gram catalyst. This is because one does not know exactly how many “catalyst molecules” there are on the surface. In biocatalysis, the TON and TOF are defined by the rate measured when all the enzyme molecules are complexed with a reactant, divided by the total enzyme concentration. Inclusion of the units of the TOF and TON in each case can save trouble when discussing catalytic activity.

2.1.1

Reaction Rates, Reaction Orders, Rate Equations, and Rate-Determining Steps

The rate of the reaction $A \rightarrow B$ (usually denoted as rate r , or ν) in a constant-volume batch reactor is simply the number of moles of **A** reacting (or of **B** forming) per unit volume per unit time [(Eq. (2.1)), where $[X]$ is the concentration of compound **X** at time t]. Traditionally, the disappearance of “reactants” on the left-hand side of the reaction equation is indicated with a minus sign.

$$\left. \begin{array}{l} A \rightarrow B \\ \text{rate} = \nu = -\frac{d[A]}{dt} = \frac{d[B]}{dt} \end{array} \right\} \quad (2.1)$$

The reaction **rate equation**, sometimes also called the reaction **rate law**, is an algebraic equation that connects the reaction rate to the time and concentration of the reactants and/or products. Denoting the rate for the disappearance of compound **A**, for example, as $-r_A$, we obtain Eq. (2.2), where k is the **reaction rate constant**.

$$\text{rate} = -r_A = k[A] \quad (2.2)$$

The reaction rate equation dictates the dimensions of k . In this case, if $[A]$ is given in moles/litre and t in seconds, k is given in litres/(moles \times seconds). In fact, k is not truly a constant, because it depends strongly on temperature (and to a lesser degree on pressure).

In more complicated cases, e.g., the reaction $A + 2B \rightarrow 3C + D$, the reaction rate is chosen arbitrarily as the consumption rate of one of the reactants, or the formation rate of one of the products (Eq. (2.3)). The reaction rate depends on temperature and concentration.

$$\left. \begin{array}{l} A + 2B \rightarrow 3C + D \\ \text{rate} = \nu = -\frac{d[A]}{dt} = -\frac{1}{2}\frac{d[B]}{dt} = \frac{1}{3}\frac{d[C]}{dt} = \frac{d[D]}{dt} \end{array} \right\} \quad (2.3)$$

The Swedish chemist and 1903 Nobel laureate Svante August Arrhenius formalized the relationship between k and T as the **Arrhenius equation** (Eq. (2.4)), where A is the **pre-exponential factor** (sometimes also called the **frequency factor**), R is the universal gas constant, roughly $2 \text{ cal mol}^{-1} \text{ K}^{-1}$, T is the absolute temperature, and E_a is the reaction **activation energy** [5]. Although the Arrhenius equation stems from empirical observations, it explains well the temperature dependence of many rate constants over a wide range of temperatures.

$$k = Ae^{-\frac{E_a}{RT}} \quad (2.4)$$

The activation energy E_a is an extremely important parameter in catalysis. It gives the height of the energy barrier that the system must overcome for the reaction to proceed. The higher the activation energy, the higher the sensitivity of k to temperature. Typical values for E_a range from $\sim 2 \text{ kcal mol}^{-1}$ to tens of kilocalories/mole. A useful rule of thumb states that the reaction rate roughly doubles for every 10°C increase in temperature. Furthermore, when E_a is less than $\sim 5 \text{ kcal mol}^{-1}$, we say that the reaction is diffusion-controlled. This means that the reaction rate is limited by how fast the molecules move toward one another. Conversely, when E_a is greater than $\sim 5 \text{ kcal mol}^{-1}$, we say that the reaction is chemically controlled.

Somewhat embarrassingly, the pre-exponential factor A does not have a clear physical description. It is attributed to entropy changes and other factors, such as substrate orientation. Typical values for A range from 10^{11} to 10^{14} s^{-1} for first-order reactions. As the exponent in the Arrhenius equation is a pure number, the units of A are the same as those of k .

Indeed, strictly speaking, the Arrhenius equation applies only to gas-phase reactions. Readers who feel uneasy about the empirical origins of the Arrhenius equation may be more comfortable with the **Eyring equation**. Developed by Henry Eyring, this equation [Eq. (2.5)], where k_b and h are Boltzmann's constant and Planck's

constant, respectively] is based on transition state theory, rather than on empirical observations [6,7].

$$k = \frac{k_b T}{h} e^{\frac{-\Delta G^\ddagger}{RT}} \quad (2.5)$$

By taking the logarithm of Equation (2.5) and substituting $\Delta G^\ddagger = \Delta H^\ddagger - T\Delta S^\ddagger$ we obtain Equation. (2.6).

$$\ln \frac{k}{T} = -\frac{\Delta H^\ddagger}{RT} + \frac{\Delta S^\ddagger}{R} + \ln \frac{k_b}{h} \quad (2.6)$$

Thus, measuring the reaction rate at different temperatures and plotting $\ln(k/T)$ against $1/T$ will give a straight line according to Eq. (2.6). The slope and the intercept of this line will give you the enthalpy of activation and the entropy of activation, respectively. All that being said, the Arrhenius equation, despite its empirical origins, will suffice for all practical purposes throughout your catalysis career. Trust me.

2.1.1.1 The Reaction Order

The rate of every chemical reaction depends in one way or another on the concentrations of the chemicals in the system. The overall rate law is often written as the product of the concentrations raised to a power. For example, for the reaction $\mathbf{A} + \mathbf{B} \rightarrow \mathbf{C}$, the rate law for the disappearance of \mathbf{A} may be written as in Eq. (2.7), where the exponents α and β represent the partial reaction order in \mathbf{A} and \mathbf{B} , respectively, and the overall reaction order is $n = \alpha + \beta$.

$$-r_A = k[\mathbf{A}]^\alpha[\mathbf{B}]^\beta \quad (2.7)$$

Partial reaction orders can be whole numbers, as in the case of the thermal (i.e., noncatalytic) reaction of nitric oxide with ozone: $\text{NO} + \text{O}_3 \rightarrow \text{NO}_2 + \text{O}_2$. When a nitric oxide molecule strikes an ozone molecule with sufficient kinetic energy, it can capture an O atom, giving nitrogen dioxide and oxygen. Here, the rate law for the disappearance of NO is given by Eq. (2.8), where $\alpha = 1$, $\beta = 1$, and $n = 2$. In such cases, where the reaction order of each species equals the stoichiometric coefficient of that species, we say that the reaction is an **elementary reaction**. However, in many cases the partial reaction orders are not integers. For example, when carbon monoxide and chlorine react to give phosgene, $\text{CO} + \text{Cl}_2 \rightarrow \text{COCl}_2$, the reaction is first order in CO, 3/2 order in Cl, and the overall order is 5/2 (see Eq. (2.9)). This is an example of a **nonelementary reaction**. If a compound slows the reaction or enhances the reverse reaction, partial reaction orders can even be negative. For example, in the water-gas shift reaction, the CO_2 product competes with the reactants for the same active site, and so the reaction shows a negative order in CO_2 [8]. Note that reaction orders of nonelementary reactions must be determined by experiment. You cannot deduce the order of a nonelementary reaction from the stoichiometric equation.

$$-r_{\text{NO}} = k[\text{NO}][\text{O}_3] \quad (2.8)$$

$$-r_{\text{CO}} = k[\text{CO}][\text{Cl}_2]^{3/2} \quad (2.9)$$

2.1.1.2 The Rate-Determining Step

A catalytic cycle consists of several elementary reactions, or steps. The experimental reaction rate is not the average or the cumulative rate of these steps. Rather, it is the rate of the slowest step(s) in the cycle. One way to illustrate this is by comparing the various reaction steps to sand grains falling in a rather curvy hourglass with two narrow openings and several wide openings, as shown on Figure 2.2a–b. The number of wide openings is irrelevant, because all of the grains will be stuck above the narrow openings. In this picture, the narrow opening represents the rate-determining step, while the wide ones represent fast steps. In the next section I will give some specific examples and explain the connection between the rate-determining step and the activation energy.

The **molecularity** of a reaction is simply the number of different molecules (or atoms or ions) that are involved in the rate-determining step. It equals 1 for a **unimolecular reaction**, 2 for a **bimolecular reaction**, and 3 for a **termolecular reaction** (see the examples in Figure 2.2b). The main difference between reaction order and molecularity is that the former follows directly from the experimental data, while the latter is based on “chemical intuition” arguments [9]. Note that termolecular reactions are extremely rare. The few cases documented are all in the gas phase, such as the reaction of boron trihalide with halide ions in the presence of various gases [10] or the reactions of alkali metal atoms with oxygen and hydroxyl ions at high temperatures [11].

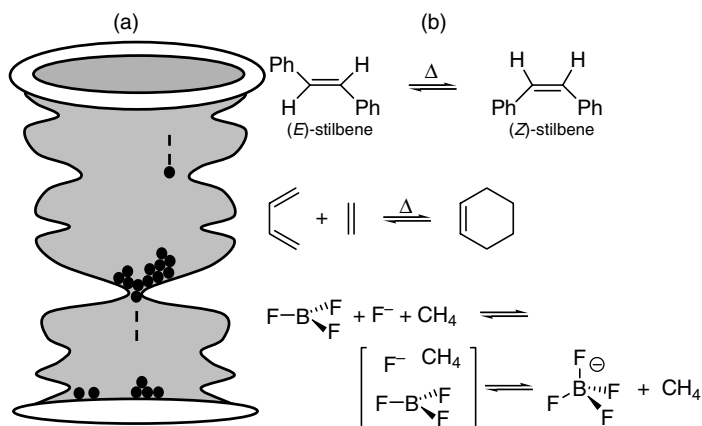


Figure 2.2 a Fast and slow steps in a catalytic cycle are analogous to the falling of sand grains through an hourglass with narrow and wide openings. b The thermal *cis/trans* isomerization of stilbene, the Diels–Alder cycloaddition of butadiene to ethene, and the fluorination of gaseous BF_3 in the presence of methane are examples of unimolecular, bimolecular, and termolecular reactions, respectively.

2.1.2

The Reaction Profile and the Reaction Coordinate

Most chemical reactions are very complicated. So complicated, in fact, that we cannot describe their mechanisms accurately. Instead, we approximate the reaction mechanism with a series of simple elementary reactions, from which we can build a model. If the model fits the experimental data well, we say that it gives a good description of the reaction mechanism.

A catalytic cycle is often made up of several steps. Each of those steps has “reactants” and “products.” The reactants can either be the products of a former step, or enter the cycle from outside (Figure 2.3). Similarly, the products of each step can either remain in the cycle as reactants for the following step, or leave the cycle. We call those reactants and products that remain in the cycle the **catalytic intermediates**.

Measuring reaction kinetics (i.e., monitoring the concentrations of reactants, catalytic intermediates, and/or products over time) often gives relevant information on the reaction mechanism, the catalytic activity, and the product selectivity. This can be done in many ways: using gas chromatography (GC), high-performance liquid chromatography (HPLC), calorimetry, or voltammetry, as well as a variety of spectroscopic techniques such as infrared or near-infrared spectroscopy, UV-visible spectroscopy, Raman spectroscopy, NMR spectroscopy, or mass spectrometry. Regardless of the method, following a reaction over time yields a so-called reaction

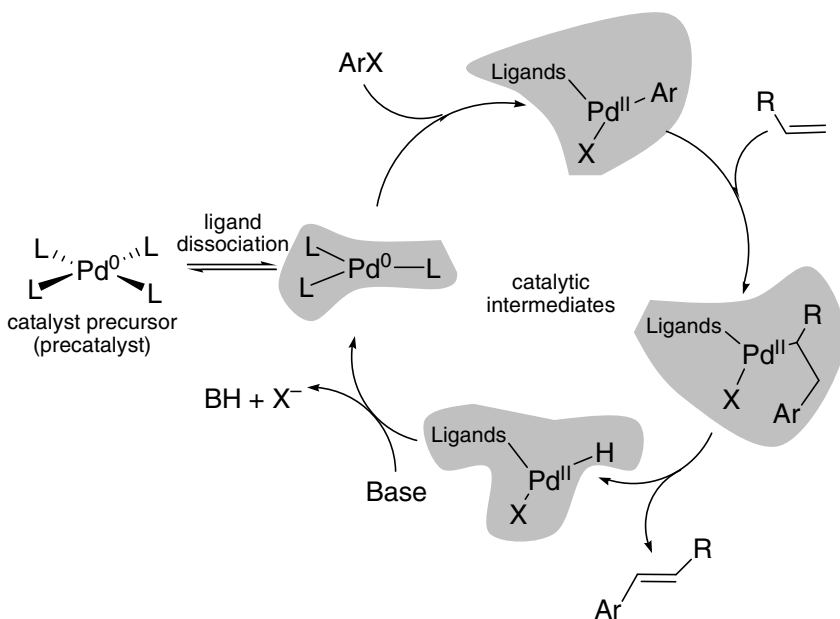


Figure 2.3 Proposed catalytic cycle for the Heck reaction between an alkene and an aryl halide in the presence of a homogeneous palladium complex.

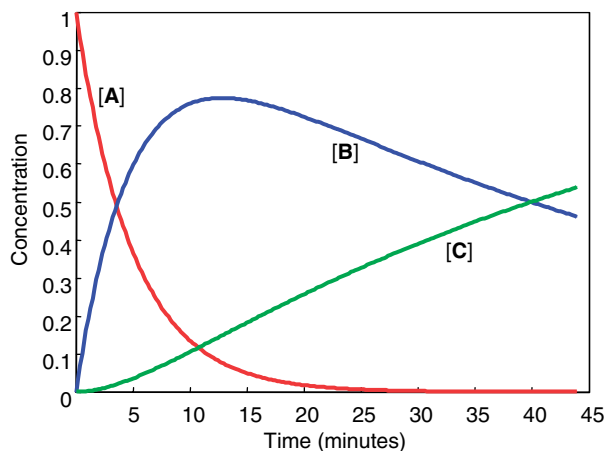


Figure 2.4 Example of concentration profiles for two consecutive first-order reactions, $A \xrightarrow{k_1} B \xrightarrow{k_2} C$, with rate constants $k_1 = 0.2 \text{ min}^{-1}$ and $k_2 = 0.02 \text{ min}^{-1}$.

profile (Figure 2.4). This is a graph that shows how the concentrations of the various species change over time. We can then interpret this profile, and formulate a reaction mechanism which agrees with the experimental data.

All catalytic cycles involve energy changes. Examining these changes is another useful method for learning about the reaction mechanism. Catalytic reactions are typically complex, involving many degrees of freedom. The corresponding energy diagrams are multidimensional, making visualization difficult. Luckily, in most cases one or two degrees of freedom are more important than the others. We call these important degrees of freedom the **reaction coordinates** (for example, in the *cis/trans* isomerization of stilbene, the important degree of freedom is the rotation around the C=C double bond). By plotting the energy changes in a catalytic system along a reaction coordinate, we obtain a simplified picture of the system. Such a diagram shows us a “slice” of the multidimensional space (Figure 2.5). In this slice we can identify and quantify the energy of the various reactants, catalytic intermediates, products, and transition states.

Reaction profiles are important because they provide information on how concentrations change over time. In most cases, the reaction profile pertains to the rate-determining step. From this we can infer the reaction order and the rate law, and calculate the rate constant k . Energy/reaction coordinate diagrams are important because they show the various energy transitions during the catalytic cycle, as well as the number of catalytic intermediates and transition states. The energy barrier for reaching each transition state is equal to the activation energy of that step. The higher the E_a , the higher the barrier. In every catalytic cycle, the highest barrier corresponds to the rate-determining step, regardless of whether it comes “early” or “late” on the reaction coordinate. If there are two (or more) barriers of similar height, it means that two (or more) of the steps are rate-determining. Note that the Arrhenius equation

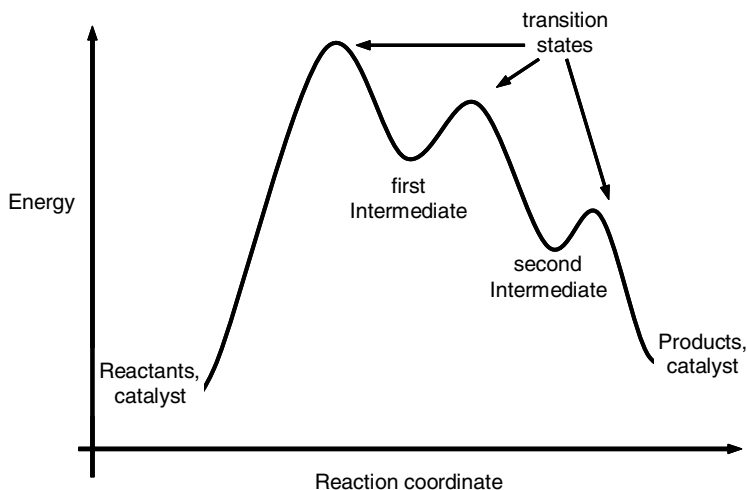


Figure 2.5 Energy/reaction coordinate diagram for a two-step reaction, with two catalytic intermediates and three transition states.

(Eq. (2.4)) ties together the reaction profiles and the energy/reaction coordinate graphs, as it relates the reaction rate constant k to the activation energy, E_a .

Note that what we see as a “hill”, the energy barrier, is in fact a saddle point between two bigger hills (see Figure 2.6). The reaction coordinate in the two-dimensional graph is just one of the system’s many degrees of freedom. Chemical reactions never climb to the tops of hills – they *always* go via saddle points. When a catalyst offers a faster reaction pathway, it is tantamount to an easier path through these mountains. The catalytic pathway may be longer and more tortuous, but its highest saddle point is lower than the highest saddle point along the noncatalytic pathway.

2.1.3

Zero-Order, First-Order, and Second-Order Kinetics

Although the overall rate equation of a catalytic cycle is often very complicated, the elementary reactions that compose the cycle are simple. They usually follow zero-order, first-order, or second-order rate laws. I give here a short derivation of these cases. This is by no means a comprehensive overview of all the known reaction types, only the most common ones [2,3,12]. Happily, in practice the simple cases discussed here suffice.

2.1.3.1 Zero-Order Rate Equations

We say that a reaction is zero order when the rate of reaction is constant, i.e., independent of the concentrations. Such a reaction will stop abruptly when the limiting reactant is completely consumed. Zero-order equations may seem dull, but they can reveal a lot about the reaction mechanism. The mathematics is very simple.

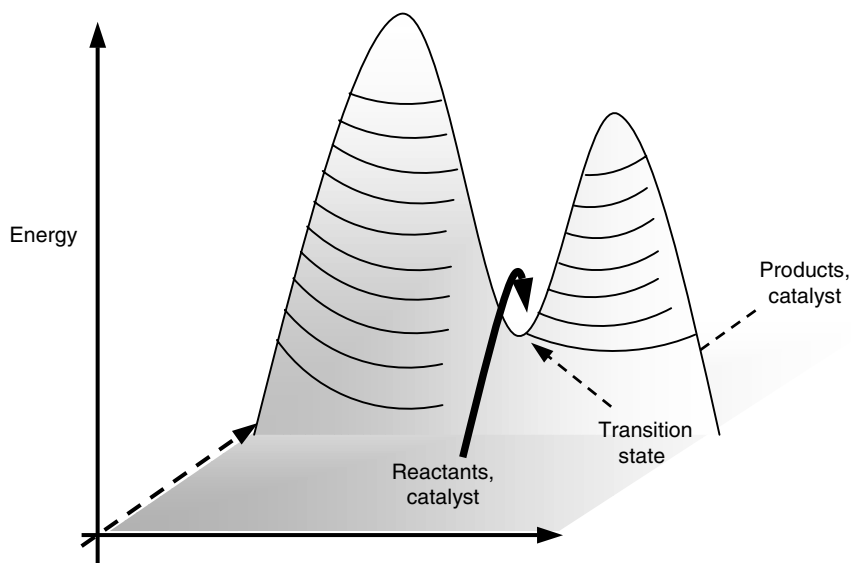


Figure 2.6 The traditional diagram of energy versus reaction coordinate is in fact only a “slice” of the multidimensional space. This slice represents just one of the degrees of freedom of the system. Going one dimension higher, we see that the transition state is not a “maximum” but a saddle point.

For example, if the reaction $A \rightarrow B$ obeys a zero-order rate law, the differential rate equation is simply,

$$-\frac{d[A]}{dt} = k \quad (2.10)$$

Integration of both sides gives Eq. (2.11), where C is the integration constant.

$$[A] = -kt + C \quad (2.11)$$

At time zero, $[A] = [A]_0$, and so . . .

$$[A] = -kt + [A]_0. \quad (2.12)$$

Thus, plotting the concentration $[A]$ versus the time t will give a straight line with a slope of $-k$ and an intercept at $[A]_0$.

2.1.3.2 First-Order Rate Equations

Let us consider the simple reaction $A \rightarrow B + C$, where $[A]_0 = a$. If after t minutes x moles of A have reacted, then $[A] = (a - x)$ and $[B] = [C] = x$. The rate of formation of B and C is dx/dt . For a first-order reaction this rate is proportional to $[A]$, so that . . .

$$\frac{dx}{dt} = k(a - x). \quad (2.13)$$

Integrating Eq. (2.13) gives us Eq. (2.14), where C is the integration constant.

$$-\ln(a-x) = kt + C \quad (2.14)$$

Often, the initial conditions are that $x=0$ at $t=0$, so $C = \ln a$, and we get...

$$\ln \frac{a}{a-x} = kt \quad (2.15)$$

or in terms of the degree of conversion, χ_A ,

$$-\ln(1-\chi_A) = kt \quad (2.16)$$

If the observed reaction is indeed first order, plotting either $\ln \frac{a}{a-x}$ against t or $-\ln(1-\chi_A)$ against t should give a straight line with slope = k .

The reaction half-life time $\tau_{1/2}$, is defined as the time at which the conversion equals 50%, i.e., when $\chi_A = 0.5$. If we substitute this in Eq. (2.11) we obtain Eq. (2.17).

$$-\ln(1-0.5) = kt$$

or

$$\tau_{1/2} = \frac{\ln 2}{k} \quad (2.17)$$

Since k is constant, this means that the half-life of a first-order reaction is always constant, and independent of the initial substrate concentrations.

2.1.3.3 Second-Order Rate Equations

Consider the reaction $A + B \rightarrow C$, where $[A]_0 = a$ and $[B]_0 = b$. If after t minutes x moles of **A** and **B** have reacted, then $[A] = (a-x)$, $[B] = (b-x)$, and $[C] = x$. The rate of formation of the product **C** is again dx/dt . For a second-order reaction, Eq. (2.18) gives the differential equation and the corresponding integrated form (assuming that $x=0$ at $t=0$).

$$\left. \begin{aligned} \frac{dx}{dt} &= k(a-x)(b-x) \\ -\frac{1}{a-b} \ln \frac{a-x}{b-x} &= kt \end{aligned} \right\} \quad (2.18)$$

The integrated form of Eq. (2.18) does not apply when $A \equiv B$, and the overall reaction is $2A \rightarrow C$. Nor does it apply when the initial concentrations are the same, i.e., when $a=b$. In such cases, the differential equation and the corresponding integrated form are:

$$\left. \begin{aligned} \frac{dx}{dt} &= k(a-x)^2 \\ \frac{1}{a-x} - \frac{1}{a} &= \frac{x}{a(a-x)} = kt \end{aligned} \right\} \quad (2.19)$$

Thus, plotting $\frac{x}{a(a-x)}$ against t should give a straight line with slope $= k$. Similarly, when expressing the reaction progress in terms of the conversion of **A**, χ_A , plotting $\frac{\chi_A}{[A]_0(1-\chi_A)}$ against t should give a straight line with slope $= k$.

The half-life time for a second-order reaction is:

$$\tau_{1/2} = \frac{1}{k[A]_0} \quad (2.20)$$

Unlike the first-order case, this half-life time depends on the initial concentration. This is not surprising: For example, in the reaction $\mathbf{A} + \mathbf{A} \rightarrow \text{products}$, two **A** molecules must collide, and this is more likely at higher $[A]_0$ values.

- **CAUTION!** Comparing k values between different types of reactions is an all-too-common mistake. Although we use the same letter k for both first-order and second-order rate constants, their units differ! A first-order rate constant has units of $[\text{time}]^{-1}$, while a second-order one has units of $[\text{time}]^{-1} [\text{concentration}]^{-1}$. Comparing these two numbers is like comparing apples and tomatoes – it is nonsense. This is also the reason why comparing the rate constants of a reaction with and without a catalyst is meaningless: Consider, for example, the noncatalytic reaction $\mathbf{A} + \mathbf{B} \rightarrow \mathbf{C}$ that obeys the second-order rate law shown in Eq. (2.21).



- If we add a catalyst, the reaction rate will change, but so will the rate law! Most likely, the new rate equation will depend on the catalyst's concentration, Eq. (2.22).



- Depending on the type of catalyst and the new steps involved, the new overall reaction order may be $n = 2$, $n = 3$, or even $n = 2.5$. The units of the two rate constants k are different, so comparing their magnitudes makes no sense (and likewise for A values). There are other measures for comparing reaction rates: for example, the reaction half-life time, $\tau_{1/2}$, or the degree of conversion at a given time t . Differences in $\tau_{1/2}$ with and without a catalyst can be considerable. For example, the noncatalytic decarboxylation of orotic acid at 25 °C has a half-life time of 78 million years. Adding the enzyme orotidine 5'-phosphate decarboxylase enhances the reaction rate by a factor of 10^{17} , reducing $\tau_{1/2}$ to 0.02 seconds [13,14]!

2.1.4

Langmuir–Hinshelwood Kinetics

The Langmuir–Hinshelwood model describes the most common situation in heterogeneous catalysis [15,16]. It assumes that the reactant must be adsorbed on the catalyst surface before it can react. The reaction then takes place at the active site, and the product is then desorbed from the catalyst back to the gas phase (Figure 2.7).

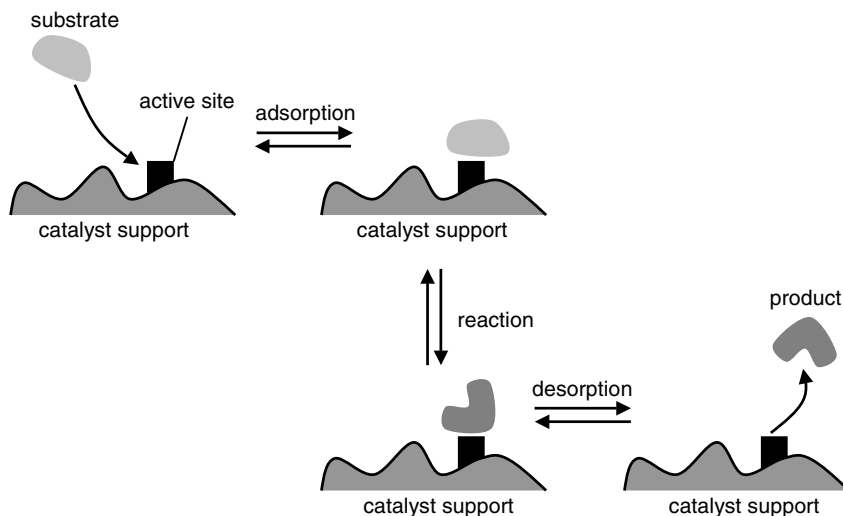


Figure 2.7 Cartoon of reaction on a catalyst surface that follows the Langmuir–Hinshelwood model.

Interestingly, this is also a good description of many (but not all) homogeneous catalysis and biocatalysis reactions. Here the reactant or the substrate first coordinates to the metal complex or to the enzyme, then a reaction occurs. Finally, the product dissociates from the catalyst and diffuses back into the solution.

Let us examine the catalytic isomerization of 2-methylheptane **A** to iso-octane **B** (Figure 2.8). This is an important process in fuel production, because of the differences in the octane number between reactant and product [12,17,18]. The

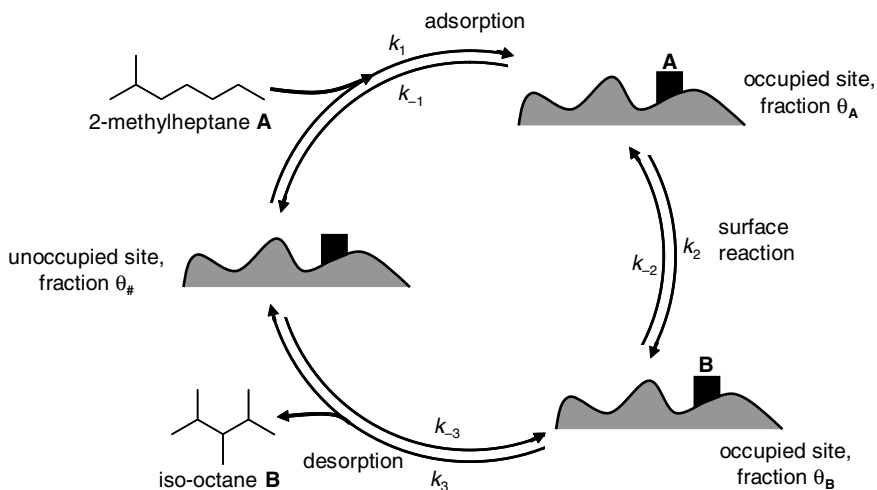


Figure 2.8 Schematic catalytic cycle for the isomerization of 2-methylheptane to iso-octane.

reaction is carried out at high temperatures in the gas phase, over a heterogeneous catalyst. We will discuss heterogeneous catalysts in detail in Chapter 4. For now, let us assume that the catalyst is a zeolite that has a total of $\#_{\text{total}}$ active sites, and that the catalytic cycle is as follows: **A** adsorbs onto a free active site **#** on the catalyst surface, forming the catalytic intermediate **A#**. This intermediate then isomerizes, giving **B#**, another catalytic intermediate. Finally, the product **B** is desorbed, leaving the active site available for adsorption of another **A** molecule, and closing the catalytic cycle. All of these steps are reversible.

Until now I have used $[X]$ to denote the concentration of **X**, regardless of whether **X** is a reactant, product, or catalytic intermediate. In heterogeneous catalysis, however, the “concentration” of a catalytic intermediate has no clear meaning. Instead, we refer to the fraction of active sites that species **X** occupies, denoting this fraction as θ_X . Thus, θ_A is the fraction of the active sites occupied by **A**, θ_B is the fraction of the active sites occupied by **B**, and $\theta_{\#}$ is the fraction of unoccupied active sites. Note that strictly speaking we should also use partial pressures instead of concentrations for gaseous reactants and products. For clarity, however, I have stayed with concentrations, keeping just one type of notation throughout the book.

Equation (2.23)–(2.25) show the three steps in this cycle and their corresponding differential rate expressions.



This leads to some complicated differential equations which are usually solved numerically. To simplify things, let us assume that the surface reaction (Eq. (2.24)) is the rate-determining step, while the adsorption and the desorption steps are at equilibrium (i.e., the net change in Eqs. (2.4) and (2.6) is zero). In this case, Eq. (2.26) apply, where K_A and K_B are the adsorption equilibrium constants for **A** and **B**, respectively.

$$\left. \begin{array}{l} \theta_{\mathbf{A}} = \frac{k_1}{k_{-1}}[\mathbf{A}]\theta_{\#} = K_{\mathbf{A}}[\mathbf{A}]\theta_{\#} \\ \text{and} \\ \theta_{\mathbf{B}} = \frac{k_{-3}}{k_3}[\mathbf{B}]\theta_{\#} = K_{\mathbf{B}}[\mathbf{B}]\theta_{\#} \end{array} \right\} \quad (2.26)$$

Substituting these values in the rate-determining step gives Eq. (2.27).

$$\text{rate} = k_2 K_A [\text{A}] \theta_{\#} - k_{-2} K_B [\text{B}] \theta_{\#} \quad (2.27)$$

Before going further, let us see if Eq. (2.28) agrees with “chemical intuition.” The rate of the isomerization $\text{A} \rightarrow \text{B}$ increases when $[\text{A}]$ is higher, as well as when there are more free active sites. Moreover, the rate equation is symmetric with respect to **A** and **B**. Indeed, this is what one would expect for this catalytic isomerization.

We can measure $[\text{A}]$ and $[\text{B}]$, and calculate the constants in Eq. (2.27). However, measuring the fraction of free active sites $\theta_{\#}$ is difficult. Luckily, we can assume that $\#_{\text{total}}$ remains constant throughout the reaction. This is a reasonable assumption, although in practise the number of active sites sometimes changes due to sintering at high temperatures, poisoning, or deactivation. We will therefore use the specific activity (i.e., the activity per active site). Summing the active site fractions θ_{X} gives Eq. (2.28), and substituting the values for θ_{A} and θ_{B} from Eq. (2.26) then gives Eq. (2.29).

$$\theta_{\#} + \theta_{\text{A}} + \theta_{\text{B}} = 1 \quad (2.28)$$

$$\theta_{\#} + K_A [\text{A}] \theta_{\#} + K_B [\text{B}] \theta_{\#} = 1$$

$$\text{or} \quad (2.29)$$

$$\theta_{\#} = \frac{1}{1 + K_A [\text{A}] + K_B [\text{B}]}$$

The overall rate equation becomes:

$$\text{rate} = \frac{(k_2 K_A [\text{A}] - k_{-2} K_B [\text{B}])}{1 + K_A [\text{A}] + K_B [\text{B}]} \quad (2.30)$$

Thus, we have simplified our system by assuming that the surface reaction is rate-determining. Remember, however, that although introducing a rate-determining step simplifies things, pinpointing this step can be difficult. There may even be more than one rate-determining step per reaction!

2.1.5

The Steady-State Approximation

Most catalytic cycles contain several steps that are intricately related. Although the rate equations of individual steps are usually simple, the overall rate equation is often very complex. Moreover, measuring the concentrations of catalytic intermediates is a difficult task. One way of overcoming these difficulties is by assuming that the concentration of the catalytic intermediates remains constant throughout the reaction – at a **steady-state concentration** (see Figure 2.9a). This is a reasonable assumption even in batch reactors, because in every cycle the catalytic intermediates are formed and consumed continuously. It certainly applies to continuous processes,

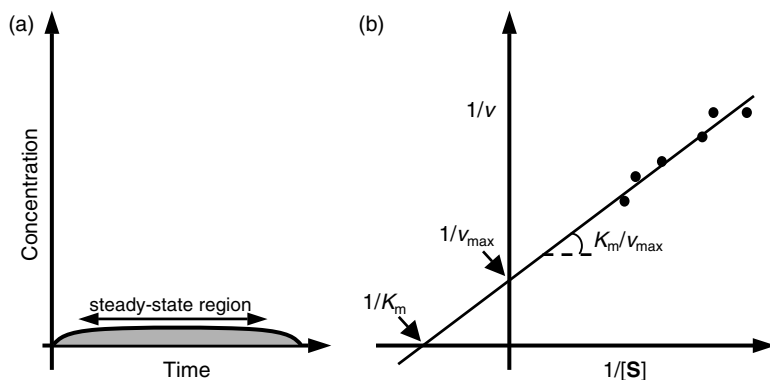


Figure 2.9 **a** Concentration profile of a steady-state intermediate; **b** the Lineweaver–Burk plot.

and this is important because all the large-scale (and also some medium- and small-scale) industrial processes are continuous ones. Such processes operate 24 h per day, seven days a week, in plug-flow reactors (PFRs) or in continuous stirred-tank reactors (CSTRs). They are never stopped, because reaching the optimal working conditions takes a long time and costs a lot of money. If you stop a large-scale continuous process for a week (for changing the catalyst, for example, or replacing a distillation unit, or sending all the workers on a joint vacation to Hawaii) you may need three to four weeks of restarting before the process conditions stabilize again. Continuous processes have neither “start” nor “end.” There is just a feed stream going in and a product stream coming out, with a small amount of active catalyst in the reactor. This is exactly the situation that the steady-state approximation describes.

The steady-state approximation applies to diverse situations in homogeneous catalysis, heterogeneous catalysis, and biocatalysis. Remember, however, that it does not apply to the “beginning” and “end” segments of batch reactions. Assuming that a species X is in a steady state does not imply that its concentration is low (although this is often the case with catalytic intermediates). It simply means that the concentration remains constant over time, i.e., $d[X]/dt = 0$. Free-radical reactions are a good example: the free-radical concentration increases in the initiation stage, then remains constant (steady-state) through the propagation stage, and finally decreases in the termination stage.

For example, if we apply the steady-state approximation to the catalytic intermediates of the 2-methylheptane/iso-octane isomerization from the previous section we obtain Eqs. (2.31)–(2.33).

$$\begin{aligned}
 \frac{d\theta_A}{dt} &= 0 \\
 \Rightarrow k_1[A]\theta_{\#} - k_{-1}\theta_A - k_{-2}\theta_A - k_{-2}\theta_B &= 0 \\
 \Rightarrow \theta_A &= \frac{k_1[A]\theta_{\#} - k_{-2}\theta_B}{k_{-1} + k_2}
 \end{aligned}
 \tag{2.31}$$

$$\begin{aligned}\frac{d\theta_{\mathbf{B}}}{dt} &= 0 \\ \Rightarrow k_2\theta_{\mathbf{A}} - k_{-2}\theta_{\mathbf{B}} - k_3\theta_{\mathbf{B}} + k_{-3}[\mathbf{B}]\theta_{\#} &= 0 \\ \Rightarrow \theta_{\mathbf{B}} &= \frac{k_2\theta_{\mathbf{A}} + k_{-3}[\mathbf{B}]\theta_{\#}}{k_{-2} + k_3}\end{aligned}\quad (2.32)$$

$$\begin{aligned}\frac{d\theta_{\#}}{dt} &= 0 \\ \Rightarrow -k_1[\mathbf{A}]\theta_{\#} + k_{-1}\theta_{\mathbf{A}} + k_3\theta_{\mathbf{B}} - k_3[\mathbf{B}]\theta_{\#} &= 0\end{aligned}\quad (2.33)$$

From these equations we can express $\theta_{\mathbf{A}}$, $\theta_{\mathbf{B}}$, and $\theta_{\#}$ as a function of $[\mathbf{A}]$ and $[\mathbf{B}]$.

2.1.6

Michaelis–Menten Kinetics

Originally published in 1913 as a rate law for enzymatic sugar inversion [19], the Michaelis–Menten rate equation is also used frequently for describing homogeneously catalyzed reactions. It describes a two-step cycle (Eqs. (2.34) and (2.35)): the catalyst (the enzyme, \mathbf{E}) first reacts reversibly with the substrate \mathbf{S} , forming an enzyme–substrate complex \mathbf{ES} (a catalytic intermediate). Subsequently, \mathbf{ES} decomposes, giving the enzyme \mathbf{E} and the product \mathbf{P} . This second step is irreversible.



If the initial concentration of the enzyme is $[\mathbf{E}]_0$, then at any time t , $[\mathbf{E}]_0 = [\mathbf{E}] + [\mathbf{ES}]$. Thus the reaction rate depends on the enzyme concentration, even though the enzyme remains unchanged at the end of the cycle. The product formation rate and the change in concentration of the catalytic intermediate \mathbf{ES} are then given by Eq. (2.36).

$$\left. \begin{aligned}\frac{d[\mathbf{P}]}{dt} &= k_2[\mathbf{ES}] \\ \text{and} \\ \frac{d[\mathbf{ES}]}{dt} &= k_1[\mathbf{E}][\mathbf{S}] - k_{-1}[\mathbf{ES}] - k_2[\mathbf{ES}]\end{aligned} \right\} \quad (2.36)$$

Assuming the steady-state approximation for $[\mathbf{ES}]$ (which is a reasonable assumption because \mathbf{ES} is a catalytic intermediate), we obtain Eq. (2.37).

$$\left. \begin{aligned}\frac{d[\mathbf{ES}]}{dt} &= 0 \\ \Rightarrow [\mathbf{ES}] &= \frac{k_1[\mathbf{E}][\mathbf{S}]}{k_{-1} + k_2}\end{aligned} \right\} \quad (2.37)$$

For the substrate, we know that $[S]_{\text{total}} = [S] + [ES]$. However, as $[E]_0 \ll [S]_0$, we can approximate that $[S]_{\text{total}} = [S]$. The Michaelis equilibrium constant, K_m , is defined as in Eq. (2.38),

$$K_m = \frac{[E][S]}{[ES]} = \frac{k_{-1} + k_2}{k_1} \quad (2.38)$$

and since

$$[E]_0 = [E] + [ES] = \frac{[ES]K_m}{[S]} + [ES] \quad (2.39)$$

the concentration of the catalytic intermediate is given by Eq. (2.40), and the product formation rate by Eq. (2.41).

$$[ES] = \frac{[E]_0[S]}{K_m + [S]} \quad (2.40)$$

$$\frac{d[P]}{dt} = k_2[ES] = \frac{k_2[E]_0[S]}{K_m + [S]} \quad (2.41)$$

We see that the rate of the enzyme-catalyzed reaction depends linearly on the enzyme concentration, and in a more complicated way on the substrate concentration. Thus, when $[S] \gg K_m$, (Eq. (2.41)) reduces to $v = k_2[E]_0$, and the reaction is zero order in $[S]$. This means that there is so much substrate that all of the enzyme's active sites are occupied. It also means that $[S]$ remains effectively unchanged, even though products are formed. This situation is known as **saturation kinetics**. The value $k_2[E]_0$ is also called the **maximum velocity** of the enzymatic reaction, and written as v_{max} .

Conversely, if $[S] \ll K_m$, (Eq. (2.42)) reduces to $v = (k_2/K_m)[E]_0[S]$. This means that the active sites on the enzyme are effectively unoccupied. The ratio k_2/K_m is also known as the enzyme's **specificity constant**, a measure of the enzyme's affinity for different substrates. Thus, if the same enzyme can catalyze the reaction of two substrates, S and S^* , the relative rates of these two reactions are compared using $(k_2/K_m)_S : (k_2/K_m)_{S^*}$. Because the specificity constant reflects both affinity and catalytic ability, it is also used for comparing different enzymes.

There are several ways of visualizing enzyme kinetic data, and calculating the values of K_m and v_{max} . Each approach has advantages and disadvantages [20,21]. One way to determine the values of K_m and v_{max} is to plot the reciprocal of the reaction velocity, $1/v$, against the reciprocal substrate concentration $1/[S]$, since

$$\left. \begin{aligned} \frac{1}{v} &= \frac{K_m + [S]}{k_2[E]_0[S]} = \frac{K_m}{k_2[E]_0} \times \frac{1}{[S]} + \frac{1}{k_2[E]_0} \\ \text{or} \\ \frac{1}{v} &= \frac{K_m}{v_{\text{max}}} \times \frac{1}{[S]} + \frac{1}{v_{\text{max}}} \end{aligned} \right\} \quad (2.42)$$

Plotting $1/v$ versus $1/[S]$ should give a straight line, with a slope of K_m/v_{max} and intercepts at $1/v_{\text{max}}$ and $-1/K_m$, respectively. This double reciprocal plot is

known as the **Lineweaver–Burk plot** (Figure 2.9b) [22]. It can give useful information, but there is a catch: although this plot is used very often in biocatalysis research, it is often misinterpreted. At low substrate concentrations (high $1/[S]$ values), small errors in the rate v will result in enormous errors in $1/v$. Conversely, the errors in $1/v$ at high substrate concentrations will be very small (indeed, one hidden “advantage” of the Lineweaver–Burk plot is that it disguises large measurement errors).

Alternatively, you can linearize the Michaelis–Menten equation by using an **Eadie–Hofstee plot** [23,24]. Here the reaction velocity, v , is plotted as a function of $v/[S]$, as shown in Eq. (2.43). This approach is more robust against error-prone data than the Lineweaver–Burk plot, because it gives equal weight to data points in any range of $[S]$ or v . The disadvantage here is that both the ordinate and the abscissa depend on v , so any experimental error will be present in both axes.

In summary, representing enzyme kinetics using linearized plots of the Michaelis–Menten equation is useful for viewing the data. However, the best way of analyzing enzyme kinetic data is by fitting them directly to the Michaelis–Menten equation using nonlinear regression [25]. Unlike in 1934, today there are computers for doing this.

$$v = -K_m \frac{v}{[S]} + v_{\max} \quad (2.43)$$

Another way of evaluating enzymatic activity is by comparing k_2 values. This first-order rate constant reflects the capacity of the enzyme–substrate complex **ES** to form the product **P**. Confusingly, k_2 is also known as the **catalytic constant** and is sometimes written as k_{cat} . It is in fact the equivalent of the enzyme’s TOF, since it defines the number of catalytic cycles the enzyme can undergo in one time unit. The k_2 (or k_{cat}) value is obtained from the initial reaction rate, and thus pertains to the rate at high substrate concentrations. Some enzymes are so fast and so selective that their k_2/K_m ratio approaches molecular diffusion rates (10^8 – 10^9 M s^{-1}). This means that every substrate/enzyme collision is fruitful, and the reaction rate is limited only by how fast the substrate molecules diffuse to the enzyme. Such enzymes are called **kinetically perfect enzymes** [26].

2.1.7

Consecutive and Parallel First-Order Reactions

A catalytic cycle is a sequence of steps. When one step is much slower than the others, we say that this step is rate determining and we ignore, for kinetics purposes, the other (fast) steps. Nevertheless, sometimes there are two slow steps with similar rates, and sometimes the rate of a specific step changes in the course of the reaction or under different conditions. One common situation is that of two consecutive first-order reactions, as in Eq. (2.44).



Here, k_1 and k_2 are both first-order rate constants, with the subscripts indicating the first and second reaction, respectively. Adding the intermediate **B** complicates the reaction dynamics considerably. If the initial concentration of **A** is $[A]_0$ and the initial concentrations of **B** and **C** are both zero, the reaction profiles are given by Eq. (2.45).

$$\left. \begin{aligned} [A] &= [A]_0 e^{-k_1 t} \\ [B] &= [A]_0 \frac{k_1}{k_2 - k_1} (e^{-k_1 t} - e^{-k_2 t}) \\ [C] &= \frac{[A]_0}{k_2 - k_1} (-k_2 e^{-k_1 t} + k_1 e^{-k_2 t}) + [A]_0 \end{aligned} \right\} \quad (2.45)$$

I recommend that you write out Eq. (2.45) and confirm that if one of the steps becomes rate determining (i.e., if $k_1 \gg k_2$ or $k_2 \gg k_1$) the rate laws reduce to a simple first order. Although this is still a relatively simple system, it has no analytic solution. There is no explicit expression for k_1 and k_2 which is analogous to the solutions for first-order or second-order equations. This is often the case with complex kinetics. Such systems are usually solved numerically [27].

Parallel reactions are very common in chemistry. They play a key role in catalysis, because the catalyst effectively creates a parallel alternative to the noncatalyzed reaction. In many cases a catalytic reaction will yield several products, because one of the catalytic intermediates can react via two different pathways. The general scheme for two parallel reactions is shown in Eq. (2.46), and the corresponding differential rate equations for **B** and **C** are Eq. (2.47).



$$\left. \begin{aligned} \frac{d[B]}{dt} &= k_1([A]_0 - [B] - [C]) \\ \frac{d[C]}{dt} &= k_2([A]_0 - [B] - [C]) \end{aligned} \right\} \quad (2.47)$$

If the initial concentration of **A** is $[A]_0$ and the initial concentrations of **B** and **C** are both zero, the corresponding reaction profiles are given by Eq. (2.48).

$$\left. \begin{aligned} [A] &= [A]_0 e^{-(k_1 + k_2)t} \\ [B] &= \frac{k_1 [A]_0}{k_1 + k_2} [1 - e^{-(k_1 + k_2)t}] \\ [C] &= \frac{k_2 [A]_0}{k_1 + k_2} [1 - e^{-(k_1 + k_2)t}] \end{aligned} \right\} \quad (2.48)$$

The product selectivity is determined by the ratio k_1/k_2 . If k_1 and k_2 pertain to the high barriers in the overall catalytic cycle, the parallel reaction is also rate determining (Figure 2.10a). If there is another, higher, barrier “earlier” in the cycle, then the selectivity is not connected to the rate-determining step (Figure 2.10b). This complicates things, since kinetic studies usually give information only about the rate-determining step(s).

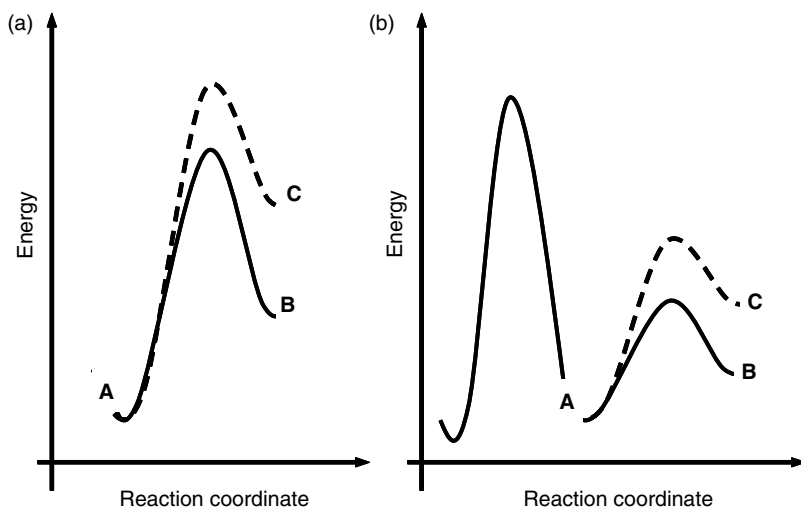


Figure 2.10 Energy/reaction coordinate diagrams for a generic parallel reaction. The parallel reaction determines the product selectivity, and may be a rate-determining or b not rate-determining.

2.1.8

Pre-Equilibrium, “Catalyst Reservoirs,” and Catalyst Precursors

Often, what we call “the catalyst” is only a **catalyst precursor**. When we add this precursor to the reaction, the catalytic cycle commences. In such cases, the real active catalyst forms *in situ*, either by decomposition of the precursor or by its reaction with one of the reagents. Sometimes, when the substrate is consumed completely, the catalyst reverts to its precursor configuration. The precursor and the active catalyst are frequently in equilibrium, with the precursor acting as a “**catalyst reservoir**” which supplies the catalytic cycle continuously with a small amount of active intermediate. This situation is known as **pre-equilibrium** (Figure 2.11, inset). For example, in homogeneous catalysis, two active catalytic intermediates may dimerize. The stable dimer (the catalyst precursor) is the reservoir for the monomer (the active catalytic intermediate). Denoting the dimer as **D** and the active catalytic intermediate as **Q**, and assuming that **Q** reacts with the substrate **S**, giving the product **P**, we obtain Eq. (2.49).



From Eq. (2.49) we derive the differential rate equations Eq. (2.50).

$$\left. \begin{array}{l} \frac{d[\text{D}]}{dt} = -k_1[\text{D}] + 4k_{-1}([\text{D}]_0 - [\text{D}])^2 \\ \frac{d[\text{S}]}{dt} = -2k_2([\text{D}]_0 - [\text{D}])[\text{S}] \end{array} \right\} \quad (2.50)$$

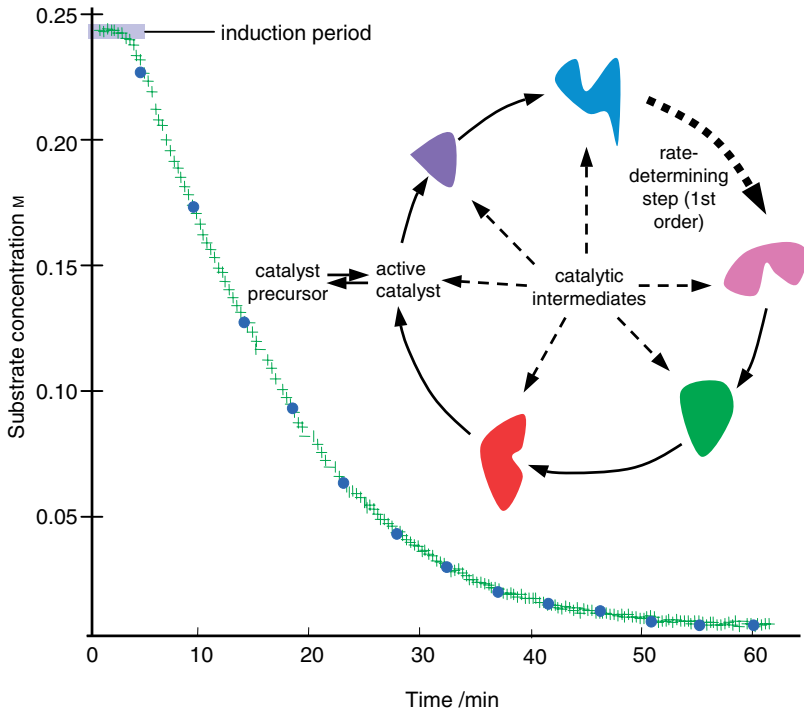


Figure 2.11 Reaction profile showing the substrate conversion in a pre-equilibrium system followed by first-order kinetics. Note the importance of frequent sampling; in this case, sampling every 5 min would not show the induction period (compare the + and • symbols). The inset shows a generic catalytic cycle with a pre-equilibrium step.

Here one usually resorts to numerical methods. Surprisingly, in this case the differential equations do have an analytic solution, although it is quite daunting, namely Eqs. (2.51) and (2.52), where $\phi = \sqrt{k_1(k_1 + 16[\mathbf{D}]_0 k_{-1})}$.

$$[\mathbf{D}] = \frac{1}{8k_{-1}} \left[k_1 + 8[\mathbf{D}]_0 k_{-1} - \phi \tanh \left(\frac{\phi t}{2} + \operatorname{arctanh} \frac{k_1}{\phi} \right) \right] \quad (2.51)$$

$$[\mathbf{S}] = 2^{-\frac{k_2}{k_{-1}}} [\mathbf{S}]_0 e^{\frac{k_1 k_2 t}{4k_{-1}}} \left(\frac{[\mathbf{D}]_0 k_{-1}}{k_1 + 16[\mathbf{D}]_0 k_{-1}} \right)^{-\frac{k_2}{4k_{-1}}} \cosh \left[\frac{\phi t}{2} + \operatorname{arctanh} \frac{k_1}{\phi} \right]^{-\frac{k_2}{2k_{-1}}} \quad (2.52)$$

Figure 2.11 shows the corresponding reaction profile. It begins with an induction period (the small plateau at low t values), and then proceeds as a first-order reaction. Once the system reaches the equilibrium between the precursor \mathbf{D} and the active catalytic intermediate \mathbf{Q} , the overall reaction rate reflects the first-order rate-

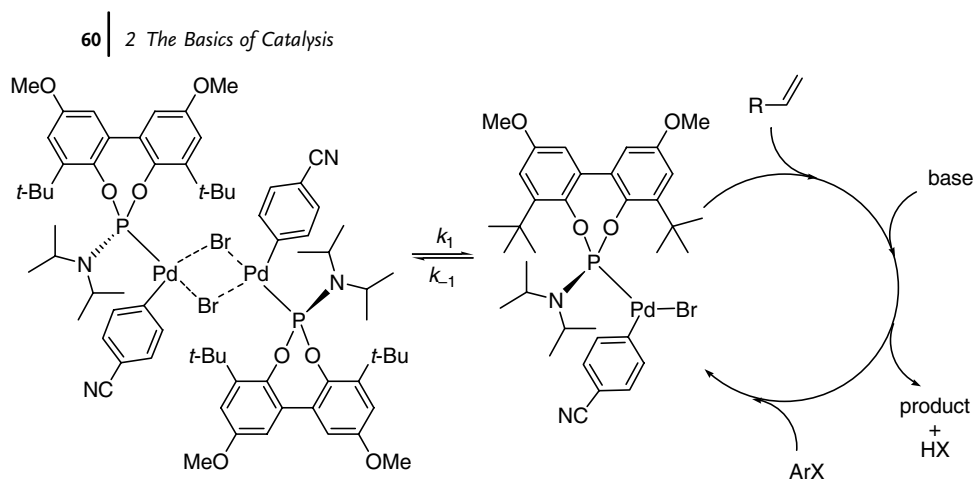


Figure 2.12 Dimer–monomer pre-equilibrium and catalytic cycle for the Heck coupling of *p*-bromocyanobenzene and *n*-butyl acrylate.

determining step in Eq. (2.49). Indeed, this type of reaction profile (induction period followed by first-order or second-order kinetics) indicates a catalyst precursor \rightleftharpoons active intermediate pre-equilibrium process.

One example of such a pre-equilibrium is the palladium-catalyzed Heck cross-coupling between *p*-bromocyanobenzene and *n*-butyl acrylate. This reaction is often studied because it is fast, selective, and easy to run in the lab. Nearly every type of Pd species will catalyze such Heck reactions (or, more accurately, nearly every Pd precursor will transform in the presence of the reactants into an active catalytic intermediate), from heterogeneous Pd/C [28,29] to homogeneous PdCl₂ [30]. In this example, the catalyst precursor is a dimer of two catalytic intermediates. Each intermediate containing a Pd center coordinated to a monodentate phosphoramidite ligand, a Br[−] anion, and an aryl ring [31]. Figure 2.12 shows the dimer–monomer equilibrium and the adjacent catalytic cycle. Monitoring the reactant concentration over time gives a reaction profile like that shown in Figure 2.11, which indicates pre-equilibrium followed by a first-order reaction.

2.2 Practical Approaches in Kinetic Studies

The literature abounds with papers on kinetic and mechanistic studies. There are no set rules for finding out reaction mechanisms. Searching for the mechanism of a chemical reaction is challenging, frequently frustrating, and sometimes rewarding [32]. Monitoring reaction profiles and analyzing reaction kinetics is very useful for testing mechanistic assumptions. The catalytic cycle is a “black box”, and kinetic studies help you look into parts of this box. They give us direct information on the species involved in the rate-determining step, and sometimes also indirect information on the fast steps [33]. Determining the reaction order and the rate law is the

fundamental challenge in kinetic studies. The rate law is closely related to the reaction mechanism. Understanding the mechanism increases your chances of designing a better catalyst, and/or finding improved reaction conditions.

2.2.1

Initial Reaction Rates and Concentration Effects

Measuring the initial reaction rate is a good method for determining the rate equation when you have little or no prior information on the reaction. The reason is that when t is close to t_0 the experimental conditions are well defined, and the initial reaction rate, v_0 , reflects these conditions. For elementary reactions, the reaction order is derived directly from the stoichiometry, and one can easily calculate the rate constant. Conversely, for nonelementary reactions (i.e., when the partial reaction orders for each component may differ from the stoichiometry of that component), the reaction order must first be found by experiment. Once you find the reaction order, you can derive the rate equation and calculate the rate constant. A simple solution is running several reactions and quantifying the concentration effects of each component. This gives the partial reaction order for each component. In general, for a system with n reagents you need $n + 1$ initial rate measurements under different conditions for determining the reaction rate law.

As an example, consider the reaction $\mathbf{A} + \mathbf{B} \rightarrow \mathbf{C}$, and let us assume that this is a nonelementary reaction. The rate equation in this case is Eq. (2.53), and we must find the values of α , β , and k . We do this by designing experiments in a way that isolates the contribution of each reactant to the initial rate, as shown in Table 2.1.

$$\text{rate} = k[\mathbf{A}]^\alpha [\mathbf{B}]^\beta \quad (2.53)$$

Comparing the initial rates for runs 1 and 2, where $[\mathbf{B}]_0$ is doubled but $[\mathbf{A}]_0$ is unchanged, we see that the rate also doubles. Therefore this reaction is first order in \mathbf{B} ($\beta = 1$). Similarly, comparing the initial rates for runs 2 and 3, where $[\mathbf{A}]_0$ is doubled but $[\mathbf{B}]_0$ is unchanged, shows that the doubling of $[\mathbf{A}]_0$ does not affect v_0 . This means that the reaction is zero order in $[\mathbf{A}]$ ($\alpha = 0$). The overall rate equation is therefore Eq. (2.54).

$$\text{rate} = k[\mathbf{A}]^0 [\mathbf{B}]^1 = k[\mathbf{B}] \quad (2.54)$$

Table 2.1 Measured concentrations of alkene **A** over time.

Run	$[\mathbf{A}]_0/\text{M}$	$[\mathbf{B}]_0/\text{M}$	$v_0/\text{M min}^{-1}$
1	1.00	1.00	0.0162
2	1.00	2.00	0.0324
3	2.00	2.00	0.0324

We can easily calculate k from any of the above experiments by substituting the v_0 and $[\mathbf{B}]_0$ values into Eq. (2.54). For example, substituting the values for run 2 ($[\mathbf{B}]_0 = 2.00\text{ M}$ and $v_0 = 0.0324\text{ min}^{-1}$) gives Eq. (2.55).

$$k = \frac{v_0}{[\mathbf{B}]_0} = \frac{0.0324\text{ M min}^{-1}}{2.00\text{ M}} = 0.0162\text{ min}^{-1} \quad (2.55)$$

2.2.1.1 Concentration Effects

One can also validate a proposed catalytic cycle by changing the concentrations of various species and comparing the resulting reaction profiles. For example, suppose that you run a homogeneously catalyzed reaction, but your “catalyst” is really only a catalyst precursor, and a ligand must dissociate from it to give the active catalytic intermediate. In such a case, adding more ligand should retard the reaction, as the excess ligand would drive the dissociation/association equilibrium towards the inactive catalyst precursor.

2.2.2

Creating Pseudo Order Conditions

By using a large excess of a reagent you can effectively remove that reagent from the reaction rate equation. The reagent does not disappear, of course, but because its concentration is high compared with the change of concentration caused by the reaction, it remains effectively constant. This lowers the overall reaction order, creating a pseudo order that gives information on the role of the remaining reagents. For example, for the second-order elementary reaction $\mathbf{A} + \mathbf{B} \rightarrow \mathbf{C}$, the rate equation for a stoichiometric mixture of \mathbf{A} and \mathbf{B} is Eq. (2.56), where k is the second-order rate constant.

$$\text{rate} = k[\mathbf{A}][\mathbf{B}] \quad (2.56)$$

If we run the same reaction starting from a 200:1 mole/mole mixture of \mathbf{A} and \mathbf{B} , the change in $[\mathbf{A}]$ will never be more than 0.5%, because even at full conversion there will still be 199 equivalents of \mathbf{A} left. This means that $[\mathbf{A}] = [\mathbf{A}]_0$, giving a pseudo first-order reaction profile that depends only on $[\mathbf{B}]$. In the corresponding rate equation (Eq. (2.57)), the pseudo first-order constant $k' = k[\mathbf{A}]_0$. Pseudo order conditions are very useful for isolating the contribution of a chemical species to the rate-determining step.

$$\text{rate} = k'[\mathbf{B}] \quad (2.57)$$

Note that the definition of “a large excess” depends on your analytical method. The excess must be sufficiently large for the change in concentration to be within the experimental error range. For example, when using GC analysis, the total measurement error may be $\pm 1\%$. In this case, a 100-fold excess will work just as well as a 1000-fold excess.

2.2.3

What You See versus What You Get

Throughout this chapter we assume that by measuring concentration changes, we can easily determine the reaction order. Sometimes this is indeed so: you try fitting either $-\ln(1 - \chi_A)$ or $\chi_A(1 - \chi_A)$ to the reaction profiles, then compare the R^2 (correlation coefficient) values and find that one equation fits much better than the other. However, sometimes the differences are small, or you do not have enough sampling points, or you may be sampling at the wrong times. A detailed discussion on sampling and statistical relevance is out of the scope of this book, but there are several texts that explain the importance of these points [34,35]. The maxim “garbage in/garbage out” is very relevant here, because inaccurate reaction profiles often lead to erroneous conclusions. Proper validation of every kinetic model is essential (see also the discussion on model validation and “separating knowledge from garbage” in Chapter 6).

Another problem is that kinetic studies are limited to the species that you can “see”. You may be monitoring the wrong species. This is especially relevant in the case of catalytic intermediates, which are often present only at low concentrations and cannot be isolated *in vitro*. For example, monitoring the concentration of an organometallic complex by NMR requires a minimum concentration, regardless of whether this complex is the active catalytic intermediate or not. Sometimes the active intermediates never attain these minimum concentrations, and so you never see them. Similarly, observing a metal–ligand complex does not guarantee that this complex participates in the catalytic cycle. One way to solve this problem is by combining two or more monitoring methods. Computer simulations are also useful,

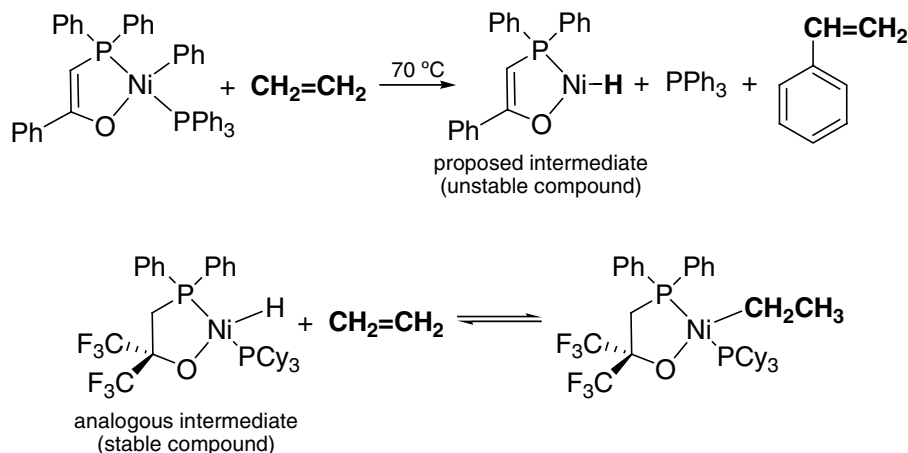


Figure 2.13 Stoichiometric reactions with isolated catalytic intermediates can provide support for the mechanism (or sometimes disprove it).

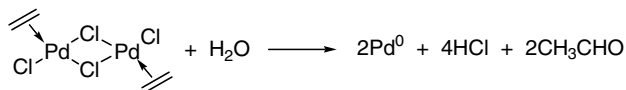


Figure 2.14 Decomposition of the binuclear complex $\text{Pd}_2\text{Cl}_4(\text{C}_2\text{H}_4)_2$ in the presence of water.

as they can visualize intermediates that cannot be seen experimentally. Chapter 6 gives more details on the various computational approaches in catalysis research.

2.2.4

Learning from Stoichiometric Experiments

Performing reactions with stoichiometric amounts of catalyst is one of the most useful techniques in catalysis research. Such reactions often give valuable information on specific steps in the catalytic cycle. If you can isolate one of the catalytic intermediates, you can examine the role of this intermediate in a stoichiometric reaction with the appropriate reagent in the catalytic cycle. In this way you can isolate one or more steps from the cycle and analyze their kinetics. If a specific catalytic intermediate is unstable, there may be a stable analogue that can be isolated and tested. For example, Keim and co-workers postulated the P–O nickel hydride complex shown in Figure 2.13 as a catalytic intermediate in the oligomerization cycle of the Shell higher olefins process (SHOP) based on *in situ* NMR studies [36]. They isolated an analogous hydride complex and showed that it underwent reversible insertion with ethylene, supporting the catalytic cycle [37].

Another example is the palladium-catalyzed oxidation of ethylene to acetaldehyde in the presence of oxygen and cupric salts, the so-called Wacker reaction. This catalytic cycle combines two stoichiometric processes, which involve first the reduction of Pd^{II} to Pd^0 , followed by reoxidation with Cu^{II} . The understanding of the first step of this process came from the earlier work of Kharasch et al., who showed that the stoichiometric dinuclear complex shown in Figure 2.14 decomposed in the presence of water to acetaldehyde (ethanal), Pd^0 and HCl [38].

2.3

An Overview of Some Basic Concepts in Catalysis

If we look at the entire reaction system as a “black box,” it seems that the catalyst simply “lowers the activation energy.” We now know that this is true in only a few cases. In most cases, the catalyst actually opens an alternative reaction pathway. This pathway is often more complicated, and includes several catalytic intermediates. However, the highest activation barrier in the catalytic pathway is still lower than that of the noncatalytic one. We also know that the catalyst does not and cannot change the thermodynamics, and that it catalyzes both the forward and reverse reactions (just as a pathway between mountains eases crossing in both directions). This means that the best catalyst for the reaction $\text{A} + \text{B} \rightarrow \text{C}$ is also the best catalyst for the reaction

$C \rightarrow A + B$. Now that we have some background on the kinetics of various reaction types, let us examine some common qualitative concepts in catalysis.

2.3.1

Catalyst/Substrate Interactions and Sabatier's Principle

The interaction between the catalyst and the substrates, intermediates, and products is extremely important. If it is too weak, the substrate will drift away from the catalyst and no reaction will take place. Conversely, if it is too strong, the substrate (or the product) will never leave the catalyst, causing poisoning or inhibition (see below). Thus, even without complicated equations, we see that some catalyst/substrate interactions should be "just right" – not too weak and not too strong. This qualitative concept is known as **Sabatier's principle**, named after the French chemist Paul Sabatier, who shared the 1912 Nobel Prize in chemistry with Victor Grignard. Figure 2.15 (left) shows how the reaction rate depends on the heat of adsorption [39]. At first, as the heat of adsorption increases, the reaction rate also increases. More substrates bind to the catalyst and there is a higher chance of reaction. When the heat of adsorption is too strong, however, the reaction rate starts to decrease, because now the substrates (or products) do not leave the catalyst. This type of plot is called a **volcano plot**, and is quite common in catalysis [40]. For example, the activity of metal oxide catalysts in cyclohexane dehydrogenation depends on their position in the periodic table [41], as does that of transition metal sulfides in hydrodesulfurization (Figure 2.15, right [42]).

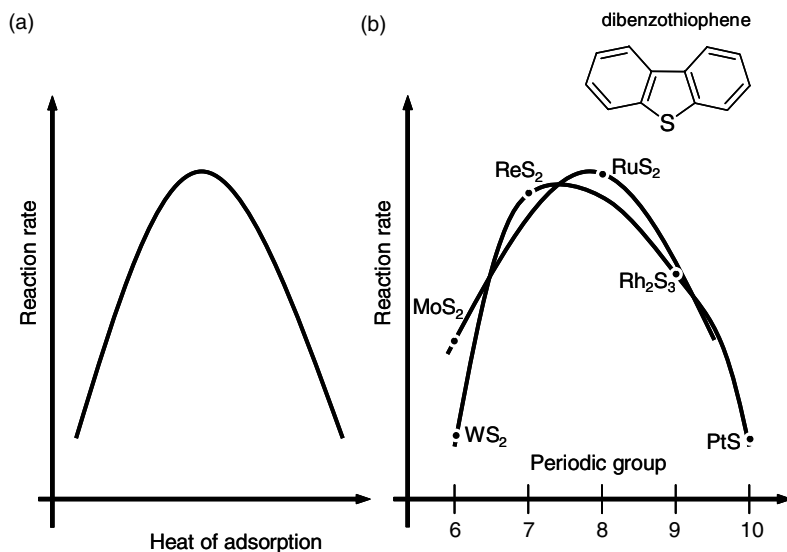


Figure 2.15 Examples of volcano plots, describing the reaction rate as a function of the heat of adsorption (*left*), and the activity of the second-row and third-row transition metal sulfides in the hydrodesulfurization of dibenzothiophene (*right*).

2.3.2

Catalyst Deactivation, Sintering, and Thermal Degradation

Up to now we have neglected any problems in the course of the reaction. In practice, however, catalytic systems exhibit all sorts of unwanted effects. Catalytic intermediates (or the active sites) can lose or gain activity as the reaction progresses, because catalysts are often sensitive to changes in acidity/basicity, temperature, pressure, and phase composition. Moreover, as the conversion increases, products and by-products can bind to the catalyst, thereby changing the preferred reaction pathway. Such processes are known as deactivation, sintering, inhibition, or poisoning.

2.3.2.1 Catalyst Deactivation

This is a general term for a common situation in catalysis, where a catalyst becomes less active as the reaction progresses. An organometallic complex catalyst, for example, may dimerize or oligomerize, reducing the concentration of active catalytic intermediates. Often, the activity depends on specific ligating groups. If these are destroyed via side-reactions – e.g., due to pH changes, oxidative degradation, increasing temperature, or the formation of additional phases – the catalyst will deactivate. When a catalyst deactivates, the reaction profile deviates from the “ideal” rate law. The deactivation can follow a first-order (e.g., thermal decomposition) or second-order (e.g., dimerization) rate law. Nevertheless, many deactivation processes are very complicated, and incorporating them into the kinetic scheme is difficult. Although it sounds trivial, switching to a more stable catalyst is still the best way of avoiding deactivation problems.

Deactivation may seem less important, but designing effective catalysts hinges on our understanding of the various deactivation processes [43,44]. One such example is the family of tetraamido macrocycle ligands (TAML) developed by Collins and co-workers [45]. Manganese and iron complexes of these ligands activate H_2O_2 , probably via metal–oxo catalytic intermediates [46]. This makes them good catalysts for cleaning up aqueous waste effluents. Collins used an iterative design approach [47], studying the deactivation by oxidative degradation and identifying the vulnerable site (Figure 2.16). This increased the robustness in each new generation of ligands.

2.3.2.2 Catalyst Sintering and Thermal Degradation

Catalyst deactivation via thermal degradation or sintering is a common phenomenon in heterogeneous catalysis. At high temperatures, the support pore structure may collapse, and the size and shape of the metal crystallites can change. This decreases the catalyst’s surface area and the number of active sites [48]. The temperature at which this happens varies, but many metals are already sensitive to sintering at $\sim 200^\circ\text{C}$ below their melting point. Automotive catalysts are a good example where sintering is a problem, because the catalytic converter is installed near the engine. Three-way catalysts must typically operate at temperatures as high as 1000°C [49]. Figure 2.17 illustrates the sintering of a metal catalyst on a porous solid support. This can occur by two pathways: atom migration and crystallite migration [50]. In the

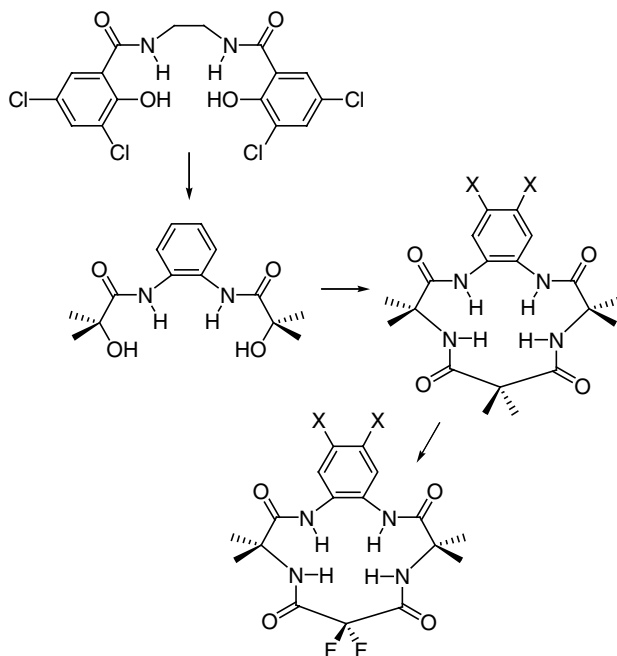


Figure 2.16 The development of tetradentate ligand systems for H_2O_2 activation.

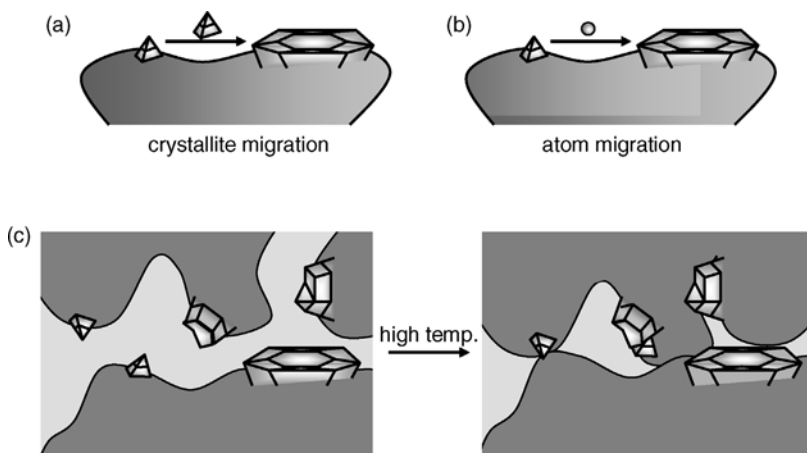


Figure 2.17 Different aspects of catalyst sintering: **a** crystallite migration; **b** atom migration; **c** phase transformation of the support at high temperatures.

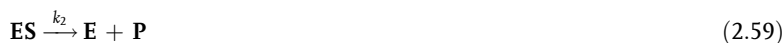
former, metal atoms migrate from one crystallite to another via the surface or the gas phase. Smaller crystals are more likely to lose atoms this way, because they have a higher surface area and correspondingly a higher proportion of atoms at high-energy sites. Thus, the big clusters get bigger and the small clusters become even smaller. Conversely, in the crystallite migration model, entire metal crystallites migrate on the support surface, collide, and coalesce [51,52].

Sintering is a complex process [43,53]. It depends on temperature, support composition, support porosity, type of active metal, and surrounding atmosphere. At lower temperatures (typically $\sim 600^\circ\text{C}$ for noble metals) the primary sintering route is atom transfer from small metal particles via surface diffusion. Crystallite migration becomes important at higher temperatures. As a rule of thumb, a metal catalyst will start sintering when the temperature is roughly half of the metal's melting point. Another type of sintering occurs when the crystal phases of the support itself transform. This happens only at very high temperatures (typically above 1000°C). Such transformations collapse the pore structure, thereby reducing the surface area and blocking access to active sites.

2.3.3

Catalyst Inhibition

Catalyst inhibition is traditionally associated with biocatalytic processes, but can also apply to homogeneous and heterogeneous catalysis. **Competitive inhibition** is analogous to **competitive adsorption** in gas/solid heterogeneous catalysis, where two molecules from the gas phase compete for the same active site on the catalyst surface. A competitive inhibitor is any chemical species **I** which can bind to the same site as the substrate, or to another site on the enzyme (an **allosteric site**). The overall reaction scheme is then given by Eqs. (2.58)–(2.60), where **EI** indicates an enzyme–inhibitor complex.



Thus, every **EI** complex reduces the amount of enzyme available for catalysis, regardless of where the inhibitor binds. As shown in Eq. (2.60), inhibition is a reversible process. The degree of reversibility depends on the ratio $k_i : k_{-i}$, or in other words, on the inhibitor binding equilibrium constant, K_i .

A **noncompetitive inhibitor** binds only at an allosteric site. This changes the properties of the active site and stops or retards the catalytic activity [54]. The structure and shape of the enzyme change, reducing the “active enzyme” concentration and decreasing v_{max} . Since the inhibitor does not compete with the substrate, increasing the substrate concentration does not help here. Nature uses competitive product

inhibition to ensure that reactions do not proceed too far. Noncompetitive inhibitors are important in drug research, e.g. as drugs for treating Alzheimer's disease [55].

2.3.3.1 Catalyst Poisoning

This is basically a bad case of inhibition. When an inhibitor bonds irreversibly to the catalyst, we say that it “poisons” the catalyst. In enzymatic catalysis, Eq. (2.60) becomes irreversible. If there is enough poison, the catalytic cycle will grind to a halt. In heterogeneous catalysis people distinguish between “permanent poisons” and “temporary poisons” [56]. For the latter, the catalyst can be regenerated, usually by recalcining (burning off the poison at high temperature). Like sintering and inhibition, poisoning depends on temperature and reaction conditions. Poisons can be selective for a certain catalyst, or for certain reactions. Coke, sulfur, and phosphorus are common poisons in automotive catalysis, as was lead when it was still being added to gasoline as an “anti-knocking” agent [57].

2.4 Exercises

- The molecular formula of **A** is C_4H_6 . When 1 mole of **A** was mixed with 1 mol of Br_2 , the flask became hot. A colorless product **B** was observed by gas chromatography. In another experiment, 1 mol of **A** was mixed with 1.5 mol of Br_2 ; the flask became hot but the color of the solution remained red. In a third experiment, UV light was shone on a flask containing **A**, and the product **C** was observed. Kinetic studies showed that the formation of **B** and **C** both fit to second-order rate laws.
 - Write out the rate equations for the formation of **B** and **C**.
 - Draw the structures of **A**, **B**, and **C** (there are three possibilities).
 - Osmium tetroxide (OsO_4) can catalyze the breaking of double bonds by ozone to form carboxylic acids. **A** (1 mol) was mixed in a closed flask with 1 mol of ozone and 0.005 mol of OsO_4 , and after 30 min a reaction sample was analyzed by GC. **A** had disappeared, but no product was observed. Explain these observations.
- Maria and Fatima performed some experiments as part of their fifth-year research project, to monitor the catalytic activity of niobium complexes in the scission of dicyclohexyldicyclopropane (Figure 2.18). They performed the reactions in well-stirred 200 mL round-bottomed flasks immersed in oil baths connected to a reflux apparatus, and measured the reaction progress by taking samples from the mixture and monitoring them by GC. Maria injected eight samples. Fatima injected only three samples. Maria ran the reaction with no catalyst, using ethanol as a solvent and heating the oil bath to $160^\circ C$. Fatima performed the reaction with 1 mol% catalyst, using ethanol as a solvent. She heated the oil bath to only $80^\circ C$. Figure 2.18 shows the results of both experiments.

Decide if the following statements are true or false, and explain your decisions.

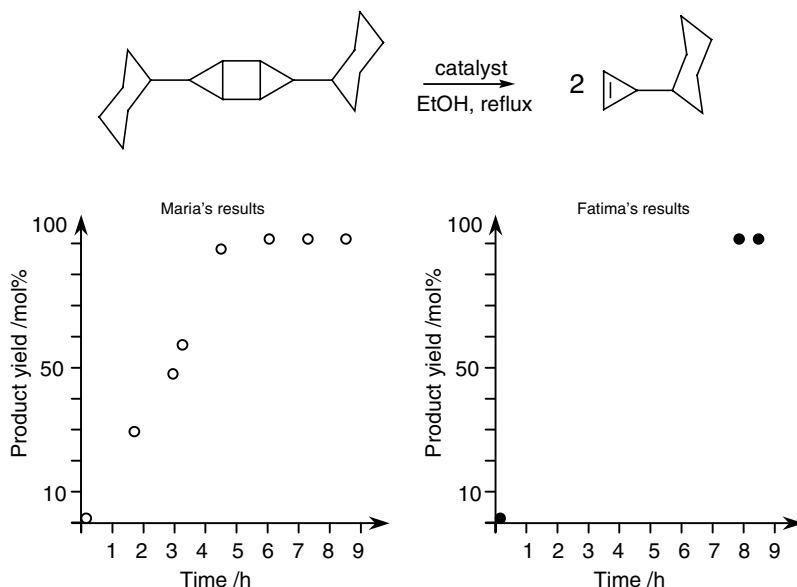


Figure 2.18 The reaction profiles obtained by Maria and Fatima.

- Maria's reaction is faster.
 - Fatima's reaction is faster.
 - If Maria repeated the reaction using two times as much dicyclohexyldicyclopropane, she would reach 50% conversion after 3 h.
 - If Fatima used 2 mol% catalyst instead of 1 mol%, her reaction would go twice as fast.
 - If there are differences in the rates of the reactions, they are due to the different temperatures in the oil baths.
3. The synthesis of lineatin, a pheromone of the insect *Trypodendron lineatum*, involves the enantioselective addition of methane to the double bond of alkene A in the presence of a chiral rhenium catalyst on silica ($\text{Re}^*/\text{silica}$; see Figure 2.19). Michael performed eight separate experiments for this reaction in a 500 mL high-pressure stirred autoclave reactor using liquid methane as a solvent and 0.05 mmol catalyst. The results are shown in Table 2.2.

In a second study, Abdelhafid performed five experiments in a 500 mL stirred tank reactor at 20 °C, using an inert organic solvent, 0.05 mmol catalyst, 1.000 mM alkene A and 1 atm of methane. In all these five experiments it was found that the reaction fitted a second-order rate law.

- Write out the rate equation that fits Michael's results.
- Calculate the value of the rate constant that Michael found.
- Write out the rate equation fits Abdelhafid's results.

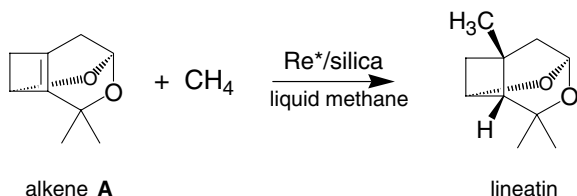


Figure 2.19 The methane asymmetric addition step in the synthesis of lineatin.

- (d) What is the reason for the different results observed by Michael and Abdelhafid?
- (e) Both students repeated their first experiment again without changing conditions but using CD_4 instead of methane. What did they observe? Will the kinetics change?
4. The acid-catalyzed reaction $\text{A} \xrightarrow{\text{acid}} \text{B}$ follows first-order kinetics. Which **one** of the following five sentences is true? Prove that your answer is correct.
- (a) If it takes 20 min to reach 50% conversion at 300 K, it will take 200 min to reach 99.9% conversion at 300 K.
- (b) If it takes 20 min to reach 50% conversion at 300 K, it will take 40 min to reach 99.9% conversion at 300 K.
- (c) If it takes 20 min to reach 50% conversion at 300 K, it will take 320 min to reach 99.9% conversion at 300 K.
- (d) Regardless of the time it takes to reach 50% conversion, an acid-catalyzed reaction will never reach more than 90% conversion.
- (e) If it takes 20 min to reach 50% conversion at 300 K, it will take 30 min to reach 99.9% conversion at 300 K.
5. The epoxidation of cyclobutene (**1**) to cyclobutane oxide (**2**) with nitrous oxide (Figure 2.20) was studied by Useless Polymers Inc. as a possible step in the route to 1,2-cyclobutadiol. Researchers Hannah and John chose two catalysts for kinetic studies, catalyst **A** and catalyst **B**.

Table 2.2 Measured concentrations of alkene **A** over time.

Experiment	Time/min	[A]/mM	Time/min	[A]/mM
1	0.0	0.500	120.0	0.248
2	0.0	1.000	120.0	0.503
3	0.0	1.200	120.0	0.611
4	0.0	1.600	120.0	0.788
5	0.0	2.000	120.0	0.986
6	0.0	3.200	120.0	1.603
7	0.0	4.400	120.0	1.566
8	0.0	6.000	120.0	2.989

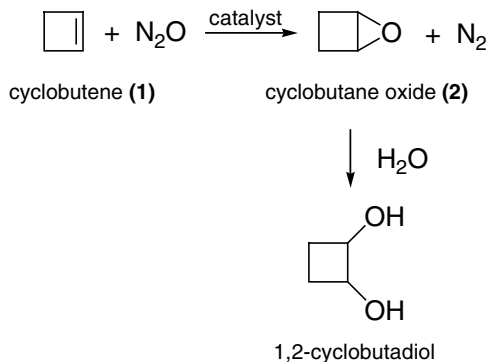


Figure 2.20 Epoxidation of cyclobutane to cyclobutane oxide with nitrous oxide.

Hannah ran a reaction with catalyst **A**, using a 25 M solution of cyclobutene, and got the following results:

Time/min	0.00	6.00	12.00	18.00	24.00	30.00	36.00	42.00	48.00	54.00	60.00
[1]/M	25.00	20.07	16.11	12.94	10.39	8.34	6.69	5.37	4.31	3.46	2.78
[2]/M	0.00	4.93	8.89	12.06	14.61	16.66	18.31	19.63	20.69	21.54	22.22

Repeating the reaction with catalyst **A**, using an 18 M solution of cyclobutene, she got:

Time/min	0.00	6.00	12.00	18.00	24.00	30.00	36.00	42.00	48.00	54.00	60.00
[1]/M	18.00	14.45	11.60	9.31	7.48	6.00	4.82	3.87	3.11	2.49	2.00
[2]/M	0.00	3.55	6.40	8.69	10.52	12.00	13.18	14.13	14.89	15.51	16.00

John ran the reaction with catalyst **B**, using a 20 M solution of cyclobutene, and got the following results:

Time/min	0.00	3.00	6.00	9.00	12.00	15.00	18.00	21.00	24.00	27.00	30.00
[1]/M	20.00	17.39	15.38	13.79	12.50	11.43	10.53	9.76	9.09	8.51	8.00
[2]/M	0.00	2.61	4.62	6.21	7.50	8.57	9.47	10.24	10.91	11.49	12.00

Repeating the reaction with catalyst **B**, using a 15 M solution of cyclobutene, he got:

Time/min	0.00	10.00	20.00	30.00	40.00	50.00	60.00	70.00	80.00	90.00	100.00
[1]/M	15.00	10.91	8.57	7.06	6.00	5.22	4.62	4.14	3.75	3.43	3.16
[2]/M	0.00	4.09	6.43	7.94	9.00	9.78	10.38	10.86	11.25	11.57	11.84

- Write out a rate equation that fits Hannah's data.
- Calculate the rate constant that Hannah found. What type of rate constant is it?
- Write out a rate equation that fits to John's data.
- Calculate the rate constant that John found. What type of rate constant is it?
- Compare the two rate constants that you calculated. Which is larger? and what does this mean?

References

- 1 Atkins, P.W. (1994) *Physical Chemistry*. Oxford University Press, Oxford, ISBN 0-19-855730-2.
- 2 Fogler, H.S. (1992) *Elements of Chemical Reaction Engineering*, Prentice-Hall, London, ISBN 0-13-253220-4.
- 3 Levenspiel, O. (1999) *Chemical Reaction Engineering*, Wiley, New York, ISBN 0-471-25424-X.
- 4 Donati, G. and Paludetto, R. (1999) Batch and semi-batch catalytic reactors (from theory to practice). *Catalysis Today*, **52**, 183.
- 5 Arrhenius, S. (1899) On the theory of chemical reaction velocity. *Zeit. Phys. Chem.*, **28**, 317.
- 6 Eyring, H. (1935) The activated complex and the absolute rate of chemical reactions. *Chem. Rev.*, **17**, 65.
- 7 Laidler, K.J. and Tweeddale, A. (1971) Current status of Eyring's rate theory. *Adv. Chem. Phys.*, **21**, 113.
- 8 Koryabkina, N.A., Phatak, A.A., Ruettinger, W.F., Farrauto, R.J. and Ribeiro, F.H. (2003) Determination of kinetic parameters for the water-gas shift reaction on copper catalysts under realistic conditions for fuel cell applications. *J. Catal.*, **217**, 233.
- 9 Laidler, K.J. and Glasstone, S. (1948) Rate, order and molecularity in chemical kinetics. *J. Chem. Educ.*, **25**, 383.
- 10 Babcock, L.M. and Streit, G.E. (1984) third-body effects in termolecular reactions Halide ion addition to boron trifluoride and boron trichloride. *J. Phys. Chem.*, **88**, 5025.
- 11 Patrick, R. and Golden, D.M. (1984) Termolecular reactions of alkali metal atoms with oxygen and hydroxyl. *Int. J. Chem. Kinet.*, **16**, 1567.
- 12 Kiperman, S.L. (1991) Kinetic models of heterogeneous catalytic reactions. *Russ. Chem. Bull.*, **40**, 2350.
- 13 Radzicka, A. and Wolfenden, R. (1995) A proficient enzyme. *Science*, **267**, 90.
- 14 Lee, J.K. and Houk, K.N. (1997) A proficient enzyme revisited: the predicted mechanism for orotidine monophosphate decarboxylase. *Science*, **276**, 942.
- 15 Murzin, D.Y. (2005) On surface heterogeneity and catalytic kinetics. *Ind. Eng. Chem. Res.*, **44**, 1688.
- 16 Petukhov, A.V. (1997) Effect of molecular mobility on kinetics of an electrochemical Langmuir–Hinshelwood reaction. *Chem. Phys. Lett.*, **277**, 539.
- 17 Jimenez, C., Romero, F.J. and Gomez, J.P. (2001) Isomerization of paraffins. *Recent Res. Dev. Pure Appl. Chem.*, **5**, 1.
- 18 Ono, Y. (2003) A survey of the mechanism in catalytic isomerization of alkanes. *Catal. Today*, **81**, 3.
- 19 Michaelis, L. and Menten, M.L. (1913) Kinetics of invertase action. *Biochem. Zeit.*, **49**, 333.
- 20 Dowd, J.E. and Riggs, D.S. (1965) A comparison of estimates of Michaelis–Menten kinetic constants from various linear transformations. *J. Biol. Chem.*, **240**, 863.
- 21 Atkins, G.L. and Nimmo, I.A. (1975) A comparison of seven methods for fitting the Michaelis–Menten equation. *Biochem. J.*, **149**, 775.
- 22 Lineweaver, H. and Burk, D. (1934) Determination of enzyme dissociation constants. *J. Am. Chem. Soc.*, **56**, 658.
- 23 Eadie, G.S. (1942) The inhibition of cholinesterase by physostigmine and prostigmine. *J. Biol. Chem.*, **146**, 85.
- 24 Hofstee, B.H. (1959) Non-inverted versus inverted plots in enzyme kinetics. *Nature*, **184**, 1296.
- 25 Frank, I.E. (1995) Modern nonlinear regression methods. *Chemom. Intell. Lab. Syst.*, **27**, 1.
- 26 Simopoulos, T.T. and Jencks, W.P. (1994) Alkaline phosphatase is an almost perfect enzyme. *Biochemistry*, **33**, 10, 375.
- 27 Iron, D., Boelens, H.F.M., Westerhuis, J.A. and Rothenberg, G. (2003) Kinetic studies

- of cascade reactions in high-throughput systems. *Anal. Chem.*, **75**, 6701.
- 28** Wall, V.M., Eisenstadt, A., Ager, D.J. and Laneman, S.A. (1999) The Heck reaction and cinnamic acid synthesis by heterogeneous catalysis: palladium on carbon catalyst gives improved production. *Platinum Met. Rev.*, **43**, 138.
- 29** Mukhopadhyay, S., Rothenberg, G., Joshi, A., Baidossi, M. and Sasson, Y. (2002) Heterogeneous palladium-catalyzed Heck reaction of aryl chlorides and styrene in water under mild conditions. *Adv. Synth. Catal.*, **344**, 348.
- 30** Beletskaya, I.P. and Cheprakov, A.V. (2000) The Heck reaction as a sharpening stone of palladium catalysis. *Chem. Rev.*, **100**, 3009.
- 31** Rothenberg, G., Cruz, S.C., Van Strijdonck, G.P.F. and Hoefsloot, H.C.J. (2004) Detailed mechanistic studies using *in situ* spectroscopic analysis: a look at little-known regions of the Heck reaction. *Adv. Synth. Catal.*, **346**, 467.
- 32** Grossman, R.B. (2003) *The Art of Writing Reasonable Organic Reaction Mechanisms*, Springer, Berlin, ISBN 0-387-95468-6.
- 33** Guengerich, F.P., Krauser, J.A. and Johnson, W.W. (2004) Rate-limiting steps in oxidations catalyzed by rabbit cytochrome P450 1A2. *Biochemistry*, **43** (10), 775.
- 34** Westerhuis, J.A., Boelens, H.F.M., Iron, D. and Rothenberg, G. (2004) Model selection and optimal sampling in high-throughput experimentation. *Anal. Chem.*, **76**, 3171.
- 35** Tranter, R.L. (2000) *Design and Analysis in Chemical Research*, CRC Press, Sheffield, ISBN 1-85075-994-4.
- 36** Keim, W. (1983) Nickel hydrides: catalysis in oligomerization and polymerization reactions of olefins. *Ann. N.Y. Acad. Sci.*, **415**, 191.
- 37** Müller, U., Keim, W., Krüger, C. and Betz, P. (1989) $[\{\text{Ph}_2\text{PCH}_2\text{C}(\text{CF}_3)_2\text{O}\}\text{NiH}(\text{PCy}_3)]$: support for a nickel hydride mechanism in ethene oligomerization, **28**, 1011.
- 38** Kharasch, M.S., Seyler, R.C. and Mayo, F.R. (1938) Coordination compounds of palladium chloride. *J. Am. Chem. Soc.*, **60**, 882.
- 39** Logadottir, A., Rod, T.H., Norskov, J.K., Hammer, B., Dahl, S. and Jacobsen, C.J.H. (2001) The Brønsted–Evans–Polanyi relation and the volcano plot for ammonia synthesis over transition metal catalysts. *J. Catal.* **197**, 229.
- 40** Jaksic, M.M. (2001) Hypo–hyper-d-electronic interactive nature of interionic synergism in catalysis and electrocatalysis for hydrogen reactions. *Int. J. Hydr. Energy*, **26**, 559–578.
- 41** Whittingham, M.S. (1977) Volcano plots and cyclohexane dehydrogenation. *J. Catal.*, **50**, 549.
- 42** Chianelli, R.R., Pecorado, T.A., Halbert, T.R., Pan, W-H. and Stiefel, E.I. (1984) Transition metal sulfide catalysis: relation of the synergic systems to the periodic trends in hydrodesulfurization. *J. Catal.*, **86**, 226.
- 43** Moulijn, J.A., van Diepen, A.E. and Kapteijn, F. (2001) Catalyst deactivation: is it predictable? What to do? *Appl. Catal. A: Gen.*, **212**, 3.
- 44** van Leeuwen, P.W.N.M. (2001) Decomposition pathways of homogeneous catalysts. *Appl. Catal. A: Gen.*, **212**, 61.
- 45** Collins, T.J. (2002) TAML oxidant activators: a new approach to the activation of hydrogen peroxide for environmentally significant problems. *Acc. Chem. Res.*, **35**, 782.
- 46** Bartos, M.J., Gordon-Wylie, S.W., Fox, B.G., Wright, L.J., Weintraub, S.T., Kauffmann, K.E., Münck, E., Kostka, K.L., Uffelman, E.S., Rickard, C.E.F., Noon, K.R. and Collins, T.J. (1998) Designing ligands to achieve robust oxidation catalysts. Iron based systems. *Coord. Chem. Rev.*, **174**, 361.
- 47** Collins, T.J. (1994) Designing ligands for oxidizing complexes. *Acc. Chem. Res.*, **27**, 279.
- 48** Bartholomew, C.H. (2001) Mechanisms of catalyst deactivation. *Appl. Catal. A: Gen.*, **212**, 17.

- 49 Koltsakis, G.C. and Stamatelos, A.M. (1997) Catalytic automotive exhaust aftertreatment. *Prog. Ener. Combust. Sci.*, **23**, 1.
- 50 Forzatti, P. and Lietti, L. (1999) Catalyst deactivation. *Catalysis Today*, **52**, 165.
- 51 Gunter, P.L.J., Niemantsverdriet, J.W., Ribeiro, F.H. and Somorjai, G.A. (1997) Surface science approach to modeling supported catalysts. *Catal. Rev. – Sci. Eng.*, **39**, 77.
- 52 Stakheev, A.Y. and Kustov, L.M. (1999) Effects of the support on the morphology and electronic properties of supported metal clusters: modern concepts and progress in 1990s. *Appl. Catal. A: Gen.*, **188**, 3.
- 53 Datye, A.K., Xu, Q., Kharas, K.C. and McCarty, J.M. (2006) Particle size distributions in heterogeneous catalysts: what do they tell us about the sintering mechanism? *Catalysis Today*, **111**, 59.
- 54 Arias, H.R. (1996) Luminal and non-luminal non-competitive inhibitor binding sites on the nicotinic acetylcholine receptor. *Molec. Membr. Biol.*, **13**, 1.
- 55 Greig, N.H., Sambamurti, K., Yu, Q-S., Brossi, A., Bruinsma, G.B. and Lahiri, D.K. (2005) An overview of phenserine tartrate, a novel acetylcholinesterase inhibitor for the treatment of Alzheimer's disease. *Curr. Alzheimer Res.*, **2**, 281.
- 56 Boitiaux, J.P., Cosyns, J. and Verna, F. (1987) Poisoning of hydrogenation catalysts. How to cope with this general problem? *Stud. Surf. Sci. Catal.*, **34**, 105.
- 57 Shelef, M., Otto, K. and Otto, N.C. (1978) Poisoning of automotive catalysts. *Adv. Catal.*, **27**, 311.

3

Homogeneous Catalysis

Homogeneous catalysis covers all the systems where the catalyst and the reactant(s) are in the same phase. In this Chapter I will concentrate on liquid-phase homogeneous catalysis, which is the most common situation. Although there are several important all-gaseous catalytic processes (e.g., the chlorine-catalyzed decomposition of atmospheric ozone [1,2]) the bulk of the research focuses on the liquid phase (all-solid catalytic processes are problematic by definition [3]). Note that our definition of “liquid phase” does include reactions where one or more of the reactants is in a gas/liquid or vapour/liquid equilibrium. Figure 3.1 shows two such examples: in catalytic hydrogenation reactions, we simply write the “H₂” in the reaction equation. Although hydrogen is a gas, some of it dissolves in the liquid and participates in the catalytic cycle. Another example is the **hydroformylation reaction**, an important industrial process in which a hydrogen molecule and a C≡O group are added to an alkene [4]. This system typically includes a liquid olefin, a dissolved organometallic complex, H₂ gas, and CO gas. However, because the actual reaction occurs with dissolved hydrogen and dissolved CO, it is classified as a homogeneously catalyzed liquid-phase reaction. In such cases, we will assume that there are no mass-transfer problems, and there is always enough dissolved gas to carry out the reaction.

Although heterogeneous catalysis accounts for more than 90% by volume of all industrial catalytic processes, homogeneous catalysis is catching up. The main advantage of homogeneous catalysis is the high activity and selectivity, which can be tuned by changing the catalyst’s molecular properties. The main disadvantage is the problem of catalyst separation and recovery. This often prevents scientific successes from becoming commercial ones.

3.1

Metal Complex Catalysis in the Liquid Phase

While the term “homogeneous catalysis” pertains to all those reaction systems where the catalyst and the substrate are in the same phase, many chemists identify it with “liquid-phase reactions catalyzed by organometallic complexes.” Indeed, this fast-growing field attracts most of the research effort in homogeneous catalysis. New

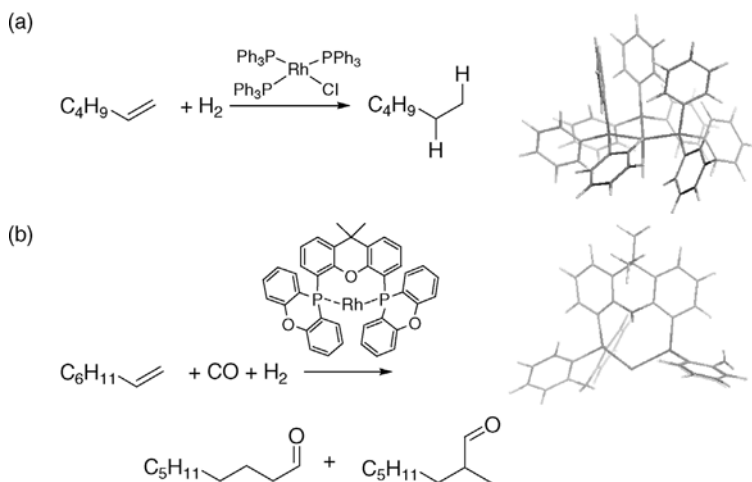


Figure 3.1 **a** Hydrogenation of 1-hexene to hexane in the presence of Wilkinson's catalyst, $\text{Rh}[\text{P}(\text{Ph}_3)_3]\text{Cl}$; **b** hydroformylation of 1-octene to the linear nonanal and the branched 2-methyloctanal [5]. The 3D representations on the right show the crowding around the Rh atom in each case (geometry optimized using molecular mechanics). As we shall see, the ligand's bulk and rigidity often govern the catalytic activity and selectivity.

synthetic protocols, as well as cheaper and better analysis instruments and computational models, play an important role in this. The development of *in situ* IR and NMR analysis techniques enables today's chemist to study reaction kinetics, and examine catalytic intermediates under true reaction conditions. This leads to a better understanding of reaction mechanisms and exciting new reactions. Homogeneous catalysis using organometallic complexes is also advancing into the modern fine-chemicals and bulk-chemicals industry. Significantly, two of the seven Nobel Prizes in chemistry given this century were awarded for achievements in homogeneous catalysis: In 2001 William Knowles [6] and Ryoji Noyori [7] shared the prize with Barry Sharpless [8] for their contributions to asymmetric hydrogenation and oxidation catalysis, respectively. Four years later, Yves Chauvin [9], Robert Grubbs [10], and Richard Schrock [11] shared the prize for their contribution to metathesis catalysis.

This section outlines the elementary steps in homogeneous catalysis using organometallic complexes, showing the role that these steps play in various catalytic cycles and industrial processes.

3.1.1

Elementary Steps in Homogeneous Catalysis

Every catalytic cycle is a sequence of simple chemical reactions. These **elementary steps** are the building blocks from which you can construct the "story behind the reaction" (better known as the reaction mechanism). Understanding these steps is often easier in homogeneous catalysis than in heterogeneous catalysis and

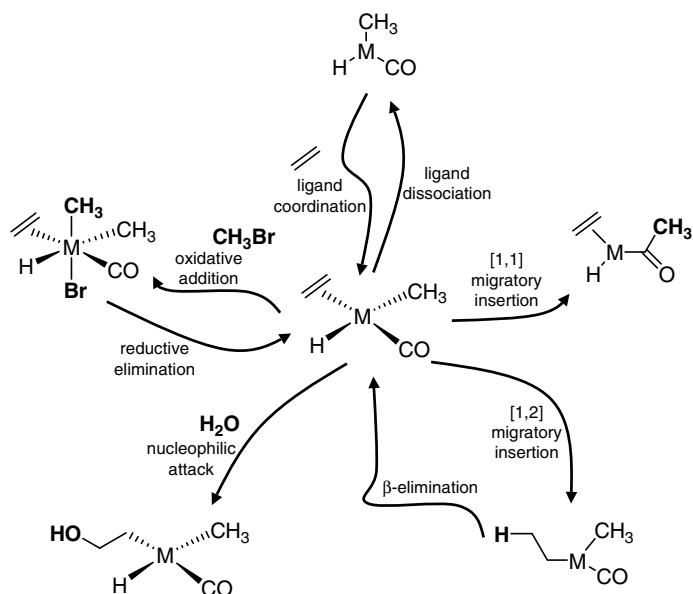


Figure 3.2 The main elementary steps in homogeneous catalysis.

biocatalysis, because the molecular nature of the catalyst simplifies things. Depending on the degree of detail, chemists divide the elementary steps into different categories [12]. Here I will use six main categories, summarized in Figure 3.2: dissociation and coordination; oxidative addition; reductive elimination; insertion and migration; de-insertion and β -elimination; and nucleophilic attack on a coordinated substrate. Most of the reactions fall into one of these categories. Additional, less common reaction types will be dealt with at the end of this section. I assume that you are familiar with the basic concepts of electronic structure, complex formation, electron donors/acceptors, electron counting, oxidation states, and ligand field theory. A detailed explanation of these is given in inorganic chemistry textbooks [13]. For a comprehensive advanced text on organometallic chemistry, see Crabtree's excellent book [14].

3.1.1.1 Ligand Exchange: Dissociation and Coordination

Before any catalysis can occur, at least one of the substrates must coordinate to the catalyst. This means that the catalyst must have a vacant active site. In homogeneous metal complex catalysis and biocatalysis, this will be a vacant coordination site at the metal atom. In heterogeneous catalysis, the vacant site could be a metal crystallite or an ion on the surface. For the latter, we speak of “desorption” and “adsorption” instead of dissociation and coordination. Remember that our reactions are not in vacuum, so there is no “vacant site”. Thus, before any chemical species can coordinate to the metal complex (or to the active site in heterogeneous catalysis or biocatalysis) the species already occupying this space must first vacate it. This happens constantly, as the system is dynamic (Figure 3.3) [15]. At any given moment

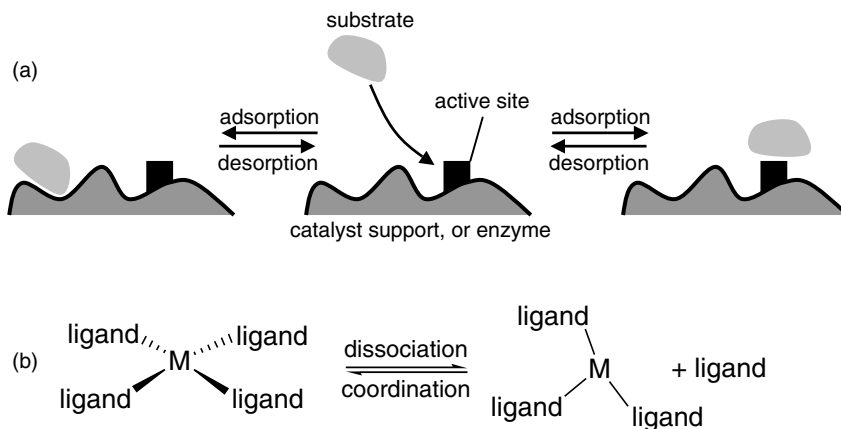


Figure 3.3 **a** Dynamic adsorption/desorption in heterogeneous catalysis and in enzymatic systems occurs both at active sites and elsewhere on the support; **b** similar coordination/dissociation occurs also in homogeneous complexes.

in a heterogeneously catalyzed system, molecules are adsorbed to and desorbed from the catalyst, some at the active site and some elsewhere on the support. The same is also true for enzymatic systems. Similarly, in liquid-phase homogeneously catalyzed reactions, solvent molecules, ligands, and substrates compete for the metal coordination sites.

The high substrate/catalyst ratios mean that there is an excess of substrate (and later, an excess of product) with respect to the catalyst. In homogeneous catalysis there is also often an excess of solvent and sometimes an excess of ligands. All these species vie for coordination at the active site. We have already encountered one such situation in Chapter 2, when we discussed the Michaelis–Menten equation and saturation kinetics. This competition can enhance the rate of reaction, but also retard it. If the active site is always occupied by excess ligand, solvent, or even product, the reaction will stop. Indeed, the rate equation for a catalytic reaction can include a ligand concentration element with negative order. We say in such cases that the ligand inhibits the reaction. A similar thing can happen in heterogeneous catalysis: let us imagine that the two reactants **A** and **B** can both be adsorbed on the catalyst, but the adsorption of **A** is much more exothermic than that of **B**. If we increase the partial pressure p_A , more **A** will be adsorbed, expelling **B** from the surface and preventing the surface reaction between adsorbed **A** and adsorbed **B**. In this case, the rate equation would show a negative order in **A**.

In homogeneous catalysis, one species can also coordinate to the metal *before* the other has left. The two situations (first dissociation, then coordination; or first coordination, then dissociation) are similar to the S_N1 and S_N2 nucleophilic substitution mechanisms. Figure 3.4 illustrates these two cases, using as an example the reaction of the $Ni(CO)_4$ complex with acetone (dimethyl ketone) in THF. In the first case, a CO ligand dissociates from the complex, leaving a vacant position that is immediately filled by a solvent molecule. Then, the solvent is replaced by an acetone

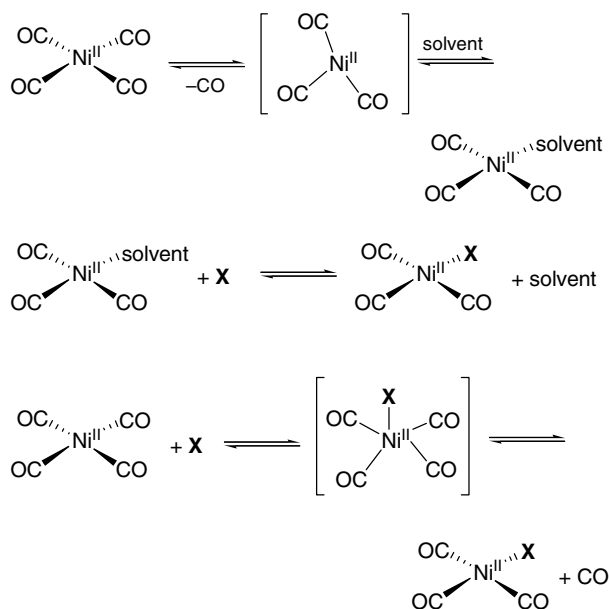


Figure 3.4 a Dissociative and b associative ligand exchange from $\text{Ni}(\text{CO})_4$.

molecule. Both reactions are equilibrium processes. The first step is the rate-determining (slow) step, while the second is fast. This $\text{S}_{\text{N}}1$ -type mechanism is also known as a **dissociative mechanism**, or (**D**). In the second case, the acetone molecule first coordinates to the Ni atom, creating a five-coordinated complex. Immediately, this complex ejects a CO ligand, yielding the $\text{Ni}(\text{CO})_3(\text{acetone})$ product. This $\text{S}_{\text{N}}2$ -type mechanism is also known as an **associative mechanism**, or (**A**). Dissociative mechanisms are common for six-coordinate 18-electron species like $\text{Cr}(\text{CO})_6$. Associative ones are observed for unsaturated species, such as $\text{IrCl}(\text{CO})[\text{P}(\text{C}_6\text{H}_5)_3]_2$ (see below).

3.1.1.2 Oxidative Addition

In **oxidative addition**, a metal **M** inserts into a covalent bond of a compound **X–Y**. The **X–Y** bond is broken and two new bonds form: **M–X** and **M–Y**. The metal “loses” two valence electrons and gains two new ligands, **X** and **Y**. Oxidative addition is a key step in many catalytic cycles. Often, it is the slow (i.e., rate-determining) step, because a covalent bond (usually in the substrate) is broken. This creates a metastable species that easily reacts further in the cycle. Figure 3.5 shows the general scheme for oxidative addition as well as a specific example of the addition of methyl iodide to *trans*- $\text{IrCl}(\text{CO})[\text{P}(\text{C}_6\text{H}_5)_3]_2$. This iridium complex, first prepared by Vaska and Di Luzio in 1961, is known as “Vaska’s complex” [16–18]. It is a 16-electron unsaturated complex which easily undergoes a two-electron oxidative addition with a variety of compounds, giving a saturated 18-electron complex. In this case, the oxidation state of the iridium metal increases from Ir^{I} to Ir^{III} . Note that the starting complex is a 16-electron four-coordinated one with a square-planar structure, while the product complex is 18-electron and octahedral.

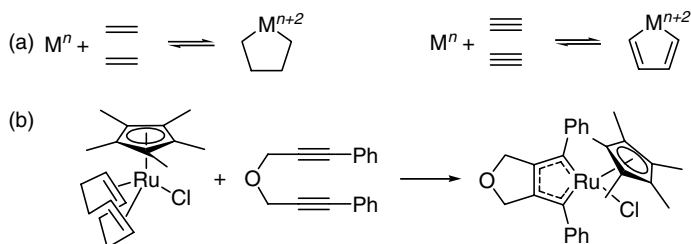


Figure 3.7 **a** Generic equations for cyclometallation; **b** formation of a ruthenacyclopentadiene complex via cyclometallation of a diacetylene.

3.1.1.3 Reductive Elimination

Formally speaking, reductive elimination is the opposite of oxidative addition: Starting from a metal M bonded to X and Y , a new $X-Y$ bond forms and the $M-X$ and $M-Y$ bonds break. The free $X-Y$ species leaves the complex, and the metal loses two ligands and “gains” two valence electrons. Reductive elimination is observed mostly for transition elements, and especially for noble metals such as Pd, Pt, Rh, and Ir in their higher oxidation states (II, III, and IV). In many catalytic cycles, the reactant enters the cycle in an oxidative addition step, and part of it leaves the intermediate in a reductive elimination step [22]. Figure 3.8 shows a generic reductive elimination reaction, and an example of reductive elimination of HCN from a nickel complex.

Reductive eliminations are the equilibrium opposites of the corresponding oxidative additions, based on the principle of microscopic reversibility. Note that while oxidative addition can yield both *cis* and *trans* products, reductive elimination proceeds only from the *cis* configuration. Ligands with electron-withdrawing groups enhance reductive elimination rates, because they stabilize the resulting electron-rich metal center. Conversely, the presence of ligands with electron-donating groups will retard the reductive elimination step. There are examples where the reductive elimination has no known oxidative addition counterpart, because of the high kinetic barrier for adding the “hidden” C–C bond of an alkene to the transition metal center [23]. One such example is the reductive elimination creating new aliphatic C–C bonds shown in Figure 3.9. Here, the energy gained by creating the Pd–ethyl

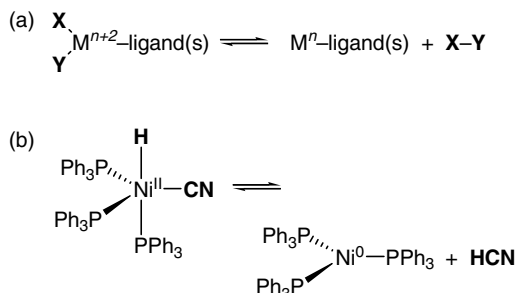


Figure 3.8 **a** Generic reductive elimination reaction; **b** reductive elimination of HCN from a nickel complex.

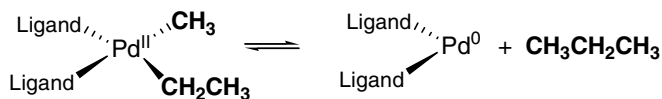


Figure 3.9 Carbon–carbon bond formation via reductive elimination from a palladium complex.

and Pd–methyl bonds does not compensate for the energy lost in breaking the aliphatic C–C bond.

This is a good example that demonstrates why catalysis research is so exciting and important. Discovering the “missing catalyst” which can undergo facile oxidative addition with aliphatic C–C and C–H bonds would have enormous implications for the chemical industry. Alkanes are the most abundant and the cheapest organic starting materials. If we had a catalyst which could activate such bonds, we could use alkanes directly in many industrial processes. Such a catalyst would change the chemical industry all over the world. In many ways, direct C–H activation and alkane functionalization are the “holy grail” of homogeneous catalysis research [24,25].

3.1.1.4 Insertion and Migration

An insertion or migration step involves the introduction of one unsaturated ligand into another metal–ligand bond on the same complex. Insertion and reductive elimination are common bond-forming steps, just as oxidative addition is a common bond-breaking step. The term “insertion” is somewhat problematic, because recent research has shown that in many cases it is the “end group” which migrates to the “inserting group”. The correct term therefore is **migratory insertion**, but many texts still use simply “insertion”. There is a difference between migration and insertion products where chelating complexes are concerned: Insertion changes the positional geometry, migration does not. For example, for the square-planar Pd complex shown in Figure 3.10, CO insertion into the Pd–Me bond results in a *cis* configuration with the ligating P atom. Conversely, migration of the Me group will retain the original *trans* configuration.

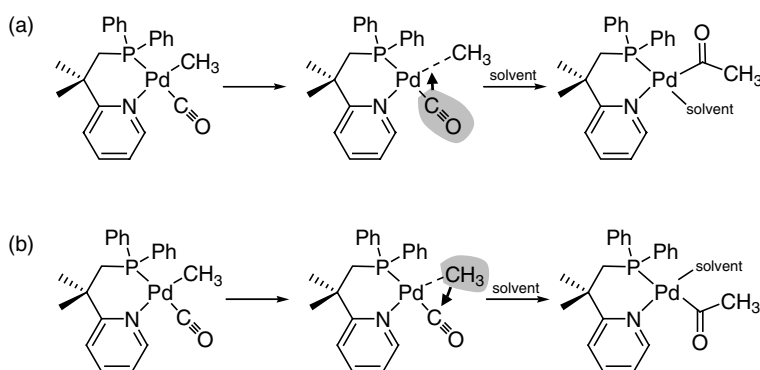


Figure 3.10 Examples of **a** CO insertion and **b** CH₃ migration, in a square-planar Pd complex with a P–N chelating ligand. Note that the migration mechanism retains the *cis* configuration between the CO group and the chelate nitrogen atom.

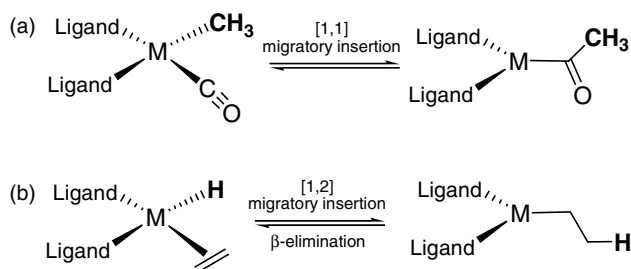


Figure 3.11 Examples of [1,1] and [1,2] migratory insertion reactions.

For (migratory) insertion to occur, the two groups must be in *cis* positions. The metal “loses” one ligand, and a new bond forms between the two old ligands. The common insertion reactions are either [1,1] or [1,2]. In [1,1] insertions, the metal atom and the “end group” end up bonded to the same atom of the “inserting group”. Conversely, in [1,2] insertions, the metal atom and the “end group” end up on adjacent atoms of the “inserting group”. [1,1] insertions are typical of η^1 -bonded ligands such as CO, while η^2 -bonded ligands such as ethene typically undergo [1,2] insertions (Figure 3.11).

3.1.1.5 De-insertion and β -Elimination

De-insertion is simply an insertion in reverse. In the special case where the de-inserting group is an alkene, the reaction is known as a β -hydride elimination (or simply β -elimination). A hydride is abstracted from the β -carbon, giving an alkene and a new M–H or M–R bond (Figure 3.12). Often the reaction proceeds via an agostic intermediate (see Section 3.1.2.2). The metal gains a new ligand (the hydride), and the electron count of the complex increases by two. Insertion creates a vacant site on the complex, while β -elimination requires one, and it must be *cis* to the eliminating group. Insertion and de-insertion reactions are always in equilibrium. In some cases, it is possible to determine this equilibrium using, for example, NMR spectroscopy. Some texts refer to de-insertion (or β -elimination) as extrusion. Alkyl ligands without β -hydrogen atoms may eliminate a hydride from the α , γ , or δ positions.

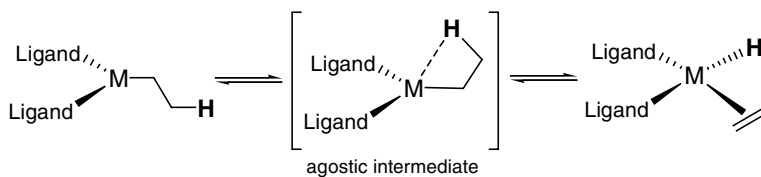


Figure 3.12 Generic equation for β -hydride elimination from a transition metal–alkyl complex.

3.1.1.6 Nucleophilic Attack on a Coordinated Substrate

The electronic properties of a molecule change when it coordinates to a metal center. Importantly, this change can activate the substrate toward nucleophilic or electrophilic attack by another molecule. Activation toward nucleophilic attack is more common because in most cases the coordinating molecule donates electrons to the

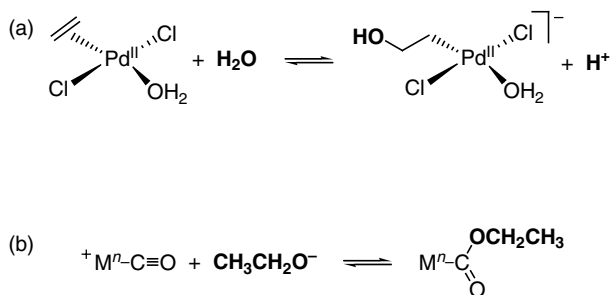


Figure 3.13 **a** Nucleophilic attack of water on coordinated ethene in the Wacker oxidation cycle; **b** attack of ethoxide on coordinated CO.

metal center (in many cases the metal center is positively charged). A good example is the activation of ethene by palladium with subsequent attack by water in the Wacker process for manufacturing acetaldehyde (ethanal) (Figure 3.13a). Coordinated carbon monoxide is another ligand that is susceptible to nucleophilic attack. The product is analogous to that of a migration (or insertion) step (Figure 3.13b). However, the difference is that here the attacking nucleophile is not coordinated to the metal center before the reaction.

3.1.1.7 Other Reaction Types

α -Hydride Elimination and α -Abstraction This reaction is analogous to β -hydride elimination, but here the hydride (or hydrogen atom) is transferred from the α -position of a ligand to the metal center, where it coordinates as a hydride (Figure 3.14a). Note that α -hydride elimination cannot occur in d^0 or d^1 complexes, because it involves a formal oxidation of the metal (just like oxidative addition). Instead, such complexes undergo α -abstraction reactions, where the α -hydrogen transfers directly to an adjacent ligand rather than to the metal center, with no change

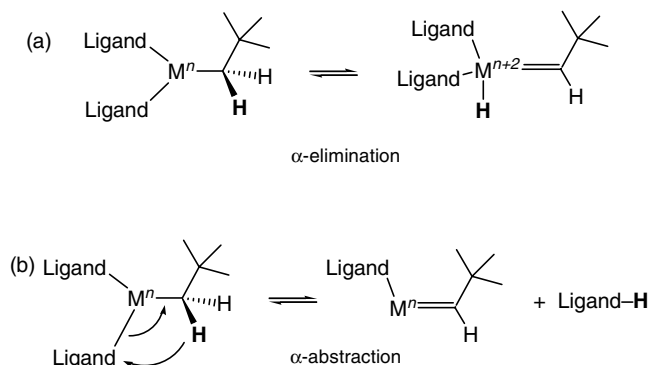


Figure 3.14 Generic examples of **a** α -elimination and **b** α -abstraction.

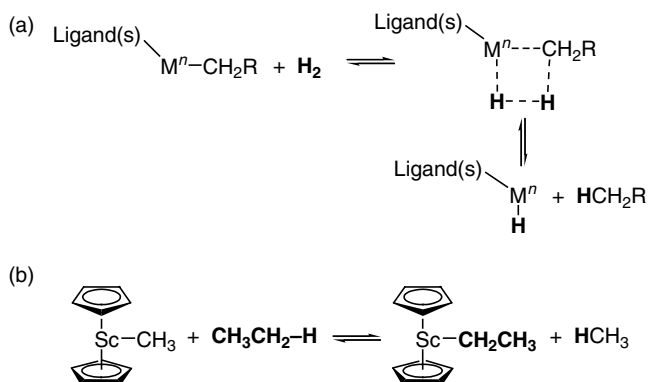


Figure 3.15 a Generic formula and b example of α -bond metathesis.

in the metal oxidation state (Figure 3.14b). α -Abstraction reactions are known for several early transition metals such as Ta, Nb [26], Ti [27,28], and Zr in their highest oxidation state (d^0) [29,30]. They are used for synthesizing alkyldiene complexes (“Schrock carbenes”) and alkyldiyne complexes [31], which are used as metathesis catalysts [32].

σ -Bond Metathesis This reaction is analogous to the classic metathesis reaction [33]. Instead of switching between the two alkenes, however, a σ bond from an incoming ligand replaces the σ bond of an existing ligand (Figure 3.15). It is basically a [2 + 2] addition followed by a [2 + 2] dissociation, with a four-center intermediate. The incoming ligand is most often a hydrocarbon or a hydrogen molecule. σ -Bond metathesis does not change the metal oxidation state. Although it is known for both early and late transition metal alkyl complexes, it is more common with d^0 transition metals. This is because such complexes cannot exchange ligands via oxidative addition. Lanthanide complexes are also prone to this reaction, because they are usually stable in their M^{3+} oxidation state. Note that although the pathway differs, the final result of σ -bond metathesis is equivalent to oxidative addition followed by reductive elimination.

Orthometallation This is an electrophilic substitution reaction which occurs when the metal is already bonded to the adding molecule (Figure 3.16) [34,35]. In the orthometallation of aromatic rings, the C–H at the *ortho* position is substituted by the metal via a Wheland-type intermediate, forming a cyclic organometallic intermediate that can react further with an alkene [36]. This yields the original metal complex plus a product with a new C–C bond. In orthometallation, the formal oxidation state of the metal center does not change. Orthometallation reactions that result in the activation of C–H, C–C, or C–F bonds are especially noteworthy, because these are strong bonds with a limited chemical reactivity. Such reactions are known with Pd^{II} [37], Ru^{II} , and Rh^{I} [38].

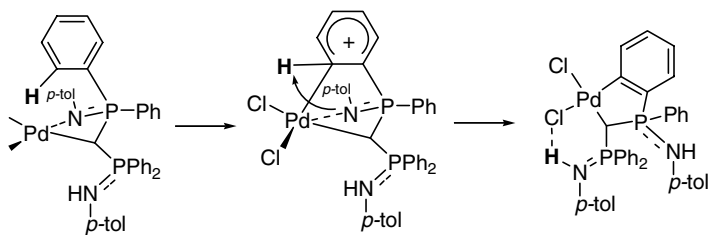


Figure 3.16 Orthometallation of a Pd-organoimine complex.

3.1.2

Structure/Activity Relationships in Homogeneous Catalysis

The metal and its immediate environment (i.e., the ligands and the solvent) are the crucial factors which control the catalytic activity. We can try and quantify these factors by studying the reaction kinetics, drawing catalytic cycles, and (hopefully) predicting the outcome for new metal–ligand complexes [39]. Understanding the chemical meaning behind these factors is like solving a cryptic crossword puzzle – it often looks impossible at first, but once you find the right answer you know that it is the right one. In this section, I will give a qualitative outline of the key structure/activity concepts in homogeneous catalysis. Chapter 6 gives a detailed quantitative treatment of these concepts using descriptor models and statistical analysis methods. In general, we can divide the structure/activity effects into two classes: steric effects and electronic effects (stereo-electronic interaction factors will be discussed in Chapter 6). This simple and rather rough division works surprisingly well, and, importantly, makes it easy for us to understand because it tallies with what “chemical intuition” tells us.

3.1.2.1 Steric Effects: Ligand Size, Flexibility, and Symmetry

Let us start by examining the main steric factors of size, flexibility, and symmetry [40]. The ligand size is important simply because the space around the metal center is limited. If the ligand(s) occupy too much of this space, the substrate cannot coordinate. Ligand dissociation frees part of the space around the metal, creating a **reaction pocket**. The size of this reaction pocket depends on the size of the remaining ligands. Figure 3.17 shows the structures of $\text{Ni}[\text{P}(\text{Ph})_3]_4$ (no access to the Ni atom) and $\text{Ni}[\text{P}(\text{Ph})_3]_3$. Calculating the size of a ligand is difficult, especially for large and unsymmetrical ligands. Chadwick Tolman, an American chemist working at Du Pont Central Research, proposed in the 1970s a general measure for the size of phosphorus ligands [41]. He used a cone that encompasses the ligand, with the metal center in its apex and the P atom situated 2.28 Å away from it (Figure 3.18). This measure, known as **Tolman’s cone angle**, θ , uses the van der Waals radii and gives good correlations for symmetric PR_3 ligands. Cone angle values typically range from 87° for $\text{L} = \text{PH}_3$ all the way up to 212° for $\text{L} = \text{P}(\text{mesityl})_3$. Tolman’s cone angle model is elegant, intuitive and simple, but it also has limitations. Substituents groups on ligands bound to the same metal center may mesh, permitting closer packing than

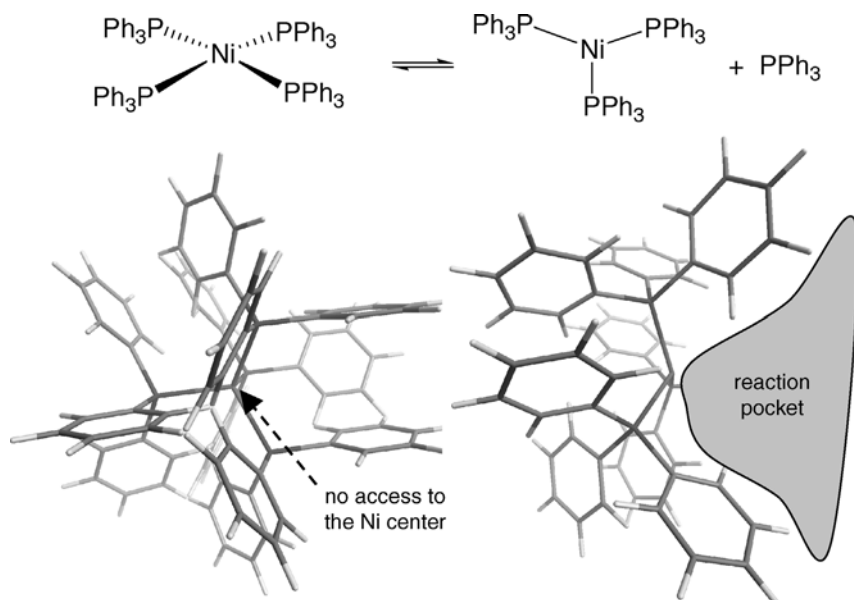


Figure 3.17 Schematic drawing and 3D structure of Ni[P(Ph)₃]₄, also showing the reaction pocket created by the dissociation of one of the triphenylphosphine ligands.

would be expected from cone angle values. Moreover, when the ligand environment is crowded, low-energy bending distortions can occur. Another problem is that ligands rarely form perfect cones; in some cases the part near the metal center is important, while in others a section far from the metal plays a determining role.

There are several modifications and extensions of the cone angle concept. These include mathematical methods, calculations based on X-ray structural data [42,43], and solid angle measurements [44–46]. White and coworkers proposed in 1993 the **ligand bulk radius**, R_{\max} , the **solid angle**, Ω_{\max} , and the **sphere occupation** parameters (Figure 3.19) [47,48]. Here the ligand size is viewed as a radial distribution function [49], measured along a growing sphere that is centered on the metal atom. This creates a steric profile in which the sphere radius is correlated with the bulk of the ligand. R_{\max} is the distance between the metal atom and the bulkiest cross-section of the ligand. This measure gives a better representation of the 3D structure of the complex than the cone angle. Ω_{\max} is the solid angle at this cross-section. For calculating the solid angle, the ligand atoms are projected onto the metal surface and the portion of the surface covered is determined [50]. The sphere occupation parameter, S_{occ} , measures the percentage of the approach sphere occupied by the ligand. The larger S_{occ} , the smaller the reaction pocket.

Ligand size can influence the coordination/dissociation equilibrium dramatically. This is extremely important, as the dissociation of a ligand is often the step that transforms the catalyst precursor into the active catalytic species. Figure 3.20 shows the dissociation equilibrium for NiL₄ complexes with different phosphite ligands. Although the difference in the cone angles is small, changing from P(O-*p*-tolyl)₃

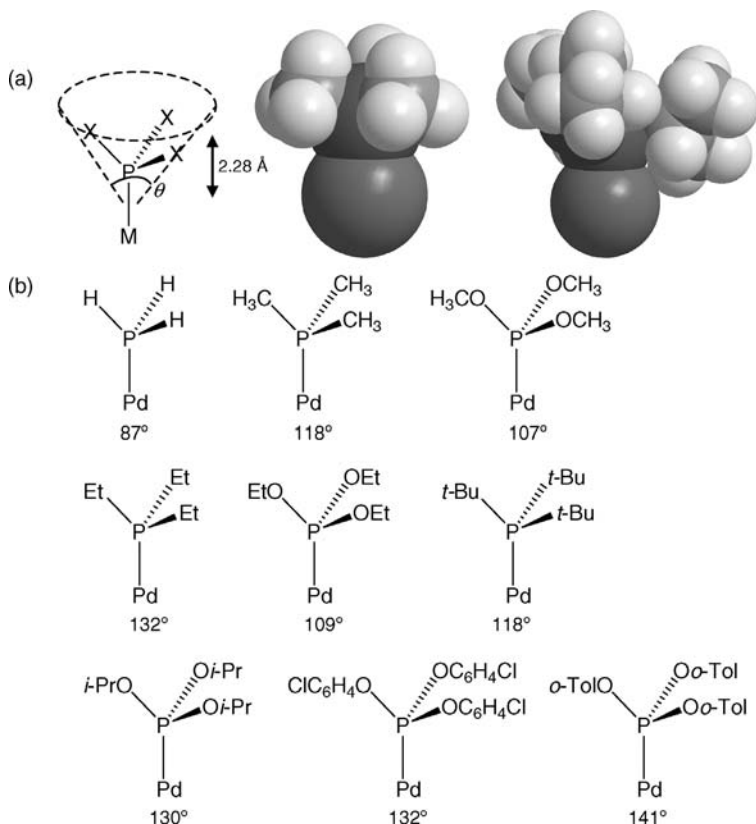


Figure 3.18 a Schematic drawing and space-filling model showing the calculation of the cone angle for symmetric and nonsymmetric ligands; b examples of some ligands with their respective cone angle values.

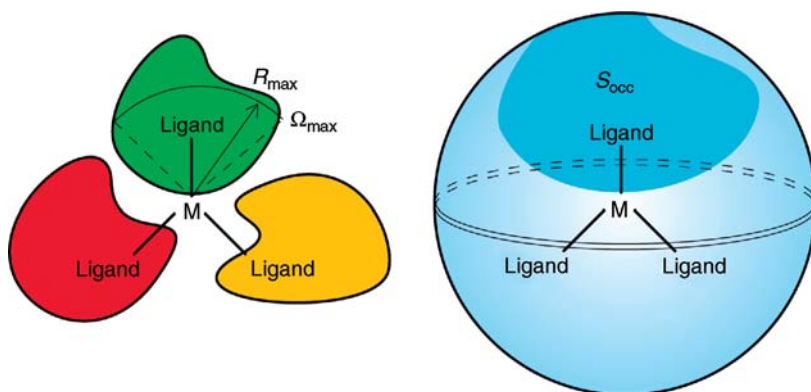


Figure 3.19 Schematic representation of the bulk radius R_{\max} , the solid angle Ω_{\max} , and the sphere occupation parameter S_{occ} .

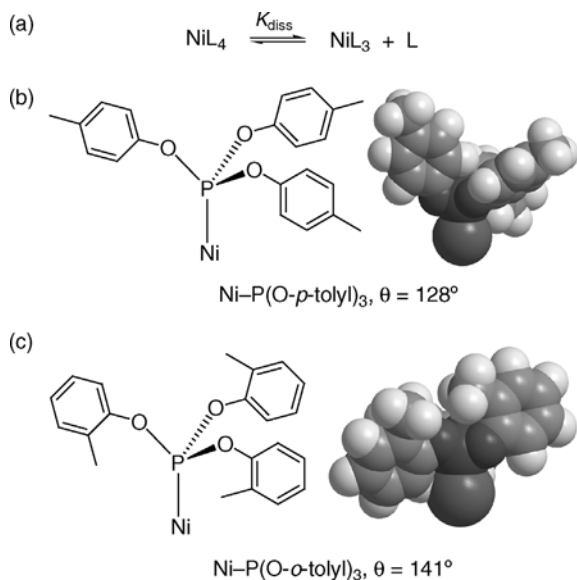


Figure 3.20 a Ligand dissociation equilibrium from a nickel complex, and corresponding structures and space-filling models of the b *p*-tolyl- and *o*-tolylphosphite ligands. The 3D models show the larger cone angle forced by the ortho methyl groups.

($\theta = 128^\circ$) to P(O-*o*-tolyl)₃ ($\theta = 141^\circ$) increases the dissociation equilibrium constant by eight orders of magnitude! Indeed, thanks to the severe **steric crowding**, it was possible to isolate and identify the unsaturated NiL₃ and NiL₂ complexes in the case of P(O-*o*-tolyl)₃ [51,52].

The concept of ligand sterics was extended to bidentate (chelating) ligands also. In this case the key parameter is the **ligand bite angle** α , highlighted by the Dutch chemist Piet van Leeuwen (Figure 3.21) [53,54]. This angle can be measured experimentally or calculated with molecular modeling techniques [55]. It correlates well with the product yield for several catalytic reactions [56–58]. Generally, the larger the bite angle, the more space the chelating ligand occupies, and consequently the smaller the reaction pocket [59]. The value of α is a compromise between the ligand's preferred bite angle and the type and number of d orbitals available from the metal. Another parameter for characterizing bidentate ligands is their **flexibility** (Figure 3.21b). This is the range of bite angle values for ligand geometries with energies slightly above that of the minimized structure (structures with energies within 3 kcal mol⁻¹ of the minimum are considered to be in the flexibility range). In the Xantphos example, square-planar complexes are disfavoured (10 kcal mol⁻¹ above the minimum), while tetrahedral and trigonal-bipyramidal ones are closer to the minimum energy and therefore more likely. The ligand flexibility is a theoretical parameter. Unlike the bite angle, it cannot be measured experimentally. The flexibility can be seen as the ability of a ligand to change its bite angle (and consequently its coordination state) in the course of the catalytic cycle.

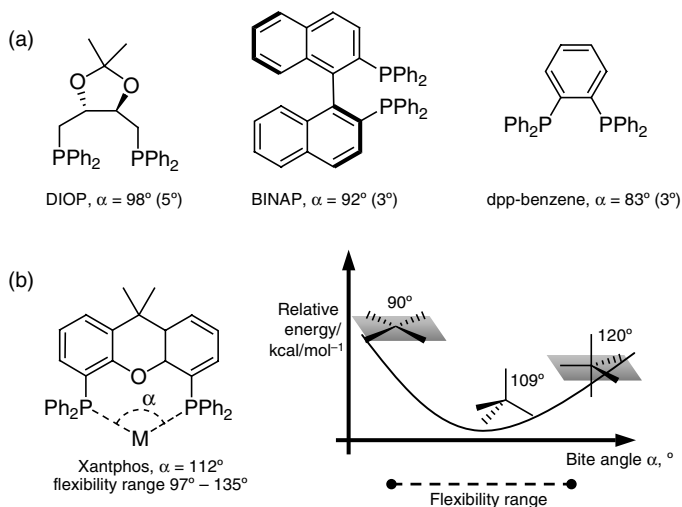


Figure 3.21 a Examples of bidentate phosphine ligands and their corresponding bite angles (the numbers in parentheses show the standard deviation for the angles calculated using various methods [55,60]); b a flexibility profile for the Xantphos ligand, showing how the energy changes with the bite angle.

The symmetry of the ligand can influence the product stereoselectivity and enantioselectivity. Enantiomerically pure chemicals are extremely important for the agrochemical, pharmaceutical, and food industries. Many of the bidentate ligands used in these processes feature C_2 -type symmetry, dividing the space around the metal center into two “empty quadrants” and two “full quadrants” (see Section 3.1.3 on asymmetric homogeneous catalysis) [61,62]. Ligand symmetry is also important in polymerization catalysis [63], where it can influence the polymer’s tacticity (Figure 3.22).

3.1.2.2 Electronic Effects of Ligands, Substrates, and Solvents

Any species that coordinates to the metal center can change the electron density of the metal by “pushing” or “pulling” electrons [64]. This is especially important in elementary steps that involve a change in the metal oxidation state, such as oxidative addition and reductive elimination. Tolman quantified the electronic effects of phosphorus ligands by measuring the symmetric stretching vibration frequency of the corresponding $M(L)(CO)_{n-1}$ complexes [65]. The stretching vibration of the C–O *trans* to the ligand L depends on whether the ligand is a σ -donor or a π -acceptor (Figure 3.23). A strong σ -donor ligand will increase the electron density at the metal center. This in turn will result in more back-donation to the C–O antibonding π^* orbital, weakening the C–O bond and shifting the C–O stretch to longer wavelengths. Conversely, a strong π -acceptor ligand will decrease the electron density at the metal center, resulting in less back-donation to the C–O antibonding π^* orbital, and shifting the C–O stretch to lower wavelengths. Thus, the electronic effects of phosphorus ligands (and other homologous series of ligands) can be compared using the C–O bond stretch frequencies, provided the comparison is made for a particular metal.

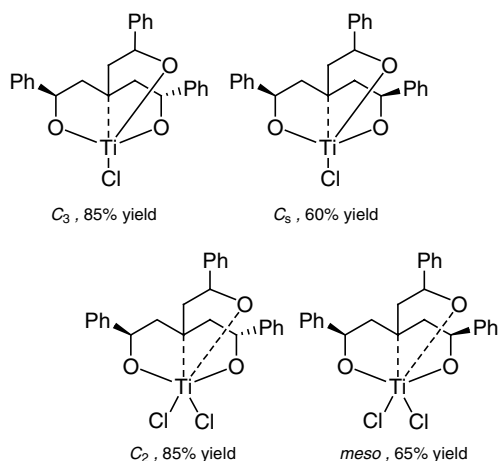


Figure 3.22 Structures of four similar titanium catalyst precursors with different symmetries, used in the polymerization of 1-hexene, and the corresponding isotactic poly(hexene) product yields.

Although C–H bonds are relatively inactive, hydrogen atoms of coordinated alkyl species do interact with the metal center [66]. This three-way C–H–M bond is called an **agostic interaction** (from the Greek $\alpha\gamma\sigma\tau\omicron\zeta$, to hold on to oneself) [67]. Agostic interactions are known for many complexes (Figure 3.24) [68,69], and feature in several important elementary steps, such as reductive elimination. They are more common with d^0 metal centers [70].

3.1.3

Asymmetric Homogeneous Catalysis

The biggest impact of homogeneous catalysis is in the synthesis of chiral molecules, especially of enantiomerically pure products. Most natural products are chiral, and in many cases different enantiomers exhibit radically different properties. Moreover,

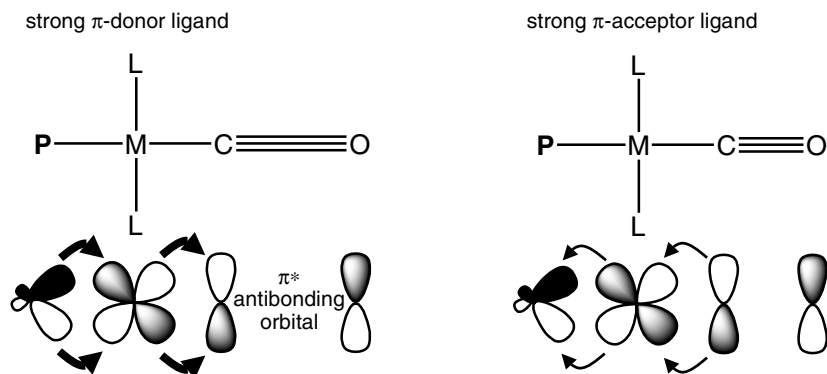


Figure 3.23 How the ligand donor/acceptor properties influence the C–O bonded *trans* to this ligand.

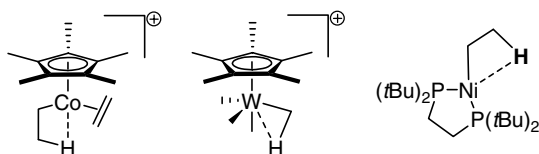


Figure 3.24 Examples of organometallic complexes of Co, W, and Ni which exhibit agostic interactions.

different enantiomers can cause completely different effects *in vivo*. Perhaps the most compelling example is that of the drug **thalidomide**, administered in racemic form as a sedative to pregnant women in the 1960s. Of the two enantiomers (Figure 3.25), (*R*)-Thalidomide was indeed a sedative, but (*S*)-thalidomide was a teratogenic compound that caused malformations in the fetuses. This tragic case led to strict regulations on the testing of enantiomers [71], and boosted the search for methods for making enantiopure products. In 2000, worldwide sales of enantiomerically pure products topped €90 billion (\$120 billion). Incidentally, it was shown later that in the specific case of thalidomide, using the pure (*R*) compound would not have solved the problem because it racemizes *in vivo*.

Apart from using asymmetric catalysis, there are two other approaches for making enantiopure compounds. The first is to use biochemical processes. These are becoming increasingly popular as our understanding of enzymes and our degree of control over enzymatic reactions improves (see Chapter 5 for details). Nevertheless, today's enzymatic processes are still limited in their reaction conditions and by their specificity – you need the right enzyme for converting your substrate. Another limitation of enzymes is that they cannot catalyze the synthesis of “unnatural products,” such as *D*-amino acids or other unnatural isomers.

The second alternative is first to make the racemate, and then to resolve the desired enantiomer. However, such resolution is often time-consuming, laborious, and (for industry) very expensive. Conversely, asymmetric homogeneous catalysis gives access to a wide range of enantiopure organic substances from achiral precursors. The chiral catalyst complex directs the orientation of the substrate, giving preference

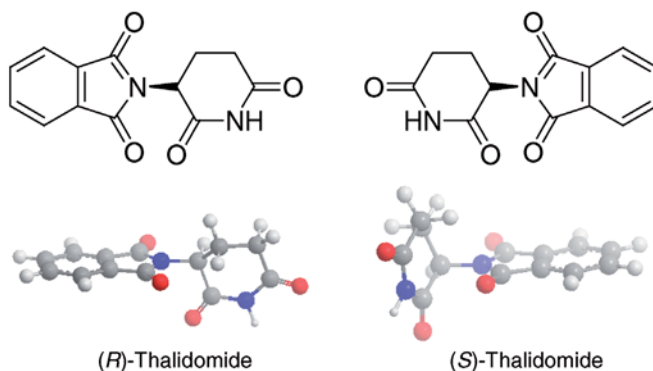


Figure 3.25 Chemical structures and optimized geometries of (*R*)- and (*S*)-thalidomide.

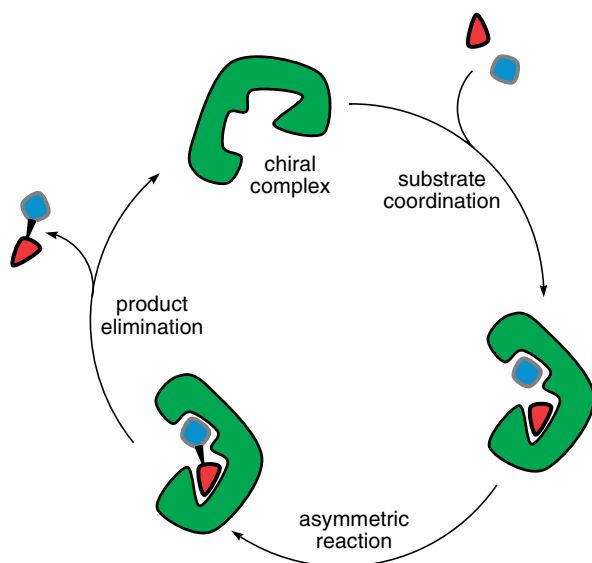


Figure 3.26 The concept of asymmetric catalysis using an organometallic complex with a chiral ligand.

to one product enantiomer over the other (Figure 3.26). Enantioselectivity ranges from 50:50 (0% *ee*, nonselective reaction) to 100:0 (100% *ee*, enantiospecific reaction). The metal atoms are achiral, so the chirality must come from the ligands.

One of the earliest examples of such catalysis was demonstrated in 1966 by the Japanese chemist Hitosi Nozaki, who reacted styrene and ethyl diazoacetate in the presence of a chiral Schiff base–Cu^I complex [72–74]. Although the initial enantioselectivity was modest (<10% *ee*), the principle was proven. Some years later, the companies Sumitomo and Merck used similar copper catalysts for asymmetric cyclopropanation on a multikilogram scale, in the production of various insecticides and antibiotics [75]. One of Nozaki's PhD students at that time was Rioji Noyori, who later developed the BINAP asymmetric hydrogenation catalysts for which he received the 2001 Nobel Prize in Chemistry [7].

On the other side of the Pacific, William Knowles and his colleagues at Monsanto discovered that chiral phosphane ligands can catalyze the asymmetric hydrogenation of enamide double bonds [62]. Fortunately for them, just then a new prodrug for treating Parkinson's disease came on the market: A relatively rare amino acid, 3,4-dihydroxy-*L*-phenylalanine (*L*-DOPA; see Figure 3.27a). Unlike dopamine, *L*-DOPA can cross the blood–brain barrier, and then metabolize to dopamine in the brain. Knowles screened several chiral phosphane ligands, believing that the P atom itself must be the asymmetric center. In 1972, however, the French chemist Henry Kagan disproved this with DIOP, demonstrating the efficiency of bidentate ligands with chiral backbones [76]. Monsanto finally settled on a bidentate chiral phosphane, (*R,R*)-DiPAMP, which yielded *L*-DOPA with 95% *ee*. Although these catalysts were expensive, they had such high TOFs that the substrate/catalyst ratios used were as high as 20 000:1. Moreover, the chiral hydrogenation product crystallized nicely out of

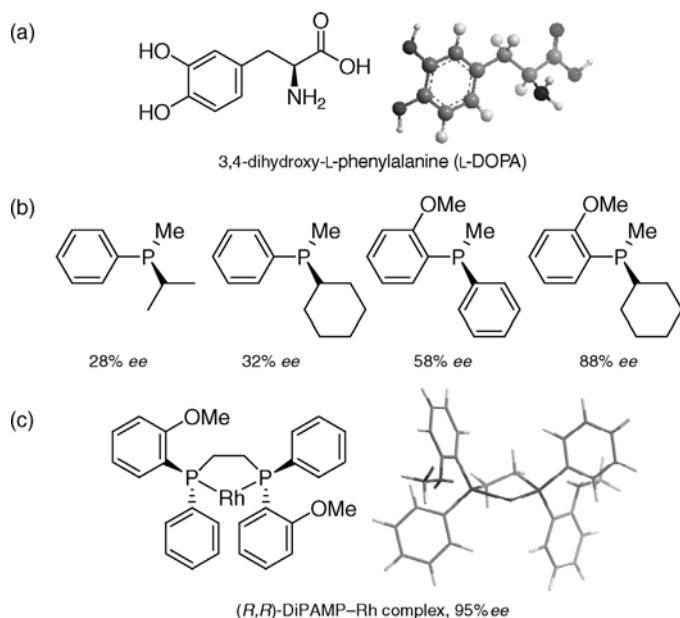


Figure 3.27 a Chemical structure and 3D representation of L-DOPA; b of the chiral ligands tested by Monsanto with their corresponding *ee* values; c the Rh complex used in the large-scale commercial process.

the reaction mixture, leaving the catalyst and remaining reactant in the mother liquor. The new route competed successfully with the racemate resolution route of Hoffman–La Roche, and L-DOPA became the first large-scale pharmaceutical manufactured by asymmetric homogeneous catalysis. Monsanto's success with L-DOPA inspired other companies to invest in large-scale homogeneous asymmetric catalytic processes, including the 10 000 tons per year Metolachlor process of Ciba–Geigy discussed in Section 3.1.4.4.

Noyori's BINAP catalysts deserve special attention because their chirality is based on the bulkiness of the naphthalene groups, rather than on carbon or phosphorus asymmetric centers (Figure 3.28, inset) [77]. One of the many examples of asymmetric catalysis using BINAP is the synthesis of (–)-menthol, an important additive for flavors, fragrances, and pharmaceuticals. Starting from myrcene, the process is carried out by Takasago International on a multi-ton scale. The key step is the isomerization of geranyldiethylamine to (*R*)-citronellal enamine [78], which is then hydrolyzed to (*R*)-citronellal with nearly 99% *ee*.

3.1.4

Industrial Examples

An increasing number of industrial processes use homogeneous catalysis. In this section, I highlight four examples which demonstrate the utility of homogeneous

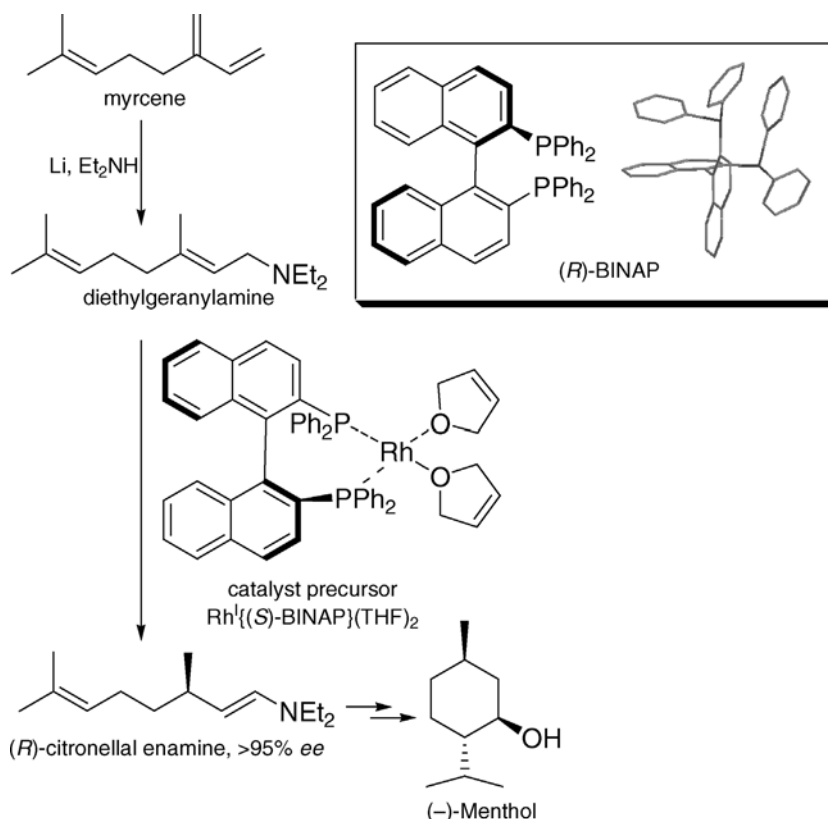


Figure 3.28 An (S)-BINAP–Rh complex catalyzes the asymmetric isomerization step in the synthesis of (–)-menthol from myrcene. The inset shows the chemical structure and 3D representation of the (R)-BINAP ligand (2,2'-bis(diphenylphosphanyl)-1,1'-binaphthyl; hydrogen atoms are omitted for clarity). Note that BINAP ligands contain no asymmetric atoms, but the entire molecule has a C_2 symmetry due to the high barrier for rotation around the naphthyl–naphthyl bond.

catalysis across the board, from bulk chemicals to pharmaceuticals. In all these cases (and many more) the use of homogeneous catalysis has led to cleaner, simpler, and safer processes. One reason for choosing these examples is that, unlike many industrial processes, they are well documented in the primary literature. The references provide additional technical details, as well as insight into the decision-making process which turned the scientific discoveries into large-scale industrial processes.

3.1.4.1 The Shell Higher Olefins Process (SHOP)

The Shell higher olefins process, or SHOP, is one of the most important large-scale processes in the chemical industry which uses homogeneous catalysis [79]. In this process, ethene is oligomerized to medium- and long-chain α -olefins. The products

are used worldwide as monomers (C_4 – C_{10}) and plasticizers (C_6 – C_{10}), as well as for manufacturing biodegradable detergents (C_{12} – C_{20}). The overall process combines oligomerization, isomerization, and metathesis steps. This gives an important advantage, because the α -olefins market demand often changes, and production must track these changes. The SHOP can be adapted to market demands because it produces a controlled distribution of α -olefins. If the current monomers market demands, for example, C_4 – C_{10} olefins, these are recovered by distillation, while the remainder are isomerized and metathesized to C_{11} – C_{20} . This fraction is then sold to the biodegradable detergents market.

The catalytic cycle of the oligomerization process is based on a homogeneous nickel complex [80]. Keim et al. showed that the catalyst precursor can be any one of a number of complexes. These usually include a phosphorus–oxygen chelate, e.g., the η^3 -(C_8H_{13})((C_6H_5)₂PCH₂COO)Ni complex **A** shown in Figure 3.29a [81,82]. In the first step, the catalyst precursor converts to the active catalytic intermediate, a nickel hydride complex. This is followed by a sequence of ethene insertions (propagation steps). At each stage, the olefin product can undergo β -elimination, giving an oligomer of a different length and regenerating the original nickel hydride complex. By studying many different nickel complexes, Keim showed that the “chelate part” of

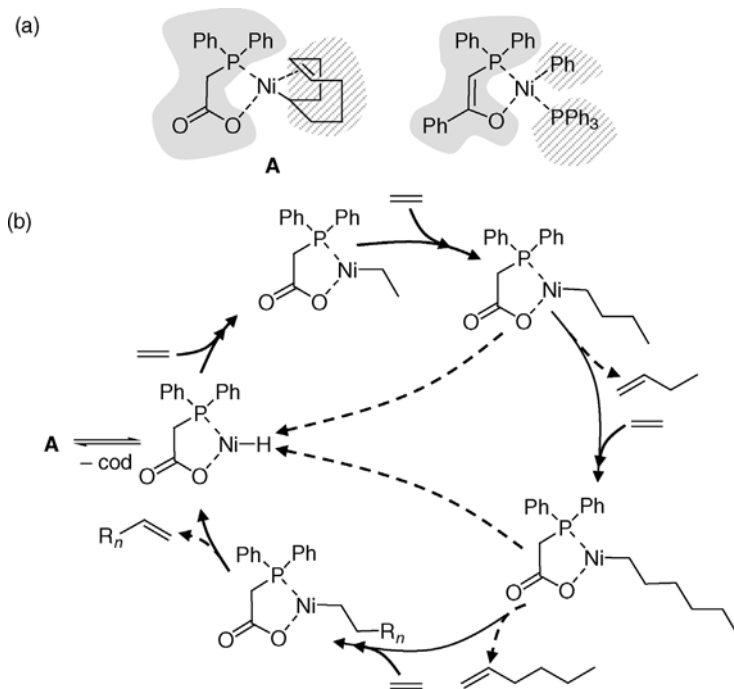


Figure 3.29 a Two examples of nickel catalyst precursors, highlighting the “chelate part” and the “organic part”; b a simplified catalytic cycle for the SHOP oligomerization step (the reverse reaction arrows are omitted, for clarity).

the complex controls the product selectivity (i.e., the oligomer length), while the “organic part” stabilizes the complex [80,83,84].

3.1.4.2 The Wacker Oxidation Process

In the late 1950s, researchers at the *Consortium für Elektrochemische Industrie* discovered that passing a mixture of ethene, hydrogen, and oxygen over heterogeneous Pd/C yielded acetaldehyde (ethanal) [85,86]. This discovery led ultimately to the homogeneous Wacker oxidation process for oxidizing olefins to carbonyl compounds. As we shall see, the process combines two catalytic cycles and uses two homogeneous catalysts. In the decades that followed, the Wacker process became increasingly important, as it provided a simple route to acetaldehyde which was used for making acetic acid (ethanoic acid). When the methanol carbonylation route to acetic acid was developed, the industrial importance of the Wacker process declined. Nevertheless, the Wacker oxidation is an excellent example for demonstrating the concept of catalyst regeneration and dual-catalyst cycles.

The Wacker process has three main steps. In the first step, ethene reacts with a Pd^{II} salt and water to give acetaldehyde, Pd⁰, and two protons. In the second step, Pd⁰ is re-oxidized by two equivalents of Cu^{II}, giving Pd^{II} and two equivalents of Cu^I. Finally, the Cu^I is re-oxidized by oxygen under acidic conditions, giving one equivalent of water and the regenerated Cu^{II} salt. As Figure 3.30 shows, all three steps are stoichiometric reactions, but taken together they form a dual-catalytic cycle. Note that although the net reaction is indeed the oxidation of ethene with oxygen to acetaldehyde, the oxygen atom in the acetaldehyde molecule does not come from the dioxygen molecule, but rather from the water!

The catalytic cycle for the Pd part is shown in Figure 3.31, which also demonstrates several of the elementary steps covered in Section 3.1. We start with [Pd^{II}Cl₄]²⁻ as the catalyst precursor. Exchange of two of the chloride ligands for ethene and water is

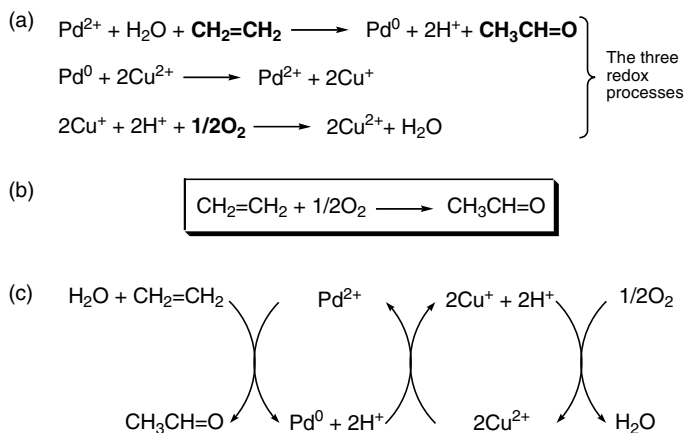


Figure 3.30 **a** The three stoichiometric redox reactions and **b** the net reaction of the Wacker oxidation system; **c** a simplified representation of the Pd and the Cu catalytic cycles (the “reverse reaction” arrows are omitted, for clarity).

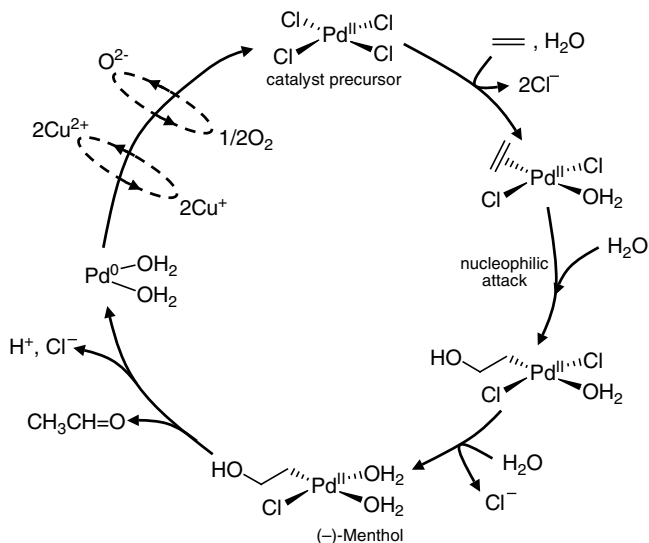


Figure 3.31 Simplified schematic of the palladium Wacker catalytic cycle for oxidizing ethene to acetaldehyde (the “reverse reaction” arrows are omitted, for clarity). The broken circles represent the copper and oxygen redox cycles.

followed by nucleophilic attack of water on the coordinated ethene. This nucleophilic attack is the “trademark” of Wacker-type oxidations. Another chloride ligand is then exchanged by water, followed by β -hydride abstraction and coordination of the vinyl alcohol. The vinyl group then inserts into the Pd–H bond, the last chloride is exchanged for water, and the product together with a proton is eliminated from the complex, giving a $\text{Pd}^0(\text{H}_2\text{O})_2$ species [87]. These last steps are complicated, because the product does not form simply by elimination and subsequent tautomerization of vinyl alcohol (ethenol). When the reaction was performed in D_2O , the acetaldehyde product contained no deuterium atoms (vinyl alcohol and D_2O undergo fast H/D exchange, so this rules out any vinyl alcohol intermediate) [88].

The exact catalytic cycle is still under debate [89]. Studies of model compounds provide insight into the mechanism, but these model reactions differ from the actual catalytic cycle, and so may follow a different mechanistic pathway [90–92]. Kinetic studies show that the conversion of ethene follows the rate law in Eq. (3.1). This supports a pre-equilibrium that involves the dissociation of two chloride ions and one proton, thus explaining the sensitivity of the reaction to the presence of chloride ions.

$$\text{rate} = \frac{d[\text{C}_2\text{H}_4]}{dt} = k \frac{[\text{Pd}^{\text{II}}][\text{C}_2\text{H}_4]}{[\text{H}^+][\text{Cl}^-]^2} \quad (3.1)$$

3.1.4.3 The Du Pont Synthesis of Adiponitrile

Hexane dinitrile (adiponitrile; ADN, $\text{NC}-(\text{CH}_2)_4-\text{CN}$), is a key intermediate in the manufacture of nylon 6.6, the most important polyamide. It is made via double

hydrocyanation of butadiene, in one of the largest industrial processes involving homogeneous catalysis. The product is hydrogenated to the nylon monomer hexamethylenediamine (hexane-1,6-diamine, $\text{H}_2\text{N}-(\text{CH}_2)_6-\text{NH}_2$). The Du Pont adiponitrile process is especially interesting, because the research on this process in the 1960s and 1970s also highlighted several important concepts in homogeneous catalysis and organometallic chemistry [93]. These include the 16/18 electron rule, the ligand cone angle, and the importance of ligand steric and electronic effects [94].

The nickel-catalyzed hydrocyanation of butadiene is a two-step process (Figure 3.32). In the first step, HCN is added to butadiene in the presence of a nickel-tetrakis(phosphite) complex. This gives the desired linear product, 3-pentenenitrile (3PN), and an unwanted branched by-product, 2-methyl-3-butenitrile (2M3BN). The products are separated by distillation, and the 2M3BN is then isomerized to 3PN. In the second step, 3PN is isomerized to 4PN (using the same nickel catalyst), followed by anti-Markovnikov HCN addition to the terminal double bond. The second step is further complicated by the fact that there is another isomerization product, $\text{CH}_3\text{CH}_2\text{CH}=\text{CHCN}$ or 2PN, which is thermodynamically more stable than 4PN. In fact, the equilibrium ratio of 3PN/2PN/4PN is only 20:78:1.6. Fortunately, the reaction kinetics favor the formation of 4PN [95].

The catalytic cycle for the first hydrocyanation step involves several elementary reactions (Figure 3.33). Note the π -allyl complex **B** that forms when butadiene adds to the nickel hydride intermediate **A**. In this case, the relative rates of the two reductive elimination pathways from **B** determine the linear/branched product distribution. As we saw above, the ligand size is important for the dissociation/coordination equilibria. Switching between Ni^0 and Ni^{II} involves a change in complex geometry, from tetrahedral to square-planar, respectively. Larger phosphite ligands can destabilize the square-planar configuration, promoting reductive elimination and

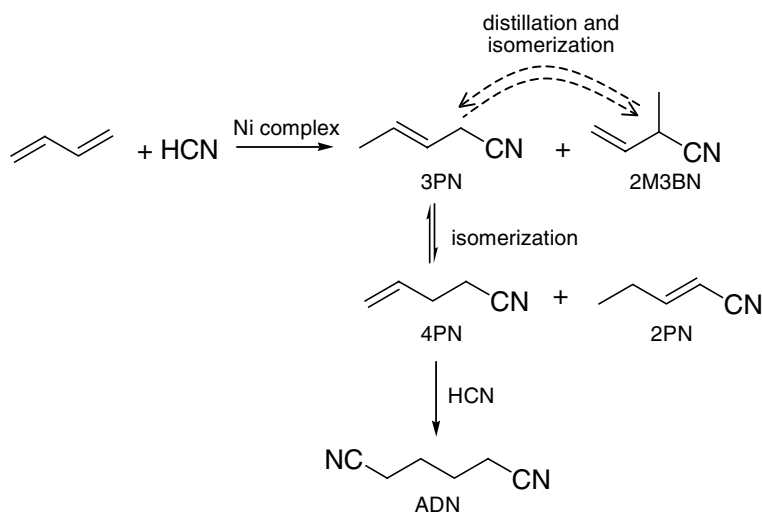


Figure 3.32 The two-step Ni-catalyzed hydrocyanation of butadiene.

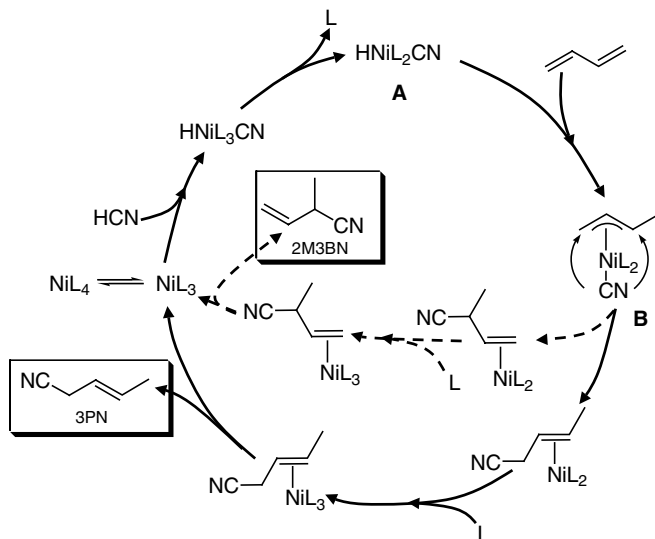


Figure 3.33 The hydrocyanation catalytic cycle, starting from a NiL_4 catalyst precursor. The broken curves show the formation of the 2M3BN by-product (the “reverse reaction” arrows are omitted, for clarity).

enhancing catalytic activity. Indeed, it was suggested that bidentate phosphine ligands with large bite angles work similarly [96]. However, it might be that the “bite angle effect” is simply a size effect in this case [97].

The final step is the hydrocyanation of the 3PN/4PN mixture (Figure 3.34a). The main product is the linear ADN, with two branched by-products: 2-methylglutaronitrile (MGN) and ethylsuccinonitrile (ESN). Adding a Lewis acid co-catalyst significantly improves the TON and the product selectivity of the second hydrocyanation step. Lewis acids such as $ZnCl_2$, $ZnBr_2$, or $AlCl_3$ can coordinate to the lone pair of the cyanide nitrogen atom, facilitating the C–C bond formation. Moreover, bulky Lewis acids can increase the selectivity to the linear product: Adding BPh_3 in the second hydrocyanation step increases the yield of adiponitrile from 77% to 98% (Figure 3.34b).

3.1.4.4 The Ciba–Geigy Metolachlor Process

The asymmetric synthesis of (*S*)-metolachlor, commercialized by Ciba–Geigy in 1996, is a *tour de force* of homogeneous catalysis [98,99]. Metolachlor (2-chloro-*N*-(6-ethyl-*o*-tolyl)-*N*-(2-methoxy-1-methylethyl)acetamide, or *N*-chloroacetyl-*N*-alkoxyalkyl-2-ethyl-6-methylaniline) is the active ingredient of the herbicide Dual Magnum[®], used for protecting corn and other crops. It has two chiral elements: an asymmetric carbon atom, and a chiral axis (similarly to BINAP). This means that there are four possible stereoisomers, but only the (*S*) isomers are active herbicides (Figure 3.35a). Since 1976, Dual was marketed using a racemic mixture of all four isomers. Meanwhile, Hans-Ulrich Blaser and co-workers at Ciba–Geigy tried to find a protocol for producing the active (*S*) isomers via asymmetric catalysis. In the final

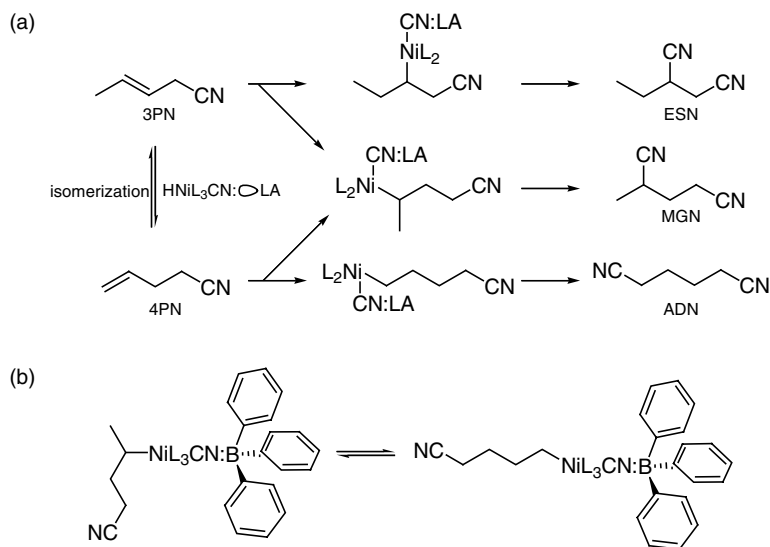


Figure 3.34 **a** Formation of the various products in the second hydrocyanation step, co-catalyzed by Lewis acids (LA); **b** bulky Lewis acids such as BPh_3 shift the linear/branched product equilibrium toward the desired linear product.

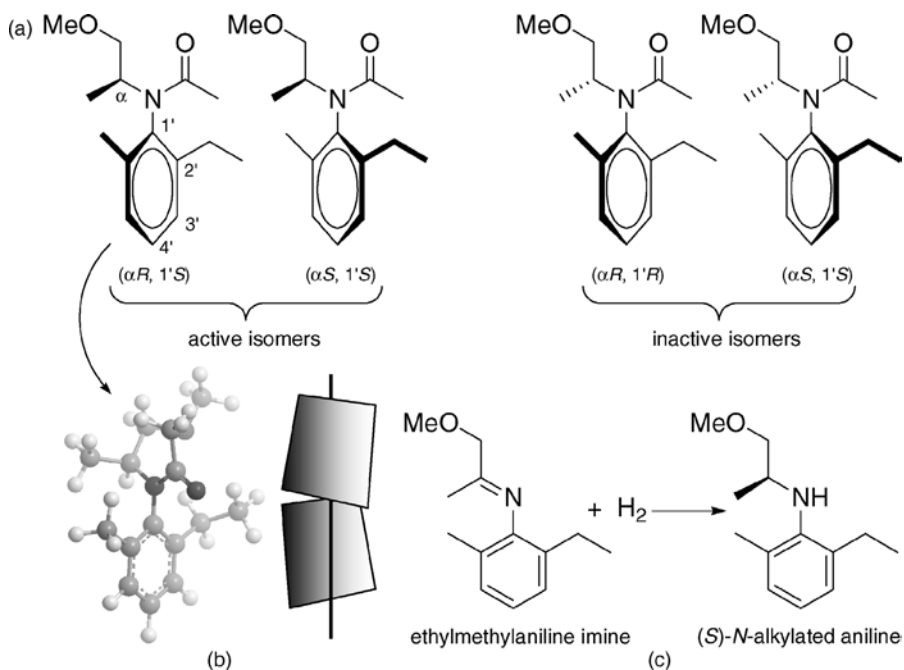


Figure 3.35 **a** Chemical structures of the four stereoisomers of metolachlor; **b** 3D representation of the $(\alpha,R,1'S)$ isomer, showing the chiral axis and **c** the asymmetric imine hydrogenation step.

process, the key step was the asymmetric hydrogenation of 2-ethyl-6-methylaniline imine to the corresponding *N*-alkylated aniline (Figure 3.35c). The main challenge was to find a catalyst that gave both high *ee* values and high activity (TON and TOF) [100]. Given the low price of the product and the high price of asymmetric hydrogenation catalysts (such as the diphosphine–Rh complexes used in Monsanto’s successful l-DOPA process), Ciba–Geigy had to find a catalyst that would give TONs higher than 40 000(!) for a competitive commercial process. Blaser’s group screened many Rh and Ir complexes [101,102]. They discovered several highly active catalysts, and also some very selective ones, but they could not find a catalyst that combined the high activity *and* the high selectivity.

The breakthrough came in 1987, with the preparation and testing of new bidentate ligands based on ferrocenyl backbones (Figure 3.36). This family of ligands was named after Josi Puelo, the technician who prepared the first **Josiphos ligand** [103,104]. The Josiphos–Rh complexes showed excellent selectivity in enamide hydrogenation. While this was not exactly what was needed for the metolachlor process, it showed promise and these ligands were developed further. In 1992 the reward came in the form of the xylyphos ligand. The Ir–xylyphos complex shown in Figure 3.36b gave a TON of 35 000, with 80% *ee* at 55 °C and 80 bar H₂ after 48 h. When the reaction conditions had been optimized, the final industrial process gave 79% *ee*, TON > 1 000 000, and TOF > 500 000. Ciba–Geigy now produces more than 10 000 tpa (tons per annum) of metolachlor using this method. Although the iridium metal is recovered at the end of the reaction, the xylyphos ligand is destroyed. Nevertheless, the process is a commercial success, thanks to the high substrate/catalyst ratio (34 g iridium and 70 g xylyphos suffice for making 10 t of *N*-alkylated aniline, with 99.6% conversion after 2 h).

3.2 Homogeneous Catalysis without Metals

3.2.1 Classic Acid/Base Catalysis

Several important chemical reactions are catalyzed simply by H⁺ or OH[−] ions. Examples include aldol reactions, esterifications and trans-esterifications, and

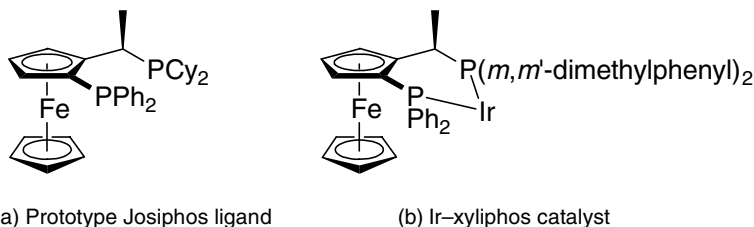


Figure 3.36 a The original Josiphos ligand; b the Ir–xylyphos complex used in the Ciba–Geigy metolachlor process.

synthesis of nitroaromatics such as 2-methyl-1,3,5-trinitrobenzene (better known as trinitrotoluene, or TNT). Brønsted acids catalyze reactions by protonating nucleophilic sites such as lone pairs on O or N atoms or alkene π -bonds. This activates the molecule toward nucleophilic attack. The strength of the acid and the stability of the cation produced determine the protonation equilibrium. There are two types of acid/base catalysis: general and specific [105]. In **general acid catalysis**, all the proton-donating species contribute to the reaction rate acceleration. Conversely, in **specific acid catalysis**, the reaction rate is proportional to the concentration of the protonated solvent molecules SH^+ . The acid catalyst itself only contributes to the rate acceleration by shifting the chemical equilibrium $\text{S} + \text{AH} \rightleftharpoons \text{SH}^+ + \text{A}^-$ in favor of the SH^+ species.

3.2.2

Organocatalysis

In organocatalysis, the catalysts are small organic molecules, predominantly composed of C, H, O, N, S, and P atoms. These molecules are often Lewis acids or bases, so organocatalysis is a subtype of acid catalysis. Organocatalysts display several advantages over organometallic complexes: They are typically inexpensive, readily available, and many of them are air- and water-stable. The fact that they contain no metals is an advantage in itself: There is no need for metal separation and recovery at the end of the reaction. Moreover, organocatalysts are usually much less toxic than their organometallic counterparts. Although the majority of the research effort worldwide in homogeneous catalysis centers on organometallic complexes, interest in organocatalysts is growing. Figure 3.37 shows an example of the Knoevenagel condensation (the reaction of a carbon acid with an aldehyde that yields α,β -unsaturated compounds) catalyzed by piperidine. The piperidine molecule abstracts one of the acidic hydrogens, forming an enol intermediate which reacts with the aldehyde. Nor is organocatalysis limited to carbonyl chemistry: Suzuki [106,107] and Sonogashira [108] cross-coupling reactions, which typically require transition-metal catalysts, can now also be performed under metal-free conditions.

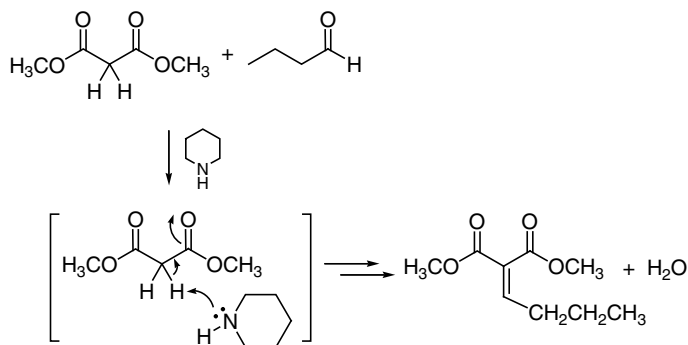


Figure 3.37 Piperidine, an organocatalyst, catalyzes the Knoevenagel condensation between dimethyl maleate (2-butenedioic acid) and butyraldehyde (butanal).

Notwithstanding the progress in other reaction types, the main thrust in organocatalysis research centers is on enantioselective catalysis applications [109,110], of which amine-based asymmetric catalysts form the majority [111]. Most of the reactions proceed via the enamine catalytic cycle (Figure 3.38a) or via imonium intermediates. The most common (and most successful) catalysts for such reactions are proline derivatives. Thanks to its secondary amine functionality and relatively high pK_a value, proline (pyrrolidine-2-carboxylic acid) is a good

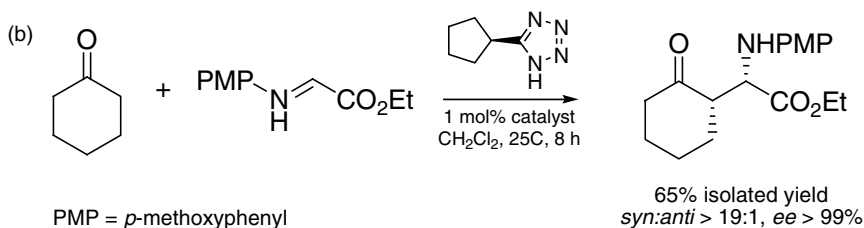
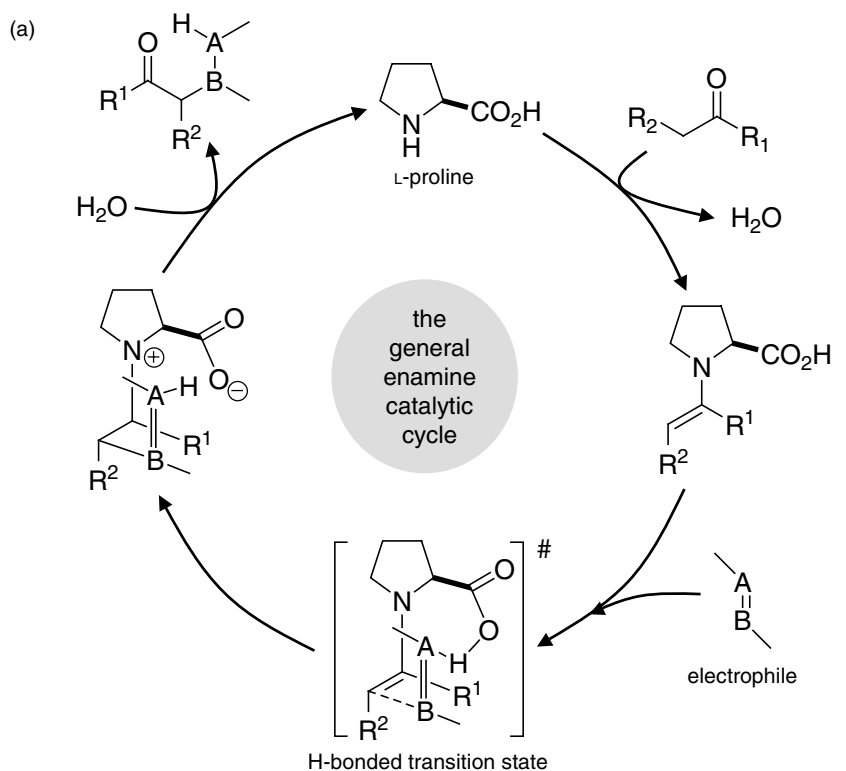


Figure 3.38 a The general enamine catalytic cycle in the presence of L-proline; b an example of an asymmetric Mannich-type addition of cyclohexanone to iminoethyl glyoxalate, catalyzed by a proline tetrazole derivative.

nucleophile as well as a Brønsted acid, making it a bifunctional organocatalyst. Numerous proline derivatives and analogues have been synthesized, some of which are very effective organocatalysts. For example, the tetrazole derivative (Figure 3.38b) gives high diastereoselectivity and $>99\%$ *ee* in the asymmetric Mannich reaction [112]. The fact that this catalyst also works well in organic solvents such as dichloromethane, THF, and acetonitrile makes it a good candidate for practical applications.

Another example, which shows the degree of control one can obtain with organocatalysis, comes from the elegant experiments of Hiemstra and co-workers. They designed *Cinchona* alkaloid based organocatalysts for the Henry reaction (an aldol-type reaction between an aldehyde and nitromethane) [113]. By connecting a thiourea group to the *Cinchona* skeleton, they obtained a bifunctional catalyst that could interact simultaneously with both substrates, giving good yields and *ee* values (Figure 3.39). Moreover, nitroalcohols with the opposite configuration were prepared by using the pseudo enantiomer as a catalyst.

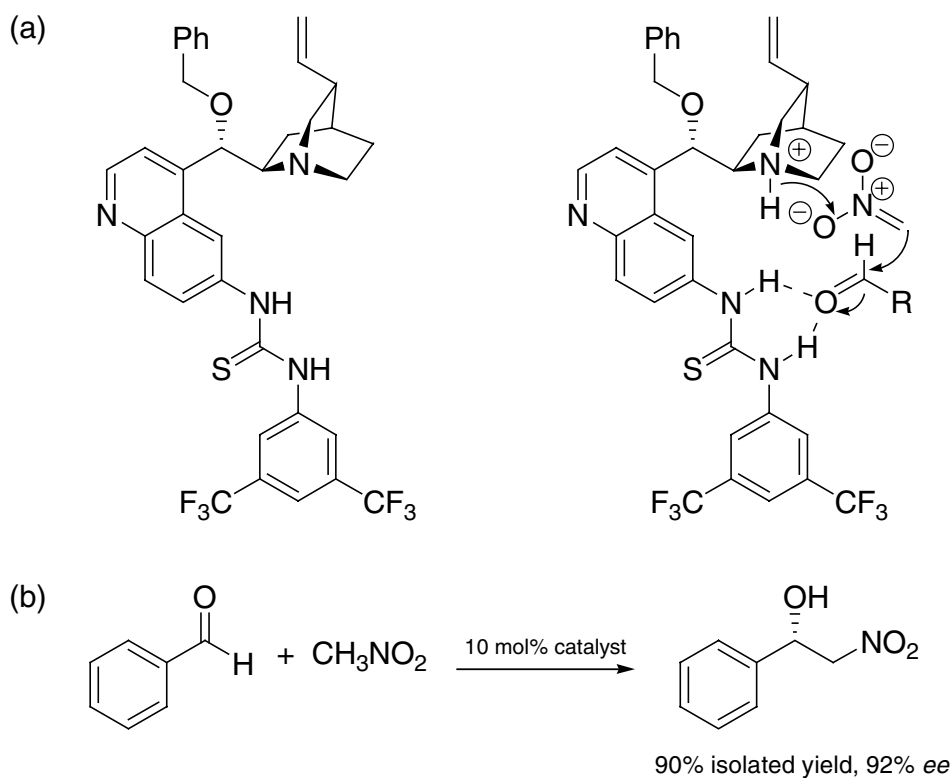


Figure 3.39 **a** The structure and proposed mode of action of the modified *Cinchona* alkaloid catalyst; **b** an example of the catalytic Henry reaction between benzaldehyde and nitromethane.

3.3

Scaling up Homogeneous Reactions: Pros and Cons

Despite their industrial importance, scale-up issues are all too often ignored by academic researchers. This is a pity, because assessment of the practical possibilities of large-scale catalyst manufacture and recovery/recycling at an early stage in the project increases the chances of a successful application.

3.3.1

Catalyst Recovery and Recycling

Organometallic synthesis and ligand design give a high degree of molecular control over the catalyst precursor structures. Thanks to this, homogeneous catalysts are usually more active and selective than their heterogeneous counterparts. Moreover, homogeneously catalyzed reactions are not hampered by surface effects, phase-transfer limitations or mass-transfer problems. All the catalytic sites are accessible and every single metal atom is a potential active site. Despite these advantages, and the increasingly important position of homogeneous catalysis in academia and industry [114], many homogeneous catalytic systems have not been commercialized due to difficulties in catalyst separation, recovery, and recycling. Product distillation, which is the most common separation method in large-scale processing, requires elevated temperatures (unless the product is very volatile). Most homogeneous catalysts are thermally sensitive, and decompose below 150 °C. Thus distillation, even at reduced pressure, will lead to catalyst decomposition. Indeed, most commercial processes using homogeneous catalysis either involve volatile substrates and products or do not contain thermally sensitive organic ligands [115]. Low-pressure distillation is also problematic, because a catalyst optimized for working under the high-pressure reaction conditions may undergo undesirable side-reactions under reduced pressure.

Catalyst separation and recovery are crucial factors in process economics for two main reasons. First and foremost, the catalyst is often very expensive compared to the substrates and products. Operating profit margins in the bulk chemical industry are typically 200–300%. This means that the end product sells for about two to three times the cost of the raw materials. If the catalyst is 1000 times more expensive than the product, which is often the case for noble metal complexes, losing even a fraction of it will render the entire process uneconomic. Second, any catalyst remaining with the product may create problems downstream in the process. It may change the selectivity of subsequent steps, bind to and thereby poison other catalysts, or corrode equipment (in the case of acid/base catalysts). Even if the catalyst is not expensive, catalyst impurities in the product may be unacceptable. A typical example is the manufacturing of biodiesel by esterification of free fatty acids with methanol. This reaction proceeds smoothly in the presence of 1 mol% sulfuric acid, a cheap and readily available catalyst. The problem is that the current standards for diesel prohibit more than 20 ppm sulfur, because of the environmental effects of the resulting SO_x emissions. Reducing the sulfur content from 1% to less than 20 ppm is a nearly impossible task, encouraging the search for alternative, solid-acid, catalysts.

Industry employs several techniques for solving these problems [116]. The most common are selective product crystallization, where the catalyst and the excess substrates and reagents are left in the liquid phase, and catalyst precipitation and filtration, where the catalyst is precipitated as a salt from the organic reaction mixture. Other techniques include flash distillation of the product under high vacuum, and liquid/liquid extraction of the catalyst from the reaction mixture.

An interesting alternative is to use supercritical solvents [117], notably supercritical carbon dioxide (scCO₂) [115]. Supercritical fluids are gases which are compressed above their critical temperature and pressure. They dissolve many apolar and medium-polar organic molecules and are fully miscible with all permanent gases, avoiding any phase-transfer problems. At the end of the reaction, the supercritical solvent can simply be decompressed back to a gas and removed [118]. The relatively low critical temperature and pressure of CO₂ (31.1 °C and 73.8 bar) make it ideal for this purpose [119]. Although most metal-containing complexes are poorly soluble in scCO₂, adding fluorocarbon chains [120] or using trialkylphosphines can solve this difficulty [121]. However, this does not overcome the main problem of separating the catalyst from the product. Leitner and co-workers achieved this by using an elegant system in which an iridium hydrogenation catalyst is soluble in scCO₂ in the presence of the substrate, but precipitates once the substrate is consumed [122]. Alternative solutions employ temperature and pressure swings to precipitate the catalyst and then decompression for removing the product [120].

A relatively new concept combines nanoporous membranes and high-molecular-weight transition-metal complexes [123]. Thanks to advances in membrane technology, both organic and ceramic ultrafiltration and nanofiltration membranes are commercially available. Such membranes can effectively filter species with diameters of a few nanometers (nanofiltration) to tens and hundreds of nanometers (ultrafiltration). These diameters match with those of dendrimers and macromolecules, respectively. Moreover, the membranes can be made to withstand organic solvents, varied pH values, and a wide range of temperatures [124]. Thus, homogeneous catalyst separation and continuous processing are physically possible, provided that the homogeneous catalyst is large enough to be retained by the membrane. Applications include hydrovinylation [125], allylic amination [126], and Kharasch addition [127]. There are several approaches for making high-molecular-weight homogeneous catalysts. Attaching the ligand by covalent bonding to a soluble oligomer or polymer is one simple and effective option. Plenio and co-workers demonstrated this approach by binding phosphine ligands to poly(methylstyrene) (PMS, M_w ca. 5000 Da; Figure 3.40) or to poly(ethylene glycol) monomethyl ether (MeOPEG, M_w ca. 2000 Da). They then reacted this polyfunctional ligand with Pd^{II} or Pd⁰ precursors, and obtained a multisite homogeneous Pd catalyst that could be retained by nanofiltration [128] or liquid/liquid extraction [129]. These catalysts were used successfully in various C–C cross-coupling reactions. Other approaches include use of shape-persistent dendrimers [130,131], or attachment of large “external units” onto single metal–ligand complexes.

Anchoring the catalyst to a solid support is another popular option. Although such systems are no longer truly “homogeneous,” I include them in this chapter because

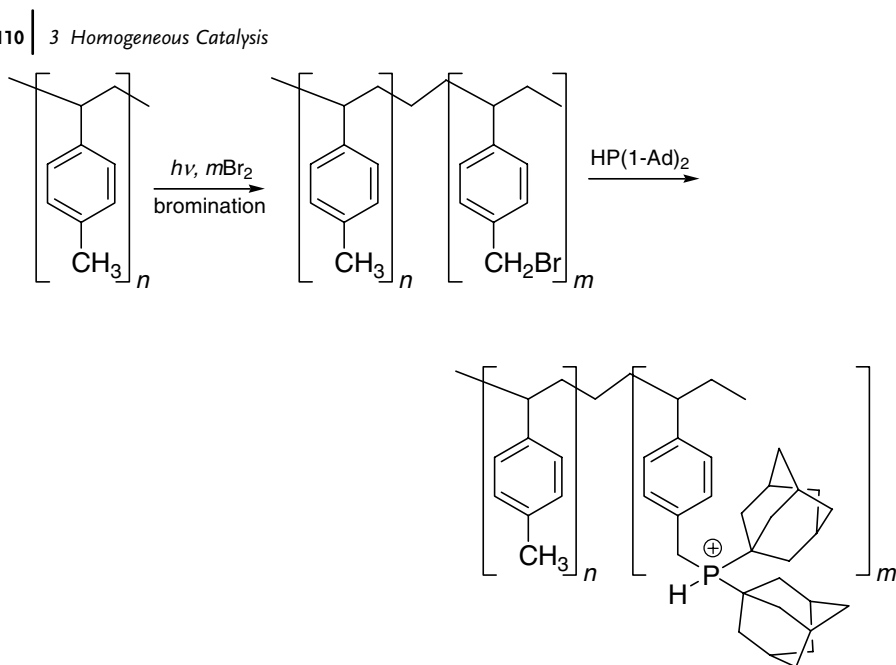


Figure 3.40 Plenio's multisite phosphine ligand based on poly(methylstyrene).

they follow the same principles as their homogeneous counterparts. These “hybrid catalysts” are described in Section 3.3.2. Another type of hybrid approach is to design heterogeneous catalysts based on surface organometallic chemistry [132,133]. This approach is covered further in Chapter 4.

3.3.2

Hybrid Catalysts: Bridging the Homogeneous/Heterogeneous Gap

Combining the advantages of homogeneous catalysts (synthesis-tunable catalyst properties and no mass-transfer limitations) and heterogeneous ones (easy separation and high thermal stability) is a key challenge for the chemical industry. Several ingenious and elegant approaches for such “heterogenization of homogeneous catalysts” have been developed. Examples include immobilization of metal complexes onto solid supports, and design of “**ship-in-a-bottle catalysts**”. Heterogenization by anchoring the homogeneous catalyst to a solid support is the most common approach [134–136]. There are several ways of doing this. The simplest is by ion exchange, substituting an inactive cation on the surface with an active metal ion [137]. Unfortunately, this simple substitution works both ways, often resulting in the metal complex leaching back into solution [138]. Indeed, leaching is *the* problem of hybrid catalysts, and often proving that a hybrid catalyst does not leach is problematic [139,140].

Another option is encapsulating the homogeneous complex in an (inorganic) cage, creating a ship-in-a-bottle hybrid catalyst. Zeolites are often used for trapping large

organometallic complexes inside the crystalline zeolite cage [141]. The catalyst is trapped, but the smaller substrate and product molecules can diffuse in and out of the zeolite pores. A variety of reactions are reported, including selective oxidation of terpenes [142] and hydrogenation of alkenes [143].

3.4

“Click Chemistry” and Homogeneous Catalysis

“Click chemistry” is a good example of how homogeneous catalysis can advance the principles of green chemistry. It represents a family of chemical reactions for joining organic molecules with heteroatom links. Originally coined by Sharpless and co-workers, this term is now used universally for describing fast and high-yielding catalytic reactions [144]. A **click reaction** must fulfill several stringent requirements according to Sharpless’s definition. It must be modular, wide in scope, give very high yields, be stereospecific (though not necessarily enantiospecific), and generate only inoffensive by-products that are easily removed by nonchromatographic methods. Moreover, the reaction conditions must be simple, preferably using no solvents (or using just water as a solvent). The product isolation must also be simple, using crystallization or distillation. This long list of requirements means that many reactions are precluded from the click repertoire, but those remaining fit extremely well with the principles of green chemistry. Indeed, the vision of click chemistry is obtaining diverse chemical functionality based on “a few good reactions”, and many of these reactions feature 100% atom economy. Thanks to their modularity and ease of operation, click reactions are popular in drug discovery [145].

Click reactions are driven by thermodynamics. The substrates are “spring-loaded” with energy that is released upon reaction. Typically, the energy difference between substrates and products in click reactions is >20 kcal/mole. This large energy difference means that often only one product is formed. Because of the high energy “loaded” in the substrates, a catalyst is not always necessary – some of these reactants form autocatalytic mixtures that must be handled carefully! However, in many cases the activation barrier is sufficiently high for no reaction to occur until a catalyst is added. One classic example is the ring-opening/rearrangement of acylaziridine. This example shows how choosing the right homogeneous catalyst can cause a radical shift in the reaction pathway. Acylaziridines are energy-intensive because of the tension in the three-membered ring. In the presence of Lewis acid catalysts, they can undergo facile ring-opening as well as isomerization. Lectka and co-workers showed that the Lewis acid catalyst controls the reaction pathway (Figure 3.41) [146]. In the presence of a nucleophile but without a catalyst, no reaction occurs. By adding an “oxophilic” Lewis acid catalyst such as $\text{Ti}(\text{OiPr})_4$, one promotes the fast ring-opening to give the *trans*-disubstituted cyclohexene. Surprisingly, if you add an “azaphilic” Lewis acid catalyst such as $\text{Cu}(\text{OTf})_2$, an entirely different reaction occurs: The acylaziridine rearranges to give a five-membered ring, which is bonded *cis* to the cyclohexane backbone. Without any Lewis acid, nothing happens.

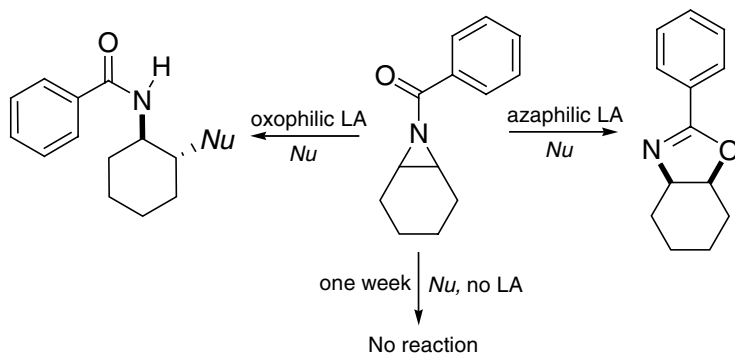


Figure 3.41 The two pathways for the Lewis-acid-catalyzed ring-opening of aziridines.

Perhaps the most famous click reaction is the Huisgen-type [3 + 2] cycloaddition of azides and alkynes to triazoles (Figure 3.42) [147–149]. This reaction demonstrates two important advantages of catalysis: improved reaction conditions and improved product selectivity. The noncatalytic variant usually requires elevated temperatures, and yields a 1:1 mixture of the 1,4 and the 1,5 regioisomers (note that this reaction features 100% atom economy, so there are no by-products). Using a Cu^{I} catalyst, the reaction can be carried out in a water/*t*-BuOH mixture at room temperature, and gives only the 1,4 regioisomer in high yields. Interestingly, almost any type of copper species can catalyze this reaction. Copper shavings, copper powder, and copper nanoparticles [150] are oxidised *in situ* to Cu^{I} , while a variety of Cu^{II} salts can be used as catalyst in the presence of a mild reductant such as ascorbic acid (vitamin C) [151]. The reaction tolerates a wide range of functional groups and conditions, and has been applied in solid-phase synthesis [152], polymer synthesis [153,154], dendrimer synthesis [155], and even for constructing peptide bond surrogates [156].

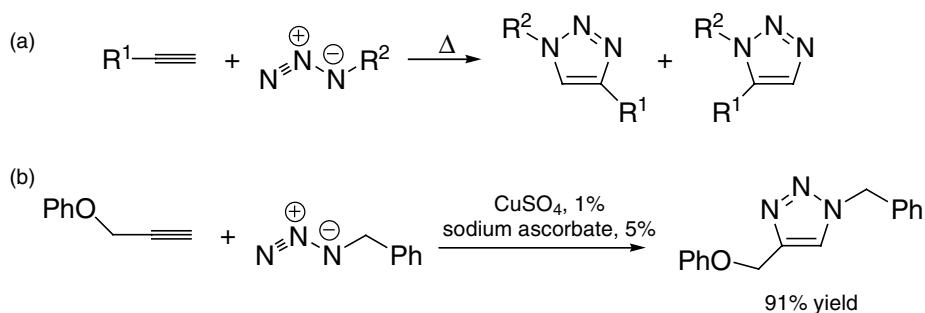


Figure 3.42 **a** General reaction scheme for the thermal Huisgen cycloaddition; **b** the copper-catalyzed reaction between phenyl propargyl ether (phenyl 2-propynyl ether) and benzyl azide. The catalytic reaction is performed in the presence of a reductant (sodium ascorbate) and gives just one of the product isomers in high yield.

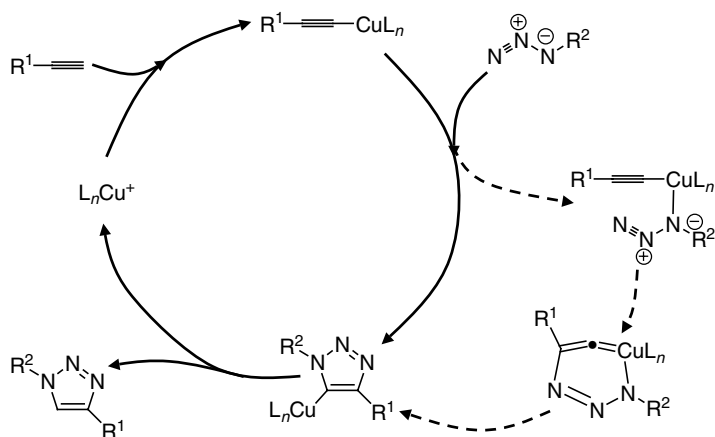


Figure 3.43 The proposed catalytic cycle for the Huisgen [3 + 2] cycloaddition, showing the “direct” and “indirect” routes.

The catalytic cycle is an interesting one, and demonstrates how computational chemistry complements mechanistic investigations [157,158]. It “begins” with a reaction between the Cu^{I} salt and the terminal acetylenic carbon (Figure 3.43). This gives a copper acetylide, a species well known from the Glaser [159], Stephens–Castro [160], and Sonogashira [161] reactions. One could expect that this intermediate would react directly with the azide in a single-step [3 + 2] cycloaddition. However, evidence from density functional theory (DFT) calculations [158] points to a stepwise reaction, where the azide first coordinates to the copper center and subsequently forms a six-membered heterocyclic intermediate which rearranges to the product.

3.5 Exercises

- Describe in your own words the main advantages and disadvantages of homogeneous catalysis. Based on the industrial examples given in this chapter, what are the main barriers for commercializing large-scale homogeneously catalyzed processes?
- The Sonogashira cross-coupling of bromoalkenes is a useful method for making C–C bonds to terminal acetylenes [161]. It tolerates a variety of functional groups, and is catalyzed by a combination of Pd and Cu, through a cuprous acetylide intermediate.
 - Complete the catalytic cycle of the Sonogashira reaction shown in Figure 3.44, by filling in the names of the elementary steps and the missing catalytic intermediates.
 - What is the oxidation state of the Pd atom in each of these intermediates?
 - Suggest an experiment which would enable you to determine which of the steps **A**, **B**, or **C** is rate-determining.

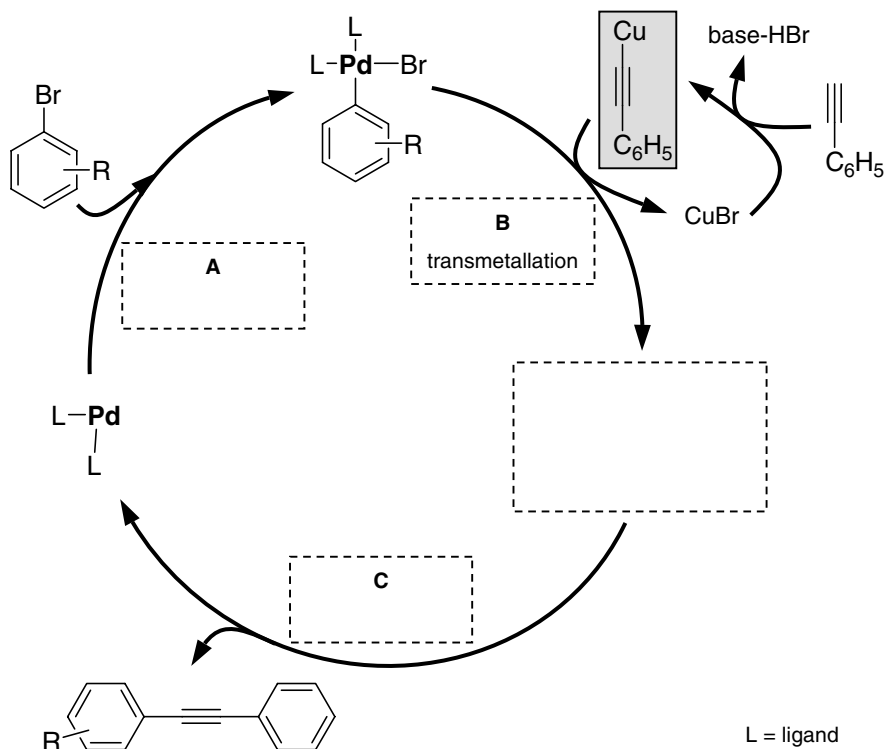


Figure 3.44 Catalytic cycle for the Pd-catalyzed Sonogashira cross-coupling; the cuprous acetylide intermediate is highlighted in gray.

3. Hydrosilylation (the addition of R_3SiH to a double bond) is an important reaction in the silicone polymer industry. It is used for “curing” silicone rubber, by cross-linking polymer chains. The reaction is catalyzed by Pt and Rh complexes, following the cycle shown in Figure 3.45.

- Complete the cycle shown in Figure 3.45, by filling in the names of the elementary steps and the missing catalytic intermediates.
- What is the oxidation state of the Pt in each of these catalytic intermediates?
- The hydrosilylation of 1-hexene was carried out in two different experiments: one with Me_3SiH and one with Me_3SiD . The relative reaction rate ratio (also called the k_H/k_D ratio) was 5.4:1. Based on this information, which step in the cycle is rate-determining?
- The hydrosilylation of polymer A is carried out in the presence of H_2PtCl_6 as catalyst precursor. The catalyst is not recoverable because the polymer forms a hard gel. If the price of Pt is €32 (\$44) per gram and the sale price of the hardened polymer is €1500 (\$2000) per ton, what is the minimum catalyst TON for an economically viable process?

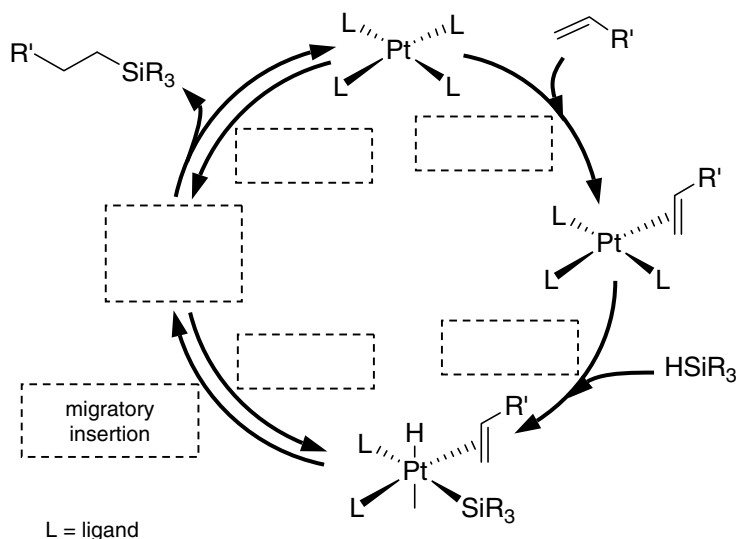


Figure 3.45 Catalytic hydrosilylation cycle in the presence of a Pt catalyst, using H_2PtCl_6 as the catalyst precursor.

4. The oxidation of 3-carene to 3-carene-5-one (Figure 3.46) is a key step in the synthesis of the pyrethroid ester insecticide Deltamethrin [162,163]. This reaction is performed with air as the oxidant, catalyzed by 2 mol% of a Cr-pyridine complex (the catalyst precursors are CrCl_3 and pyridine). Table 3.1 shows the turnover frequencies obtained using various Cr/pyridine ratios.

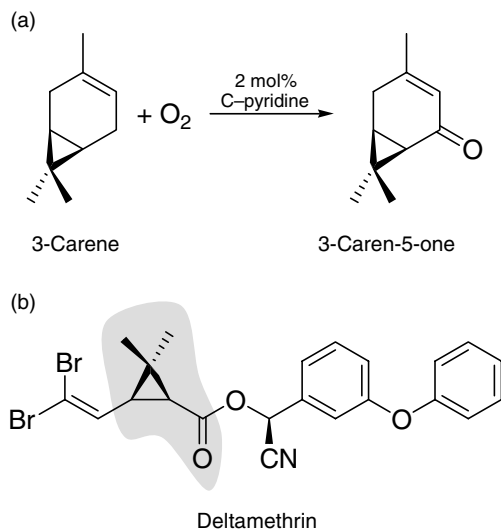


Figure 3.46 a Catalytic oxidation of 3-carene to 3-carene-5-one; **b** molecular structure of Deltamethrin, showing the incorporation of the carenone precursor in the final product.

Table 3.1 Turnover frequencies for the air oxidation of 3-carene.

CrCl ₃ /pyridine ratio	1:10	1:3	1:2	1:1	2:1
TOF/min ⁻¹	86	650	832	468	342

- (a) Draw a graph of the TOF dependence on the Cr/pyridine ratio. What can you learn about the reaction from the shape of this graph?
- (b) Suggest two structures for catalytic intermediates that may participate in the carene oxidation cycle.
- (c) Kinetic studies showed that this oxidation involves free-radical intermediates, and that the reaction is much faster if 1 mol% of carene hydroperoxide is added. Suggest a mechanism that accounts for these observations. Would you expect the same effect if you added 1 mol% of *t*-butyl hydroperoxide instead?
5. (a) Explain how the bite angle and the flexibility of a bidentate ligand are related to the reaction pocket, and why these concepts are important in homogeneous catalysis.
- (b) Examine the seven bidentate phosphine ligands A–G shown in Figure 3.47 and rank them in order of flexibility.
- (c) Test your answer by building these ligands using plastic molecular models (if you don't have such models, go and buy some – they are fun, inexpensive, and a great tool for understanding chemical reactions). What is the key to the flexibility in these seven ligands?
6. Explain the difference between Tolman's cone angle, the ligand bulk radius, and the solid angle. Which of these parameters would you use for characterizing the size of the following ligands: PPh₃; P(*o*-O-tolyl)₃; P(Ph)₂(*t*-butyl); 2,2'-bis(diphenylphosphanyl)-1,1'-binaphthyl (BINAP); and DIOP (see structure E in Figure 3.47).

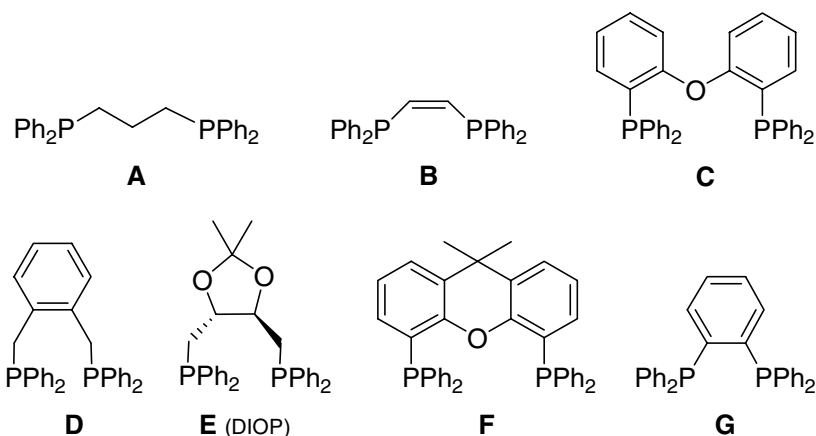
**Figure 3.47** Molecular structures of various bidentate phosphine ligands.

Table 3.2 Butadiene dimerization and trimerization yields with different catalysts.

Catalyst precursor	Yield/%	
	cyclooctadiene	cyclododecatriene
$(\text{C}_6\text{H}_5\text{O})_3\text{P}-\text{Ni}$	50	35
$(p\text{-CH}_3\text{-C}_6\text{H}_4\text{O})_3\text{P}-\text{Ni}$	52	35
$(o\text{-CH}_3\text{-C}_6\text{H}_4\text{O})_3\text{P}-\text{Ni}$	70	10
$(p\text{-C}_6\text{H}_5\text{-C}_6\text{H}_4\text{O})_3\text{P}-\text{Ni}$	65	17
$(o\text{-C}_6\text{H}_5\text{-C}_6\text{H}_4\text{O})_3\text{P}-\text{Ni}$	95	<1

7. Nickel–triarylphosphite complexes catalyze the dimerisation of butadiene to cyclooctadiene. Cyclododecatriene is an unwanted by-product, which results from trimerization catalyzed by the same catalyst. Table 3.2 shows the product yields using various ligand–metal complexes (the remainder in each case is a tarry polymeric material).

- Draw a simple catalytic cycle for the dimerization and trimerization reactions which accounts for the data shown in Table 3.2.
 - What is the reason for the difference in selectivity between the various catalysts? Why do some of the catalysts give less tarry material?
 - Draw the structures of the catalyst precursors in Table 3.2. Which descriptor plays the key role here?
 - Ethene trimerization is an important industrial process. Assume that the reaction mechanism for ethene is similar to that of butadiene. What ligand–metal complex would you suggest for maximizing the yield of ethene trimerization?
8. You are in charge of scaling up an asymmetric oxidation process for making 10 tpa (tons per annum) of a pharmaceutical intermediate which sells at €5000 (\$6750) per kg. The lab-scale reaction uses 2 mol% of a Ru–ligand complex as a catalyst and DMSO as solvent. List the factors you must consider when planning your scaleup operation. How would your list change if the product were a polymerization additive with a market price of €50 (\$67) per kg?

References

- Anderson, J.G., Margitan, J.J. and Stedman, D.H. (1977) Atomic chlorine and the chlorine monoxide radical in the stratosphere: three *in situ* observations. *Science*, **198**, 501.
- Rycroft, M.J. (1987) Where has all the ozone gone? *Phys. Bull.*, **38**, 410.
- Rothenberg, G., Downie, A.P., Raston, C.L. and Scott, J.L. (2001) Understanding solid/solid organic reactions. *J. Am. Chem. Soc.*, **123**, 8701.
- Trzeciak, A.M. and Ziolkowski, J.J. (1999) Perspectives of rhodium organometallic catalysis. Fundamental and applied

- aspects of hydroformylation. *Coord. Chem. Rev.*, **190–192**, 883.
- 5 van der Veen, L.A., Kamer, P.C.J. and van Leeuwen, P.W.N.M. (1999) New phosphacyclic diphosphines for rhodium-catalyzed hydroformylation. *Organometallics*, **18**, 4765.
 - 6 Knowles, W.S. (2002) Asymmetric hydrogenations (Nobel Lecture). *Angew. Chem. Int. Ed.*, **41**, 1998.
 - 7 Noyori, R. (2003) Asymmetric catalysis: science and opportunities (Nobel Lecture 2001). *Adv. Synth. Catal.*, **345**, 15.
 - 8 Sharpless, K.B. (2002) Searching for new reactivity (Nobel Lecture). *Angew. Chem. Int. Ed.*, **41**, 2024.
 - 9 Chauvin, Y. (2006) Olefin metathesis: the early days (Nobel Lecture). *Angew. Chem. Int. Ed.*, **45**, 3740.
 - 10 Grubbs, R.H. (2006) Olefin-metathesis catalysts for the preparation of molecules and materials (Nobel Lecture). *Angew. Chem. Int. Ed.*, **45**, 3760.
 - 11 Schrock, R.R. (2006) Multiple metal-carbon bonds for catalytic metathesis reactions (Nobel Lecture). *Angew. Chem. Int. Ed.*, **45**, 3748.
 - 12 Niu, S. and Hall, M.B. (2000) Theoretical studies on reactions of transition-metal complexes. *Chem. Rev.*, **100**, 353.
 - 13 Huheey, J.E., Keiter, E.A. and Keiter, R.L. (1993) *Inorganic Chemistry*, Harper Collins, New York, ISBN 0-06-042995-X.
 - 14 Crabtree, R.H. (2005) *The Organometallic Chemistry of the Transition Metals*, Wiley-VCH, Weinheim, ISBN 0-471-66256-9.
 - 15 Vaska, L. (1968) Reversible activation of covalent molecules by transition-metal complexes. The role of the covalent molecule. *Acc. Chem. Res.*, **1**, 335.
 - 16 Vaska, L. and DiLuzio, J.W. (1961) Carbonyl and hydrido-carbonyl complexes of iridium by reaction with alcohols-hydrido complexes by reaction with acid. *J. Am. Chem. Soc.*, **83**, 2784.
 - 17 Vaska, L. and DiLuzio, J.W. (1961) Complex carbonyl hydrides of osmium and ruthenium. *J. Am. Chem. Soc.*, **83**, 1262.
 - 18 Vaska, L. and DiLuzio, J.W. (1962) The origin of hydrogen in metal hydride complexes formed by reaction with alcohols. *J. Am. Chem. Soc.*, **84**, 4989.
 - 19 Baar, C.R., Jenkins, H.A., Vittal, J.J., Yap, G.P.A. and Puddephatt, R.J. (1998) Stereoselectivity in organometallic reactions: oxidative addition of alkyl halides to platinum(II). *Organometallics*, **17**, 2805.
 - 20 Amatore, C. and Jutand, A. (2000) Anionic Pd(0) and Pd(II) intermediates in palladium-catalyzed Heck and cross-coupling reactions. *Acc. Chem. Res.*, **33**, 314.
 - 21 Yamamoto, Y., Arakawa, T. and Itoh, K. (2004) Synthesis of naphthoquinone-fused cyclobutadiene ruthenium complexes. *Organometallics*, **23**, 3610.
 - 22 Gillie, A. and Stille, J.K. (1980) Mechanisms of 1,1-reductive elimination from palladium. *J. Am. Chem. Soc.*, **102**, 4933.
 - 23 Rybtchinski, B. and Milstein, D. (1999) Metal insertion into C–C bonds in solution. *Angew. Chem. Int. Ed.*, **38**, 871.
 - 24 Arndtsen, B.A., Bergman, R.G., Mobley, T.A. and Peterson, T.A. (1995) Selective intermolecular carbon-hydrogen bond activation by synthetic metal complexes in homogeneous solution. *Acc. Chem. Res.*, **28**, 154.
 - 25 Godula, K. and Sames, D. (2006) C–H bond functionalization in complex organic synthesis. *Science*, **312**, 67.
 - 26 Rupprecht, G.A., Messerle, L.W., Fellmann, J.D. and Schrock, R.R. (1980) Multiple metal-carbon bonds. 15. Octahedral alkylidene complexes of niobium and tantalum by ligand-promoted α abstraction. *J. Am. Chem. Soc.*, **102**, 6236.
 - 27 Basuli, F., Bailey, B.C., Huffman, J.C. and Mindiola, D.J., (2005) Intramolecular C–H activation reactions derived from a terminal titanium neopentylidene functionality. Redox-controlled 1,2-addition and α -hydrogen abstraction reactions. *Organometallics* **24**, 3321.

- 28 Basuli, F., Bailey, B.C., Tomaszewski, J., Huffman, J.C. and Mindiola, D.J. (2003) A terminal and four-coordinate titanium alkylidene prepared by oxidatively induced α -hydrogen abstraction. *J. Am. Chem. Soc.*, **125**, 6052.
- 29 Weng, W., Yang, L., Foxman, B.M. and Ozerov, O.V. (2004) Chelate-enforced phosphine coordination enables α -abstraction to give zirconium alkylidenes. *Organometallics*, **23**, 4700.
- 30 Fryzuk, M.D., Mao, S.S.H., Zaworotko, M.J. and MacGillivray, L.R. (1993) The first stable zirconium alkylidene complex formed via α -hydrogen abstraction: synthesis and X-ray crystal structure of $[\eta^5\text{-C}_5\text{H}_3\text{-1,3-(SiMe}_2\text{CH}_2\text{PPri}_2)_2\text{]Zr:CHPh(Cl)}$. *J. Am. Chem. Soc.*, **115**, 5336.
- 31 Schrock, R.R. (1979) Alkylidene complexes of niobium and tantalum. *Acc. Chem. Res.*, **12**, 98.
- 32 Schrock, R.R. (2005) High oxidation state alkylidene and alkylidyne complexes. *Chem. Commun.*, 2773.
- 33 Grubbs, R.H. (2003) *Handbook of Metathesis*, Wiley-VCH, Weinheim, ISBN 3-527-30616-1.
- 34 van der Boom, M.E. and Milstein, D. (2003) Cyclometalated phosphine-based pincer complexes: mechanistic insight in catalysis, coordination, and bond activation. *Chem. Rev.*, **103**, 1759.
- 35 Mohr, F., Priver, S.H., Bhargava, S.K. and Bennett, M.A. (2006) Ortho-metallated transition metal complexes derived from tertiary phosphine and arsine ligands. *Coord. Chem. Rev.*, **250**, 1851.
- 36 Avis, M.W., van der Boom, M.E., Elsevier, C.J., Smeets, W.J.J. and Spek, A.L. (1997) Reactions of bis(iminophosphoranes) with palladium(II) dichloride: metal-induced tautomerization orthopalladation and unexpected platinum-assisted [2 + 2]cycloaddition of an aryl-nitrile with a phosphinimine moiety. *J. Organomet. Chem.*, **527**, 263.
- 37 Dupont, J., Consorti Crestina, S. and Spencer, J. (2005) The potential of palladacycles: more than just precatalysts. *Chem. Rev.*, **105**, 2527.
- 38 Ritleng, V., Sirlin, C. and Pfeffer, M. (2002) Ru-, Rh-, and Pd-catalyzed C–C bond formation involving C–H activation and addition on unsaturated substrates: reactions and mechanistic aspects. *Chem. Rev.*, **102**, 1731.
- 39 Hageman, J.A., Westerhuis, J.A., Frühauf, H.W. and Rothenberg, G. (2006) Design and assembly of virtual homogeneous catalyst libraries – towards in silico catalyst optimisation. *Adv. Synth. Catal.*, **348**, 361.
- 40 Brown, T.L. and Lee, K.J. (1993) Ligand steric properties. *Coord. Chem. Rev.*, **128**, 89.
- 41 Tolman, C.A. (1977) Steric effects of phosphorus ligands in organometallic chemistry and homogeneous catalysis. *Chem. Rev.*, **77**, 313.
- 42 Alyea, E.C., Dias, S.A., Ferguson, G. and Restivo, R.J. (1977) Structural studies of steric effects in phosphine complexes. Synthesis and crystal and molecular structure of the dinitrato (tricyclohexylphosphine)mercury(II) dimer. *Inorg. Chem.*, **16**, 2329.
- 43 Alyea, E.C., Dias, S.A., Ferguson, G. and Parvez, M. (1979) Structural studies of steric effects in phosphine complexes. Part 6. The synthesis, characterization and molecular structure of the dinitro (trimesitylphosphine)mercury(II) dimer. *Inorg. Chim. Acta*, **37**, 45.
- 44 Immirzi, A. and Musco, A. (1977) A method to measure the size of phosphorus ligands in coordination complexes. *Inorg. Chim. Acta*, **25**, L41.
- 45 White, D.P., Anthony, J.C. and Oyefeso, A.O. (1999) Computational measurement of steric effects: the size of organic substituents computed by ligand repulsive energies. *J. Org. Chem.*, **64**, 7707.
- 46 Guezi, I.A. and Wendt, M. (2006) An improved method for the computation of ligand steric effects based on solid angles. *Dalton Trans.*, 3991.

- 47 White, D., Taverner, B.C., Leach, P.G.L. and Coville, N.J. (1993) Quantification of substituent and ligand size by the use of solid angles. *J. Comp. Chem.*, **14**, 1042.
- 48 White, D., Taverner, B.C., Leach, P.G.L. and Coville, N.J. (1994) Solid angles. 1. The radial profile. *J. Organomet. Chem.*, **478**, 205.
- 49 Korsunsky, V.I. (2000) The investigation of structure of heavy metal clusters and polynuclear complexes in powder samples with the radial distribution function method. *Coord. Chem. Rev.*, **199**, 55.
- 50 White, D., Taverner, B.C., Coville, N.J. and Wade, P.W. (1995) Solid angles. 3. The role of conformers in solid angle calculations. *J. Organomet. Chem.*, **495**, 41.
- 51 Gosser, L.W. and Tolman, C.A. (1970) New three-coordinate complex of nickel (0). Tris(tri-*o*-tolyl phosphite)nickel. *Inorg. Chem.*, **9**, 2350.
- 52 Seidel, W.C. and Tolman, C.A. (1970) Ethylene [bis(tri-*o*-tolyl phosphite)] nickel (0). *Inorg. Chem.*, **9**, 2354.
- 53 van Leeuwen, P.W.N.M., Kamer, P.C.J., Reek, J.N.H. and Dierkes, P. (2000) Ligand bite angle effects in metal-catalyzed C–C bond formation. *Chem. Rev.*, **100**, 2741.
- 54 Dierkes, P. and van Leeuwen, P.W.N.M. (1999) The bite angle makes the difference: a practical ligand parameter for diphosphine ligands. *J. Chem. Soc., Dalton Trans.*, 1519.
- 55 Casey, C.P., Whiteker, G.T., Melville, M.G., Petrovich, L.M., Gavney, J.A., Jr. and Powell, D.R. (1992) Diphosphines with natural bite angles near 120 Deg increase selectivity for *n*-aldehyde formation in rhodium-catalyzed hydroformylation. *J. Am. Chem. Soc.*, **114**, 5535.
- 56 Kamer, P.C.J., Reek, J.N.H. and van Leeuwen, P.W.N.M. (1998) Designing ligands with the right bite. *Chemtech*, **28**, 27.
- 57 Kamer, P.C.J., van Leeuwen, P.W.N.M. and Reek, J.N.H. (2001) Wide bite angle diphosphines: Xantphos ligands in transition metal complexes and catalysis. *Acc. Chem. Res.*, **34**, 895.
- 58 Lenero, K.A., Kranenburg, M., Guari, Y., Kamer, P.C.J., van Leeuwen, P.W.N.M., Sabo-Etienne, S. and Chaudret, B. (2003) Ruthenium dihydrogen complexes with wide bite angle diphosphines. *Inorg. Chem.*, **42**, 2859.
- 59 Van Leeuwen, P.W.N.M., Kamer, P.C.J. and Reek, J.N.H. (1999) The bite angle makes the catalyst. *Pure Appl. Chem.*, **71**, 1443.
- 60 Kranenburg, M., van der Burgt, Y.E.M., Kamer, P.C.J., van Leeuwen, P.W.N.M., Goubitz, K. and Fraanje, J. (1995) New diphosphine ligands based on heterocyclic aromatics inducing very high regioselectivity in rhodium-catalyzed hydroformylation: effect of the bite angle. *Organometallics*, **14**, 3081.
- 61 Dahlenburg, L. (2003) P-modular homochiral bis(phosphines) with 1,2-disubstituted cyclopentane backbones in asymmetric hydrogenation. *Eur. J. Inorg. Chem.*, 2733.
- 62 Knowles, W.S. (1983) Asymmetric hydrogenation. *Acc. Chem. Res.*, **16**, 106.
- 63 Sudhakar, P. and Sundararajan, G. (2005) Tuning the reactivity of *N,O,O*-non-metallocene catalysts for α -olefin polymerization: issues related to ligand symmetry and derivatization. *Macromol. Rapid Commun.*, **26**, 1854.
- 64 Tolman, C.A. (1974) Olefin complexes of nickel(0). III. Formation constants of (olefin)bis(tri-*o*-tolyl phosphite) nickel complexes. *J. Am. Chem. Soc.*, **96**, 2780.
- 65 Tolman, C.A. (1970) Electron donor–acceptor properties of phosphorus ligands. Substituent additivity. *J. Am. Chem. Soc.*, **92**, 2953.
- 66 Mashima, K. and Nakamura, A. (1992) Agostic interaction in early transition metal alkyls and their role in catalytic activity for olefin polymerizations. *J. Organomet. Chem.*, **428**, 49.

- 67 Brookhart, M. and Green, M.L.H. (1983) Carbon–hydrogen–transition metal bonds. *J. Organomet. Chem.*, **250**, 395.
- 68 Conroy-Lewis, F.M., Mole, L., Redhouse, A.D., Litster, S.A. and Spencer, J.L. (1991) Synthesis of coordinatively unsaturated diphosphine nickel(II) and palladium(II) β -agostic ethyl cations: X-ray crystal structure of $[\text{Ni}[\textit{tert}\text{-Bu}_2\text{P}(\text{CH}_2)_2\text{PBu}\text{-tert}_2](\text{C}_2\text{H}_5)][\text{BF}_4]$. *J. Chem. Soc., Chem. Commun.*, 1601.
- 69 Green, M.L.H., Hughes, A.K., Popham, N.A., Stephens, A.H.H. and Wong, L.L. (1992) Nuclear magnetic resonance studies on partially deuteriated transition metal–methyl derivatives. *J. Chem. Soc., Dalton Trans.*, 3077.
- 70 Scherer, W. and McGrady, G.S. (2004) Agostic interactions in d^0 metal alkyl complexes. *Angew. Chem. Int. Ed.*, **43**, 1782.
- 71 Stinson, S.C. (1992) *Chem. Eng. News*, **70**, 46.
- 72 Nozaki, H., Moriuti, S., Yamabe, M. and Noyori, R. (1966) Reactions of diphenyldiazomethane in the presence of bis(acetylacetonato)copper(II). Modified diphenylmethylene reactions. *Tetrahedron Lett.*, 59.
- 73 Nozaki, H., Takaya, H., Moriuti, S. and Noyori, R. (1968) Homogeneous catalysis in the decomposition of diazo compounds by copper chelates. Asymmetric carbenoid reactions. *Tetrahedron*, **24**, 3655.
- 74 Nozaki, H., Moriuti, S., Takaya, H. and Noyori, R. (1966) Asymmetric induction in carbenoid reactions by means of a dissymmetric copper chelate. *Tetrahedron Lett.*, 5239.
- 75 Aratani, T. (1985) Catalytic asymmetric synthesis of cyclopropanecarboxylic acids: an application of chiral copper carbenoid reaction. *Pure Appl. Chem.*, **57**, 1839.
- 76 Kagan, H.B. and Phat, D.-T. (1972) Asymmetric catalytic reduction with transition metal complexes. I. Catalytic system of rhodium(I) with (–)-2,3-O-isopropylidene-2,3-dihydroxy-1,4-bis(diphenylphosphino)butane, a new chiral diphosphine. *J. Am. Chem. Soc.*, **94**, 6429.
- 77 Takaya, H., Mashima, K., Koyano, K., Yagi, M., Kumobayashi, H., Taketomi, T., Akutagawa, S. and Noyori, R. (1986) Practical synthesis of (R)- or (S)-2,2'-bis(diarylphosphino)-1,1'-binaphthyls (BINAPs). *J. Org. Chem.*, **51**, 629.
- 78 Masashi, Y. and Noyori, R. (1992) Ab initio molecular orbital study on rhodium (I)-catalyzed isomerization of allylic amines to enamines. *Organometallics*, **11**, 3167.
- 79 Lutz, E.F. (1986) Shell Higher Olefins Process. *J. Chem. Educ.*, **63**, 202.
- 80 Keim, W. (1987) Mechanistic considerations for the linear carbon–carbon linkage of monoolefins. *New J. Chem.*, **11**, 531.
- 81 Keim, W. (1994) Organometallic complexes as catalyst precursors: Value and usefulness. *New J. Chem.*, **18**, 93.
- 82 Peuckert, M. and Keim, W. (1983) A new nickel complex for the oligomerization of ethylene. *Organometallics*, **2**, 594.
- 83 Keim, W. (1989) Organometallic complexes as catalyst precursors: advantages and disadvantages. *J. Mol. Catal.*, **52**, 19.
- 84 Keim, W., Behr, A., Gruber, B., Hoffmann, B., Kowaldt, F.H., Kuerschner, U., Limbaecker, B. and Sistig, F.P. (1986) Reactions of chelate ylides with nickel(0) complexes. *Organometallics*, **5**, 2356.
- 85 Smidt, J., Hafner, W., Jira, R., Sedlmeier, J., Sieber, R., Ruttinger, R. and Kojer, H. (1959) Catalytic reactions of olefins on compounds of the platinum group. *Angew. Chem.*, **71**, 176.
- 86 Smidt, J. and Sieber, R. (1959) Reactions of palladium dichloride with olefinic double bonds. *Angew. Chem.*, **71**, 626.
- 87 Moiseev, I.I., Levanda, O.G. and Vargaftik, M.N. (1974) Kinetics of olefin oxidation by tetrachloropalladate in aqueous solution. *J. Am. Chem. Soc.*, **96**, 1003.

- 88 Smidt, J., Hafner, W., Jira, R., Sieber, R., Sedlmeier, J. and Sabel, A. (1962) The oxidation of olefins with palladium chloride catalysts. *Angew. Chem. Int. Ed. Engl.*, **1**, 80.
- 89 Takacs, J.M. and Jiang, X.-t. (2003) The Wacker reaction and related alkene oxidation reactions. *Curr. Org. Chem.*, **7**, 369.
- 90 Bäckvall, J.E., Åkermark, B. and Ljunggren, S.O. (1979) Stereochemistry and mechanism for the palladium(II)-catalyzed oxidation of ethene in water (the Wacker process). *J. Am. Chem. Soc.*, **101**, 2411.
- 91 Nelson, D.J., Li, R. and Brammer, C. (2001) Correlation of relative rates of PdCl₂ oxidation of functionalized acyclic alkenes versus alkene ionization potentials, HOMOs, and LUMOs. *J. Am. Chem. Soc.*, **123**, 1564.
- 92 Hamed, O., Henry, P.M. and Thompson, C. (1999) Palladium(II)-catalyzed exchange and isomerization reactions. 17. Exchange of chiral allyl alcohols with hydroxide, methoxide, and phenyl at high [Cl⁻]. Stereochemistry of the Wacker reaction. *J. Org. Chem.*, **64**, 7745.
- 93 Tolman, C.A. (1986) Steric and electronic effects in olefin hydrocyanation at Du Pont. *J. Chem. Educ.*, **63**, 199.
- 94 Tolman, C.A. (1972) The 16- and 18-electron rule in organometallic chemistry and homogeneous catalysis. *Chem. Soc. Rev.*, **1**, 337.
- 95 McKinney, R.J. (1985) Kinetic control in catalytic olefin isomerization. An explanation for the apparent contra-thermodynamic isomerization of 3-pentenitrile. *Organometallics*, **4**, 1142.
- 96 Goertz, W., Keim, W., Vogt, D., Englert, U., Boele, M.D.K., van der Veen, L.A., Kamer, P.C.J. and van Leeuwen, P.W.N.M. (1998) Electronic effects in the nickel-catalyzed hydrocyanation of styrene applying chelating phosphorus ligands with large bite angles. *J. Chem. Soc., Dalton Trans.*, 2981.
- 97 Freixa, Z. and van Leeuwen, P.W.N.M. (2003) Bite angle effects in diphosphine metal catalysts: Steric or electronic? *Dalton Trans.*, 1890.
- 98 Blaser, H.-U. (2002) The chiral switch of (S)-metolachlor: A personal account of an industrial odyssey in asymmetric catalysis. *Adv. Synth. Catal.*, **344**, 17.
- 99 Blaser, H.-U. and Spindler, F. (1998) Enantioselective catalysis for agrochemicals. The case histories of (S)-metolachlor, (R)-metalaxyl and clozylacon. *Top. Catal.*, **4**, 275.
- 100 Ng Cheong Chan, Y. and Osborn, J.A. (1990) Iridium(III) hydride complexes for the catalytic enantioselective hydrogenation of imines. *J. Am. Chem. Soc.*, **112**, 9400.
- 101 Spindler, F., Pugin, B. and Blaser, H.U. (1990) New diphosphonioiridium catalysts for the enantioselective hydrogenation of N-arylketimines. *Angew. Chem. Int. Ed. Engl.*, **29**, 558.
- 102 Spindler, F., Pugin, B., Jalett, H.-P., Buser, H.-P., Pittelkow, U. and Blaser, H.-U. (1996) A technically useful catalyst for the homogeneous enantioselective hydrogenation of N-aryl imines: A case study. *Chem. Ind. (Dekker) Catal. Org. React.*, **68**, 153.
- 103 Togni, A. (1996) Developing new chiral ferrocenyl ligands for asymmetric catalysis. A personal account. *Chimia*, **50**, 86.
- 104 Togni, A. (1996) Planar-chiral ferrocenes: Synthetic methods and applications. *Angew. Chem. Int. Ed. Engl.*, **35**, 1475.
- 105 Kwan, E.E. (2005) Factors affecting the relative efficiency of general acid catalysis. *J. Chem. Educ.*, **82**, 1026.
- 106 Leadbeater, N.E. and Marco, M. (2003) Transition-metal-free Suzuki-type coupling reactions. *Angew. Chem. Int. Ed.*, **42**, 1407.
- 107 Leadbeater, N.E. and Marco, M. (2003) Transition-metal-free Suzuki-type coupling reactions: scope and limitations of the methodology. *J. Org. Chem.*, **68**, 5660.

- 108 Leadbeater, N.E., Marco, M. and Tominack, B.J. (2003) First examples of transition-metal free Sonogashira-type couplings. *Org. Lett.*, **5**, 3919.
- 109 Berkessel, A. and Gröger, H. (2005) *Asymmetric Organocatalysis*, Wiley-VCH, Weinheim, ISBN 3-527-30517-3.
- 110 Dalco, P.I. and Moisan, L. (2004) In the golden age of organocatalysis. *Angew. Chem. Int. Ed.*, **43**, 5138.
- 111 Westermann, B. (2003) Asymmetric catalytic aza-Henry reactions leading to 1,2-diamines and 1,2-diaminocarboxylic acids. *Angew. Chem. Int. Ed.*, **42**, 151.
- 112 Cobb, A.J.A., Shaw, D.M., Longbottom, D.A., Gold, J.B. and Ley, S.V. (2005) Organocatalysis with proline derivatives: improved catalysts for the asymmetric Mannich, nitro-Michael and aldol reactions. *Org. Biomol. Chem.*, **3**, 84.
- 113 Marcelli, T., van der Haas, R.N.S., van Maarseveen, J.H. and Hiemstra, H. (2006) Asymmetric organocatalytic Henry reaction. *Angew. Chem. Int. Ed.*, **45**, 929.
- 114 Cornils, B. and Herrmann, W.A. (2003) Concepts in homogeneous catalysis: the industrial view. *J. Catal.*, **216**, 23.
- 115 Cole-Hamilton, D.J. (2003) Homogeneous catalysis – new approaches to catalyst separation, recovery, and recycling. *Science*, **299**, 1702.
- 116 Bhanage, B.M. and Arai, M. (2001) Catalyst product separation techniques in Heck reaction. *Catal. Rev. - Sci. Eng.*, **43**, 315.
- 117 Jessop, P.G., Ikariya, T. and Noyori, R. (1999) Homogeneous catalysis in supercritical fluids. *Chem. Rev.*, **99**, 475.
- 118 Pereda, S., Bottini, S.B. and Brignole, E.A. (2005) Supercritical fluids and phase behavior in heterogeneous gas-liquid catalytic reactions. *Appl. Catal. A: Gen.*, **281**, 129.
- 119 Webb, P.B., Kunene, T.E. and Cole-Hamilton, D.J. (2005) Continuous flow homogeneous hydroformylation of alkenes using supercritical fluids. *Green Chem.*, **7**, 373.
- 120 Koch, D. and Leitner, W. (1998) Rhodium-catalyzed hydroformylation in supercritical carbon dioxide. *J. Am. Chem. Soc.*, **120**, **13**, 398.
- 121 Sellin, M.F., Bach, I., Webster, J.M., Montilla, F., Rosa, V., Aviles, T., Poliakov, M. and Cole-Hamilton, D.J. (2002) Hydroformylation of alkenes in supercritical carbon dioxide catalysed by rhodium trialkylphosphine complexes. *J. Chem. Soc., Dalton Trans.*, 4569.
- 122 Kainz, S., Brinkmann, A., Leitner, W. and Pfaltz, A. (1999) Iridium-catalyzed enantioselective hydrogenation of imines in supercritical carbon dioxide. *J. Am. Chem. Soc.*, **121**, 6421.
- 123 Mueller, C., Nijkamp, M.G. and Vogt, D. (2005) Continuous homogeneous catalysis. *Eur. J. Inorg. Chem.*, 4011.
- 124 Vankelecom, I.F.J. (2002) Polymeric membranes in catalytic reactors. *Chem. Rev.*, **102**, 3779.
- 125 Eggeling, E.B., Hovestad, N.J., Jastrzebski, J.T.B.H., Vogt, D. and van Koten, G. (2000) Phosphino carboxylic acid ester functionalized carbosilane dendrimers: nanoscale ligands for the Pd-catalyzed hydrovinylation reaction in a membrane reactor. *J. Org. Chem.*, **65**, 8857.
- 126 de Groot, D., de Waal, B.F.M., Reek, J.N.H., Schenning, A.P.H.J., Kamer, P.C.J., Meijer, E.W. and van Leeuwen, P.W.N.M. (2001) Noncovalently functionalized dendrimers as recyclable catalysts. *J. Am. Chem. Soc.*, **123**, 8453.
- 127 Kleij, A.W., Gossage, R.A., Gebbink, R.J.M.K., Brinkmann, N., Reijerse, E.J., Kragl, U., Lutz, M., Spek, A.L. and van Koten, G. (2000) A “dendritic effect” in homogeneous catalysis with carbosilane-supported arylnickel(II) catalysts: observation of active-site proximity effects in atom-transfer radical addition. *J. Am. Chem. Soc.*, **122**, **12**, 112.
- 128 Datta, A., Ebert, K. and Plenio, H. (2003) Nanofiltration for homogeneous catalysis separation: soluble polymer-supported

- palladium catalysts for Heck, Sonogashira, and Suzuki coupling of aryl halides. *Organometallics*, **22**, 4685.
- 129** An der Heiden, M. and Plenio, H. (2004) Homogeneous catalysts supported on soluble polymers: biphasic Suzuki–Miyaura coupling of aryl chlorides using phase-tagged palladium–phosphine catalysts. *Chem. Eur. J.*, **10**, 1789.
- 130** Dijkstra, H.P., Ronde, N., van Klink, G.P.M., Vogt, D. and van Koten, G. (2003) Application of a homogeneous dodecakis (NCN–Pd^{II}) catalyst in a nanofiltration membrane reactor under continuous reaction conditions. *Adv. Synth. Catal.*, **345**, 364.
- 131** Dijkstra, H.P., Kruithof, C.A., Ronde, N., van de Coevering, R., Ramon, D.J., Vogt, D., van Klink, G.P.M. and van Koten, G. (2003) Shape-persistent nanosize organometallic complexes: synthesis and application in a nanofiltration membrane reactor. *J. Org. Chem.*, **68**, 675.
- 132** Copéret, C., Chabanas, M., Saint-Arroman, R.P. and Basset, J.-M. (2003) Homogeneous and heterogeneous catalysis: bridging the gap through surface organometallic chemistry. *Angew. Chem. Int. Ed.*, **42**, 156.
- 133** Scott, S.L., Basset, J.M., Nicolai, G.P., Santini, C.C., Candy, J.P., Lecuyer, C., Quignard, F. and Choplin, A. (1994) Surface organometallic chemistry: a molecular approach to surface catalysis. *New J. Chem.*, **18**, 115.
- 134** Park, E.D., Lee, K.H. and Lee, J.S. (2000) Easily separable molecular catalysis. *Catalysis Today*, **63**, 147.
- 135** Clark, J.H., MacQuarrie, D.J. and Tavener, S.J. (2006) The application of modified mesoporous silicas in liquid phase catalysis. *Dalton Trans.*, 4297.
- 136** Jackson, T., Clark, J.H., Macquarrie, D.J. and Brophy, J.H. (2004) Base catalyst immobilised on silica coated reactor walls for use in continuous flow systems. *Green Chem.*, **6**, 193.
- 137** Simons, C., Hanefeld, U., Arends, I.W.C.E., Sheldon, R.A. and Maschmeyer, T. (2004) Noncovalent anchoring of asymmetric hydrogenation catalysts on a new mesoporous aluminosilicate: application and solvent effects. *Chem. Eur. J.*, **10**, 5829.
- 138** Lempers, H.E.B. and Sheldon, R.A. (1998) The stability of chromium in CrAPO-5, CrAPO-11, and CrS-1 during liquid phase oxidations. *J. Catal.*, **175**, 62.
- 139** Arends, I.W.C.E. and Sheldon, R.A. (2001) Activities and stabilities of heterogeneous catalysts in selective liquid phase oxidations: recent developments. *Appl. Catal., A: Gen.*, **212**, 175.
- 140** Sheldon, R.A., Wallau, M., Arends, I.W.C.E. and Schuchardt, U. (1998) Heterogeneous catalysts for liquid-phase oxidations: philosophers' stones or Trojan horses? *Acc. Chem. Res.*, **31**, 485.
- 141** Corma, A. and Garcia, H. (2004) Supramolecular host–guest systems in zeolites prepared by ship-in-a-bottle synthesis. *Eur. J. Inorg. Chem.*, 1143.
- 142** Heinrichs, C. and Holderich, W.F. (1999) Novel zeolitic hosts for “ship-in-a-bottle” catalysts. *Catal. Lett.*, **58**, 75.
- 143** Zsigmond, A., Bogar, K. and Notheisz, F. (2003) Comparative study of “ship-in-a-bottle” and anchored heterogenized Rh complexes. *J. Catal.*, **213**, 103.
- 144** Kolb, H.C., Finn, M.G. and Sharpless, K.B. (2001) Click chemistry: diverse chemical function from a few good reactions. *Angew. Chem. Int. Ed.*, **40**, 2004.
- 145** Kolb, H.C. and Sharpless, K.B. (2003) The growing impact of click chemistry on drug discovery. *Drug Discov. Today*, **8**, 1128.
- 146** Ferraris, D., Drury, W.J., Cox, C. and Lectka, T. (1998) “Orthogonal” Lewis acids: catalyzed ring opening and rearrangement of acylaziridines. *J. Org. Chem.*, **63**, 4568.
- 147** Huisgen, R. (1989) Kinetics and reaction mechanisms: selected examples from the experience of forty years. *Pure Appl. Chem.*, **61**, 613.
- 148** Huisgen, R., Szeimies, G. and Moebius, L. (1967) 1,3-Dipolar cycloadditions.

- XXXII. Kinetics of the addition of organic azides to carbon-carbon multiple bonds. *Chem. Ber.*, **100**, 2494.
- 149** Gothelf, K.V. and Jørgensen, K.A. (1998) Asymmetric 1,3-dipolar cycloaddition reactions. *Chem. Rev.*, **98**, 863.
- 150** Durán Páchon, L., van Maarseveen, J.H. and Rothenberg, G. (2005) Click chemistry: copper clusters catalyze the cycloaddition of azides with terminal alkynes. *Adv. Synth. Catal.*, **347**, 811.
- 151** Creutz, C. (1981) Complexities of ascorbate as a reducing agent. *Inorg. Chem.*, **20**, 4449.
- 152** Tornøe, C.W., Christensen, C. and Meldal, M. (2002) Peptidotriazoles on solid phase: [1,2,3]-triazoles by regioselective copper(I)-catalyzed 1,3-dipolar cycloadditions of terminal alkynes to azides. *J. Org. Chem.*, **67**, 3057.
- 153** Diaz, D.D., Punna, S., Holzer, P., McPherson, A.K., Sharpless, K.B., Fokin, V.V. and Finn, M.G. (2004) Click chemistry in materials synthesis. 1. Adhesive polymers from copper-catalyzed azide-alkyne cycloaddition. *J. Polym. Sci. Polym. Chem.*, **42**, 4392.
- 154** Scheel, A.J., Komber, H. and Voit, B.I. (2004) Novel hyperbranched poly([1,2,3]-triazole)s derived from AB₂ monomers by a 1,3-dipolar cycloaddition. *Macromol. Rapid Commun.*, **25**, 1175.
- 155** Wu, P., Feldman, A.K., Nugent, A.K., Hawker, C.J., Scheel, A., Voit, B., Pyun, J., Frechet, J.M.J., Sharpless, K.B. and Fokin, V.V. (2004) Efficiency and fidelity in a click-chemistry route to triazole dendrimers by the copper(I)-catalyzed ligation of azides and alkynes. *Angew. Chem. Int. Ed.*, **43**, 3928.
- 156** Horne, W.S., Yadav, M.K., Stout, C.D. and Ghadiri, M.R. (2004) Heterocyclic peptide backbone modifications in an α -helical coiled coil. *J. Am. Chem. Soc.*, **126** (15), 366.
- 157** Rodionov, V.O., Fokin, V.V. and Finn, M.G. (2005) Mechanism of the ligand-free CuI-catalyzed azide-alkyne cycloaddition reaction. *Angew. Chem. Int. Ed.*, **44**, 2210.
- 158** Himo, F., Lovell, T., Hilgraf, R., Rostovtsev, V.V., Noodleman, L., Sharpless, K.B. and Fokin, V.V. (2005) Copper(I)-catalyzed synthesis of azoles. DFT study predicts unprecedented reactivity and intermediates. *J. Am. Chem. Soc.*, **127**, 210.
- 159** Siemsen, P., Livingston, R.C. and Diederich, F. (2000) Acetylenic coupling: A powerful tool in molecular construction. *Angew. Chem. Int. Ed.*, **39**, 2632.
- 160** Stephens, R.D. and Castro, C.E. (1963) The substitution of aryl iodides with cuprous acetylides. A synthesis of tolans and heterocyclics. *J. Org. Chem.*, **28**, 3313.
- 161** Sonogashira, K., Tohda, Y. and Hagihara, N. (1975) A convenient synthesis of acetylenes: catalytic substitutions of acetylenic hydrogen with bromoalkenes, iodoarenes and bromopyridines. *Tetrahedron Lett.*, **16**, 4467.
- 162** Rothenberg, G., Yatziv, Y. and Sasson, Y. (1998) Comparative autoxidation of 3-carene and α -pinene: factors governing regioselective hydrogen abstraction reactions. *Tetrahedron*, **54**, 593.
- 163** Mestres, R. and Mestres, G. (1992) Deltamethrin: Uses and environmental safety. *Rev. Environ. Contam. Toxicol.*, **124**, 1.

4

Heterogeneous Catalysis

Heterogeneous catalysis influenced our lives greatly in the 20th century. In 1908, the German chemist Fritz Haber succeeded in synthesizing ammonia by feeding N_2 and H_2 at high pressures over an osmium catalyst. This discovery was picked up by Carl Bosch and Alwin Mittasch at BASF, who tested over 2500 different materials until they found an iron-based compound which was active enough and cheap enough to serve as a commercial catalyst. The Haber–Bosch ammonia synthesis has become one of the most important chemical processes worldwide, earning Haber the 1918 Nobel Prize in chemistry. Nitrogen fixation provided mankind with a much-needed fertilizer, improving crop yields for the world's growing population. Ironically, the same process also provided raw materials for making explosives, strengthening Germany's position in World War I. Mittasch's magnetite catalyst (with some modifications) is still used today on a gigantic scale – a staggering 110 million tons of ammonia was produced in 2005, accounting for 1% of the global energy consumption.

The 1930s saw the development of three important types of **refinery catalysts**, for hydrocarbon cracking, alkylation, and dehydrogenation. Once again, heterogeneous catalysis played a major role in warfare, this time in WW II. Using new cracking and alkylation catalysts, the Allied forces produced higher-octane aviation fuel, which gave the Spitfires superior performance over the Messerschmitts in the famous Battle of Britain. Similarly, catalytic dehydrogenation of methylcyclohexane supplied both sides with the necessary toluene for making TNT.

Another important catalytic process which emerged out of political turmoil was the Fischer–Tropsch synthesis. Germany and Japan had an abundance of coal, but no reliable source of petroleum. The Co/Fe-catalyzed Fischer–Tropsch process converted coal to syngas, further reaction of which gave a liquid mixture rich in C_5 – C_{11} olefins and paraffins. South Africa also used this process for converting coal during the apartheid period, to compensate for its shortage of petroleum supply. Interestingly, Fischer–Tropsch-type processes are now back in demand, as governments seek sulfur-free fuels and alternatives to petroleum [1].

Today, heterogeneous catalysis dominates the petrochemicals and the bulk chemicals industry [2]. The sales of refinery catalysts topped €2 billion (\$2.7 billion) in 2005,

Table 4.1 Examples of major industrial processes using heterogeneous catalysis.

Process	Catalyst	Reactants	Products	End usage
Haber-Bosch NH ₃ synthesis	magnetite (Fe)	H ₂ , N ₂	NH ₃	fertilizer, gunpowder, explosives
Methanol synthesis [11]	Cu/ZnO/Al ₂ O ₃	CO, CO ₂ , H ₂	CH ₃ OH	bulk chemicals, fuel
Fischer-Tropsch [12]	Co, Fe	coal, natural gas	C ₅ -C ₁₁ hydrocarbons	automotive fuel
Cracking [13]	clays	long alkanes, C ₁₂ +	C ₇ -C ₉ alkanes	fuel, detergents
Alkylation [14]	zeolites, clays, silicates	C ₃ -C ₅ alkanes	C ₇ -C ₉ isoalkanes	high-octane fuel
Dehydrogenation/reforming	Pt/Al ₂ O ₃	alkanes	alkenes	polymers, bulk chemicals
Hydrodesulfurization [15,16]	Co/Mo sulfides	diesel fuel	sulfur-free diesel	automotive fuel
Hydrocracking [2]	Pt on zeolites or aluminosilicates	aromatics mixture	saturated hydrocarbons	automotive/aviation fuel
Isomerization [17]	H-ZSM-5 zeolites	xylenes, toluene	p-xylene	polymers, bulk chemicals
Polymerization [18]	Ti, Ziegler-Natta	ethene	poly(ethylene)	polymers, bulk chemicals
Oxidation [19]	vanadium oxide	xylenes	phthalic acids	polymers

with an expected annual growth of 3.24% [3]. Not surprisingly, the biggest demand for these catalysts comes from the stricter legislation on sulfur content in diesel and gasoline. Table 4.1 gives some examples of the key processes, catalysts, and products involved. In the last two decades, with the advancement of green chemistry, heterogeneous catalysis has moved into the fine-chemicals and pharmaceuticals industry also [4]. Solid catalysts are also used in clean energy applications such as fuel cells [5,6], solar energy conversion [7,8], and energy storage cycles [9,10].

At first glance, heterogeneous catalysis seems overwhelming. It is the most varied and the most complicated of the three catalysis subdisciplines, combining physical chemistry, inorganic chemistry, organic and organometallic chemistry, surface science, and materials science. There are numerous books on various aspects of heterogeneous catalysis, several dedicated journals, and over 18 000 research papers. Fortunately, these varied applications are based on a few fundamental principles. This chapter explains the scientific fundamentals, illustrating them through a number of industrial examples. I will focus on the physical chemistry and materials science issues, rather than on the engineering aspects. An excellent detailed discussion of the latter is given in the comprehensive handbook by Ertl, Knözinger, and Weitkamp [20].

Note that the distinction between “heterogeneous catalysis” and “homogeneous catalysis” or “biocatalysis” is subjective. A typical enzyme is so much larger than its substrate, and the reaction environment it presents is so different from the surrounding solvent, that it qualifies as a “heterogeneous catalyst.” Similarly, there are soluble catalysts (e.g., surfactant-stabilized metal nanoparticles [21]) which are on the borderline between “homogeneous” and “heterogeneous” systems. To avoid confusion, this chapter focuses on three cases only: classic gas/solid systems, liquid/solid systems, and liquid/liquid systems. Reactions involving immobilized organometallic complexes or immobilized enzymes are discussed in Chapters 3 and 5, respectively.

4.1 Classic Gas/Solid Systems

The classic gas/solid heterogeneous catalysis comprises the bulk of catalytic processing. Over 90 vol% of the chemicals worldwide are manufactured with the aid of solid catalysts. Typically, the gaseous reactants are fed over the catalyst bed, usually at high temperatures, and sometimes at high pressures. These conditions are suitable for continuous processes, e.g., using plug-flow reactors. From the outside, the process seems extremely simple: reactants enter the reactor, and products leave it (Figure 4.1, left). Inside, things are much more complicated: reactants must diffuse through the catalyst pores, adsorb on its surface, travel to the active site, react there, and desorb back to the gas phase (Figure 4.1, right). All of these steps happen at the molecular level (also called the **microscopic level**, although in reality it is nanoscopic, rather than microscopic). However, the catalyst itself is a macroscopic object, with an intricate surface structure, and physical interactions at the **macroscopic level** also affect the

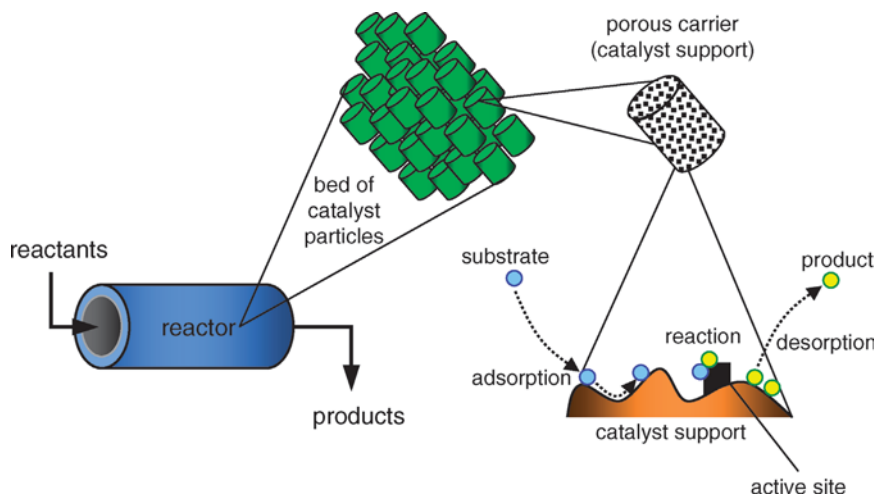


Figure 4.1 A plug-flow catalytic reactor at various zoom-in levels.

reaction outcome. This is the difference between homogeneous and heterogeneous catalysis, and this is what makes heterogeneous catalysis so complicated.

In every gas/solid catalytic cycle, at least one of the reactants must at some point be adsorbed on the catalyst surface. Let us consider the reaction $A + B \rightarrow C$. There are two options (Figure 4.2): In the first, both reactants **A** and **B** are first adsorbed on the catalyst, migrate to each other, and react on the surface, giving the product **C**, which is desorbed into the gas phase. This pathway, which we have already met in Chapter 2, is the **Langmuir–Hinshelwood mechanism**. The other option is that **A** is adsorbed on the catalyst surface, and **B** subsequently reacts with it from the gas phase to give **C** (the so-called **Eley–Rideal mechanism** [22]). The Langmuir–Hinshelwood mechanism is much more common, partly because many reactants are activated by the adsorption on the catalyst surface.

The surface interactions hold the key to the catalyst's activity, selectivity, and stability. Unlike the situation for molecular catalysts, the bulk parameters such as particle size, shape, and mechanical strength are crucial here. Particle size is directly related to the accessible active surface area. Platinum, for example, is an excellent catalyst for alkane dehydrogenation, but it is also very expensive (ca. €32/g or \$44/g

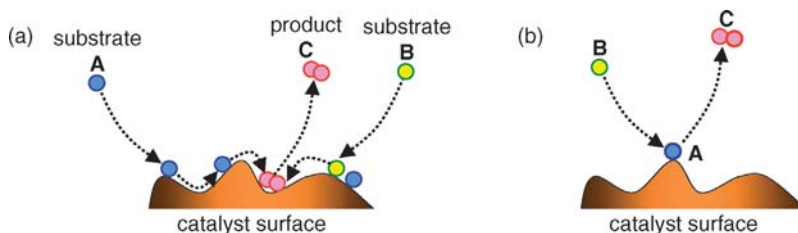


Figure 4.2 The two main mechanisms in gas/solid heterogeneous catalysis: **a** Langmuir–Hinshelwood; **b** Eley–Rideal.

in February, 2007). Suppose you use a cubic centimeter of Pt as your catalyst. This cube would weigh 21.3 g, and cost about €700 (\$1000). The available surface area of such a cube would be only 5 cm^2 , because one side would have to be attached to the reactor. Now, if you break this cube into 10^{12} smaller cubes, each of which has $1\text{ }\mu\text{m}$ sides, the total available surface area would be $5 \times 10^{12}\text{ }\mu\text{m}^2$, or $50\,000\text{ cm}^2$. State-of-the-art catalyst synthesis methods can produce particles as small as 2 nm , with correspondingly huge surface areas. Interestingly, reducing the particle size can also cause undesired effects, due to surface penetration by foreign atoms [23,24]. One reason why Pt is an excellent oxidation catalyst is that O_2 is readily adsorbed on Pt particles, dissociating to two O atoms which react with a variety of substrates. When the particles are very small ($<10\text{ nm}$), they react with oxygen and form platinum oxide. The resulting strong Pt–O bond lowers the catalytic activity, despite the large metal surface area.

Placing all these small particles in one reactor at high temperatures would cause very high back-pressures and agglomeration. This can be avoided by coating the active metal particles on a (porous) support with a high surface area, e.g., silica, alumina, zeolites, or carbon. The shape and mechanical strength of the catalyst particles are also important, especially in large-scale applications (refinery reactors can be 20 m high, holding as much as 50 tons of catalyst). They determine the packing in the reactor, and ultimately the flow of the gaseous reactants and products to and from the catalyst.

Two other crucial factors are mass transfer and heat transfer. In Chapter 3 we assumed that the reactions were homogeneous and well stirred, so that every substrate molecule had an equal chance of getting to the catalytic intermediates. Here the situation is different. When a molecule reaches the macroscopic catalyst particle, there is no guarantee that it will react further. In porous materials, the reactant must first diffuse into the pores. Once adsorbed, the molecule may need to travel on the surface, in order to reach the active site. The same holds for the exit of the product molecule, as well as for the transfer of heat to and from the reaction site. In many gas/solid systems, the product is “hot” as it leaves the catalyst, and carries the excess energy out with it. This energy must dissipate through the catalyst particles and the reactor wall. Uneven heat transfer can lead to hotspots, sintering, and runaway reactions.

4.1.1

The Concept of the Active Site

The fact that heterogeneous catalysis occurs at a surface really complicates things, because surfaces are not nearly as nice and uniform as we like to think. At the microscopic level, metal crystal surfaces show various steps and kinks (Figure 4.3). Strikingly, it is often precisely at these irregular points that catalysis happens. This is because the surface atoms at those spots are not fully coordinated, and thus have more options for interacting with substrate molecules. This concept of active sites was put forward in the 1920s by the British chemist Hugh Taylor, who also suggested that active sites on the surfaces can be few and far between [25–27]. Today, we know

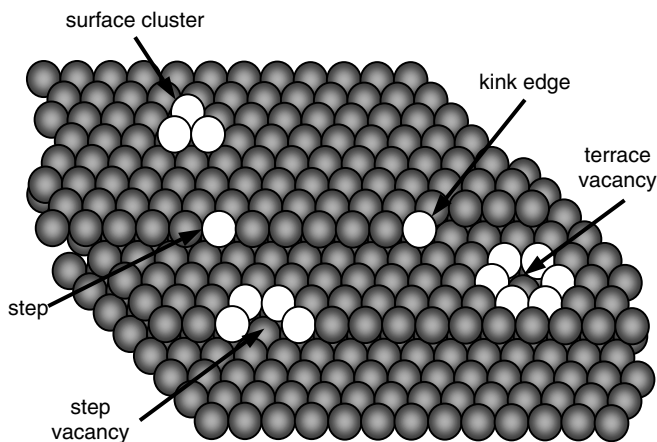


Figure 4.3 Schematic representation of a solid catalyst crystal surface.

that Taylor was right, and that in many cases what we call “the catalyst” is made up mostly of inactive surface, with a few very active spots. Figure 4.3 shows a schematic drawing of a catalyst particle, indicating the various irregularities at the surface.

Note that the catalytic active site is often not the energetically preferred site for adsorption (i.e., there are other sites on the surface where adsorption would be more exothermic). The most favored site for adsorption may be “too good”, in the sense that any species that are adsorbed on it would simply stay there. The active site follows Sabatier’s principle – reactants should be able to be adsorbed there, but after the reaction they should also be able to leave.

Ideally, the active sites should all be identical, and isolated from each other. This is seldom the case, because industrial heterogeneous catalysts are often amorphous, multicomponent and multiphase solids, containing many types of active sites. Nevertheless, there is one important exception: zeolites. These highly crystalline materials can be synthesized to exacting specifications, including the setup of identical active sites at uniform distances. As we shall see, this is one of the key advantages of zeolites, which are the preferred catalysts today for many industrial processes.

4.1.2

Model Catalyst Systems

About 800 000 tons of solid catalysts are prepared and used every year worldwide, but this does not mean that we understand how they work. Catalyst synthesis and treatment recipes are often based on empirical studies, handed down the generations like ancient medicines. Since chemists dislike ignorance even more than nature abhors a vacuum, much research is done to find out how solid catalysts work. And, since the real industrial catalysts are usually multicomponent, nonuniform solids, much of this research is done on simplified model systems [28].

This difference between the model catalysts and the real ones is a major debating point in the catalysis community. Industrial catalysts are usually porous,

high-surface-area materials (typically $50\text{--}400\text{ m}^2\text{ g}^{-1}$). They can be amorphous or microcrystalline materials, and can contain different phases. Furthermore, their surface composition can change in the course of the installation time, due to ion diffusion from the bulk, high-temperature/pressure effects, or impurities in the feed. Conversely, model catalysts are well-defined materials, often examined under “clean” laboratory conditions (low pressures or even ultra-high vacuum, low temperatures, pure component feed streams, and small reactors, with no sintering problems from uneven heat transfer). Given these differences, does studying such model systems make sense? The answer is yes, as long as you are aware of the model’s limitations. That being said, much effort is directed at “bridging the gap” between model systems and real catalysts, with catalyst characterization done as close as possible to the real process conditions (*operando* conditions) [29–31].

The most common model systems for heterogeneous catalysis are single crystals. These are highly uniform and pure materials. They are easy to characterize and study in detail, both under ultra-high-vacuum conditions and under simulated process conditions [32]. Despite the gap between the single-crystal catalyst and the real catalyst, one can learn much about the catalytic cycle by studying single-crystal systems [33]. The model systems provide a firm scientific basis for developing new concepts and ideas, which can then be tested in real-life situations [34].

Single crystals are particularly useful for determining structure/activity relationships. There is a host of characterization methods available for measuring the heats of adsorption and desorption, the sticking probabilities, and the rate of surface reactions. Indeed, such measurements show that different crystal facets can have completely different catalytic properties! Figure 4.4 shows the rate of dissociative adsorption of nitrogen on Fe single crystals. This dissociation is a key step in the ammonia synthesis process (in October 2007, as this book was being published, Gerhard Ertl was awarded the Nobel Prize in chemistry for studies on model catalysts that led to an understanding of this process). The large differences in dissociative adsorption between the [1,1,1] and the [1,1,0] planes correlate well with the activity of these planes in ammonia synthesis under simulated industrial conditions [35].

By cutting the crystal in specific directions, you can control the number and type of steps and kinks on its surface. In this way, you can study the performance of specific surface irregularities under controlled conditions. For example, Davis et al. showed that in platinum-catalyzed hydrogenolysis, the kink sites on the Pt surface were more active than the [1,1,1] sites [36]. Although the concentration of kinks on the surface was only 5%, they represented over 90% of the catalytic activity, demonstrating Taylor’s active-site principle. Single crystals can also be used for studying the effects of multicomponent catalysts and promoters, which are closer to the complex industrial formulations. Catalytic reforming, for example, is carried out in the presence of a Pt/Re/S catalyst. By depositing Pt and S over Re crystals, and *vice versa*, Kim and Somorjai determined the role played by each of the catalyst’s components [37].

Other common model catalyst systems include thin metal and oxide films [38,39], glassy metals [40], supported catalysts based on chemical vapor deposition [41], and

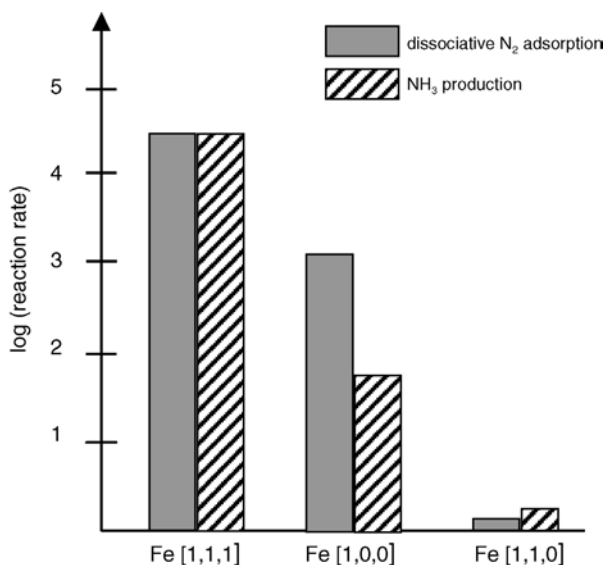


Figure 4.4 Relative rates of dissociative N₂ adsorption (gray bars) and ammonia synthesis (hatched bars) on different planes of Fe single crystals.

supported homometallic and bimetallic clusters and oxides [42–44]. Just like single crystals, these model systems are relatively well defined, enabling the study of discrete steps in the catalytic cycle.

4.1.3

Real Catalysts: Promoters, Modifiers, and Poisons

In contrast with the clean and well-defined model systems, commercial catalysts usually consist of several phases containing a number of species. These are due to impurities, as well as to small amounts of **promoters** or **modifiers**, which are added intentionally during the catalyst synthesis. Adding these compounds improves the catalyst activity, selectivity, stability, and/or accessibility. Alkali metals such as K and Na are often used as **activity modifiers** or **electronic promoters**. Figure 4.5 shows how small amounts of alkali promote the dissociative chemisorption of molecules such as N₂ and CO on the surface of transition metals through electron donation. The electropositive alkali atom donates electron density to the transition metal. This increases the back-donation into the π^* antibonding orbital of the substrate, and facilitates the substrate decomposition. Note that although the promoter activates the surrounding sites, it is not an active catalyst itself, so it effectively blocks the site it is sitting on.

Because their surface energy is lower than that of transition metals, the alkali ions segregate to the upper layers of the catalyst, resulting in high surface concentrations: Adding 0.5% Na during the catalyst synthesis can give as much as 10% Na on the surface. Ammonia synthesis, for example, is carried out over a magnetite (iron-based

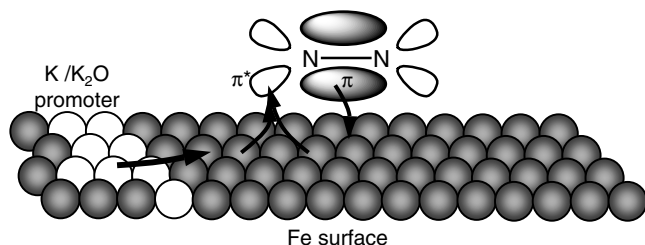


Figure 4.5 An activity promoter lowers the antibonding LUMO of the incoming N₂ molecule, facilitating its dissociation on the catalyst surface.

oxide) catalyst, with two promoters: Al₂O₃ and K₂O. The alumina improves the catalyst's stability, by preventing the sintering of Fe particles (it is a so-called **textural modifier**). The potassium oxide interacts with the orbitals of incoming N₂ molecules, facilitating the dissociation of N₂ on the surface [45]. Single-crystal studies show that when potassium is added to the [1,0,0] face of an Fe crystal, the rate of ammonia synthesis increases by a factor of 300, confirming that the rate-determining step in ammonia synthesis is indeed the dissociative chemisorption of N₂.

Unlike promoters, poisons are usually electronegative atoms, such as C, S, P, and Cl. A poisoning atom or ion blocks sites on the surface, and also reduces the metal/substrate interaction. Being electronegative, they lower the electron density at the active site, decreasing the back-donation and retarding the dissociation of substrates such as CO and N₂. Poisons are not all bad – they can enhance product selectivity by demoting side-reactions. For example, adding 1–2 ppm of ethene dichloride (1,2-dichloroethane) to the Ag-catalyzed ethene epoxidation process deposits Cl atoms on the catalyst surface. This retards the total oxidation of ethene to CO₂ and H₂O, increasing the selectivity to ethene oxide (epoxyethane, oxirane).

Promoters, poisons, and modifiers are ubiquitous throughout the chemical industry. They are often added during the catalyst optimization stage or even in the pilot stage. A catalyst may need a promoter which has no initial effect, for example, but increases long-term stability (which also requires many hours of on-stream testing). Another frequent reason for adding promoters and modifiers is when more stringent regulations demand the adaptation of existing catalysts and processes. Generally speaking, promoter effects are based on empirical observations and trial-and-error experiments. They are rarely understood. Moreover, many academic researchers eschew promoters, preferring to work with well-defined and simpler catalyst systems.

4.1.4

Preparation of Solid Catalysts: Black Magic Revealed

The complex and diverse synthesis protocols of solid catalysts sometimes give the impression of alchemy, instead of 21st-century chemistry. The final catalytic properties depend strongly on every step of the preparation, as well as on the purity (and

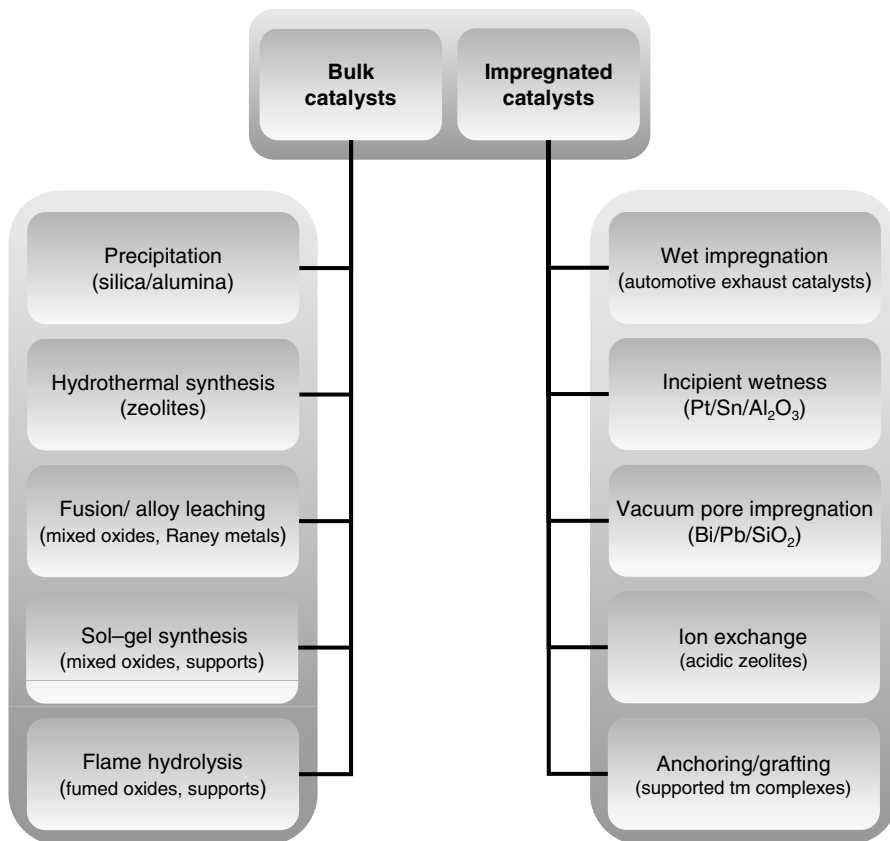


Figure 4.6 Types and examples of solid catalysts, grouped by preparation method (tm = transition metal).

impurity!) of the starting materials. Small changes in drying temperatures, aging times, solvent compositions, or stirring rates can affect the catalyst performance. For this reason, most companies never publish the intimate details of their catalyst synthesis procedures. To simplify things, I will divide the synthesis protocols into a number of common unit operations, and the solid catalysts in two basic preparation classes: bulk catalysts, and impregnated/supported catalysts (Figure 4.6) [46,47].

Figure 4.7 summarizes the main unit operations and stages in the synthesis of solid catalysts, discussed in the following sections. Bulk catalysts are typically made by precipitation, hydrothermal synthesis, or fusion. They are (mixed) metals or oxides and, as their name suggests, the entire catalyst is made of active material. The silica/alumina hydrocracking catalysts, zeolites, the ammonia synthesis catalyst, and the Raney metals all belong to this class. Impregnated catalysts are commonly used in the case of precious metals or unstable compounds. Here, the active metal precursor is deposited on a porous bulk support. This support can be an oxide (e.g., silica, titania, alumina or ceria), an activated carbon, or even an organic or hybrid polymer resin.

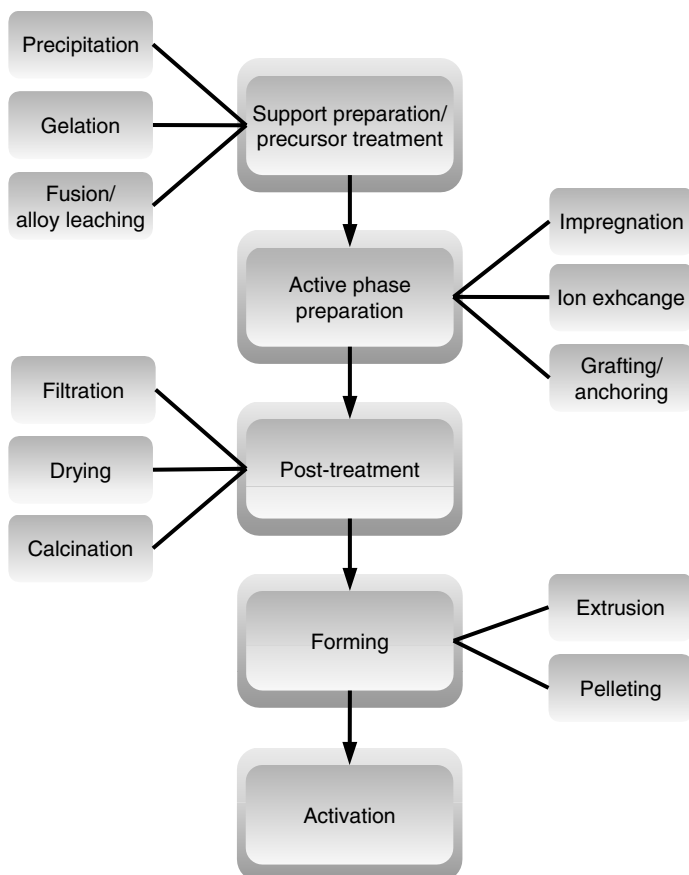


Figure 4.7 Flowchart summarizing the main unit operations and stages in solid catalyst synthesis (different synthesis protocols may include fewer/more operations).

The supports themselves are usually made by the bulk methods. Examples of impregnated catalysts include the Pd/C hydrogenation catalysts, the Pt/Sn/Al₂O₃ dehydrogenation catalysts and the automotive three-way catalysts. There are also catalysts made by hybrid synthesis approaches, e.g., where the active precursors are mixed with a powdered support, and the mixture is then agglomerated.

4.1.4.1 High-Temperature Fusion and Alloy Leaching

Metallic alloys and some mixed-oxide catalysts can be prepared by co-melting and fusion of the metal (oxide) precursors at high temperatures. The melting enables intimate mixing of the precursor atoms and clusters, creating highly pure, well-dispersed solids. Furthermore, a range of different phases can be obtained by controlling the cooling of the melt. Alloys and mixed-oxide catalysts are usually referred to by combining the formulas of their precursors with a dash, e.g., as V₂O₅–MoO₃, or simply as V–Mo–O. One interesting option is the preparation of

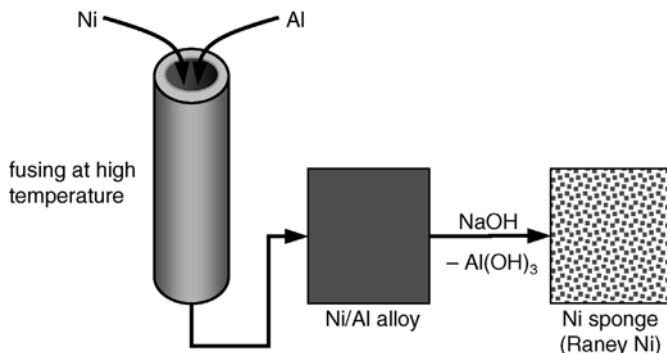


Figure 4.8 The Raney process, in which a metal/aluminum alloy is prepared by fusion, and subsequently the aluminum is dissolved by aqueous NaOH, leaving a “metallic sponge.”

metallic glasses as a new type of catalyst [48]. The disadvantage of the melting/fusion option is that it is an energy-intensive process which requires special equipment, especially compared to the precipitation–calcination protocols.

The preparation of **skeletal catalysts** is worth a special mention. In 1924, the American engineer Murray Raney discovered that metal alloy leaching gave superior hydrogenation catalysts. He made a 50 : 50 Ni/Al alloy by fusion, and then leached out the Al with aqueous NaOH (Figure 4.8). The resulting “nickel sponge,” commonly known as **Raney nickel**, was much more active than the current commercial catalysts. Curiously, Raney hit on the best formula for the alloy right from the start – detailed studies showed that the 50:50 combination was the optimal one, as some alumina was left inside which stabilized the catalyst [49]. In 1963, W. R. Grace & Co. bought the rights to Raney’s patents and trademarks. Today, skeletal catalysts (mostly Ni and Cu) are used in hydrogenation, ammonolysis, and reductive alkylation. The catalysts are ready to use, requiring no reduction or other activation, and have a high metal surface area. Since the catalyst particles are heavy, they are easily separated from the products by settling/decantation. Unlike many other catalysts, Raney metals are stable in alkaline liquids. They are also highly pyrophoric, and are therefore stored under water [50].

4.1.4.2 Slurry Precipitation and Co-precipitation

Precipitation methods are used for making several important catalysts and support materials, including silica, alumina, and the Cu/ZnO/Al₂O₃ methanol synthesis catalyst. Precipitation can give high-purity materials, and co-precipitation can give stoichiometric mixtures with well-defined mixed crystallites. However, unlike fusion, which needs no additional reagents, precipitation requires a solvent and a precipitating agent. This means added costs for catalyst separation and waste disposal.

Typically, the precursor solutions (usually aqueous salt solutions) are mixed, and the desired salt is precipitated as a gel by adding an acid/base or another reagent. Precipitation has three stages: supersaturation, nucleation, and growth. The

resulting gel is aged, filtered, washed, dried, and finally calcined. Different precursor/precipitator combinations can be used. The steam reforming Ni/Al₂O₃ catalysts, for example, can be prepared by co-precipitating the nitrate precursors in the presence of NaOH [51] or by combining an alkaline NaAlO₂ solution with an acidic nickel nitrate solution.

Some bulk catalysts are produced directly from their active components by slurry mixing, using either a small amount of water or of alcohol as solvent. For example, the FeSbO₄ catalyst used in the ammoxidation of propene to acrylonitrile is prepared by adding Sb₂O₃ powder to a warm solution of FeNO₃·9H₂O, and then raising the pH of the slurry using aqueous ammonia [52]. The precipitate is filtered, dried, and calcined at high temperature, resulting in the rutile-structured solid mixed oxide.

4.1.4.3 Impregnation of Porous Supports

Impregnation is a common method of making supported catalysts [53] such as the reforming catalyst Pt/Al₂O₃. In **wet impregnation**, the (porous) support is immersed in a solution of the catalyst precursor. The precursor is either adsorbed spontaneously on the support, or precipitated there by changing the pH or by inducing another chemical reaction. The resulting catalyst is then filtered, dried, and calcined. For example, Pt/Al₂O₃ is prepared by mixing porous alumina with a chloroplatinic acid solution (Eq. (4.1)). The solvent is evaporated, leaving the solute dispersed on the surface. The catalyst is dried and the supported Pt^{IV} ions are reduced to Pt⁰ with hydrogen gas (the notation (Pt)_n indicates a Pt cluster, which can contain hundreds or even thousands of atoms, depending on the degree of aggregation during the reduction step).



One drawback of this method is the large volumes of aqueous waste involved. This can be overcome using the **incipient wetness** method, by which a solution of the active precursor is added to the dry support powder until the mixture becomes “slightly tacky”, indicating that the pores of the support are filled with the liquid. Another variation is **vacuum pore impregnation**, in which the support is first dried and then placed under vacuum, emptying the pores of air. A volume of precursor solution equivalent to the pore volume is then mixed with the support under vacuum, and this solution is absorbed in the pores of the seemingly-dry powder. High loadings of active material can be achieved by drying the catalyst and repeating the impregnation process. Figure 4.9 shows a simple reactor for vacuum pore impregnation, suitable for preparing gram quantities of catalyst [54].

4.1.4.4 Hydrothermal Synthesis

As the name implies, hydrothermal treatments involve the heating of precipitates, gels, or flocculates in the presence of water. These treatments are typically carried out in an autoclave at 100–300 °C, and result in textural and/or structural changes, including crystal and/or particle growth, changes in crystal structure, and transformation of amorphous solids into crystalline ones.

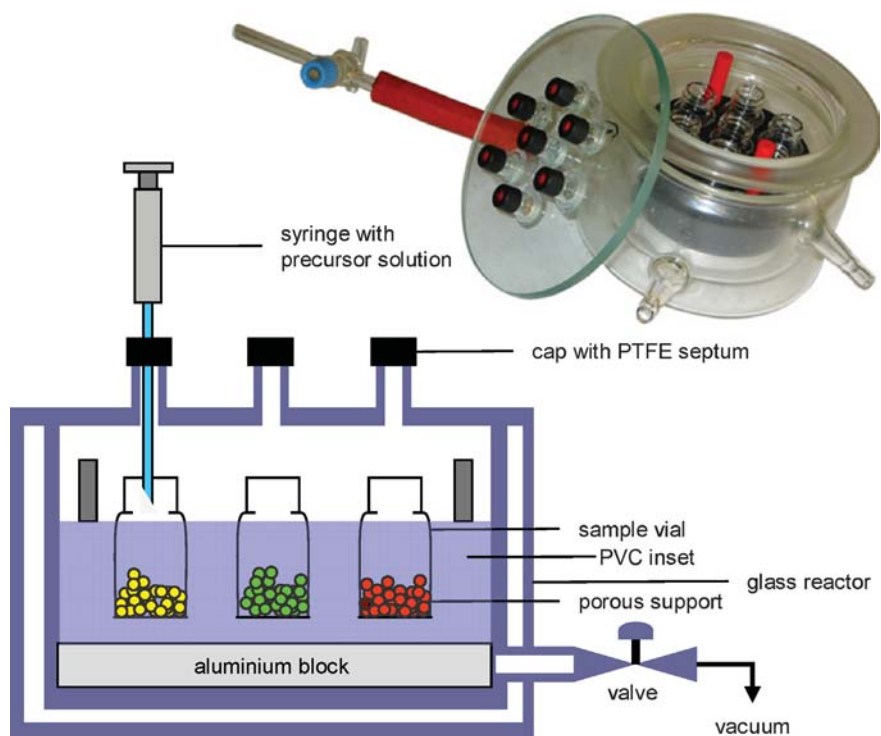


Figure 4.9 Photograph and schematic of a lab-scale parallel reactor for vacuum pore impregnation.

The most important application of hydrothermal synthesis is the manufacture of **zeolites** [55,56]. Typically, zeolites are made from sodium silicate and sodium aluminate precursors at 100–150°C. A supersaturated solution of the precursors is converted into a microporous crystalline material, where the substitution of Al^{3+} in place of the tetrahedral Si^{4+} requires the presence of an extra cation (in this case, Na^+). Like many other crystallizations, zeolite formation is a slow process. Moreover, the type of the zeolite depends strongly on the synthesis conditions. In the early 1970s, researchers at Mobil Oil discovered that adding small amounts of alkylammonium salts to the precursor solution gave new and special zeolites, with unusual pore dimensions. The organic salts act as templates, directing the growth of the zeolite crystals. Surprisingly, the researchers also found that adding the alkylammonium salts resulted in a higher Si/Al ratio, creating so-called high-silica zeolites. The zeolite pores are nanometric channels and cavities (cages), which is why zeolites are also known as **molecular sieves** [57]. Figure 4.10 shows the steps involved in the hydrothermal synthesis of ZSM-5, the most famous synthetic zeolite (the acronym stands for Zeolite Socony Mobil no. 5, as it was the fifth material made in the program; the official generic name of this zeolite topology is MFI).

Ion exchange of the Na^+ cations with NH_4^+ , and subsequent drying and calcination, gives the **solid acid** H-ZSM-5, used in synthetic gasoline manufacture and

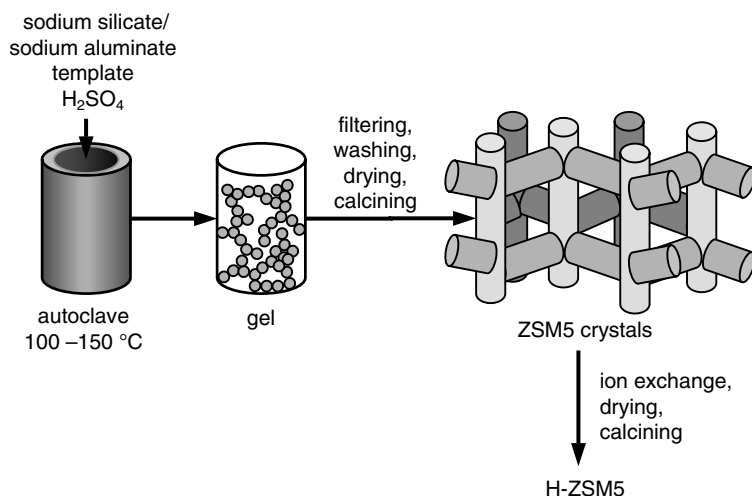


Figure 4.10 Hydrothermal synthesis of ZSM-5 with subsequent ion exchange.

selective isomerization processes [57,58]. Such solid Brønsted acids have an important advantage over HF, HCl, or H_2SO_4 : They are easily isolated from the product mixture and require no neutralization [59]. This means no salt waste, and considering the enormous production volumes in the petrochemical industry, this is a big advantage even when the acid is used in catalytic amounts [60]. The same is true for the fine-chemicals and pharmaceuticals industry [61], where production volumes are smaller but acids are often used as stoichiometric reagents.

Figure 4.11 shows an example of how ZSM-5 is applied as a catalyst for xylene production. The zeolite has two channel types – vertical and horizontal – which form a zigzag 3D connected structure [62,63]. Methanol and toluene react in the presence of the Brønsted acid sites, giving a mixture of xylenes inside the zeolite cages. However, while benzene, toluene, and *p*-xylene can easily diffuse in and out of the channels, the bulkier *m*- and *o*-xylene remain trapped inside the cages, and eventually isomerize (the disproportionation of *o*-xylene to trimethylbenzene and toluene involves a bulky biaryl transition structure, which does not fit in the zeolite cage). For more information on zeolite studies using computer simulations, see Chapter 6.

4.1.4.5 Drying, Calcination, Activation, and Forming

The majority of the preparation protocols involve solvents (mostly water), which must be removed. Drying crystalline solids is straightforward, but flocculates and hydrogels are tricky. The reason is that these gels can contain as much as 90% water, and removing this water can make the porous structure collapse. The solution is a stepwise drying, where the water is first removed at a constant rate from the outside surface of the hydrogel. The gel mass shrinks, giving a dry **xerogel**, which still contains 25–30% water in its pores. This xerogel is either transferred directly to the forming stage (see below), or calcined first at high temperature. The **calcination** process (drying at high temperature, typically $300-800\text{ }^\circ\text{C}$, either in air or in a

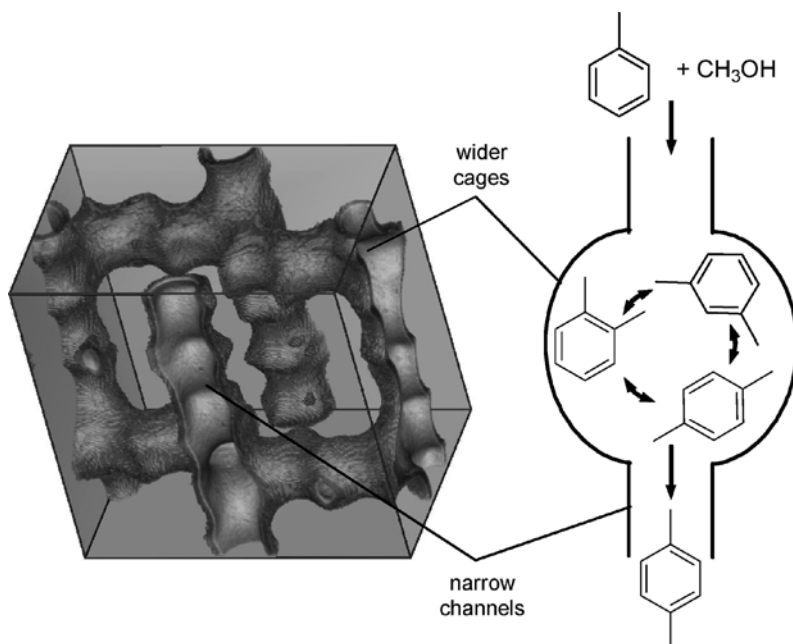


Figure 4.11 Computer simulation of the MFI-type zeolite H-ZSM5 (left), and scheme showing the shape-selective formation of *p*-xylene in the cage (right). Thanks to Dr. Edith Beerdsen for the simulation snapshot.

synthetic gas mixture) removes all the water from the catalyst, decomposes the nitrate/carbonate precursors, and forms metal-oxide links with the support. Depending on the temperature, calcination can also dehydrate surface hydroxyl groups. This is very important as it alters the catalyst surface hydrophobicity. Like drying, calcination should be carried out in a controlled manner, to avoid pore collapse.

Once the required microscopic properties are achieved, most industrial catalysts are **formed** into macroscopic spheres or pellets [64]. The chemical industry uses hundreds of thousands of tons of catalysts every year, most of them in very large reactors. For these applications, the technical macroscopic parameters of the catalyst are of utmost importance. These include the particle size, mechanical strength (preventing attrition and dust formation), bulk thermal expansion coefficients, filtration properties (catalyst recovery from a slurry reactor), stickiness/flocculation properties, and bulk density. The size and shape of the catalyst particles determine the flow of gases in the catalyst bed, as well as the pressure drop over the reactor. If the catalyst particles are not well formed and robust, they will be crushed, and break down to a powder (attrition), clogging the reactor and reducing effectiveness. Catalyst size and shape are a compromise – smaller particles give higher activity, but also increase the pressure drop over the catalyst bed. Roughly speaking, catalyst forms are divided in pellets, beads or granules, spheres, and extrudates. Small spherical particles (10–100 μm) are usually prepared by **spray drying**: the hydrogel or sol solution is

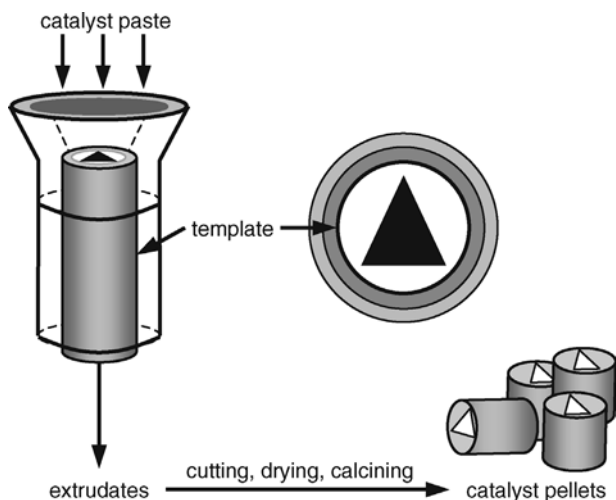


Figure 4.12 Extrusion templates enable the design of catalyst pellets with different shapes and sizes.

sprayed into a hot chamber [65]. The solvent evaporates, causing agglomeration of the catalyst particles. These catalyst spheres are typically used in fluidized-bed reactors. Larger spheres, in the millimeter range, are usually prepared by granulation, “snowball rolling,” or by the so-called oil-drop method [66].

Pelleting or **tableting** is done by compacting the catalyst powder, together with a binder, under high pressure. In **extrusion**, the powder is first made into a paste, together with a binder. Clays, starch, and alumina are commonly used as binders, depending on the rheological and mechanical properties required. This paste is forced through a former (Figure 4.12) very similar to a spaghetti machine, which determines the macroscopic shape of the extrudates. The extrudates are then cut, dried, and calcined, giving the final catalyst particles. An interesting alternative to pellets is to coat the active catalyst on a monolith support [67]. The latter is usually made from ceramic [68] or stainless steel, with a honeycomb structure of channels, each $\sim 1 \text{ mm}^2$. The most famous application of catalytic monolith reactors is the catalytic converter (see Section 4.1.7).

Depending on the final application, the catalyst may require activation prior to the reaction. For example, if you prepare Pd/silica by impregnating the silica support with a $\text{Pd}(\text{NO}_3)_2$ precursor, and then calcining and burning out the nitrates as nitrogen oxides, the calcination will also oxidize the Pd. Such catalysts are usually activated by treatment with H_2 , reducing the oxides at the active site back to Pd^0 .

4.1.5

Selecting the Right Support

The catalyst support should provide optimal dispersion of the active component, good accessibility, and stability against sintering. In many solid catalysts, the active

component is a small metal cluster, while the support is a hard and unreactive material with a high melting point. Silica, titania, alumina, and porous carbon are typical examples. However, organic and hybrid organic/inorganic polymers can also be used as solid supports [60]. Note that the choice of support can influence various catalytic parameters [69].

Although most supports are chemically inactive, some applications benefit from active supports. Cerium oxide and ceria-based mixed oxides ($\text{Ce}_x\text{M}_{1-x}\text{O}_y$), for example, are versatile solid oxygen exchangers. At temperatures above 350°C , the $\text{Ce}^{3+} \rightleftharpoons \text{Ce}^{4+} + e^-$ redox cycle facilitates oxygen storage and release from the fluorite lattice. This makes them ideal as catalyst supports for direct oxidation applications [70], such as automotive three-way catalysis [71] and hydrocarbon fuel cells [72,73]. Sometimes the support itself is also a catalyst, creating a bifunctional catalytic system. Converting *n*-heptane to isoheptane, for example, requires both a dehydrogenation catalyst (such as $\text{Pt}/\text{Al}_2\text{O}_3$) and an isomerization catalyst (such as silica/alumina). Impregnating a porous silica/alumina support with Pt particles creates a bifunctional system which can catalyze both processes simultaneously.

Specific Surface Area In general, the larger the surface area, the better the dispersion and the more catalyst you will get for your money. Most catalyst supports are porous materials, which means that the surface is “inside the catalyst,” i.e., in the pores. The specific surface areas of metal oxides such as silica or alumina are typically $100\text{--}300\text{ m}^2\text{ g}^{-1}$, while some porous carbons have surface areas as high as $3000\text{ m}^2\text{ g}^{-1}$ (three-quarters of the minimum area of a standard FIFA soccer field). To see what these numbers mean, we should compare them with the size of the active site and the substrate/product molecules. Suppose, for example, that you are making an oxidation catalyst, chromium oxide on alumina. The specific surface area of your alumina is $200\text{ m}^2\text{ g}^{-1}$ (the term “specific” denotes that a quantity is “per gram”). How much Cr should you impregnate on your support, if the active sites must be separate from each other?

In this context, “separate sites” means that each Cr atom is far enough from its neighbor, so that reactions at one site will not affect the other. If the substrate and product molecules are small, e.g., they are simple aromatics or diterpenes, then an area of 1 nm^2 per active site would suffice (Figure 4.13). Since 200 m^2 equals $2 \times 10^{20}\text{ nm}^2$, each gram of your alumina can accommodate roughly 0.1 mmol of Cr precursor on separate sites (in real catalysts, the active component atoms are often clustered as nanoparticles).

Substrate Accessibility Porous materials are divided according to their pore size. This can be measured using adsorption techniques (the principles of adsorption are outlined below). According to the International Union of Pure and Applied Chemistry (IUPAC), **microporous** materials have pores under 2 nm in diameter, **mesoporous** materials have pores of 2–50 nm diameter, and any material with an average pore diameter above 50 nm is **macroporous** [74]. The pores must be sufficiently large for substrates to enter and products to exit. Pores come in different shapes and sizes (Figure 4.14). Some materials have large pores with narrow pore mouths, known as

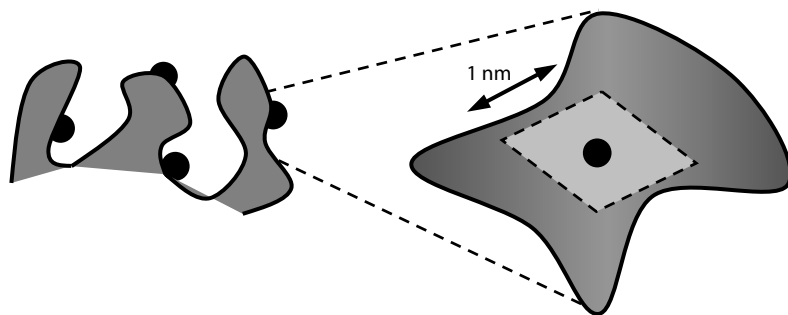


Figure 4.13 A porous alumina support particle with well-dispersed active sites (*left*), and zoom-in view of a single active site (*right*).

“ink bottle” pores. Others, e.g., zeolites, have a channel-and-cage structure. In such cases, large product molecules may be trapped inside the pores. By measuring the adsorption of molecular probes of different sizes, you can determine the fraction of the surface area that a given substrate can access.

Catalyst Stability As we have already seen in Chapter 2, catalyst deactivation is a key issue. Some deactivation processes, such as coking or poisoning, depend less on the type of support and more on the reaction itself. Sintering, on the other hand, depends strongly on the degree of dispersion of the active material, as well as on the stability of the support at high temperatures. Gas/solid catalytic systems are typically applied in large-scale continuous processes, giving preference for catalysts which remain stable for months and even years on stream. Temperature stability is important because higher temperature often means higher space–time yield, and thus higher profits. For example, polymeric ion-exchange resins such as Amberlyst and Nafion are good solid acid catalysts for fatty acid esterification, but only at temperatures below 130 °C [75]. Above this temperature, the support decomposes and loses its catalytic activity. High-temperature esterification and transesterification applications, such as biodiesel production from mixed oil/fat feeds, use instead inorganic solid acids [76] (see also the industrial examples in Section 4.3).

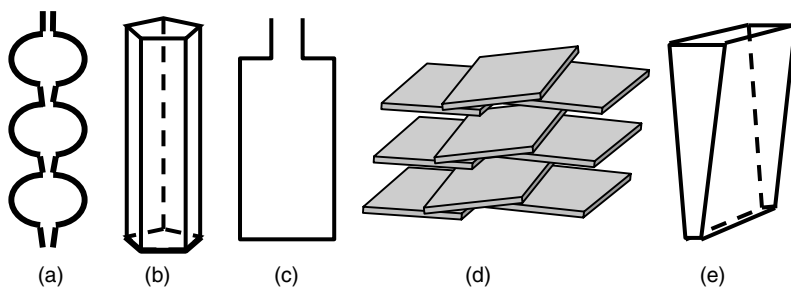


Figure 4.14 Pores may vary in size, shape, and connectivity: **a** channel/cage structures; **b** polygonal capillaries; **c** “ink bottle” pores; **d** laminae; **e** slit pores.

4.1.6

Catalyst Characterization

Theoretical models based on first principles, such as Langmuir's adsorption model, help us understand what is happening at the catalyst surface. However, there is (still) no substitute for empirical evidence, and most of the papers published on heterogeneous catalysis include a characterization of surfaces and surface-bound species. Chemists are faced with a plethora of characterization methods, from micrometer-scale particle size measurement, all the way to ångström-scale atomic force microscopy [77]. Some methods require UHV conditions and room temperature, while others work at 200 bar and 750 °C. Some methods use real industrial catalysts, while others require very clean single-crystal model catalysts. In this book, I will focus on four main areas: classic surface characterization methods, temperature-programmed techniques, spectroscopy and microscopy, and analysis of macroscopic properties. For more details on the specific methods see the references in each section, as well as the books by Niemantsverdriet [78] and Thomas [79].

- **CAUTION!** The plethora of catalyst characterization methods makes it easy to see what you want to see. Always try and validate your results, by combining different characterization approaches.

4.1.6.1 Traditional Surface Characterization Methods

In any gas/solid catalytic system, the reactant must first be adsorbed on the catalyst surface. This is why surface characterization is so important. Studying the adsorption of various molecules under controlled conditions yields information regarding the catalyst surface area, pore volume, and pore size distribution [80]. The key factor here is **accessibility**. Sophisticated spectroscopic analysis of single-crystal models can tell us a lot about what goes on at the active site, but the molecules must get there first.

There are two types of adsorption. In physical adsorption, or **physisorption**, the molecules are attached to the surface through Van der Waals interactions. The corresponding heats of adsorption are relatively low, ca. 3–10 kcal mol⁻¹. Conversely, chemical adsorption, or **chemisorption**, involves the breaking and creation of chemical bonds, with heats of adsorption ranging between 20 and 100 kcal mol⁻¹. Both adsorption types are used in characterization studies. Physisorption is used for determining the total surface area and pore volume, usually at temperatures that are close to the boiling point of the adsorbate. Nitrogen adsorption at 77 K, for example, is used as a standard comparison by many DIN and ISO norms. Conversely, chemisorption is used for measuring specific chemical entities (such as Brønsted acid sites) on the surface.

Determining the Surface Area The total surface area of a solid is related to the volume of gas that is adsorbed on this surface at a given temperature and pressure. An **adsorption isotherm** is a graph which shows how the amount adsorbed depends on the equilibrium pressure of the gas, at constant temperature. Empirically speaking, there are only six types of isotherms (Figure 4.15), regardless of the gas and the solid

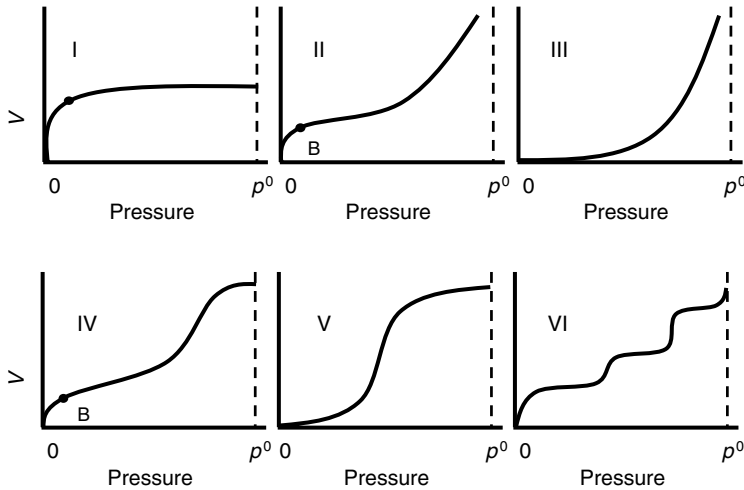


Figure 4.15 The six types of adsorption isotherms (V = volume adsorbed): Type I shows a monolayer (Langmuir isotherm); types II and III show multilayer adsorption; type IV shows first a monolayer, followed by filling of mesopores. The “knee” in isotherms I, II, and IV, indicated by a black dot, indicates the point of monolayer formation (point “B”).

in question. Type I isotherms are typical for adsorption on microporous materials, such as molecular sieves and some activated carbons. Type II isotherms describe a multilayer adsorption on a nonporous or macroporous material. In the case of isotherm types III and V, we see no monolayer formation – the incoming molecule is adsorbed preferentially on another adsorbed molecule, rather than on an “empty” site. This is what happens, for example, when H_2O is adsorbed on a hydrophobic material. For heterogeneous catalysis applications, the most important materials are those with type IV isotherms (monolayer formation followed by filling of mesopores). This is because most of the substrates and products we deal with are within the mesopore diameter range (2–50 nm).

There are several theoretical derivations of adsorption isotherms. The simple Langmuir equation [Eq. (4.2), named after the American chemist and 1932 Nobel laureate Irving Langmuir], describes the formation of a monolayer on a surface [81]. This corresponds to the type I isotherm shown in Figure 4.15. Here V is the amount adsorbed, V_m is the amount adsorbed in one monolayer, p is the pressure and b is the adsorption coefficient, which depends exponentially on the heat of adsorption.

$$\frac{V}{V_m} = \frac{bp}{1 + bp} \quad (4.2)$$

Langmuir’s model includes three strong simplifications:

- 1st All of the adsorption sites on the solid are equal.
- 2nd Molecules are adsorbed only on the surface, not on top of each other.

3rd There are no lateral interactions (it does not matter whether neighboring sites are occupied or not).

Real catalysts are usually more complicated. Adsorption sites differ in their energy and accessibility, and there are often strong lateral interactions, especially at high surface coverage. One way to bridge these differences is by describing the overall adsorption as a sum of several Langmuir isotherms.

Another common model which also describes multilayer adsorption is the Brunauer–Emmett–Teller equation [Eqs. (4.3) and (4.4), often called the BET equation or the BET method], published in 1938 [82]. Here V is the amount adsorbed, V_m is the amount adsorbed in one monolayer, p is the pressure, p^0 is the saturation pressure, C is a constant which relates to the net heat of adsorption, and N [in the cases of Eq. (4.4)] is the maximum number of layers which can form in a pore.

$$V = V_m \frac{C(p/p^0)}{[1 - (p/p^0)][1 + (C - 1)(p/p^0)]} \quad (4.3)$$

$$V = V_m \frac{C(p/p^0)}{1 - (p/p^0)} \times \frac{1 - (N + 1)(p/p^0)^N + N(p/p^0)^{N+1}}{1 + (C - 1)(p/p^0)^N - C(p/p^0)^{N+1}} \quad (4.4)$$

Using these equations, we can estimate the number of molecules in a monolayer for compounds with type I, II, and IV isotherms. From that, we can determine the solid's **monolayer capacity**. This is the amount of adsorbate needed to cover 1 g of solid. The **specific surface area** for this solid is given dividing this capacity by the average area which one adsorbate molecule occupies. To obtain meaningful values, the dimensions of the adsorbate must be small compared to the pore diameter. The best results are obtained with small spheres, e.g., Ar or Kr. For practical and traditional reasons, however, N_2 adsorption at 77 K is used as the IUPAC standard, even though it is not a spherical molecule.

The **pore volume** and the **pore size distribution** can be estimated from gas adsorption [83], while the hysteresis of the adsorption isotherms can give an idea as to the pore shape. In the pores, because of the confined space, a gas will condense to a liquid at pressures below its saturated vapor pressure. The Kelvin equation (Eq. (4.5)) gives this pressure ratio for cylindrical pores of radius r , where γ is the liquid surface tension, V is the molar volume of the liquid, R is the gas constant ($\sim 2 \text{ cal mol}^{-1} \text{ K}^{-1}$), and T is the temperature. This equation forms the basis of several methods for obtaining pore-size distributions [84,85].

$$\ln \frac{p^0}{p} = \frac{2\gamma V}{rRT} \quad (4.5)$$

Another method of estimating the pore size distribution of meso- and macropores is by **mercury porosimetry**. Here one measures the volume of mercury, a nonwetting liquid, which is forced under pressure into the pores of a catalyst sample immersed in mercury. The pressure required to intrude mercury into the sample's pores is inversely proportional to the pore size [86]. For cylindrical pores of radius r , this

pressure is given by the Washburn equation (Eq. (4.6)) [87,88], where γ is the surface tension of the liquid, and α is the contact angle. Despite the fact that real pores are rarely cylindrical, this method gives good estimates of pore size distributions. However, owing to the high contact angle and surface tension of mercury (ca. 140° and $4.8 \times 10^9 \text{ N m}^{-1}$), the measurements are limited to pores wider than $\sim 3 \text{ nm}$ (even these require pressures greater than 4000 bar).

$$r = \frac{2\gamma \cos \alpha}{p} \quad (4.6)$$

4.1.6.2 Temperature-Programmed Techniques

Temperature-programmed (TP) techniques measure the reactivity of a solid as a function of the temperature under controlled conditions [89]. The temperature at which species react on the surface (or indeed are desorbed from it) reflects the bond strength of this species. Different chemical species react at different temperatures, displaying distinct maxima in the TP profile. The more reactive species react at lower temperatures, and *vice versa*. The most common TP techniques are temperature-programmed desorption (TPD, sometimes also referred to as flash desorption spectroscopy), reduction (TPR), sulfiding (TPS), and oxidation (TPO). Although these techniques are older and simpler than the latest spectroscopic methods, they can give important information on the type of bonds and functional groups on the surface. Furthermore, they have the advantage of operating under realistic process conditions. Using TPO and TPR, for example, you can monitor the changes that the catalyst precursor goes through during the calcination and activation steps.

Figure 4.16 shows a general schematic of a TP setup, as well as examples of TPR profiles. The gas reagent (H_2 , $\text{H}_2/\text{H}_2\text{S}$, or O_2 , depending on the method) is pumped over the catalyst while the temperature is increased. As the temperature rises, the reactant consumption and/or the product formation are measured. This is often done by comparing the thermal conductivity of the gas before and after the reactor, using a thermal conductivity detector (TCD). Alternatively, one can determine the composition of the gas phase at the reactor exit using gas chromatography, mass spectrometry, or other methods [90].

4.1.6.3 Spectroscopy and Microscopy

This is the fastest-growing area in catalyst characterization. Using a host of methods (and acronyms), samples are bombarded with photons, electrons, and ions, giving chemists large amounts of data on what is happening at the catalyst surface. Until recently, many of these methods were restricted to UHV conditions and/or low temperatures, creating a temperature and pressure gap between the study conditions and the real process. However, *in situ* and *operando* spectroscopic methods are closing this gap fast, and on-line spectroscopic monitoring of gas/solid catalytic processes is becoming more and more common [91]. I will outline here the principles of five key method “families” (X-ray diffraction, X-ray photoelectron spectroscopy, electron

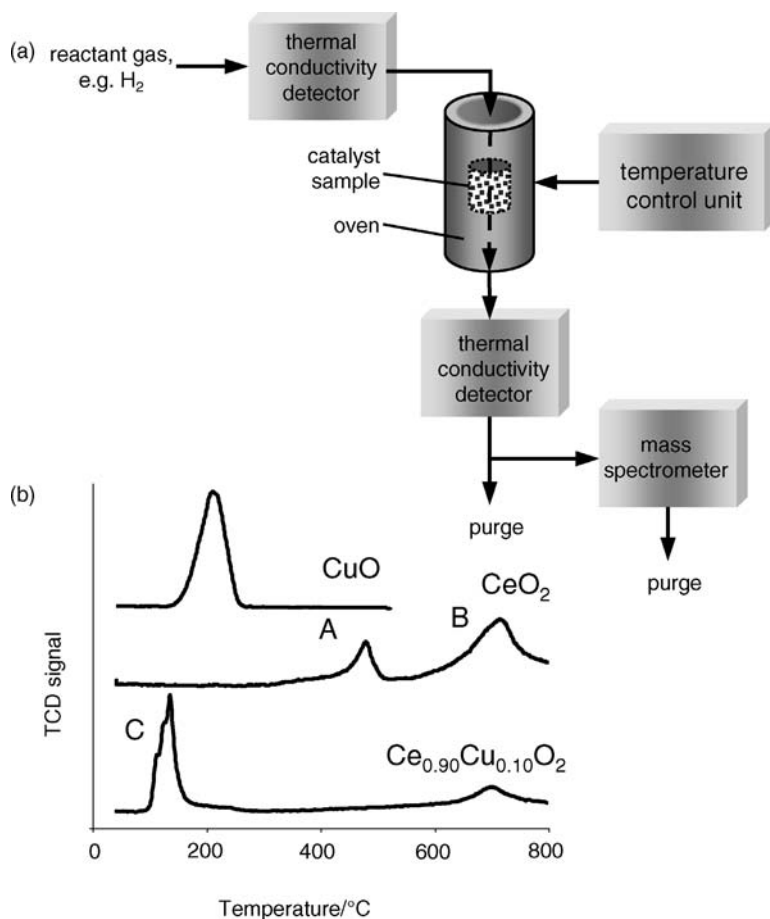


Figure 4.16 a Schematic of a temperature-programmed analysis setup; b TPR profile of CuO, CeO₂, and a copper-doped ceria sample, Ce_{0.9}Cu_{0.1}O₂, showing the effect of Cu doping on the reduction temperature.

microscopy, solid-state nuclear magnetic resonance spectroscopy, and infrared spectroscopy). A detailed overview of these and many other methods is given in specialized textbooks and reviews [78,92,93].

X-ray diffraction (XRD) is used for identifying the crystalline phases and estimating particle sizes. It is based on the elastic scattering of X-ray photons by atoms in a periodic lattice. A beam of X-rays (wavelength $\lambda \sim 0.5\text{--}2 \text{ \AA}$) hits the catalyst sample, and is diffracted by the crystalline phases in the catalyst according to Bragg's law, (Eq. (4.7)), where $n = 1, 2, \dots$, d is the spacing between atomic planes in the crystalline phase, and θ is the diffraction angle.

$$n\lambda = 2d \sin \theta \quad (4.7)$$

The intensity of the diffracted X-rays is plotted as a function of the diffraction angle and the sample orientation. This diffraction pattern is used for identifying the crystalline phases and measuring the size and lattice spacing of the crystallites. Crystalline phases of unknown samples can be identified by comparing the X-ray diffraction pattern with known patterns of metals and oxides (the International Centre for Diffraction Data, ICDD database, lists approximately 100 000 diffraction patterns of solids). Since XRD is based on interference between reflecting X-rays from lattice planes, it requires sufficient long-range order. Noncrystalline catalysts, such as silica/alumina gels used for hydrocarbon cracking, will show either broad and weak diffraction lines, or even no diffraction at all.

Small-angle X-ray scattering (SAXS) works similarly, but while XRD covers the 10° – 180° scattering range, SAXS deals with 2θ angles less than 2° . This enables the determination of catalyst particle size in the 50–500 nm range. In some cases, SAXS can also be used for determining the particles' surface area, giving comparable results to BET adsorption studies [94,95].

X-ray photoelectron spectroscopy (XPS) was developed in the mid-1960s by the Swedish physicist and 1981 Nobel laureate Kai Siegbahn [96]. XPS (originally called electron spectroscopy for chemical analysis, or ESCA) is a straightforward and useful technique for identifying atoms at the catalyst surface [97]. It is based on the photoelectric effect, in which photons from a "soft" X-ray source such as Al K_α or Mg K_α penetrate the first few atomic layers under the surface, and interact with the inner-shell electrons. The sample absorbs the energy of the photon, $h\nu$, and ejects an electron with a kinetic energy E_{kin} , as shown in Eq. (4.8). The difference between the two energies equals roughly to the electron's bonding energy, E_b , with a correction factor ϕ that accounts for the difference between the work function of the sample and that of the spectrometer. Since each element has a characteristic set of bonding energies, the XPS peak areas can be used (with appropriate sensitivity factors) to determine the surface composition of the material.

$$E_{\text{kin}} = h\nu - E_b - \phi \quad (4.8)$$

XPS can be used for analyzing the relative elemental concentrations at the surface, as well as for analyzing elemental oxidation states (E_{kin} varies with the oxidation state of a certain element, as the electrons of a cation are bound more strongly than those of a neutral atom). The probe depth ranges from 2 to 20 atomic layers, depending on the material, the photoelectron energy, and the angle of the measurement. The technique requires UHV conditions, and can detect all the elements except hydrogen and helium.

Electron microscopy is used for determining the size, shape, and composition of supported particles [93]. A **transmission electron microscope (TEM)** is like an optical microscope in which the optical lenses have been replaced by electromagnetic ones. An electron beam hits the sample, and the transmitted electrons are magnified by the electromagnetic lenses. The optics bring the scattered electrons from the same point in the sample to the same point in the image (the so-called bright-field image). A conventional TEM can magnify $\times 300\,000$, with a resolution of 0.5 nm, whereas a

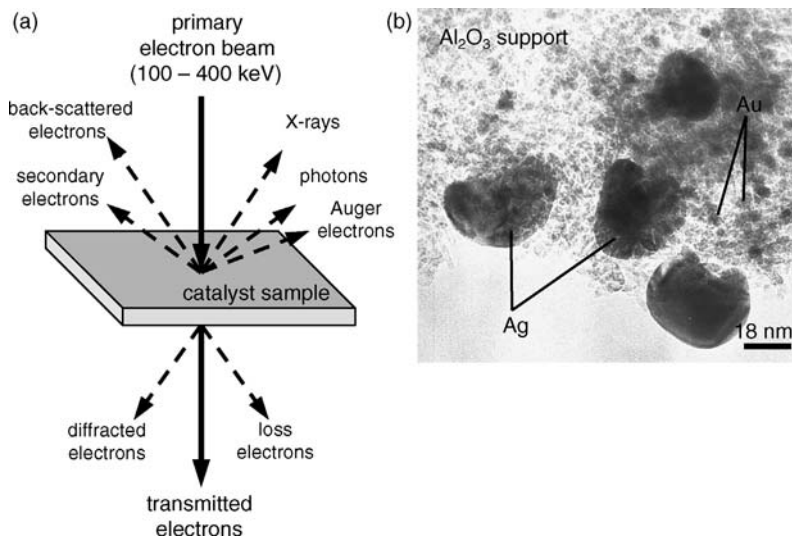


Figure 4.17 a An electron beam hitting the catalyst surface sets off several processes; the electrons that are transmitted through the sample are used for generating b the TEM image (showing gold and silver nanoparticles supported on γ -alumina [98]).

high-resolution apparatus can magnify $\times 1000\,000$, giving atomic resolution. The contrasts in the image reflect the different scattering processes, and the interactions between the transmitted electrons and different atoms in the sample (typically, the metal has a much higher electron density than the support, and appears darker in the TEM image). Thus, supported metal particles appear as dark spots, while the support itself appears as a lighter background (see the example of Au and Ag nanoparticles supported on γ -alumina in Figure 4.17b).

In **scanning electron microscopy (SEM)**, a high-energy (typically 10 keV) electron beam is scanned over a small rectangular area of the sample. This generates low-energy secondary electrons, some of which escape from the surface. These secondary electrons are detected by attracting them onto a phosphor screen, and measuring the light intensity with a photomultiplier. Some of the beam's electrons strike atomic nuclei, and “bounce back.” These electrons, known as back-scattered primaries, give information on the surface topography, and on the average atomic number in the scanned area. The microscope records the secondary and back-scattered electrons as a function of the beam's position. The surfaces that face the detector appear brighter than those set at an angle, creating contrast in the image. Because the secondary electrons originate mainly from the surface, whereas the back-scattered electrons arise from the bulk, SEM gives a 3D image of the catalyst, albeit at a lower resolution than TEM. Figure 4.18 shows a scanning electron micrograph of porous and hollow polyelectrolyte microcapsules, which were used by Eiser and co-workers as supports for noble metal clusters within their onion-like shell structure [99].

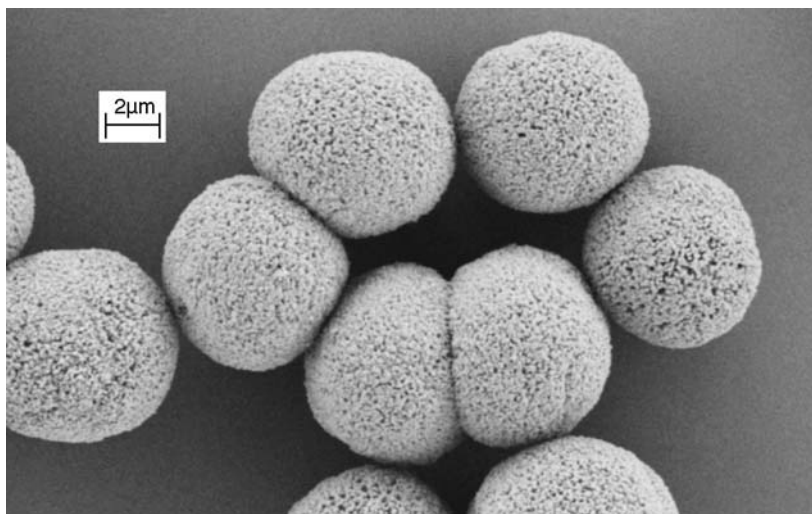


Figure 4.18 Scanning electron micrograph of “polyelectrolyte onions,” which can trap active metal clusters within their shell thickness, showing the porous 3D structure at the capsule surface.

Solid-State Nuclear Magnetic Resonance Spectroscopy (SS-NMR) The principles of solid-state NMR are identical to those of liquid-phase NMR [100]. However, NMR spectra of solid samples are more complex, since there is no isotropic averaging of NMR interactions in the solid state. The motion of the nuclei is restricted, and orientation-dependent, anisotropic characteristics appear in the spectra. This, together with the magnetic influences of neighboring atoms, causes a broadening of the peaks (for comparison, the ^1H NMR spectrum of water at room temperature is ~ 0.1 Hz, while that of ice is $\sim 10^5$ Hz). Nevertheless, solid-state NMR spectra contain much more information than solution spectra. Determination of the magnitudes and orientation dependence of chemical shielding, dipolar coupling, J -coupling and quadruple interactions provides valuable chemical information about the solid materials.

Special techniques have been developed for deriving high-resolution NMR spectra of solids. The most important is **magic angle spinning** – spinning the sample rapidly at an angle of $\cos^{-1}(1/\sqrt{3})$, or $54^\circ 54'$, to the magnetic field. Spinning at this angle cancels the broadening of the chemical shift anisotropy [101]. MASNMR is now the standard method for obtaining high-resolution spectra of solids, with numerous applications in heterogeneous catalysis [102].

Infrared (IR) Spectroscopy Infrared spectroscopy is the most widely used technique for studying the surface chemistry of heterogeneous catalysts [103]. It can give information about the catalyst structure, as well as about the species adsorbed on the catalyst surface. By using probe molecules like CO, NO and NH_3 , information is obtained about the nature and environment of atoms and ions exposed on the surface. The method is based on the absorption, transmission, or reflection by a

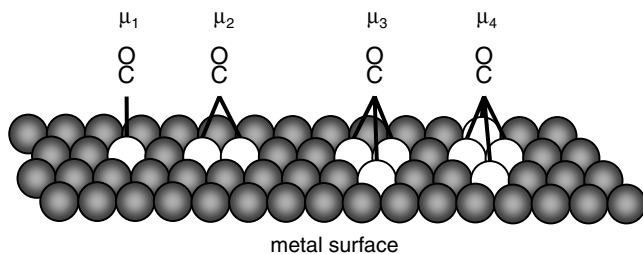


Figure 4.19 The four different adsorption configurations of CO on metal surfaces can be distinguished by their IR activity.

catalyst of infrared radiation; this excites molecular vibrations. IR spectroscopy of solid catalysts can be performed either by transmission of the IR beam through a thin section of the solid, or by its reflection from the surface. The energy of these vibrations depends on the nature and bonding of the molecules. The vibrational frequencies of surface groups and probe molecules are identified by comparing their “fingerprints” with literature databases. IR spectroscopy has two important advantages: It is nondestructive and noninvasive, and it can be adapted to measurements at high temperatures and pressures. This means that IR studies can be done under real process conditions, and even, with today’s advanced computers, using on-line analysis [104]. By using reactive probe molecules, you can qualify and quantify the type and number of active sites. For example, pyridine vapor is used for titrating Brønsted acid sites on solids, and the changes in the acid absorption bands are easily monitored using diffuse-reflectance infrared Fourier-transform spectroscopy (DRIFTS) [105,106].

IR spectroscopy can even be used for detecting the way that molecules are adsorbed on the catalyst surface. CO, for example, can form different adcomplexes on metal surfaces (Figure 4.19): linear (μ_1 , $2000\text{--}2130\text{ cm}^{-1}$); bridged between two metal atoms (μ_2 , $1860\text{--}2000\text{ cm}^{-1}$); triply bridged (μ_3 , $1800\text{--}1920\text{ cm}^{-1}$); and even quadruply bridged (μ_4 , $1650\text{--}1800\text{ cm}^{-1}$) [107]. The linear configuration is common for most group VII metals, while bridged configurations are found more with group VIII metals.

4.1.7

The Catalytic Converter: an Example from Everyday Life

Ask the average man on the street for an example of catalysis, and you will most likely hear about “the thing on the exhaust pipe that reduces engine emissions”. As we shall see, the remarkable story of the catalytic converter is not only an excellent example of catalysis, but also highlights the connection between heterogeneous catalysis, green chemistry, and sustainable development.

Today’s automotive engines emit a number of toxic pollutants: CO, unburned fuel, partially oxidized fuel, hot particulates, and nitrogen oxides (NO, N_2O , and NO_2 , collectively termed NO_x). Table 4.2 shows the typical concentrations of the exhaust gas constituents of gasoline engines [108], together with the legal emission limits set by the EU in 2005 [109].

Table 4.2 Exhaust gas constituent concentrations and their legal limits set by the EU (2005).

Compound	CO	Hydrocarbons	NO _x	H ₂	N ₂	O ₂	CO ₂	H ₂ O
Concentration/vol.%	0.680	0.075	0.105	0.230	72.5	0.51	13.5	12.5
Legal limit/g km ⁻¹	1.0	0.10	0.08	n/a	n/a	n/a	n/a	n/a

There are three strategies for reducing vehicle emissions. The first is simply driving less, using more public transportation, cycling, and/or walking. This may sound impractical, especially in places like California. Nevertheless, high gasoline prices, modern urban planning, and the increased ability to work from home are advancing this solution [110]. The second strategy is cutting the cause of emissions, by switching to cleaner fuels, e.g., hydrogen fuel cells, or hybrid electric/gasoline motors [111]. This solution is advancing rapidly, but decades will pass before such cars replace a sizable chunk of the market [112]. Thus, the most practicable solution is removing engine emissions at the exhaust outlet, using a catalytic converter.

Engines emit CO and hydrocarbons as a result of incomplete combustion. The nitrogen oxide derivatives, on the other hand, are “burned air.” We tend to think of N₂ as an inert gas, and indeed K_{eq} for the reaction $\text{N}_2 + \text{O}_2 \rightleftharpoons 2\text{NO}$ at 25 °C is only 6×10^{-31} . The picture changes at high temperatures: At 900 °C, $K_{\text{eq}} = 3 \times 10^{-7}$, and at 2200 °C, $K_{\text{eq}} = 4 \times 10^{-3}$. Interestingly, this means that if, as the temperature falls along the exhaust pipe, the reverse reaction were sufficiently fast, there would be no NO_x pollution! Unfortunately, the rate of the gas-phase reaction is too low for equilibrium to be attained during the short time that the gases spend in the exhaust pipe. We know from Chapter 2 that a catalyst never changes the thermodynamics, but it *can* change the *kinetics*, and provide a faster pathway to equilibrium. This is exactly what we need here.

The catalytic converter is based on a monolith support, a honeycomb structure of 1 mm² channels, made of cordierite (a Ca/Mg aluminate ceramic) or stainless steel [113]. The monolith must have excellent impact and thermal shock resistance, because the temperature can change by as much as 500 °C when you start the engine. Since the monolith is nonporous, it is first wash-coated with a 20–60 μm layer of γ-Al₂O₃, which has a surface area of ~200 m² g⁻¹. The whole catalyst is then impregnated with a solution of Pt, Rh, and Pd salt precursors, together with a CeO₂ layer which acts as an oxygen reservoir (Figure 4.20a) [114]. The total mass loading of noble metals is ca. 0.25%, most of which is Pt. The final catalyst is called a **three-way catalyst (TWC)**, because it converts the three main pollutants into nontoxic products (Figure 4.20b). Pt and Pd are excellent oxidation catalysts, while Rh catalyzes the reactions of NO with CO and H₂.

While most of the noble metal stays on the catalyst, small amounts do end up on the road, causing diverse environmental effects [115–117]. The concentration of Pt metals in urban road dust (especially on roundabouts) can be 100-fold higher than the normal background concentration. There is even a company in the UK that sweeps up this dust, with the aim of recovering the Pt group metals!

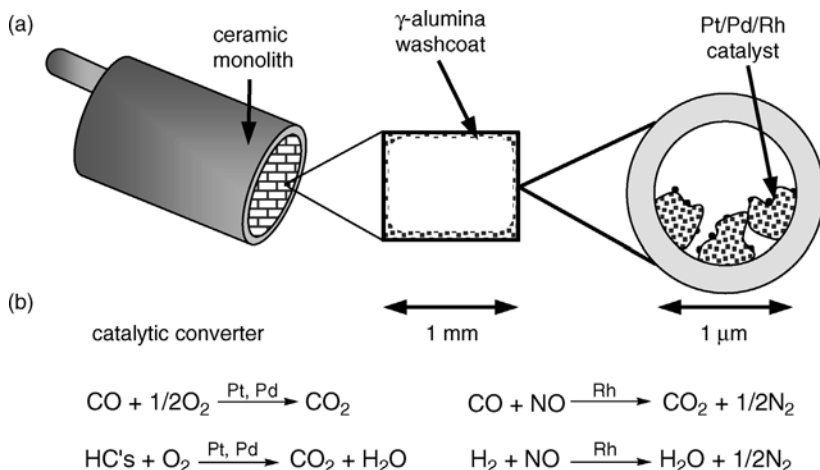


Figure 4.20 a Cartoon showing the monolith, channel washcoat, and supported active metals in the TWC; b the chemical oxidation and reduction reactions for converting the three main pollutants.

The fractional composition of the exhaust gases depends on the air-to-fuel (A/F) ratio. At low A/F ratios (rich conditions, e.g., during acceleration) the exhaust gases contain more reducing reactants (CO and HCs) than oxidizing ones (O_2 , NO_x). Conversely, high A/F ratios (lean conditions) favor the catalytic oxidation of CO and hydrocarbons. Modern cars combine the catalytic converter with an electronically controlled air/fuel management system, which maintains a near-stoichiometric A/F ratio in the combustion chamber. At this ratio, $\sim 90\%$ conversions of CO, HC, and NO_x are achieved simultaneously [118]. The engine alternates between “richer” and “leaner” operating modes. This is where the ceria or ceria/zirconia oxygen reservoir enters the picture. During the lean cycle, the storage component takes up oxygen, which it releases during the rich cycle. Depending on lattice dopants and operating conditions, ceria can store and release up to 25% of its lattice oxygen [119]. Figure 4.21 shows the qualitative effect of adding an oxygen storage component to the TWC.

4.1.8

Surface Organometallic Chemistry

Solid catalysts are macroscopic objects, but catalysis itself is primarily a molecular phenomenon. This means that many of the principles of homogeneous complexes apply to active sites. Conceptually, we can consider the support as a very large and rigid ligand, especially when the active site itself is an organometallic species which is anchored on the support. Indeed, experiments show that functional groups on surfaces exhibit chemical properties which are similar to their liquid-phase counterparts.

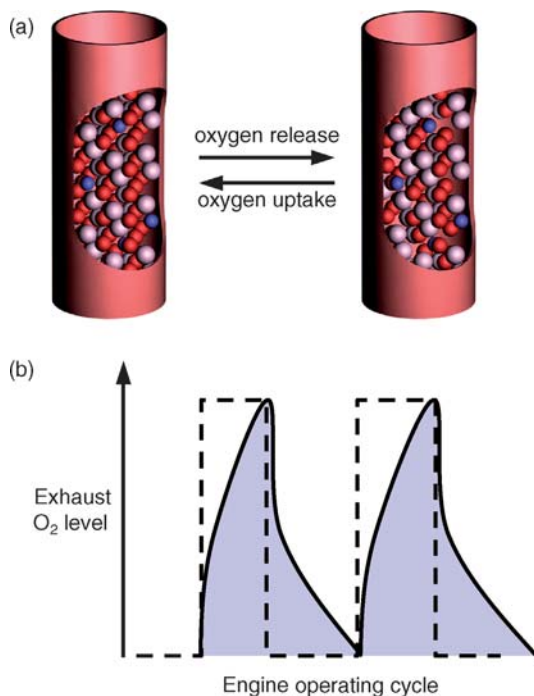


Figure 4.21 **a** Schematic showing the release of oxygen from the ceria fluorite lattice during the rich engine cycle; **b** comparison of the oxygen levels in the exhaust gas in the absence (broken line) and in the presence of an oxygen reservoir (shaded area). Thanks to Dr. Merijn Schenk for rendering the 3D fluorite crystal structures.

This concept of surface organometallic chemistry (SOMC) was developed by the French chemist Jean-Marie Basset in the 1970s [120–122]. It does not cover all situations in heterogeneous catalysis, but it has much merit because it bridges the gap between homogeneous and heterogeneous catalysis. Surface organometallic chemistry combines solid catalyst characterization and principles from solution-phase organometallic chemistry, establishing structure/activity relationships of organometallic surface species. It does not deal with adsorption or diffusion to the active site, but rather with what happens after the substrate has arrived there.

Ideally, attaching organometallic complexes to solid supports should combine the advantages of homogeneous catalysis (high TON and TOF) with those of heterogeneous catalysis (good stability and easy separation). In practice, supported organometallic complexes often display the combined drawbacks of the two methods. The reason is that instead of just one type of active site, many different types form. SOMC can be used to overcome this problem, by study and development of techniques for making single-site organometallic complexes on well-defined supports [123,124].

Naturally, SOMC depends on a good characterization and understanding of the solid support structure [125]. Silica is one of the most commonly used supports in SOMC studies, owing to its relatively simple and controllable structure [126]. The

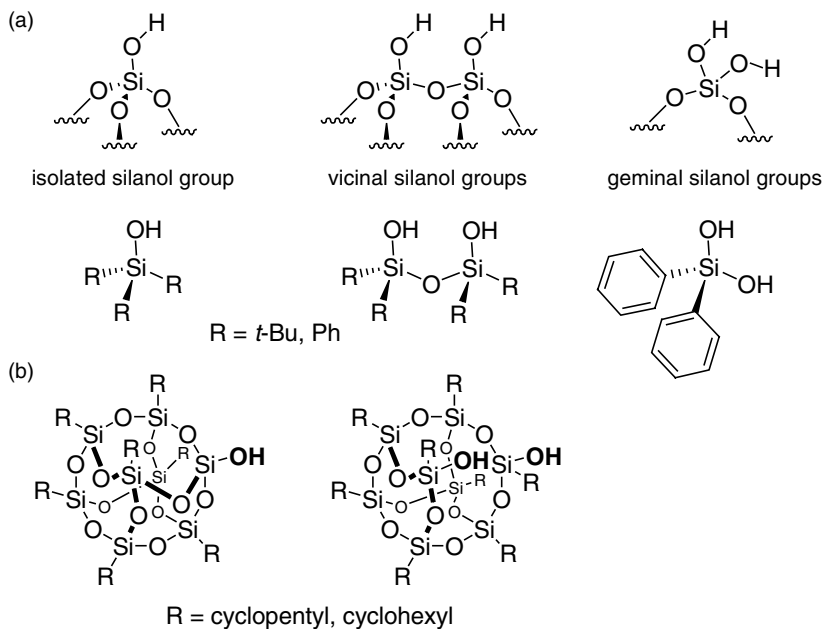


Figure 4.22 **a** The three types of silanol groups on a silica surface; **b** molecular POSS mimics of these groups.

surface of pure silica is composed of siloxane bridges ($\equiv\text{SiOSi}\equiv$) and silanol groups ($\equiv\text{SiOH}$) [127]. The type and the distribution of these groups depend on the preparation conditions, and especially on the calcination step (see Figure 4.22a). In addition to studying complexes on solid silica, SOMC research also uses complexes bound to molecular silica mimics, which range from simple organosilanols to polyhedral oligomeric silsesquioxanes (POSS; see Figure 4.22b). These large silica cages enable the use of solution-based characterization techniques, while still retaining many of the properties of solid silica [128].

SOMC has been used for studying and developing several heterogeneous catalysts, most notably for olefin polymerization (metallocene-based catalysts) and metathesis applications [129,130]. Anchoring the organometallic complexes on silica gives an active heterogeneous catalyst, which is easily separated from the product mixture (Figure 4.23). Another important application of SOMC is the preparation of well-defined surface alkoxides, which are used as oxidation and Lewis acid catalysts.

4.2

Liquid/Solid and Liquid/Liquid Catalytic Systems

Liquid/solid and liquid/liquid systems are important, because most of the chemicals we use are either liquids themselves at ambient temperature, or are dissolved in a liquid. These catalytic systems are gaining ground, as industrial attention turns to

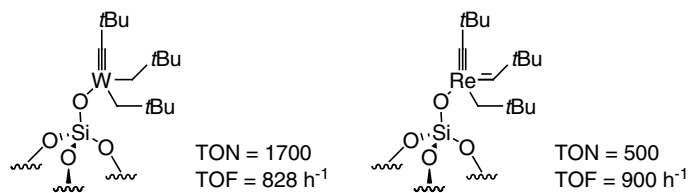


Figure 4.23 Second-generation W- and Re-alkylidene metathesis catalysts anchored on silica, with their corresponding TOF and TON values at 25°C [131].

enzymatic and water-based processes. The most common situation for biphasic liquid catalysis is an aqueous/organic system, where the substrates and/or products form the oil phase, and the catalysts and/or reagents are in the water phase. The reaction can occur either on the interface [132], or by transferring molecules between the phases using a “molecular shuttle”, a so-called **phase-transfer catalyst**. In the case of liquid/solid catalysis, the reaction takes place on the surface of the catalyst particles that are suspended in the substrate/reagent mixture.

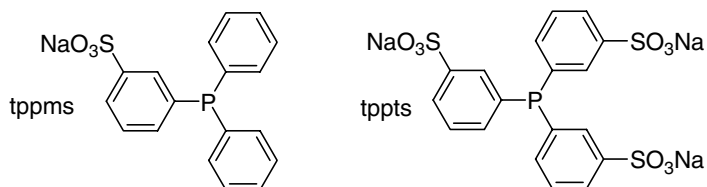
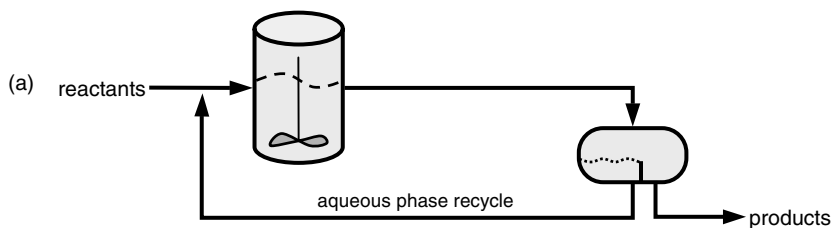
Note that catalysis is a microscopic (molecular) phenomenon, while phase separation is a macroscopic concept. This can cause some confusion, because you can define some biphasic catalytic systems as either homogeneous or heterogeneous. When the catalyst is a solid, the phase boundary is distinct, so the system is “obviously heterogeneous”; but when the catalyst is dissolved in another liquid phase, the homogeneous/heterogeneous distinction blurs. To avoid this confusion, I divide the systems according to their macroscopic behavior, classifying all liquid/liquid biphasic reactions as heterogeneous catalysis (enzyme reactions are grouped separately in Chapter 5).

4.2.1

Aqueous Biphasic Catalysis

Water is the cheapest and most eco-friendly solvent. It is nontoxic and readily available, and dissolves many inorganic and some organic reagents. Moreover, its high heat capacity and high thermal conductivity make it an ideal heat sink for controlling exothermic reactions [133]. Using water as a solvent does create some problems (e.g., cleaning aqueous waste streams containing small amounts of organics is particularly difficult), but these disadvantages are minor compared with the benefits of avoiding organic solvents [134].

In principle, most reactions catalyzed by organometallic complexes can be performed in water/oil systems by using water-soluble ligands, thus combining the advantages of high activity and selectivity with easy separation by decantation (Figure 4.24a) [134–136]. Interestingly, today’s widespread use of aqueous/organic biphasic catalysis has been influenced by the chemical industry, and specifically by the success of the Ruhrchemie/Rhône–Poulenc hydroformylation process for making butanal (the **oxo process**) [137]. This process, which came on stream in 1984, is now producing over 450 000 tpa of aldehydes in four plants. It uses a Rh-based



(b)

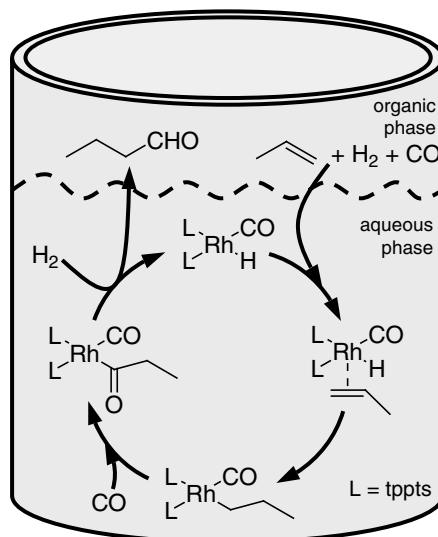


Figure 4.24 a A general process schematic for aqueous biphasic catalysis, and examples of water-soluble phosphine ligands; b the catalytic cycle for the Ruhrchemie/Rhône-Poulenc hydroformylation of propene.

catalyst with a triphenylphosphinetrisulfonate water-soluble ligand (tppts) [138]. The catalytic intermediates remain in the aqueous phase, while the reactants and products move between the phases (Figure 4.24b). The overall selectivity is >99%, with an *n*/*iso* aldehyde ratio of 96 : 4.

Another process that utilizes biphasic aqueous catalysis is the hydrodimerization of butadiene and water, run at 5000 tpa by Kuraray in Japan [138]. This process has two

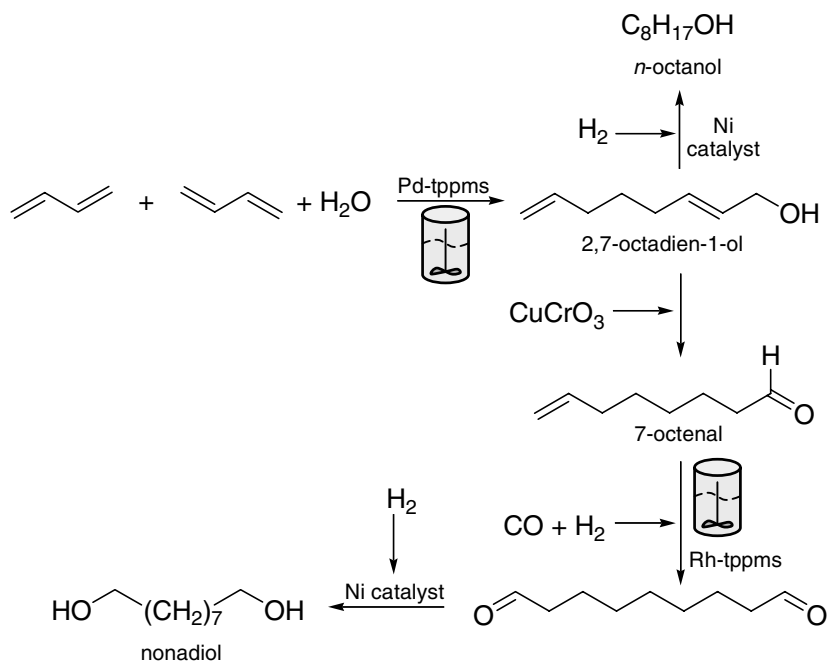


Figure 4.25 The Kuraray hydrodimerization route to *n*-octanol and 1,9-nonadiol, which includes two biphasic catalytic steps.

biphasic steps (see Figure 4.25). First, butadiene is hydrodimerized to 2,7-octadien-1-ol, using a Pd-tppps complex (tppps = $\text{PPh}_2(m\text{-C}_6\text{H}_4\text{SO}_3\text{H})$). The dienol is then either hydrogenated to *n*-octanol, or oxidized to 7-octenal which is then hydroformylated using Rh-tppts as in the Ruhrchemie process. Subsequent hydrogenation gives 1,9-nonadiol, the final product.

With the advent of green chemistry and the increasing availability of water-soluble ligands, aqueous biphasic catalysis has become a thriving research field with numerous industrial applications. In the fine-chemicals sector there are processes for C–C coupling of vitamin precursors [139] and for hydroformylation of esters of acrylic acid (2-propenoic acid) [140,141] and ω -alkene carboxylic esters [142]. Other reactions include hydrogenations [143,144], Heck reactions [145], and oligomerizations [146]. Readers wishing to explore this subject further should consult the comprehensive collection of essays edited by Cornils and Herrmann [147].

4.2.2

Fluorous Biphasic Catalysis

The fluorous biphasic concept was introduced by the Hungarian chemists István Horváth and Jozsef Rábai in 1994 [148]. A fluorous biphasic system consists of a fluorous phase (a perfluoroalkane-, perfluorodialkyl ether-, or perfluorotrialkylamine-rich phase) containing a fluorous-soluble reagent or catalyst, and a second phase,

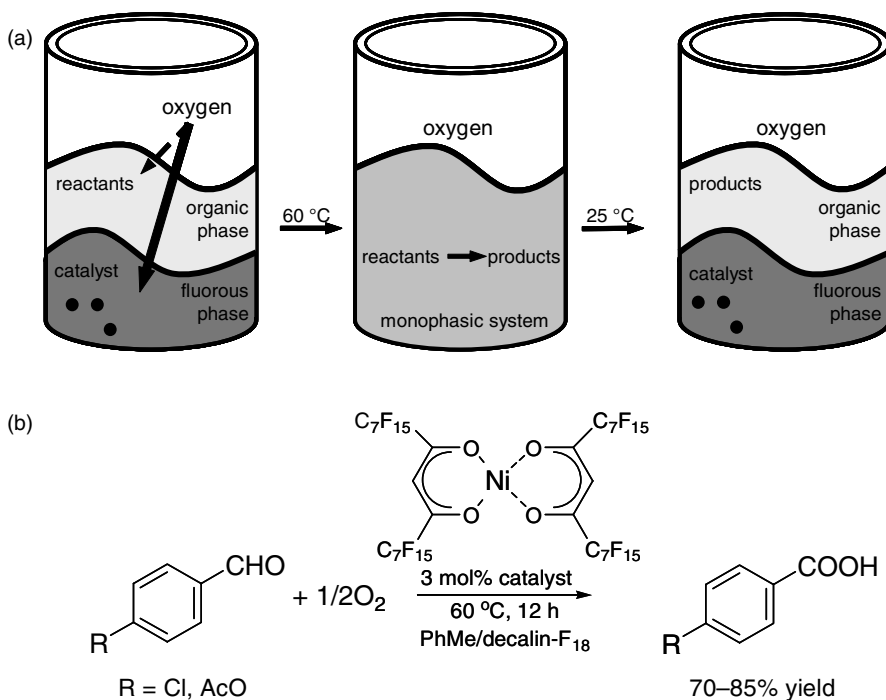


Figure 4.26 a Temperature-controlled mixing and separation of fluororous and organic phases; b its application in nickel-catalyzed oxidation of aldehydes by Klement *et al.*

which may be any organic/inorganic solvent that is sparingly miscible with the fluororous phase [149]. Reagents and catalysts can be made fluororous-soluble by decorating them with branched perfluoroalkyl chains (“fluororous ponytails”). As these ponytails can change the molecules’ electronic properties, insulating spacer groups, e.g., $-\text{CH}_2-$, are often inserted before them [150]. The fluororous phase separation is often highly temperature-dependent, which means that you can easily switch the system from biphasic to monophasic and back (Figure 4.26) [151]. The main disadvantage of fluororous solvents is their high price compared to conventional solvents.

Generally speaking, a fluororous-compatible organometallic catalyst contains at least one metal center with a fluororous ligand, $\text{L}(\text{R})_n(\text{Rf})_m$, where R denotes a regular organic residue and Rf a perfluorinated residue. The fluororous partition coefficients of such complexes depend on the type and size of the fluororous and hydrocarbon domains. Many fluororous-soluble ligands have been prepared, including phosphines [152], phosphites [148], porphyrins [153], phthalocyanines [154], diketonates [155], bipyridines [156], and tris(pyrazolyl)borates [157]. Several of these are also commercially available.

Horváth and Rábai demonstrated the efficiency of their fluororous-soluble $\text{RhP}[\text{CH}_2\text{CH}_2(\text{CF}_2)_5\text{CF}_3]_3$ catalyst in the hydroformylation of 1-decene at 100°C , using a 50:50 vol.% toluene/ $\text{C}_6\text{F}_{11}\text{CF}_3$ solvent mixture and 11 bar of 1 : 1 CO/H_2 [148].

Many examples followed, especially of oxidation reactions. Oxygen is highly soluble in fluoruous solvents, while perfluoroalkanes are highly resistant to oxidation. Moreover, most oxidations yield polar products, which are less soluble in the fluoruous phase, facilitating product separation. Klement *et al.* combined these advantages, using a perfluorinated diketone–nickel complex which catalyzed the monophasic autoxidation of various aldehydes to the carboxylic acids, obtained in 70–85% yield at 60 °C. Cooling the reaction back to 25 °C separated the phases, enabling an easy separation of product and catalyst (Figure 4.26) [155].

Interestingly, the first experiments demonstrating the fluoruous biphasic concept were actually made in 1991 by M. Vogt, a German PhD student at the Rheinisch-Westfälischen Technischen Hochschule in Aachen. Unfortunately, Vogt (and his supervisor!) never published these results except as a PhD thesis hidden at the technical school library in Aachen, so their work remained secret. It came to light only some years after the field of fluoruous biphasic chemistry was established internationally [151].

4.2.3

Biphasic Catalysis Using Ionic Liquids

Ionic liquids (ILs) are basically salts with poorly coordinated ions, resulting in low melting points. Since “low” is a relative term (NaCl, for example, is an IL between 801 °C and 1465 °C), chemists use it to refer either to salts which melt below 100 °C, or to salts that are liquid at 25 °C. The latter group is known as room-temperature ionic liquids (RTILs). In most RTILs, one of the ions is organic, with a delocalized charge. Note that ILs are not concentrated salt solutions. They are nonmolecular liquids which contain, in theory, no water (in practice, many ILs contain at least traces of water).

ILs are an exciting new class of solvents, because many functional groups show different properties in all-ionic environments (they are sometimes called **neoteric solvents**, but this just means new solvents) [158]. Moreover, ILs can be tailored for specific functions, by choosing the right cation/anion combination. There are literally millions of combinations available, and predicting their physical properties is a challenge by itself [159] (see also the discussion on data explosion in Chapter 6). Two common cation options are methylimidazolium (mim) and pyridinium (py). Figure 4.27 shows some examples of ILs based on these cations, with their respective melting points [159].

The application of ILs as solvents for transition-metal catalysis began in the 1990s, especially for reactions involving ionic intermediates, e.g., Friedel–Crafts acylations [160]. Some ILs, such as [bmim]⁺[PF₆][−], form biphasic mixtures with water, enabling the separation of water-soluble byproducts by simple extraction/decantation [161,162]. ILs are also often used in water-free biphasic systems (i.e., a mixture of IL and organic solvent) [162]. In general, ionic catalysts are much more soluble in ionic liquids than in organic solvents, thus facilitating product/catalyst separation at the end of the reaction. ILs are even used as solvents for enzymatic reactions [163]. Another interesting application for ILs is as solvents in electrochemical systems, because they are good conductors [164].


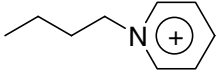
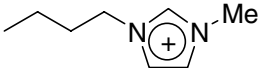
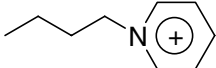
	ionic liquid	mp, °C	
 ethylmethylimidazolium (emim)	[emim] ⁺ [PF ₆] ⁻	62	 butylpyridinium (bpy)
	[emim] ⁺ [ClO ₄] ⁻	7	
	[emim] ⁺ [NO ₃] ⁻	38	
 butylmethylimidazolium (bmim)	[bmim] ⁺ [PF ₆] ⁻	11	 butylmethylpyridinium (bmpy)
	[bmim] ⁺ [Br] ⁻	77	
	[bmim] ⁺ [Cl] ⁻	41	

Figure 4.27 Examples of ILs based on mim- and on py-type cations.

ILs are also attractive candidates for replacing volatile organic compounds (VOCs) as solvents, because they have practically no vapor pressure [165]. However, the environmental impact of ILs and VOCs should be compared on the basis of life-cycle analysis, and for that we are still missing many data on the toxicity and environmental effects of ILs [166,167]. Another point is that the current prices of ILs are much higher than those of VOCs. Handy et al. recently demonstrated a handy synthesis of mim-type ILs starting from fructose, which could eventually lead to truly eco-friendly IL solvents [168].

4.2.4

Phase-Transfer Catalysis

Introduced by Charles Starks in the early 1970s [169,170], phase-transfer catalysis (PTC) is an elegant approach to reactions in multiphase systems [171]. Many chemical reactions are hampered not by inactivity of functional groups, but simply by the fact that the reactants are immiscible. PTC solves this problem by literally transferring one active species from one phase to the other. The phase-transfer catalyst acts like a **molecular shuttle bus** which goes to and fro between the phases (one of the phases can also be a solid, e.g., solid NaOH in an organic solvent). Anionic reagents, such as OH⁻ and CN⁻, are typically soluble in water but not in organic solvents, while the opposite holds for many organic reactants. PTC brings such anions into the organic phase, or in some cases to the interface between the two phases, avoiding the need for expensive and wasteful reagents. Quaternary ammonium or phosphonium salts (“quats”) and crown ethers are the most commonly used PT agents. Another bonus of PTC is that the transported reagents often show enhanced activity. The hydroxyl ion, OH⁻, is highly solvated in water, and thus less reactive. Extracting it into an organic solvent using tetrabutylammonium bromide creates a [Bu₄N]⁺[OH]⁻ ion pair, in which the OH⁻ has practically no solvation shell. This “naked OH⁻” is a much stronger base, comparable with NaOMe, NaNH₂, or NaH. The situation in which reagents are transferred from the organic phase to the aqueous phase is known as **inverse PTC** [172,173].

Phase-transfer-catalyzed reactions proceed via two main pathways. In the classic **extraction mechanism** proposed by Starks (Figure 4.28a), the quat **Q** extracts the

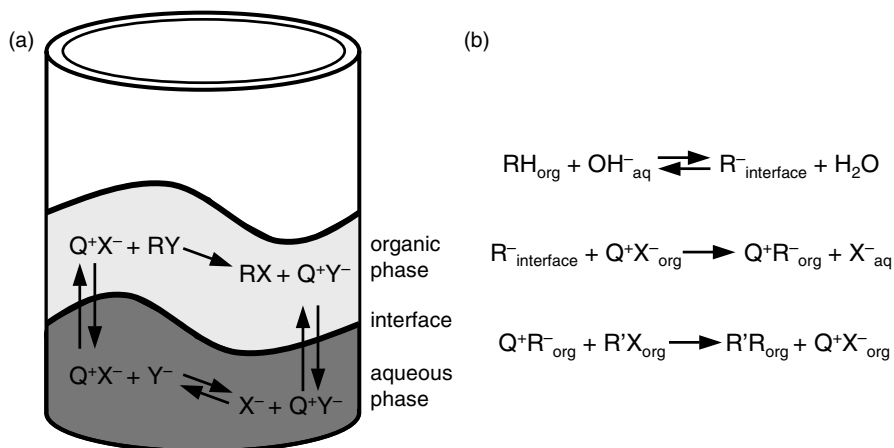


Figure 4.28 Different pathways for PTC: **a** the classic Starks extraction mechanism; **b** the Makosza interfacial mechanism.

reagent **X** from the aqueous phase to the organic phase. The reaction then takes place, and the PTC extracts the byproduct **Y** back to the aqueous phase. The alternative **interfacial mechanism**, proposed by Makosza [174], applies to many alkylations and reactions involving carbanion species. Here, a concentrated alkali solution deprotonates the organic substrate **RH** at the interface. The R^{-} anion then pairs with the quat and is transported back into the organic phase, where it reacts with the alkylating agent R' [175].

PTC has proven its usefulness in many organic transformations, e.g., in oxidation reactions using NaOCl (bleach) [176,177] or H_2O_2 [178,179], alkylation reactions [180,181], sulfanylation [182], and a variety of asymmetric reactions [183–186]. One interesting application of solid/liquid PTC in the context of green chemistry is the *in situ* generation of anhydrous HF from CaF_2 and H_2SO_4 . Anhydrous HF is an important multipurpose fluorination reagent, with a worldwide production capacity of 10^6 tpa (tons per annum). Unfortunately, it is also extremely toxic and corrosive, so its transport and storage are problematic. Using solid/liquid PTC, Sasson and co-workers generated anhydrous HF in inert organic solvents (Figure 4.29). Essentially based on the same raw materials employed in the large-scale industrial HF process, and using ambient temperatures and pressures, this technique is a simple, safe, and a cheap alternative method of hydrofluorination [187].

4.3

Advanced Process Solutions Using Heterogeneous Catalysis

Industrial heterogeneous catalysis may be an old discipline, but this does not mean that it is stagnating – far from it. New catalysts and processes are constantly being developed, combining the power of high-throughput catalyst synthesis and screening

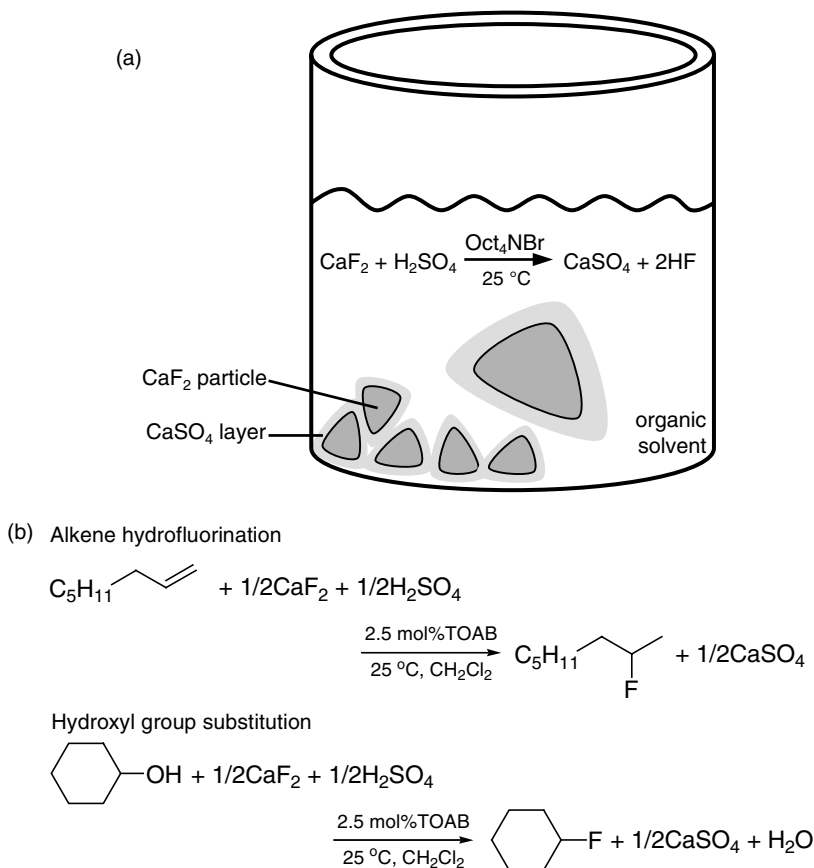


Figure 4.29 a Schematic representation of the solid/liquid HF generation system; b examples of synthetic applications.

tools, state-of-the-art characterization methods, and elegant process designs. As the examples in this section show, the right combination of tools and people can result in new processes and plants which reach both the goals of profit-making companies and of sustainable development.

4.3.1

The BP AVADA Ethyl Acetate Process

Ethyl acetate is a common solvent which is widely used in paints, pharmaceuticals, and fragrances. The two traditional production routes, acetic acid esterification and Tischencko condensation of acetaldehyde, rely on liquid acid/base catalysts which result in large aqueous waste streams. In the 1990s, BP redeployed its chemical manufacturing capacity, forcing the business unit managers to either come up with new technological solutions, or close down plants. BP's new AVADA process

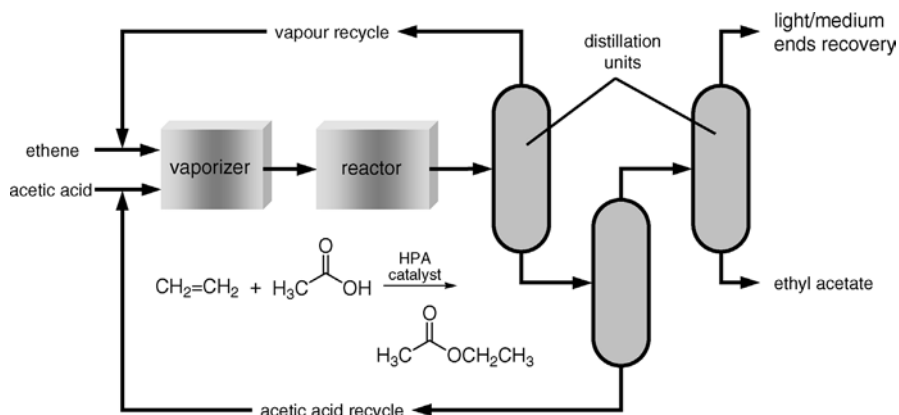


Figure 4.30 Chemical reactions and simplified process schematic for BP's AVADA ethyl acetate process.

(AdVanced Acetates by Direct Addition), which went on stream in Hull in a 220 ktpa plant in June 2001, is an excellent example of how combining heterogeneous catalysis and process innovation can create economic value and environmental benefits [188]. The AVADA process (Figure 4.30) converts ethene and acetic acid directly to ethyl acetate, cutting out the intermediate esterification step and the need for ethanol. Instead of using a liquid Brønsted acid, it uses a heteropolyacid compound which is supported on porous silica for additional stability. The process provides 99.98% pure ethyl acetate, in what is now the largest EtOAc production plant worldwide. Moreover, the simpler design requires fewer operators and saves ~20% on energy costs compared to the conventional routes. The AVADA process won the 2002 AstraZeneca Award for Excellence in Green Chemistry and Engineering.

Although the exact structure of the catalyst is undisclosed, it is most probably a “superacid” (a Keggin-type phosphotungstic heteropolyacid, with the general formula $\text{H}_3\text{PW}_n\text{M}_{12-n}\text{O}_{40}$, wherein M is tungsten or another metal). Such heteropolyacids are used in the laboratory both in solution and as solid salts [189]. Their industrial applications are limited, however, due to rapid deactivation [190]. To solve this problem, BP used a bed of porous silica beads, with the heteropolyacid impregnated in the pores.

The AVADA process combines several green chemistry principles: It uses simple, nontoxic feedstocks, converting these directly to the product. It features 100% atom economy – all the atoms in the reactants are incorporated in the product. Using a solid catalyst, the process is practically waste-free, avoiding waste stream problems. Notwithstanding these important benefits, this process was developed not because of environmental legislation or pressure groups, but following commercial considerations, demonstrating again that economic benefit is the main driver of green chemistry.

4.3.2

The ABB Lummus/Albemarle AlkyClean Process

The catalytic alkylation of isobutane with C_3 – C_5 alkenes was commercialized in the US during WW II. Blending the alkylate product with catalytically cracked gasoline provided high-octane aviation fuel. The introduction of aromatic and oxygenated fuel additives, such as methyl *t*-butyl ether (MTBE), pushed alkylation to the sidelines. However, in the 1990s, when the environmental effects of such additives were realized, alkylation regained its importance [191].

The traditional isobutane alkylation process uses H_2SO_4 or HF as catalysts. This has several serious disadvantages. First, these acids are toxic and corrosive, and transporting and storing them is a hazardous business (remember that due to the large volume of gasoline produced, the absolute catalyst amounts are very large, even when the substrate/catalyst molar ratios are high). Second, the alkylate product must be post-treated, and spent acid streams including acid-soluble oils must be disposed of. The H_2SO_4 process also has expensive cooling requirements, since its optimal temperature operating window is 4–10 °C. These disadvantages prompted an intensive search for an alternative solution using solid acid catalysts [192], but no process reached commercial realization. Rapid catalyst deactivation, inadequate catalyst regeneration schemes, concerns over process complexity, and sometimes simply insufficient evidence for breaking the “first-of-a-kind” barrier, have held clean alkylation at bay for over 40 years.

In 1999, Akzo Nobel (which later sold its catalyst division to Albemarle) patented a new technology for alkylating hydrocarbons based on a zeolite acid catalyst [193]. This new process, AlkyClean, was then designed by ABB Lummus and Albemarle, and a 10 barrels per stream day (BPSD) demonstration unit came online in Finland in 2002. AlkyClean produces a high-quality sulfur-free alkylate (96 octane), eliminating all the drawbacks of the liquid acid catalyst technologies. There are no acid-soluble oil waste streams, the reactor operates at 50–90 °C, and the catalyst is a solid, noncorrosive material, which is easily transported and stored.

The new technology employs a rugged, optimized catalyst formulation coupled with a novel (but mechanically simple) reactor design and processing scheme (Figure 4.31). The system minimizes deactivation by utilizing serial reaction stages. Slow catalyst deactivation does occur, mainly due to formation of small amounts of heavy by-products which clog the catalyst pores. To solve this problem, the process uses multiple reactors, with individual reactors cycling back and forth between on-line alkylation and mild catalyst regeneration. In the regeneration step, the olefin addition is stopped, and the heavies are removed from the catalyst using hydrogen at 250 °C (the catalyst itself remains in the reactor at all times).

4.3.3

The IFP and Yellowdiesel Processes for Biodiesel Production

Biodiesel is a renewable fuel comprising monoalkyl fatty esters. It can be made from vegetable oils, animal fat, and even recycled grease from the food industry [194,195].

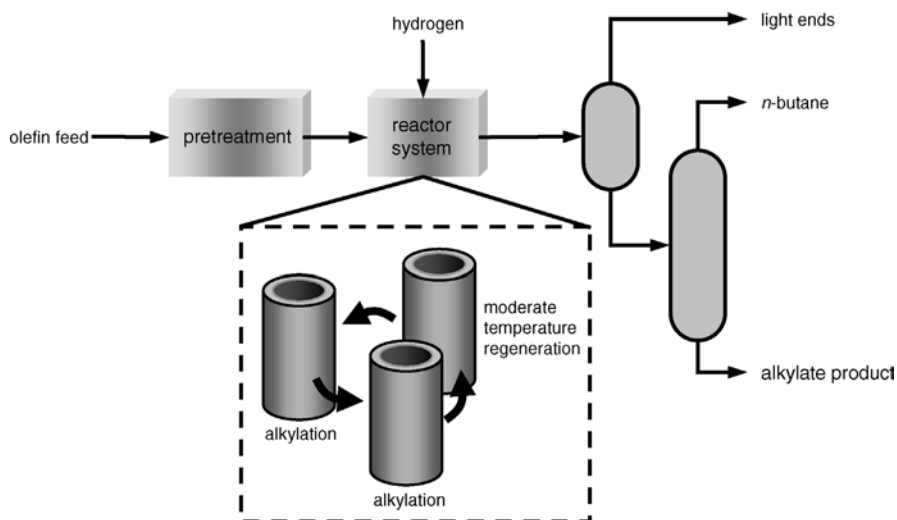


Figure 4.31 A simplified design scheme of the AlkyClean process, using three reactors in a cyclic configuration. At any given time, two reactors are used for alkylation, while the catalyst in the third reactor is regenerated.

Remarkably, it is the only alternative fuel with an overall positive life-cycle energy balance, yielding as much as 3.2 units of fuel product energy for every unit of fossil energy consumed, compared to 0.83 units for petroleum diesel. Biodiesel has several advantages over petroleum diesel: it is safe, renewable, nontoxic, and biodegradable in water (ca. 98% biodegrades in just a few weeks). It has a lower content of sulfur compounds [196], and a high flash point ($>130\text{ }^{\circ}\text{C}$). Furthermore, it is almost neutral with regard to CO_2 emissions, and emits less hydrocarbons (80%) and particulates ($\sim 50\%$) (see Table 4.3). Finally, biodiesel production enjoys a positive social impact, by enhancing rural revitalization.

Table 4.3 Average emissions from biodiesel compared to conventional diesel.

	Emission type ^[a]	
	B20/%	B100/%
Total unburned hydrocarbons	-20	-67
CO	-12	-48
CO ₂	-16	-79
Particulate matter	-12	-47
NO _x	+2	+10
SO _x	-20	-100
Polycyclic aromatic hydrocarbons (PAHs)	-13	-80
Nitrated PAHs	-50	-90

The world interest in biodiesel has accelerated tremendously, owing to recent legislation curbing vehicle emissions, and the increasing price of petroleum [196]. Although biodiesel contains no petroleum products, you can blend it with conventional diesel. B20, a blend of 80% petroleum diesel and 20% biodiesel, can be used in regular diesel engines (in fact, using B20 in buses and trucks reduces the black smoke emitted during acceleration [195]). Biodiesel can also be used in its pure form (B100), but this requires minor engine modifications [197]. Incidentally, the idea of using vegetable oil as fuel for diesel engines is over 100 years old – Rudolf Diesel himself demonstrated the performance of his engine using peanut oil as fuel [198].

The current biodiesel manufacturing processes primarily employ transesterification of triglycerides with methanol using NaOH as a base catalyst, or batch esterification of fatty acids catalyzed by H_2SO_4 [199,200]. However, these processes have several disadvantages: soap formation (with the NaOH catalyst), shifting the equilibrium to fatty esters by using an excess of alcohol that must be separated and recycled, homogeneous catalysts that require neutralization (causing salt waste streams), expensive separation of products from the reaction mixture, and relatively high investment and operating costs.

In 2005, the French petroleum institute (IFP) disclosed a novel biodiesel process, called Esterfif. Starting from triglycerides, the transesterification step was performed using a solid catalyst, a mixed Zn/Al oxide [201]. The process runs at higher temperature and pressure than the homogeneous one, and uses an excess of methanol, which is vaporized and recycled. It has two reactors and two separators, which are needed for shifting the methanolysis equilibrium (Figure 4.32). At each

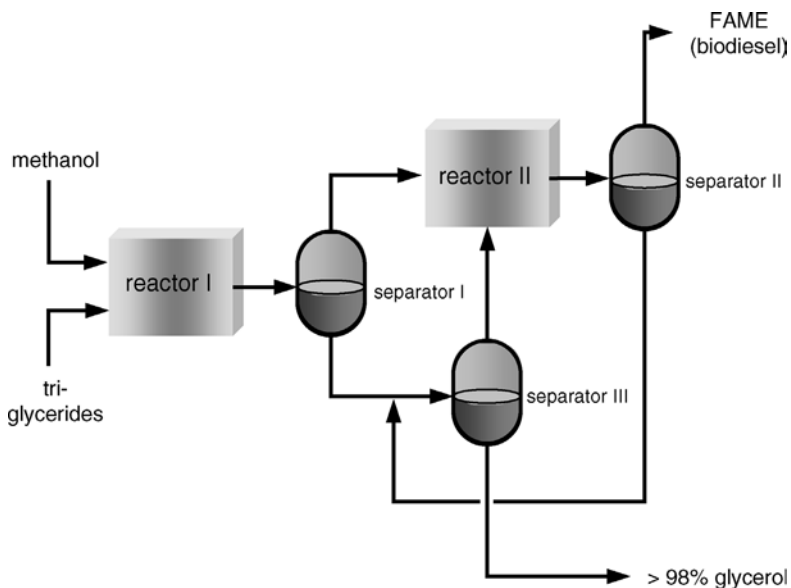


Figure 4.32 Simplified schematic of the IFP Esterfif biodiesel process, based on two consecutive reactor/separator stages.

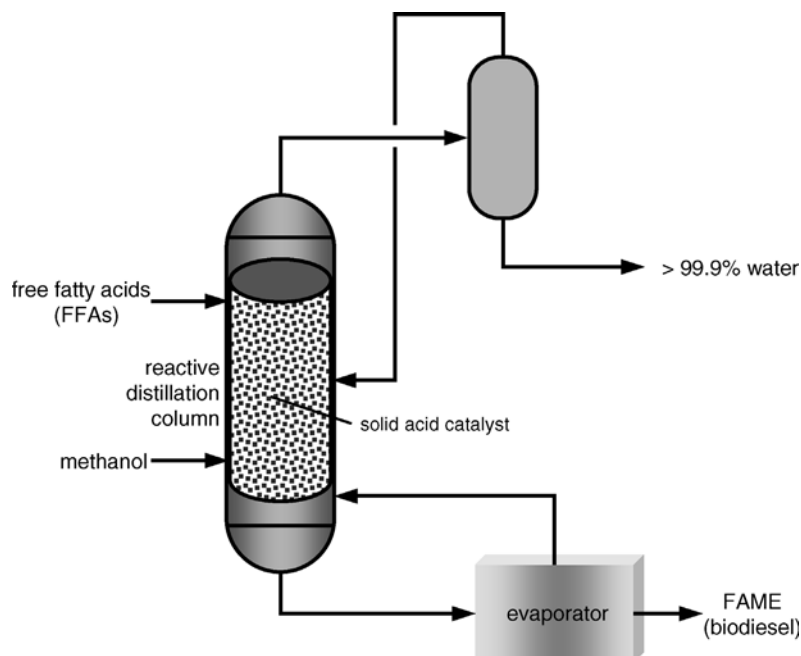


Figure 4.33 Simplified schematic of the Yellowdiesel catalytic distillation process for making biodiesel from high-FFA oils, by integrating the reaction and separation in one reactive distillation column using a solid acid catalyst.

stage the excess of methanol is removed by partial evaporation, and the esters and glycerol are separated in a settler.

A second alternative, developed by Yellowdiesel in 2006 [75,76], is especially suited to mixed feedstocks with high free fatty acid (FFA) content, such as used cooking oil and low-grade grease. The process combines the reaction and the separation in one step, using **reactive distillation** (also known as **catalytic distillation**; see Figure 4.33) [202,203]. This intensifies mass transfer, allows energy integration *in situ*, reduces equipment costs, and simplifies the process flowsheet and operation [204–206]. Furthermore, the thermodynamic equilibrium of the reaction can be shifted, by controlling the vapor/liquid equilibrium in the column. The first pilot biodiesel plant based on this process (2500 tpa), built by Fertibom, will come on stream in Rio de Janeiro in 2008.

Like the AVADA and the AlkyClean processes, these two processes also replace the liquid acid/base catalysts with solid acids and bases [192]. Although the reaction mechanism for the heterogeneous acid-catalyzed esterification is similar to the homogeneously catalyzed one [207,208], there is an important difference concerning the relationship between the surface hydrophobicity and the catalyst's activity. This is especially true for fatty acids, which are very lipophilic compounds. One can envisage three cases: First, if there are isolated Brønsted acid sites surrounded by a

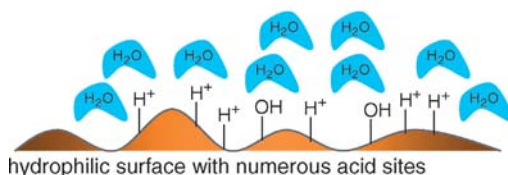
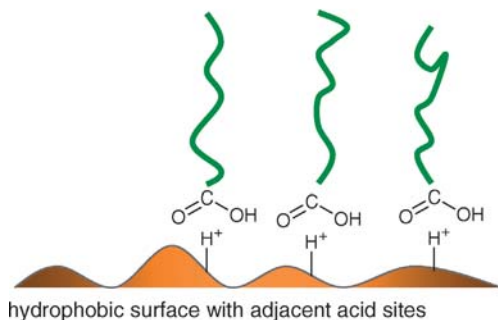
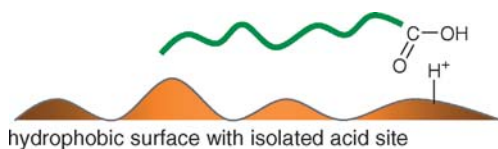


Figure 4.34 In fatty acid esterification, the catalyst surface hydrophobicity is a key factor. Too few acid sites result in low activity, but too many lead to water adsorption and deactivation.

hydrophobic environment, the hydrophobic ‘tail’ of the acid would be adsorbed parallel to the hydrophobic surface (Figure 4.34 top). Second, if there are a few acid sites in the vicinity, the fatty acid molecules could be adsorbed perpendicular to the surface, with the tails forming a local hydrophobic environment (Figure 4.34 middle). Finally, in the case of a very acidic and/or hydrophilic catalyst (many adjacent acid sites and/or hydroxyl groups), the by-product water from the esterification would be adsorbed on the surface, and the catalyst would lose its activity (the water layer would prevent the access of fatty acids to the catalyst, Figure 4.34 bottom). Thus, there is a trade-off between reactivity and surface hydrophobicity.

4.3.4

The ABB Lummus/UOP SMART Process

Styrene is one of the largest-volume production chemicals. Its global demand in 2004 reached 24 million metric tons, over half of which was used for making polystyrene. The growing demand for styrene over the past decade encouraged producers to revamp plants, increasing plant capacity while keeping capital

investment low. To this end, in 1995 ABB Lummus and UOP introduced the elegant SMART (Styrene Monomer Advanced Reheat Technology) oxidative dehydrogenation process [209].

Catalytic dehydrogenation of ethylbenzene to styrene is a well-known reaction [210], but it is endothermic, and high conversions are obtained only at high temperatures and low pressures. Moreover, in conventional dehydrogenation units, selectivity and conversion are mutually exclusive. Trade-offs must be made, and conventional plants usually operate at <70% conversion. The SMART process combines oxidative reheating technology with adiabatic dehydrogenation. Oxidation of the H₂ by-product shifts the dehydrogenation equilibrium to the products side, while simultaneously generating heat loss for the dehydrogenation reaction (Figure 4.35, inset). This results in ethylbenzene conversions of >80% per pass. The high conversion means that lower feedstock flows are needed, increasing plant production capacity by up to 50%.

Figure 4.35 shows the general process flowchart. The ethylbenzene is dehydrogenated catalytically to styrene in the presence of steam in a fixed-bed, radial-flow reactor. The heat for this reaction is supplied by catalytic combustion of the H₂ by-product with a stream of oxygen. Toluene, benzene, and some light organics are also formed. Part of the reactor effluent heat is recovered through heat exchange with the feed, and another part is used for generating steam for the process. The off-gas stream is compressed, processed, and used as fuel in the steam superheater. The condensates from the condenser and off-gas recovery section flow into the separator, where hydrocarbon and water phases separate. The dehydrogenated mixture is fractionated, recovering the styrene product, recycling ethylbenzene, and separating benzene and toluene by-products. Inhibitors are added to prevent styrene polymerization.

The SMART process is a good example of how industry can use catalysis to combine exothermic and endothermic reactions, and thus save on energy costs while at the same time increasing chemical productivity. Currently, five commercial plants run this process, producing over 1.3 million metric tons of styrene per year.

4.4

Exercises

1. *tert*-Butanol is an octane enhancer, used for replacing lead additives in gasoline. Goodfuel Inc. produces *t*-butanol by catalytic liquid-phase hydration of isobutene using the solid acid catalyst Nafion. Scientists at Goodfuel propose the mechanism shown in Figure 4.36, where {AB} indicates that A is adsorbed on B.
 - (a) Write out the overall reaction equation.
 - (b) Nafion is a mesoporous catalyst based on an organic polymer backbone. Draw the N₂ adsorption isotherm for this catalyst. Now draw the isobutene adsorption isotherm for this catalyst. What type isotherm is this?

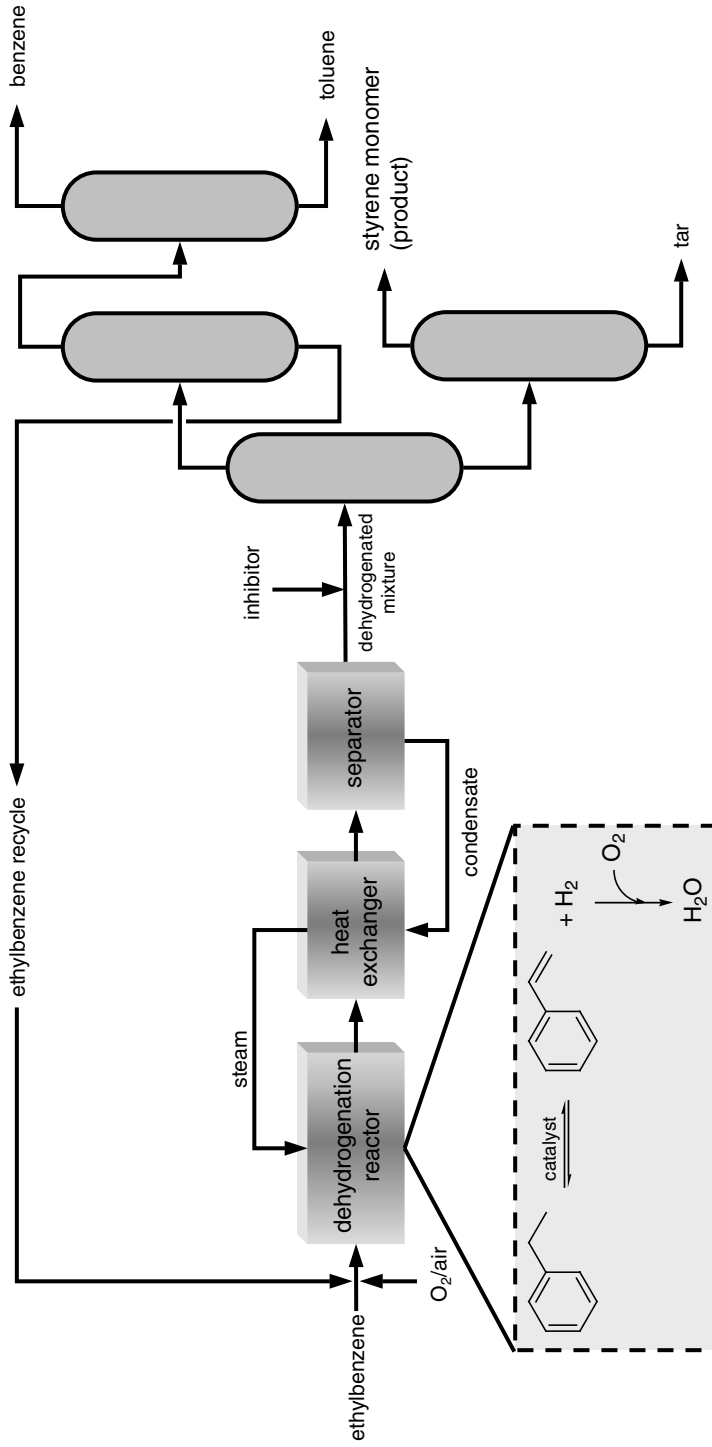


Figure 4.35 A simplified schematic of the SMART process, showing the ethylbenzene dehydrogenation (inset) and hydrogen oxidation energy exchange cycle.

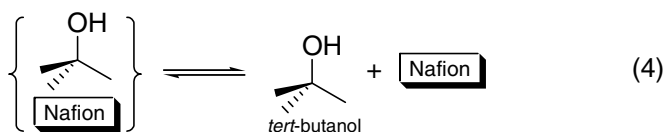
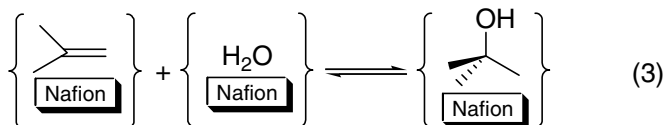
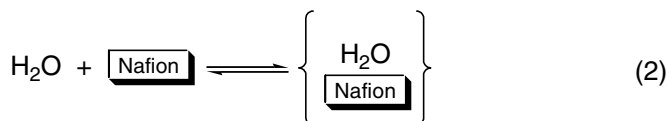
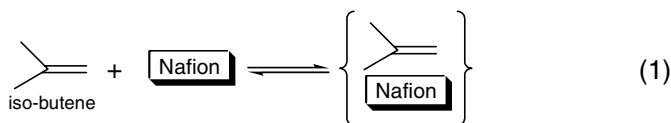


Figure 4.36 Proposed four-step mechanism for the Nafion-catalyzed synthesis of *t*-butanol.

- (c) In practice, excess *t*-butanol is added to the reaction. Explain why this excess of *t*-butanol is needed. Do you think that adding *n*-pentanol instead of *t*-butanol would have the same effect?
2. Your task is to choose the right heterogeneous catalyst for reducing a waste stream containing cyclohexanols and cyclohexanone back to cyclohexane. Your company is considering the following process options:
- H_2 gas as reducing agent; $T = 600^\circ\text{C}$; max. pressure 200 bar;
 - NaHCO_2 as reducing agent; $T = 30^\circ\text{C}$; $\text{pH} = 10.5$; max. pressure 1.1 bar;
 - $\text{CH}_3\text{CH}(\text{OH})\text{CH}_3$ as reducing agent; $T = 80^\circ\text{C}$; max. pressure 3 bar.

Search the Internet for information on chemical waste streams (both the US EPA and the EU have excellent websites on this subject), and suggest an eco-friendly active catalyst and a support for each of the three options. Suggest two methods for characterizing your catalysts before and after the reaction, and one method for characterizing at least one of the catalysts *during* the reaction (see the literature on *operando* spectroscopy [29]).

3. Nitrous oxide (N_2O , also known as “laughing gas”) is a greenhouse gas which contributes to ozone depletion in the stratosphere. It is also, however, an interesting oxidant, because it contains 36 wt.% oxygen, and gives only N_2 as by-product. The problem is that N_2O does not bond well to metals, especially in an acidic environment. Your task is to design a heterogeneous catalyst for the gas/solid reaction of nitrous oxide with propene, to make propene oxide.

- (a) Which catalyst would you choose for this process?
- (b) Write out the stoichiometric reaction equation for this process, and suggest a possible mechanism that uses your catalyst. What do you think is the rate-determining step? How would you check your hypothesis?
- (c) Do you think you could use this catalyst in a gas/liquid oxidation process to make phenol from benzene? If not, why not?
4. Draw a cartoon of molecules adsorbed on a porous solid which has both micropores and mesopores. Using this drawing, explain the terms chemisorption and physisorption.
- (a) Is it true that molecules undergo chemisorption only until a monolayer is formed, or can you get multilayer chemisorption?
- (b) Given that physisorption does occur in multilayers, how many layers of molecules can adsorb on a solid surface?
5. In a pilot process for making a pharmaceutical intermediate, the last synthetic step is a catalytic hydrogenation, using H_2 and a heterogeneous catalyst at $130^\circ C$. Researchers at the plant did three experiments. In the first run, they got $TOF = 200 \text{ min}^{-1}$. When they filtered the catalyst and reused it, they got $TOF = 33 \text{ min}^{-1}$. After filtering the catalyst again *and* calcining it in air at $450^\circ C$ for 4 h, they got $TOF = 196 \text{ min}^{-1}$ in the third run. They measured the N_2 adsorption isotherms of their catalyst before and after the first reaction (see Figure 4.37), labeled the bottle, and stored it in a cupboard containing six other catalyst samples. Unfortunately, they forgot which catalyst they used!
- (a) Decide and explain which one of the seven catalysts A–G was used in the reaction.
- (b) What is the reason for the differences in the adsorption isotherms before and after the reaction?

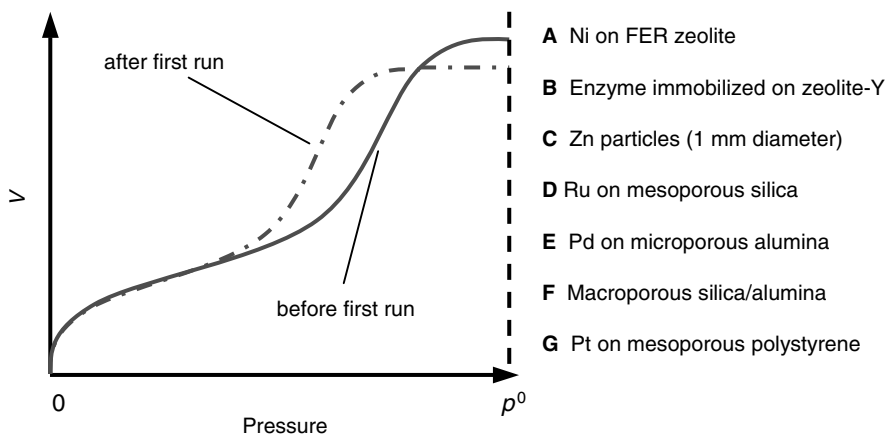


Figure 4.37 N_2 adsorption isotherm (measured at 77 K) of the catalyst before and after the first run.

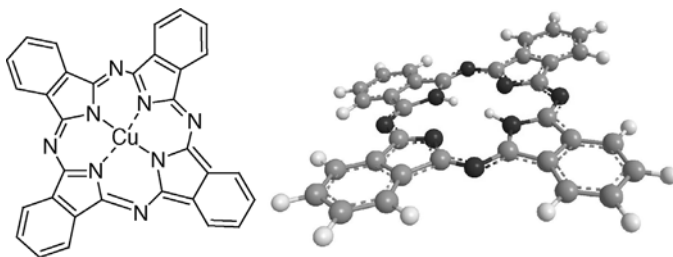


Figure 4.38 Molecular formula of Cu-phthalocyanine and optimized geometry of the phthalocyanine ligand.

- (c) Measuring just the surface area of a solid is cheaper than measuring the entire isotherm. Is saving money justified in this case?
6. Alumex is a porous silica/alumina zeolite, with cylindrical pores of 6.0 \AA diameter. Nitrogen adsorption studies show that its surface area is $500 \text{ m}^2 \text{ g}^{-1}$ and its pore volume is 0.4 mL g^{-1} . Copper phthalocyanine (Figure 4.38) is a macrocyclic pigment. It has a strong blue color. If someone has synthesized copper phthalocyanine in your lab in the past five years, it is likely that there are blue stains everywhere. Your job is to make two supported catalysts by vacuum pore impregnation. In each impregnation cycle you can fill 90% of the pore volume. In both cases the support is Alumex. For the first catalyst, the precursor is $\text{Ni}(\text{NO}_3)_2$. For the second, the precursor is copper phthalocyanine. The solubility of $\text{Ni}(\text{NO}_3)_2$ in water is 0.3 g in 1.0 g water. The solubility of copper phthalocyanine in water is 0.002 g in 1.0 g water. You may assume that the volume of the water does not change when a precursor is dissolved in it. The solubility of Alumex in water is zero. The molar mass M of copper phthalocyanine is $576.08 \text{ g mol}^{-1}$, the atomic weight of Ni is 58.7 , and the length of a typical C–C bond is 1.54 \AA .
- (a) How much $\text{Ni}(\text{NO}_3)_2$ do you need to make 5 g of a heterogeneous Ni/Alumex catalyst with a loading of $2 \text{ Ni atoms per nm}^2$? And how many impregnation cycles do you need to perform in order to make this catalyst?
- (b) How much copper phthalocyanine do you need to make 5 g of a heterogeneous Cu/Alumex catalyst with a loading of $2 \text{ Cu atoms per nm}^2$? And how many impregnation cycles do you need to perform in order to make that catalyst?

References

- 1 Agrawal, R., Singh, N.R., Ribeiro, F.H. and Delgass, W.N. (2007) Sustainable fuel for the transportation sector. *Proc. Natl. Acad. Sci. USA*, **104**, 4828.
- 2 Gary, J.H. and Handwerk, G.E. (2001) *Petroleum Refining: Technology and Economics*, CRC Press, Boca Raton, ISBN 0824704827.

- 3 Bryner, M. and Scott, A. (2006) Catalysts: fuel regulations rev up demand. *Chem. Week*, **168**, 19.
- 4 Sheldon, R.A. and van Bekkum, H. (2001) *Fine Chemicals Through Heterogeneous Catalysis*, Wiley-VCH, Weinheim, ISBN 3-527-29951-3.
- 5 Chuang, S.S.C. (2005) Catalysis of solid oxide fuel cells. *Catalysis*, **18**, 186.
- 6 Carrette, L., Friedrich, K.A. and Stimming, U. (2000) Fuel cells: principles, types, fuels, and applications. *ChemPhysChem*, **1**, 163.
- 7 Kamat, P.V. and Dimitrijevic, N.M. (1990) Colloidal semiconductors as photocatalysts for solar energy conversion. *Solar Energy*, **44**, 83.
- 8 Serpone, N. (1994) A decade of heterogeneous photocatalysis in our laboratory: pure and applied studies in energy production and environmental detoxification. *Res. Chem. Intermed.*, **20**, 953.
- 9 Zaidman, B., Wiener, H. and Sasson, Y. (1986) Formate salts as chemical carriers in hydrogen storage and transportation. *Int. J. Hydr. Energy*, **11**, 341.
- 10 Wiener, H., Zaidman, B. and Sasson, Y. (1989) Storage of energy by solutions of alkali formate salts. *Solar Energy*, **43**, 291.
- 11 Klier, K. (1982) Methanol synthesis. *Adv. Catal.*, **30**, 243.
- 12 Van der Laan, G.P. and Beenackers, A.A.C.M. (1999) Kinetics and selectivity of the Fischer–Tropsch synthesis: a literature review. *Catal. Rev. – Sci. Eng.*, **41**, 255.
- 13 Wojciechowski, B.W. (1998) The reaction mechanism of catalytic cracking: quantifying activity, selectivity, and catalyst decay. *Catal. Rev. – Sci. Eng.*, **40**, 209.
- 14 Feller, A. and Lercher, J.A. (2004) Chemistry and technology of isobutane/alkene alkylation catalyzed by liquid and solid acids. *Adv. Catal.*, **48**, 229.
- 15 Babich, I.V. and Moulijn, J.A. (2003) Science and technology of novel processes for deep desulfurization of oil refinery streams: a review. *Fuel*, **82**, 607.
- 16 Eijsbouts, S., Mayo, S.W. and Fujita, K. (2007) Unsupported transition metal sulfide catalysts: from fundamentals to industrial application. *Appl. Catal. A: Gen.*, **322**, 58.
- 17 Corma, A. (1993) Transformation of hydrocarbons on zeolite catalysts. *Catal. Lett.*, **22**, 33.
- 18 Huang, J. and Rempel, G.L. (1995) Ziegler–Natta catalysts for olefin polymerization – mechanistic insights from metallocene systems. *Prog. Polym. Sci.*, **20**, 459.
- 19 Gellings, P.J. and Bouwmeester, H.J.M. (2000) Solid state aspects of oxidation catalysis. *Catal. Today*, **58**, 1.
- 20 Ertl, G., Knozinger, H. and Weitkamp, J. (1997) *Handbook of Heterogeneous Catalysis*, Wiley-VCH, Weinheim, ISBN 3-527-29212-8.
- 21 Thathagar, M.B., Beckers, J. and Rothenberg, G. (2002) Copper-catalyzed Suzuki cross-coupling using mixed nanocluster catalysts. *J. Am. Chem. Soc.*, **124**, 11858.
- 22 Eley, D.D. and Rideal, E.K. (1940) Parahydrogen conversion on tungsten. *Nature*, **146**, 401.
- 23 Bernal, S., Calvino, J.J., Cauqui, M.A., Gatica, J.M., Larese, C., Perez Omil, J.A. and Pintado, J.M. (1999) Some recent results on metal/support interaction effects in NM/CeO₂ (NM noble metal) catalysts. *Cataly. Today*, **50**, 175.
- 24 Otto, K., Haack, L.P. and De Vries, J.E. (1992) Identification of two types of oxidized palladium on γ -alumina by X-ray photoelectron spectroscopy. *Appl. Catal. B: Environ.*, **1**, 1.
- 25 Taylor, H.S. (1920) Mechanism of catalytic processes. *J. Ind. Eng. Chem.*, **13**, 75.
- 26 Taylor, H.S. (1925) A theory of the catalytic surface. *Proc. R. Soc. (London)*, **108A**, 105.

- 27 Taylor, H.S. (1926) The mechanism of activation at catalytic surfaces. *Proc. R. Soc. (London)*, **113A**, 77.
- 28 Freund, H.J., Rupprechter, G., Baeumer, M., Risse, T., Ernst, N. and Libuda, J. (2003) From real world catalysis to surface science and back: can nanoscience help to bridge the gap? *NATO Sci. Ser., II: Math., Phys. Chem.*, **116**, 65.
- 29 Weckhuysen, B.M. (2003) Determining the active site in a catalytic process: operando spectroscopy is more than a buzzword. *Phys. Chem. Chem. Phys.*, **5**, 4351.
- 30 Banares, M.A. and Wachs, I.E. (2002) Molecular structures of supported metal oxide catalysts under different environments. *J. Raman Spectrosc.*, **33**, 359.
- 31 Stoltze, P. and Nørskov, J.K. (1985) Bridging the “pressure gap” between ultrahigh-vacuum surface physics and high-pressure catalysis. *Phys. Rev. Lett.*, **55**, 2502.
- 32 Ertl, G. (2002) Heterogeneous catalysis on atomic scale. *J. Mol. Catal. A: Chem.*, **182–183**, 5.
- 33 Ertl, G. (1994) Reactions at well-defined surfaces. *Surf. Sci.*, **299–300**, 742.
- 34 Goodman, D.W. (1996) Correlations between surface science models and “real-world” catalysts. *J. Phys. Chem.*, **100**, 13 090.
- 35 Strongin, D.R., Carrazza, J., Bare, S.R. and Somorjai, G.A. (1987) The importance of C7 sites and surface roughness in the ammonia synthesis reaction over iron. *J. Catal.*, **103**, 213.
- 36 Davis, S.M., Zaera, F. and Somorjai, G.A. (1982) The reactivity and composition of strongly adsorbed carbonaceous deposits on platinum. Model of the working hydrocarbon conversion catalyst. *J. Catal.*, **77**, 439.
- 37 Kim, C. and Somorjai, G.A. (1992) Effects of rhenium and sulfur on the reactivity and selectivity of platinum single-crystal catalysts. *J. Catal.*, **134**, 179.
- 38 Friend, C.M., Queeney, K.T. and Chen, D.A. (1999) Structure and reactivity of thin-film oxides and metals. *Appl. Surf. Sci.*, **142**, 99.
- 39 Rainer, D.R. and Goodman, D.W. (1997) Thin films as model catalysts. *NATO ASI Ser. E: Appl. Sci.*, **331**, 27.
- 40 Baiker, A. (1989) Metallic glasses in heterogeneous catalysis. *Faraday Discuss. Chem. Soc.*, **87**, 239.
- 41 Kim, S.H. and Somorjai, G.A. (2006) Surface science of single-site heterogeneous olefin polymerization catalysts. *Proc. Natl. Acad. Sci. USA*, **103**, 15 289.
- 42 Frank, M. and Baumer, M. (2000) From atoms to crystallites: adsorption on oxide-supported metal particles. *Phys. Chem. Chem. Phys.*, **2**, 3723.
- 43 Wallace, W.T., Min, B.K. and Goodman, D.W. (2005) The nucleation, growth, and stability of oxide-supported metal clusters. *Top. Catal.*, **34**, 17.
- 44 Rainer, D.R., Xu, C. and Goodman, D.W. (1997) Characterization and catalysis studies of small metal particles on planar model oxide supports. *J. Mol. Catal. A: Chem.*, **119**, 307.
- 45 Fastrup, B. (1994) Temperature programmed adsorption and desorption of nitrogen on iron ammonia synthesis catalysts, and consequences for the microkinetic analysis of NH₃ synthesis. *Top. Catal.*, **1**, 273.
- 46 Perego, C. and Villa, P. (1997) Catalyst preparation methods. *Catal. Today*, **34**, 281.
- 47 Schwarz, J.A., Contescu, C. and Contescu, A. (1995) Methods for preparation of catalytic materials. *Chem. Rev.*, **95**, 477.
- 48 Armbruster, E., Baiker, A., Baris, H., Guentherodt, H.J., Schlögl, R. and Walz, B. (1986) Ammonia synthesis over a novel catalyst prepared from an amorphous hennonacontaironnonazirconium precursor. *J. Chem. Soc., Chem. Commun.*, 299.

- 49 Raney, M. (1940) Catalysts from alloys. *Ind. Eng. Chem.*, **32**, 1199.
- 50 Smith, A.J. and Trimm, D.L. (2005) The preparation of skeletal catalysts. *Annu. Rev. Mater. Res.*, **35**, 127.
- 51 Kruissink, E.C., Van Reijen, L.L. and Ross, J.R.H. (1981) Coprecipitated nickel–alumina catalysts for methanation at high temperature. Part 1. Chemical composition and structure of the precipitates. *J. Chem. Soc., Faraday Trans. 1*, **77**, 649.
- 52 Bowker, M., Bicknell, C.R. and Kerwin, P. (1996) Ammoxidation of propane to acrylonitrile on FeSbO₄. *Appl. Catal. A: Gen.*, **136**, 205.
- 53 Komiya, M. (1985) Design and preparation of impregnated catalysts. *Catal. Rev. – Sci. Eng.*, **27**, 341.
- 54 Van der Zande, L.M., De Graaf, E.A. and Rothenberg, G. (2002) Design and parallel synthesis of novel selective hydrogen oxidation catalysts and their application in alkane dehydrogenation. *Adv. Synth. Catal.*, **344**, 884.
- 55 Cundy, C.S. and Cox, P.A. (2003) The hydrothermal synthesis of zeolites: history and development from the earliest days to the present time. *Chem. Rev.*, **103**, 663.
- 56 Cundy, C.S. and Cox, P.A. (2005) The hydrothermal synthesis of zeolites: precursors, intermediates and reaction mechanism. *Micropor. Mesopor. Mater.*, **82**, 1.
- 57 Corma, A. (1995) Inorganic solid acids and their use in acid-catalyzed hydrocarbon reactions. *Chem. Rev.*, **95**, 559.
- 58 Chang, C.D. and Silvestri, A.J. (1977) The conversion of methanol and other O-compounds to hydrocarbons over zeolite catalysts. *J. Catal.*, **47**, 249.
- 59 Okuhara, T. (2002) Water-tolerant solid acid catalysts. *Chem. Rev.*, **102**, 3641.
- 60 Harmer, M.A. and Sun, Q. (2001) Solid acid catalysis using ion-exchange resins. *Appl. Catal. A: Gen.*, **221**, 45.
- 61 Corma, A., Nemeth, L.T., Renz, M. and Valencia, S. (2001) Sn-zeolite beta as a heterogeneous chemoselective catalyst for Baeyer–Villiger oxidations. *Nature*, **412**, 423.
- 62 Olson, D.H., Kokotailo, G.T., Lawton, S.L. and Meier, W.M. (1981) Crystal structure and structure-related properties of ZSM-5. *J. Phys. Chem.*, **85**, 2238.
- 63 Kokotailo, G.T., Lawton, S.L., Olson, D.H. and Meier, W.M. (1978) Structure of synthetic zeolite ZSM-5. *Nature*, **272**, 437.
- 64 Fulton, J.W. (1986) Selecting the catalyst configuration. *Chem. Eng.*, **93**, 97.
- 65 Lukasiewicz, S.J. (1989) Spray-drying ceramic powders. *J. Am. Ceram. Soc.*, **72**, 617.
- 66 Holt, E.M. (2004) The properties and forming of catalysts and absorbents by granulation. *Powder Technol.*, **140**, 194.
- 67 Xu, X. and Moulijn, J.A. (1998) Transformation of a structured carrier into structured catalyst. *Chem. Ind. (Dekker), Struct. Catal. Reactors*, **71**, 599.
- 68 Forzatti, P., Ballardini, D. and Sighicelli, L. (1998) Preparation and characterization of extruded monolithic ceramic catalysts. *Catal. Today*, **41**, 87.
- 69 Roozeboom, F., Mittelmeijer-Hazeleger, M.C., Moulijn, J.A., Medema, J., de Beer, V.H.J. and Gellings, P.J. (1980) Vanadium oxide monolayer catalysts. 3. A Raman spectroscopic and temperature-programmed reduction study of monolayer and crystal-type vanadia on various supports. *J. Phys. Chem.*, **84**, 2783.
- 70 Trovarelli, A., de Leitenburg, C., Boaro, M. and Dolcetti, G. (1999) The utilization of ceria in industrial catalysis. *Catal. Today*, **50**, 353.
- 71 Kašpar, J., Fornasiero, P. and Graziani, M. (1999) Use of CeO₂-based oxides in the three-way catalysis. *Catal. Today*, **50**, 285.
- 72 Park, S.D., Vohs, J.M. and Gorte, R.J. (2000) Direct oxidation of hydrocarbons in a solid-oxide fuel cell. *Nature*, **404**, 265.

- 73 Murray, E.P., Tsai, T. and Barnett, S.A. (1999) A direct-methane fuel cell with a ceria-based anode. *Nature*, **400**, 649.
- 74 Rouquerol, J., Avnir, D., Fairbridge, C.W., Everett, D.H., Haynes, J.H., Pernicone, N., Ramsay, J.D.F., Sing, K.S.W. and Unger, K.K. (1994) Recommendations for the characterization of porous solids. *Pure Appl. Chem.*, **66**, 1739.
- 75 Kiss, A.A., Dimian, A.C. and Rothenberg, G. (2006) Solid acid catalysts for biodiesel production – towards sustainable energy. *Adv. Synth. Catal.*, **348**, 75.
- 76 Kiss, A.A., Omota, F., Dimian, A.C. and Rothenberg, G. (2006) The heterogeneous advantage: biodiesel by catalytic reactive distillation. *Top. Catal.*, **40**, 141.
- 77 Brazdil, J.F. (1999) Understanding catalysis using analytical characterization. *Chemtech*, **29**, 23.
- 78 Niemantsverdriet, J.W. (1995) *Spectroscopy in Catalysis*, VCH, Weinheim, ISBN 3-527-28726-4.
- 79 Thomas, J.M. and Thomas, W.J. (1997) *Principles and Practice of Heterogeneous Catalysis*, VCH, Weinheim, ISBN 3-527-29288-8.
- 80 Meyer, K., Lorenz, P., Böhl-Kuhn, B. and Klobes, P. (1994) Porous solids and their characterization. Methods of investigation and application, *Cryst. Res. Technol.*, **29**, 903.
- 81 Langmuir, I. (1915) Theory of adsorption. *Phys. Rev.*, **6**, 79.
- 82 Brunauer, S., Emmett, P.H. and Teller, E. (1938) Adsorption of gases in multimolecular layers. *J. Am. Chem. Soc.*, **60**, 309.
- 83 Rouquerol, F., Rouquerol, J. and Sing, K. (1999) *Adsorption by Powders and Porous Solids*, Academic Press, London, ISBN 0-12-598920-2.
- 84 Barrett, E.P., Joyner, L.G. and Halenda, P.P. (1951) The determination of pore volume and area distributions in porous substances. I. Computations from nitrogen isotherms. *J. Am. Chem. Soc.*, **73**, 373.
- 85 Cranston, R.W. and Inkley, F.A. (1957) The determination of pure structures from nitrogen adsorption isotherms. *Adv. Catal.*, **9**, 143.
- 86 Thompson, A.H., Katz, A.J. and Raschke, R.A. (1987) Mercury injection in porous media: a resistance devil's staircase with percolation geometry. *Phys. Rev. Lett.*, **58**, 29.
- 87 Washburn, E.W. (1921) Note on a method of determining the distribution of pore sizes in a porous material. *Proc. Natl. Acad. Sci. USA*, **7**, 115.
- 88 Washburn, E.W. (1921) Dynamics of capillary flow. *Phys. Rev.*, **17**, 374.
- 89 Boaro, M., Vicario, M., de Leitenburg, C., Dolcetti, G. and Trovarelli, A. (2003) The use of temperature-programmed and dynamic/transient methods in catalysis: characterization of ceria-based, model three-way catalysts. *Catal. Today*, **77**, 407.
- 90 Baker, R.T., Bernal, S., Blanco, G., Cordon, A.M., Pintado, J.M., Rodriguez-Izquierdo, J.M., Fally, F. and Perrichon, V. (1999) Reversible changes in the redox behavior of a $\text{Ce}_{0.68}\text{Zr}_{0.32}\text{O}_2$ mixed oxide: effect of alternating the re-oxidation temperature after reduction at 1223 K. *Chem. Commun.*, 149.
- 91 Hunger, M. (2005) Applications of *in situ* spectroscopy in zeolite catalysis. *Micropor. Mesopor. Mater.*, **82**, 241.
- 92 Busca, G. (1996) The use of vibrational spectroscopies in studies of heterogeneous catalysis by metal oxides: an introduction. *Catal. Today*, **27**, 323.
- 93 Anderson, M.W., Ohsuna, T., Sakamoto, Y., Liu, Z., Carlsson, A. and Terasaki, O. (2004) Modern microscopy methods for the structural study of porous materials. *Chem. Commun.*, 907.
- 94 Fagherazzi, G., Cocco, G., Schifflini, L., Enzo, S., Benedetti, A., Passerini, R. and Tauszik, G.R. (1978) Particle size distribution and surface area of supported metal catalysts. *Chim. e l'Industria*, **60**, 892.

- 95 Xiang, Y., Zhang, J. and Liu, C. (2000) Verification for particle size distribution of ultrafine powders by the SAXS method. *Mater. Charact.*, **44**, 435.
- 96 Siegbahn, K. (1970) Electron spectroscopy for chemical analysis (e.s.c.a.). *Phil. Trans. R. Soc.*, **268**, 33.
- 97 Brinen, J.S. (1976) Applying electron spectroscopy for chemical analysis to industrial catalysis. *Acc. Chem. Res.*, **9**, 86.
- 98 Wang, J., Boelens, H.F.M., Thathagar, M.B. and Rothenberg, G. (2004) *in situ* spectroscopic analysis of nanocluster formation. *ChemPhysChem*, **5**, 93.
- 99 Turkenburg, D.H., Antipov, A.A., Thathagar, M.B., Rothenberg, G., Sukhorukov, G.B. and Eiser, E. (2005) Palladium nanoclusters in microcapsule membranes: from synthetic shells to synthetic cells. *Phys. Chem. Chem. Phys.*, **7**, 2237.
- 100 Aliev, A.E. and Law, R.V. (2003) Solid-state NMR spectroscopy. *Nucl. Magn. Reson.*, **32**, 238.
- 101 Isbester, P.K., Kaune, L. and Munson, I.J. (1999) Magic-angle spinning NMR: a window into flow catalytic reactors. *Chemtech*, **29**, 40.
- 102 Han, X., Yan, Z., Zhang, W. and Bao, X. (2001) Applications of *in situ* NMR in catalytic processes of organic reactions. *Curr. Org. Chem.*, **5**, 1017.
- 103 Ryczkowski, J. (2001) IR spectroscopy in catalysis. *Catal. Today*, **68**, 263.
- 104 Snively, C.M., Oskarsdottir, G. and Lauterbach, J. (2001) Parallel analysis of the reaction products from combinatorial catalyst libraries. *Angew. Chem. Int. Ed.*, **40**, 3028.
- 105 Wilson, K. and Clark, J.H. (1998) Synthesis of a novel supported solid acid BF₃ catalyst. *Chem. Commun.*, 2135.
- 106 Craciun, R., Miller, D.J., Dulamita, N. and Jackson, J.E. (1996) Diffuse reflectance infrared Fourier transform spectroscopy (DRIFTS) applied in heterogeneous catalysis studies. *Prog. Catal.*, **5**, 55.
- 107 Sheppard, N. and Nguyen, T.T. (1978) The vibrational spectra of carbon monoxide chemisorbed on the surfaces of metal catalysts – a suggested scheme of interpretation. *Adv. Infrared Raman Spectrosc.*, **5**, 67.
- 108 Taylor, K.C. (1993) Nitric oxide catalysis in automotive exhaust systems. *Catal. Rev. - Sci. Eng.*, **35**, 457.
- 109 Anon (1998) Directive 98/69/EC relating to measures to be taken against air pollution by emissions from motor vehicles. *Official J. Eur. Commun.*, **L350**, 1.
- 110 Overberg, P. and Copeland, L. (2007, May 17) Drivers cut back – a 1st in 26 years. *USA Today*.
- 111 Sisiopiku, V.P., Rousseau, A., Fouad, F.H. and Peters, R.W. (2006) Technology evaluation of hydrogen light-duty vehicles. *J. Environ. Eng.*, **132**, 568.
- 112 MacLean, H.L. and Lave, L.B. (2003) Life cycle assessment of automobile/fuel options. *Environ. Sci. Technol.*, **37**, 5445.
- 113 Cybulski, A. and Moulijn, J.A. (1994) Monoliths in heterogeneous catalysis. *Catal. Rev. - Sci. Eng.*, **36**, 179.
- 114 Heck, R.M. and Farrauto, R.J. (2001) Automobile exhaust catalysts. *Appl. Catal. A: Gen.*, **221**, 443.
- 115 Rauch, S., Peucker-Ehrenbrink, B., Molina, L.T., Molina, M.J., Ramos, R. and Hemond, H.F. (2006) Platinum group elements in airborne particles in Mexico City. *Environ. Sci. Technol.*, **40**, 7554.
- 116 Hodge, V.F. and Stallard, M.O. (1986) Platinum and palladium in roadside dust. *Environ. Sci. Technol.*, **20**, 1058.
- 117 Wang, J., Zhu, R.-h. and Shi, Y.-z. (2007) Distribution of platinum group elements in road dust in the Beijing metropolitan area, China. *J. Environ. Sci.*, **19**, 29.
- 118 Muraki, H. and Zhang, G. (2000) Design of advanced automotive exhaust catalysts. *Catal. Today*, **63**, 337.
- 119 Rothenberg, G., De Graaf, E.A. and Blik, A. (2003) Solvent-free synthesis of rechargeable solid oxygen reservoirs for

- clean hydrogen oxidation. *Angew. Chem. Int. Ed.*, **42**, 3366.
- 120** Basset, J.M. and Choplin, A. (1983) Surface organometallic chemistry: a new approach to heterogeneous catalysis? *J. Mol. Catal.*, **21**, 95.
- 121** Copéret, C., Chabanas, M., Saint-Arroman, R.P. and Basset, J.-M. (2003) Homogeneous and heterogeneous catalysis: bridging the gap through surface organometallic chemistry. *Angew. Chem. Int. Ed.*, **42**, 156.
- 122** Scott, S.L., Basset, J.M., Niccolai, G.P., Santini, C.C., Candy, J.P., Lecuyer, C., Quignard, F. and Choplin, A. (1994) Surface organometallic chemistry: a molecular approach to surface catalysis. *New J. Chem.*, **18**, 115.
- 123** Jones, C.W., McKittrick, M.W., Nguyen, J.V. and Yu, K. (2005) Design of silica-tethered metal complexes for polymerization catalysis. *Top. Catal.*, **34**, 67.
- 124** McKittrick, M.W. and Jones, C.W. (2005) Modulating the reactivity of an organometallic catalyst via immobilization on a spatially patterned silica surface. *Chem. Mater.*, **17**, 4758.
- 125** Basset, J.-M., Lefebvre, F. and Santini, C. (1998) Surface organometallic chemistry: some fundamental features including the coordination effects of the support. *Coord. Chem. Rev.*, **178–180**, 1703.
- 126** Anwander, R. SOMC@PMS (2001) Surface organometallic chemistry at periodic mesoporous silica. *Chem. Mater.*, **13**, 4419.
- 127** Iler, R.K. (1979) *The Chemistry of Silica*, Wiley, New York, ISBN 978-0-471-02404-0.
- 128** Pescarmona, P.P. and Maschmeyer, T. (2001) Oligomeric silsesquioxanes: synthesis, characterization and selected applications. *Aust. J. Chem.*, **54**, 583.
- 129** McKittrick, M.W. and Jones, C.W. (2004) Toward single-site, immobilized molecular catalysts: site-isolated Ti ethylene polymerization catalysts supported on porous silica. *J. Am. Chem. Soc.*, **126**, 3052.
- 130** Lefebvre, F. and Basset, J.M. (1999) Recent applications in catalysis of surface organometallic chemistry. *J. Mol. Catal. A: Chem.*, **146**, 3.
- 131** Chabanas, M., Baudouin, A., Coperet, C. and Basset, J.-M. (2001) A highly active well-defined rhenium heterogeneous catalyst for olefin metathesis prepared via surface organometallic chemistry. *J. Am. Chem. Soc.*, **123**, 2062.
- 132** Chaudhari, R.V., Bhanage, B.M., Deshpande, R.M. and Delmas, H. (1995) Enhancement of interfacial catalysis in a biphasic system using catalyst-binding ligands. *Nature*, **373**, 501.
- 133** Narayan, S., Muldoon, J., Finn, M.G., Fokin, V.V., Kolb, H.C. and Sharpless, K.B. (2005) "On water": unique reactivity of organic compounds in aqueous suspension. *Angew. Chem. Int. Ed.*, **44**, 3275.
- 134** Kuntz, E.G. (1995) Hydrosoluble ligands for a new technology. *NATO ASI Ser. III., High Technol.*, **5**, 177.
- 135** Cornils, B. and Kuntz, E.G., (1995) Introducing TPPTS and related ligands for industrial biphasic processes. *J. Organomet. Chem.*, **502**, 177.
- 136** Kuntz, E., Amgoune, A., Lucas, C. and Godard, G. (2006) Palladium TPPTS catalyst in water: C-allylation of phenol and guaiacol with allyl alcohol and novel isomerisation of allyl ethers of phenol and guaiacol. *J. Mol. Catal. A: Chem.*, **244**, 124.
- 137** Kuntz, E.G. (1987) Homogeneous catalysis . . . in water. *Chemtech*, **17**, 570.
- 138** Cornils, B. (1999) Bulk and fine chemicals via aqueous biphasic catalysis. *J. Mol. Catal. A: Chem.*, **143**, 1.
- 139** Mercier, C. and Chabardes, P. (1995) Organometallic chemistry in industrial vitamin A and vitamin E synthesis. *Chem. Ind. (Dekker) Catal. Org. React.*, **62**, 213.
- 140** Fremy, G., Castanet, Y., Grzybek, R., Monflier, E., Mortreux, A., Trzeciak, A.M. and Ziolkowski, J.J. (1995) A new, highly selective, water-soluble rhodium catalyst for methyl acrylate hydroformylation. *J. Organomet. Chem.*, **505**, 11.

- 141 Monflier, E., Fremy, G., Castanet, Y. and Mortreux, A. (1995) Molecular recognition between chemically modified β -cyclodextrin and dec-1-ene: new prospects for biphasic hydroformylation of water-insoluble olefins. *Angew. Chem. Int. Ed. Engl.*, **34**, 2269.
- 142 Fell, B., Schobben, C. and Papadogianakis, G. (1995) Hydroformylation of homologous ω -alkenecarboxylate esters with water soluble rhodium carbonyl/tertiary phosphine complex catalyst systems. *J. Mol. Catal. A: Chem.*, **101**, 179.
- 143 Kotzabasakis, V., Georgopoulou, E., Pitsikalis, M., Hadjichristidis, N. and Papadogianakis, G. (2005) Catalytic conversions in aqueous media: a novel and efficient hydrogenation of polybutadiene-1,4-block-poly(ethylene oxide) catalyzed by Rh/TPPTS complexes in mixed micellar nanoreactors. *J. Mol. Catal. A: Chem.*, **231**, 93.
- 144 Grosselin, J.M., Mercier, C., Allmang, G. and Grass, F. (1991) Selective hydrogenation of α,β -unsaturated aldehydes in aqueous organic two-phase solvent systems using ruthenium or rhodium complexes of sulfonated phosphines. *Organometallics*, **10**, 2126.
- 145 Kiji, J., Okano, T. and Hasegawa, T. (1995) Palladium-catalyzed arylation of ethylene (the Heck reaction) under aqueous conditions. *J. Mol. Catal. A: Chem.*, **97**, 73.
- 146 Baidossi, W., Goren, N. and Blum, J. (1993) Homogeneous and biphasic oligomerization of terminal alkynes by some water soluble rhodium catalysts. *J. Mol. Catal. A: Chem.*, **85**, 153.
- 147 Cornils, B. and Herrmann, W.A. (2004) *Aqueous-Phase Organometallic Catalysis*, Wiley-VCH, Weinheim, ISBN 9783527307128.
- 148 Horváth, I.T. and Rábai, J. (1994) Facile catalyst separation without water: fluoros biphasic hydroformylation of olefins. *Science*, **266**, 72.
- 149 Horváth, I.T. (1998) Fluorous biphasic chemistry. *Acc. Chem. Res.*, **31**, 641.
- 150 Horváth, I.T., Kiss, G., Cook, R.A., Bond, J.E., Stevens, P.A., Rábai, J. and Mozeleski, E.J. (1998) Molecular engineering in homogeneous catalysis: one-phase catalysis coupled with biphasic catalyst separation. The fluoros-soluble $\text{HRh}(\text{CO})\{\text{P}[\text{CH}_2\text{CH}_2(\text{CF}_2)_5\text{CF}_3]_3\}_3$ hydroformylation system. *J. Am. Chem. Soc.*, **120**, 3133.
- 151 Cornils, B. (1997) Fluorous biphasic systems – the new phase-separation and immobilization technique. *Angew. Chem. Int. Ed. Engl.*, **36**, 2057.
- 152 Kampa, J.J., Nail, J.W. and Lagow, R.J. (1995) The synthesis of tris (perfluoroalkyl)phosphanes. *Angew. Chem. Int. Ed. Engl.*, **34**, 1241.
- 153 DiMugno, S.G., Williams, R.A. and Therien, M.J. (1994) Facile synthesis of *meso*-tetrakis(perfluoroalkyl)porphyrins: spectroscopic properties and X-ray crystal structure of highly electron-deficient 5,10,15,20-tetrakis(heptafluoropropyl) porphyrin. *J. Org. Chem.*, **59**, 6943.
- 154 Keller, T.M. and Griffith, J.R. (1979) The synthesis of a fluorinated phthalocyanine. *J. Fluor. Chem.*, **13**, 73.
- 155 Klement, I., Lutjens, H. and Knochel, P. (1997) Transition metal catalyzed oxidations in perfluorinated solvents. *Angew. Chem. Int. Ed. Engl.*, **36**, 1454.
- 156 Garelli, N. and Vierling, P. (1992) Synthesis of new amphiphilic perfluoroalkylated bipyridines. *J. Org. Chem.*, **57**, 3046.
- 157 Dias, H.V.R. and Kim, H.-J. (1996) Novel tris(pyrazolyl)borates bearing perfluoroalkyl pigtails. Syntheses and characterization of the sodium and copper(I) complexes of $[\text{HB}(3\text{-}(\text{R})\text{Pz})_3]^-$ ($\text{R} = \text{C}_2\text{F}_5, \text{C}_3\text{F}_7, \text{Pz} = \text{pyrazolyl}$). *Organometallics*, **15**, 5374.
- 158 Seddon, K.R. (1997) Ionic liquids for clean technology. *J. Chem. Technol. Biotechnol.*, **68**, 351.
- 159 Lopez-Martin, I., Burello, E., Davey, P.N., Seddon, K.R. and Rothenberg, G. (2007)

- Anion and cation effects on imidazolium salt melting points: a descriptor modelling study. *ChemPhysChem*, **8**, 690.
- 160** Earle, M.J., Seddon, K.R., Adams, C.J. and Roberts, G. (1998) Friedel–Crafts reactions in room temperature ionic liquids. *Chem. Commun.*, 2097.
- 161** Wasserscheid, P. and Welton, T. (2002) *Ionic Liquids in Synthesis*, Wiley-VCH, Weinheim, ISBN 3-527-30515-7.
- 162** Wasserscheid, P. and Keim, W. (2000) Ionic liquids – new “solutions” for transition metal catalysis. *Angew. Chem. Int. Ed.*, **39**, 3772.
- 163** Van Rantwijk, F. and Sheldon, R.A. (2007) Biocatalysis in ionic liquids. *Chem. Rev.*, **107**, 2757.
- 164** Durán Pachón, L., Elsevier, C.J. and Rothenberg, G. (2006) Electroreductive palladium-catalyzed Ullmann reactions in ionic liquids: scope and mechanism. *Adv. Synth. Catal.*, **348**, 1705.
- 165** Earle, M.J., Esperanca, J.M.S.S., Gilea, M.A., Canongia Lopes, J.N., Rebelo, L.P.N., Magee, J.W., Seddon, K.R. and Widegren, J.A. (2006) The distillation and volatility of ionic liquids. *Nature*, **439**, 831.
- 166** Kralisch, D., Stark, A., Koersten, S., Kreisel, G. and Ondruschka, B., (2005) Energetic environmental and economic balances: Spice up your ionic liquid research efficiency. *Green Chemistry*, **7**, 301.
- 167** Jessop, P.G. (2007) In pursuit of the perfect green solvent. *Can. Chem. News*, **59**, 16.
- 168** Handy, S.T., Okello, M. and Dickenson, G. (2003) Solvents from biorenewable sources: ionic liquids based on fructose. *Org. Lett.*, **5**, 2513.
- 169** Starks, C.M. (1971) Phase-transfer catalysis. I. Heterogeneous reactions involving anion transfer by quaternary ammonium and phosphonium salts. *J. Am. Chem. Soc.*, **93**, 195.
- 170** Starks, C.M. and Owens, R.M. (1973) Phase-transfer catalysis. II. Kinetic details of cyanide displacement on 1-halooctanes. *J. Am. Chem. Soc.*, **95**, 3613.
- 171** Starks, C.M., Liotta, C.L. and Halpern, M.C. (1994) *Phase-Transfer Catalysis – Fundamentals, Applications, and Industrial Perspectives*, Springer, New York, ISBN 0412040719.
- 172** Mathias, L.J. and Vaidya, R.A. (1986) Inverse phase transfer catalysis. First report of a new class of interfacial reactions. *J. Am. Chem. Soc.*, **108**, 1093.
- 173** Fife, W.K. and Xin, Y. (1987) Inverse phase-transfer catalysis: probing its mechanism with competitive transacylation. *J. Am. Chem. Soc.*, **109**, 1278.
- 174** Makosza, M. (1975) Two-phase reactions in the chemistry of carbanions and halocarbenes. A useful tool in organic synthesis. *Pure Appl. Chem.*, **43**, 439.
- 175** Mason, D., Magdassi, S. and Sasson, Y. (1990) Interfacial activity of quaternary salts as a guide to catalytic performance in phase-transfer catalysis. *J. Org. Chem.*, **55**, 2714.
- 176** Rothenberg, G. and Sasson, Y. (1996) Extending the haloform reaction to non-methyl ketones: oxidative cleavage of cycloalkanones to dicarboxylic acids using sodium hypochlorite under phase transfer catalysis conditions. *Tetrahedron*, **52**, 13641.
- 177** Abramovici, S., Neumann, R. and Sasson, Y. (1985) Sodium hypochlorite as oxidant in phase transfer catalytic systems. Part II. Oxidation of aromatic alcohols. *J. Mol. Catal.*, **29**, 299.
- 178** Bortolini, O., Conte, V., Di Furia, F. and Modena, G. (1986) Metal catalysis in oxidation by peroxides. Part 25. Molybdenum- and tungsten-catalyzed oxidations of alcohols by diluted hydrogen peroxide under phase-transfer conditions. *J. Org. Chem.*, **51**, 2661.
- 179** Barak, G. and Sasson, Y. (1989) Effect of phase-transfer catalysis on the selectivity of hydrogen peroxide oxidation of aniline. *J. Org. Chem.*, **54**, 3484.
- 180** Dehmlow, E.V., Thieser, R., Zahalka, H.A. and Sasson, Y. (1985) Applications of phase transfer catalysis, part 30. The

- mechanism of N-alkylation of weak N–H acids by phase transfer catalysis. *Tetrahedron Lett.*, **26**, 297.
- 181** Lebel, H., Morin, S. and Paquet, V. (2003) Alkylation of phosphine boranes by phase-transfer catalysis. *Org. Lett.*, **5**, 2347.
- 182** Wladislaw, B., Bueno, M.A., Marzorati, L., DiVitta, C. and Zukerman-Schpector, J. (2004) Phase transfer catalysis (PTC) sulfanylation of some 2-methylsulfinyl-cyclanones. *J. Org. Chem.*, **69**, 9296.
- 183** Lygo, B. and Andrews, B.I. (2004) Asymmetric phase-transfer catalysis utilizing chiral quaternary ammonium salts: asymmetric alkylation of glycine imines. *Acc. Chem. Res.*, **37**, 518.
- 184** Ooi, T., Uematsu, Y. and Maruoka, K. (2006) Asymmetric Strecker reaction of aldimines using aqueous potassium cyanide by phase-transfer catalysis of chiral quaternary ammonium salts with a tetranaphthyl backbone. *J. Am. Chem. Soc.*, **128**, 2548.
- 185** Park, E.J., Kim, M.H. and Kim, D.Y. (2004) Enantioselective alkylation of β -keto esters by phase-transfer catalysis using chiral quaternary ammonium salts. *J. Org. Chem.*, **69**, 6897.
- 186** Verbicky, J.W. and O'Neil, E.A. (1985) Chiral phase-transfer catalysis. Enantioselective alkylation of racemic alcohols with a nonfunctionalized optically active phase-transfer catalyst. *J. Org. Chem.*, **50**, 1786.
- 187** Rothenberg, G., Royz, M., Arrad, O. and Sasson, Y. (1999) *In situ* generation and synthetic applications of anhydrous hydrogen fluoride in a solid–liquid biphasic system. *J. Chem. Soc., Perkin Trans.*, **1**, 1491.
- 188** Ng, F.T.T., Mure, T., Jiang, M., Sultan, M., Xie, J.-h., Gayraud, P., Smith, W.J., Hague, M., Watt, R. and Hodge, S. (2005) AVADA – a new green process for the production of ethyl acetate. *Chem. Ind. (CRC Press) Catal. Org. React.*, **104**, 251.
- 189** Misono, M., Ono, I., Koyano, G. and Aoshima, A. (2000) Heteropolyacids. Versatile green catalysts usable in a variety of reaction media. *Pure Appl. Chem.*, **72**, 1305.
- 190** Janik, M.J., Davis, R.J. and Neurock, M. (2005) The relationship between adsorption and solid acidity of heteropolyacids. *Catal. Today*, **105**, 134.
- 191** Davis, J.M. and Thomas, V.M. (2006) Systematic approach to evaluating trade-offs among fuel options: the lessons of MTBE. *Ann. NY Acad. Sci.*, **1076**, 498.
- 192** Clark, J.H. (2002) Solid acids for green chemistry. *Acc. Chem. Res.*, **35**, 791.
- 193** Van Broekhoven, E.H., Cabre, F.R.M., Boggard, P., Klaver, G. and Vonhof, M. (1999) Process for alkylating hydrocarbons. US Patent 5 986 158 (to Akzo Nobel NV).
- 194** Maa, F. and Hanna, M.A. (1999) Biodiesel production: a review. *Bioresource Technol.*, **70**, 1.
- 195** Buczek, B. and Czepirski, L. (2004) Applicability of used rapeseed oil for production of biodiesel. *Inform*, **15**, 186.
- 196** Körbitz, W. (1999) Biodiesel production in Europe and North America, an encouraging prospect. *Renewable Energy*, **16**, 1078.
- 197** Demirbas, A. (2003) Current advances in alternative motor fuels. *Ener. Explor. Exploit.*, **21**, 475.
- 198** Diesel, R. (1912) The Diesel oil engine. *Engineering*, **93**, 395.
- 199** Harmer, M.A., Farneth, W.E. and Sun, Q. (1998) Towards the sulfuric acid of solids. *Adv. Mater.*, **10**, 1255.
- 200** Lotero, E., Liu, Y., Lopez, D.E., Suwannakarn, K., Bruce, D.A. and Goodwin, J.G. (2005) Synthesis of biodiesel via acid catalysis. *Ind. Eng. Chem. Res.*, **44**, 5353.
- 201** Bournay, L., Casanave, D., Delfort, B., Hillion, G. and Chodorge, J.A. (2005) New heterogeneous process for biodiesel production: a way to improve the quality and the value of the crude glycerin produced by biodiesel plants. *Catal. Today*, **106**, 190.
- 202** Omota, F., Dimian, A.C. and Bliet, A. (2003) Fatty acid esterification by reactive

- distillation: Part 2 – kinetics-based design for sulphated zirconia catalysts. *Chem. Eng. Sci.*, **58**, 3175.
- 203** Omota, F., Dimian, A.C. and Blik, A. (2003) Fatty acid esterification by reactive distillation. Part 1: Equilibrium-based design. *Chem. Eng. Sci.*, **58**, 3159.
- 204** Subawalla, H. and Fair, J.R. (1999) Design guidelines for solid-catalyzed reactive distillation systems. *Ind. Eng. Chem. Res.*, **38**, 3696.
- 205** Schoenmakers, H.G. and Bessling, B. (2003) Reactive and catalytic distillation from an industrial perspective. *Chem. Eng. Prog.*, **42**, 145.
- 206** Taylor, R. and Krishna, R. (2000) Modelling reactive distillation. *Chem. Eng. Sci.*, **55**, 5183.
- 207** Koster, R., Van der Linden, B., Poels, E. and Blik, A. (2001) The mechanism of the gas-phase esterification of acetic acid and ethanol over MCM-41. *J. Catal.*, **204**, 333.
- 208** Bambase, M.E., Jr. Nakamura, N., Tanaka, J. and Matsumura, M. (2007) Kinetics of hydroxide-catalyzed methanolysis of crude sunflower oil for the production of fuel-grade methyl esters. *J. Chem. Technol. Biotechnol.*, **82**, 273.
- 209** Dautzenberg, F.M. and Angevine, P.J. (2004) Encouraging innovation in catalysis. *Catal. Today*, **93–95**, 3.
- 210** Atkins, M.P. and Evans, G.R. (1995) A review of current processes and innovations in catalytic dehydrogenation. *Erdoel, Erdgas, Kohle*, **111**, 271.

5

Biocatalysis

Biocatalysis is as green as catalysis gets. Reaction conditions are mild, the solvent is water, and the catalysts are fully biocompatible and biodegradable [1]. Nitrogenase enzymes, for example, fix nitrogen from the air and make ammonia at ambient temperature [2], while the Haber–Bosch process requires temperatures above 700 K. Enzymes are extremely efficient catalysts. Their typical TOFs are 10^2 – 10^4 s⁻¹, and values as high as 10^8 are not unheard of. They are also highly regioselective, distinguishing between similar functional groups on a single substrate molecule, and thus eliminating the need for protecting/deprotecting steps. This means less (or no) by-products, low *E*-factors, and low *Q*-values. Another important bonus is that many enzymatic reactions are enantiospecific, generating chirally pure products. With all these advantages, the question that arises is not “Why use biocatalysis?” but rather “How come there are still any nonbiocatalytic processes?”

The answer is not that biocatalysis is a recent discovery (yeast fermentation has been used in wine-making and baking for thousands of years). Rather, at the end of the 20th century most chemists would have said that enzymes are generally expensive, inflexible in their substrate choice, and unstable at high temperatures, plus that they function poorly in organic media (admittedly, I was not the exception [3]). But times are changing. The 21st century promises to be the golden age of biotechnology and with it, biocatalysis. Genetic engineering already enables things that in the 1980s and 1990s were dismissed as fanciful dreams. The large worldwide investments in biotechnology are spinning off many new applications, and industrial biocatalysis is riding on the crest of this wave. Over 150 biocatalytic processes are running today in various industrial sectors, including the bulk chemicals and fine-chemicals industry (Figure 5.1) [4,5].

This chapter introduces the basics of biocatalysis, explaining the terminology and outlining the main mechanisms (readers wishing to delve more deeply into enzyme chemistry should consult Tim Bugg’s specialized textbook [6]). I will explain the various methods for developing new biocatalysts, and discuss the pros and cons of replacing “conventional catalysis” with biocatalytic alternatives. Armed with these basics, we will explore the state-of-the-art in enzyme engineering and development,

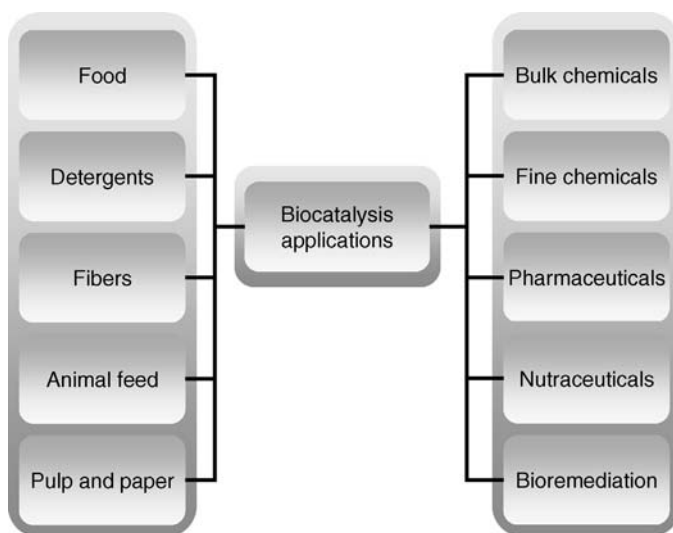


Figure 5.1 A host of new industrial sectors (*right*) are joining the traditional biocatalysis application fields (*left*).

and examine several industrial processes that use biocatalysis for eco-friendly manufacture of commodities and fine chemicals. The bulk of this chapter centers on enzymatic reactions and applications (Section 5.5 deals with nonenzymatic biocatalysis). Note that I will focus on biocatalysis applications in organic synthesis, rather than on biological transformations. An good overview of the latter is given in biochemistry textbooks [7,8]. For an advanced text on biocatalysis, see Bommarius and Riebel's book [9].

5.1 The Basics of Enzymatic Catalysis

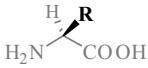
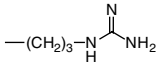
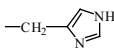
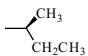
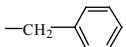
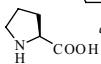
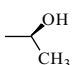
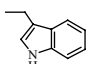
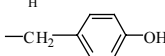
Before we start discussing enzymatic reaction mechanisms, let us try and figure out whether enzymes are “homogeneous catalysts” or “heterogeneous catalysts.” All enzymes are proteins, and large ones at that. Their typical molecular weight ranges from 20 to 200 kDa. This means that, sizewise, enzymes are much bigger than most of their substrates, so in this respect they are like heterogeneous catalysts. Like other proteins, enzymes are polypeptides, i.e., long chains of amino acids connected by amide bonds. These chains are coiled and supercoiled around themselves, often creating hydrophilic and hydrophobic regions. Therefore, unlike in homogeneous catalysis, the reaction environment at the enzyme's active site can be totally different from the outside solvent environment. So, in this respect also, enzymes are heterogeneous catalysts. Indeed, in the following sections we shall see that many of the features of catalysis at surfaces apply to enzymatic systems.

5.1.1

Terms and Definitions – The Bio Dialect

Enzymes are made from just 20 α -amino acid building blocks (structures and abbreviations are shown in Table 5.1). Each amino acid has a unique side chain, or **residue**, which can be polar, aliphatic, aromatic, acidic, or basic. The amide bonds (**peptide bonds**) make up the enzyme's backbone, and the residues determine the ultimate structure and catalytic activity of the enzyme. When the sequence of amino acids (the **primary structure**) for an enzyme is assembled *in vivo*, it folds

Table 5.1 Abbreviations and residue structures of the 20 natural (L)- α -amino acids.

Name	Three-letter abbreviation	One-letter abbreviation		Class
Alanine	Ala	A	–CH ₃	aliphatic
Arginine	Arg	R		basic
Asparagine	Asn	N	–CH ₂ CONH ₂	polar
Aspartic acid	Asp	D	–CH ₂ COOH	acidic
Cysteine	Cys	C	–CH ₂ SH	polar
Glutamic acid	Glu	E	–CH ₂ CH ₂ COOH	acidic
Glutamine	Gln	Q	–CH ₂ CH ₂ CONH ₂	polar
Glycine	Gly	G	–H	small
Histidine	His	H		basic
Isoleucine	Ile	I		aliphatic
Leucine	Leu	L	–CH ₂ CH(CH ₃) ₂	aliphatic
Lysine	Lys	K	–CH ₂ CH ₂ CH ₂ NH ₂	basic
Methionine	Met	M	–CH ₂ CH ₂ SCH ₃	aliphatic
Phenylalanine	Phe	F		aromatic
Proline	Pro	P		aliphatic
Serine	Ser	S	–CH ₂ OH	polar
Threonine	Thr	T		polar
Tryptophan	Trp	W		aromatic
Tyrosine	Tyr	Y		aromatic
Valine	Val	V	–CH(CH ₃) ₂	aliphatic

^aEntire structure.

spontaneously, giving the enzyme's three-dimensional structure (the **secondary structure** and **tertiary structure**). Remarkably, each primary structure has a unique stable tertiary structure, stabilized by hydrogen bonding, packing together of hydrophobic residues, and formation of **secondary structures** (α -helices, β -sheets, and β -turns). Note that except for glycine, all α -amino acids are chiral molecules, with "L" and "D" enantiomers. Another remarkable fact is that enzymes on Earth are composed of L-amino acids only [10,11], so they are inherently chiral (D-amino acids do appear in biological systems, but only rarely [12,13]).

The classification and naming of enzymes are somewhat complex. The first few enzymes found were given trivial (i.e., nonsystematic) names, e.g., pepsin, trypsin, lysozyme, and chymotrypsin. Later, the **common name** system was devised, by adding the suffix "-ase" to the name of the substrate (and sometimes the reaction as well). For example, "lipase" catalyzes the hydrolysis of a lipid triglyceride, "sucrase" catalyzes the hydrolysis of sucrose into glucose and fructose, and "glucose isomerase" catalyzes the isomerization of glucose to fructose. The International Enzyme Commission established a four-stage classification system for enzymes which is based on six main groups (Table 5.2). Each enzyme is assigned an identifier, called an **enzyme number**. This identifier comprises four numbers separated by periods, denoting the main group, subclass, sub-subclass, and serial number. For example, the enzyme number EC 1.1.1.1 denotes an alcohol dehydrogenase (an oxidoreductase enzyme, class 1 in Table 5.2), which acts on the CH–OH group of donors with NAD^+/NADH . Luckily, there are several on-line databases that enable the searching and cross-referencing of enzyme common names, systematic names, and structures. One user-friendly example is the Braunschweig enzyme database, or BRENDA for short [14]. It is the largest public enzyme information system worldwide, and it is available gratis for noncommercial users [15].

Enzymology has its own terminology. Reactants and reagents are generally referred to as **substrates**. Some enzymes only function when bound to additional, non-protein species. These "helpers" are called **cofactors**. The combination enzyme + cofactor is called a **holoenzyme**, while an enzyme that is missing its cofactor is called an **apoenzyme**. Cofactors can be either inorganic (e.g., metal ions) or organic. If

Table 5.2 The six classes and functions of enzymes, according to the International Enzyme Commission.

Enzyme class	Enzyme function (reactions catalyzed)
1	Oxidoreductases redox reactions
2	Transferases transfer of a functional group from one molecule to another
3	Hydrolases hydrolysis
4	Lyases adding or removal of a group to form a double bond, or addition of a group to a double bond
5	Isomerases isomerization (intramolecular rearrangement)
6	Ligases/Synthetases joining two substrates together

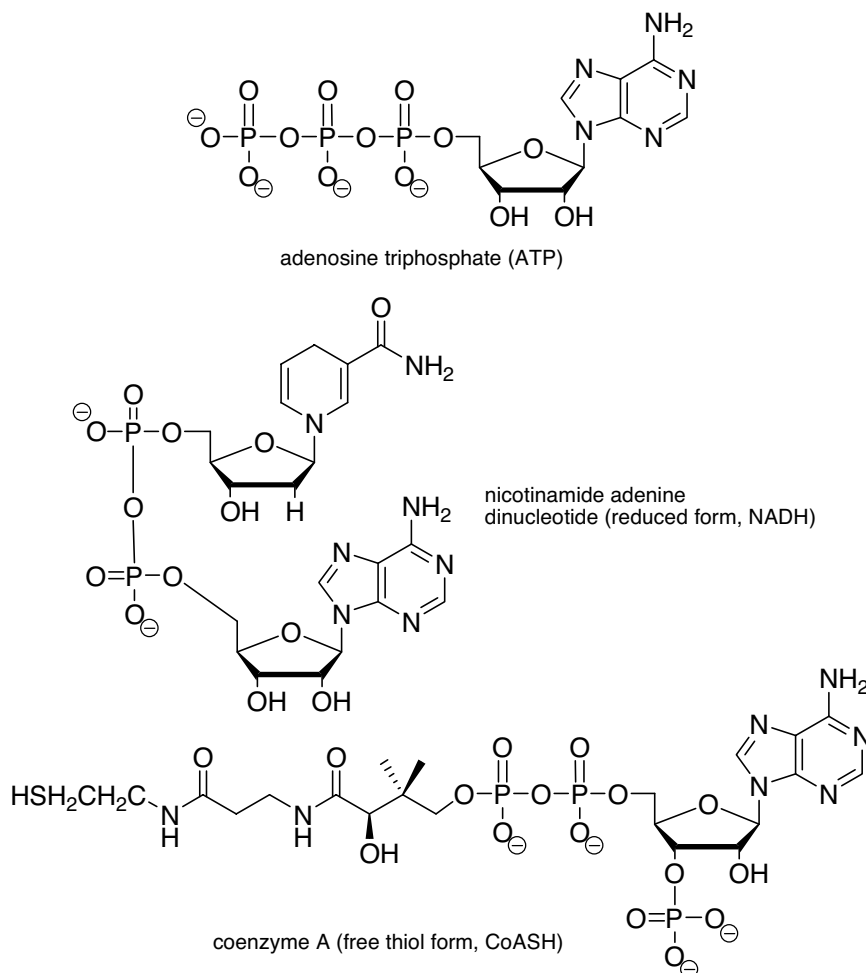


Figure 5.2 Chemical structures of three common coenzymes: NADH, ATP, and coenzyme A. Since coenzymes and cofactors are often complex and expensive molecules, their regeneration is crucial in industrial biocatalysis applications.

the cofactor is a metal, the enzyme is called a **metalloenzyme**. Confusingly, organic cofactors are also called **coenzymes**. Most coenzymes are small molecules, which transport chemical species between enzymes (see the examples in Figure 5.2). Cofactors that are bound tightly to the enzyme are referred to as **prosthetic groups**. In some cases, the cofactor itself participates in the reaction, so it is in fact a substrate, and must be regenerated before participating in another catalytic cycle. In living cells, the enzymatic cycles include cofactor/coenzyme regeneration, sometimes using a different enzyme, with the cofactor kept at a steady-state concentration. As we shall see, cofactor regeneration is one of the barriers in industrial biocatalysis because the cofactor is often more expensive than the product [16].

Rather surprisingly, the average person knows the names of several cofactors and coenzyme precursors, because many of these cannot be synthesized *in vivo*, and must be supplied in one's diet. This is the reason why a balanced diet should include retinol (vitamin A), ascorbic acid (vitamin C), tocopherol (vitamin E), thiamine (vitamin B₁), folic acid etc., as well as zinc and iron.

5.1.2

Active Sites and Substrate Binding Models

The active site of an enzyme is usually a cleft surrounded by an array of amino acid residues. Some of these residues bind the substrate (and sometimes also the cofactor/coenzyme) to the enzyme. Enzymes use four types of interactions to bind their substrates: electrostatic interactions, hydrogen bonding, van der Waals interactions, and hydrophobic interactions. The various amino acid residues (Table 5.1) are well suited to each of these binding modes. For example, substrates containing carboxylic groups ($pK_a \sim 5$) will be negatively charged at $pH = 7$, and will bind electrostatically to the protonated residues of lysine or arginine. Similarly, polar substrates can form hydrogen bonds with serine or threonine residues, and hydrophobic substrates can interact with leucine or isoleucine residues. Several cases are known where three different residues (a so-called **catalytic triad**) function as a "proton-relay" system at the same active site. Note that, in agreement with Sabatier's principle, the substrate binding at the active site is relatively weak (the binding energy is $\sim 3\text{--}10 \text{ kcal mol}^{-1}$). If the substrate bound too strongly, it would inhibit the catalytic cycle.

Enzymes owe their superb activity and selectivity to the spatial and chemical configuration of the active site. The enzyme cavity fits around the substrate (or substrates), and the multipoint contact directs it precisely to the desired reaction center. The **lock-and-key model**, introduced in 1894 by the German chemist and 1902 Nobel laureate Emil Fischer [17], is an excellent analogy (Figure 5.3a). This model was

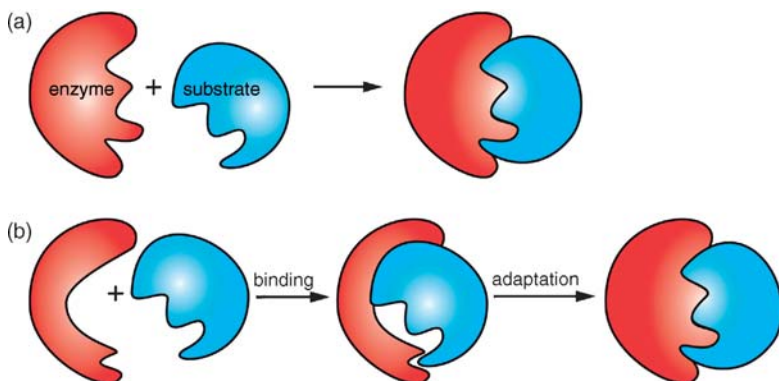


Figure 5.3 Enzyme–substrate binding: **a** Fischer's lock-and-key model; **b** Koshland's induced-fit model.

refined in 1960 by Daniel Koshland Jr. [18,19], who showed that some enzymes first bind their substrates, and then rearrange their active site accordingly (the **induced-fit model**, Figure 5.3b). Note that the enzyme–substrate complementarity applies not only to shape, but also to charge and polarity. Due to this induced fit, the binding residues at the active site destabilize the substrate, so that the enzyme–substrate complex is similar in structure to the activated complex corresponding to the transition state [20].

Some enzymes are so fast and so selective that their k_2/K_m ratio approaches the molecular diffusion rates (10^8 – 10^9 M s^{-1}). Such enzymes are called **kinetically perfect** [21]. With these enzymes, the reaction rate is diffusion controlled, and every “collision” is an effective one. However, since the active site is very small compared to the entire enzyme, there must be some extra forces which draw the substrate to the active sites (otherwise, there would be many fruitless collisions). The work of these forces was dubbed by William Jencks in 1975 as the **Circe effect** [22], after the mythological sorceress of the island of Aea, who lured Odysseus’ men to a feast and then turned them into pigs [23,24].

The binding at the active site is also responsible for the enzyme’s chiral recognition ability and enantiospecificity. Figure 5.4a shows the binding of a chiral substrate at an active site that contains three binding residues and a reactive coenzyme. One enantiomer binds well and reacts, while the other is always mismatched at two of its binding positions. The same principle applies to prochiral substrates: The enzyme’s active site can distinguish between pro-*S* and pro-*R* substrates, and also between *Re* and *Si* faces of planar prochiral molecules (Figure 5.4b).

There is an interesting parallel between substrate binding and adsorption. Since each enzyme molecule has one active site, and since these active sites all have the same structure, we can think of enzyme molecules in solution as a surface with many equivalent active sites. In this case, k_1 in the Michaelis–Menten kinetics (Eq. 5.1; see Chapter 2 for a detailed discussion) represents the rate of adsorption, k_{-1} the rate of desorption, and k_2 the rate of the surface reaction followed by fast product desorption. Moreover, this system fits the assumptions of the Langmuir isotherm (all sites identical, one molecule per site, no lateral interactions) even better than the active sites on some real solid catalysts!



5.1.3

Intramolecular Reactions and Proximity Effects

The secret behind the superb catalytic performance of enzymes is that when an enzyme binds the substrates and cofactors, it turns the uncatalyzed intermolecular reaction into an intramolecular reaction [25]. In general, intramolecular reactions are faster than intermolecular ones, because the reacting groups are already close to each other. This **proximity effect** increases the effective concentration, and with it the rate

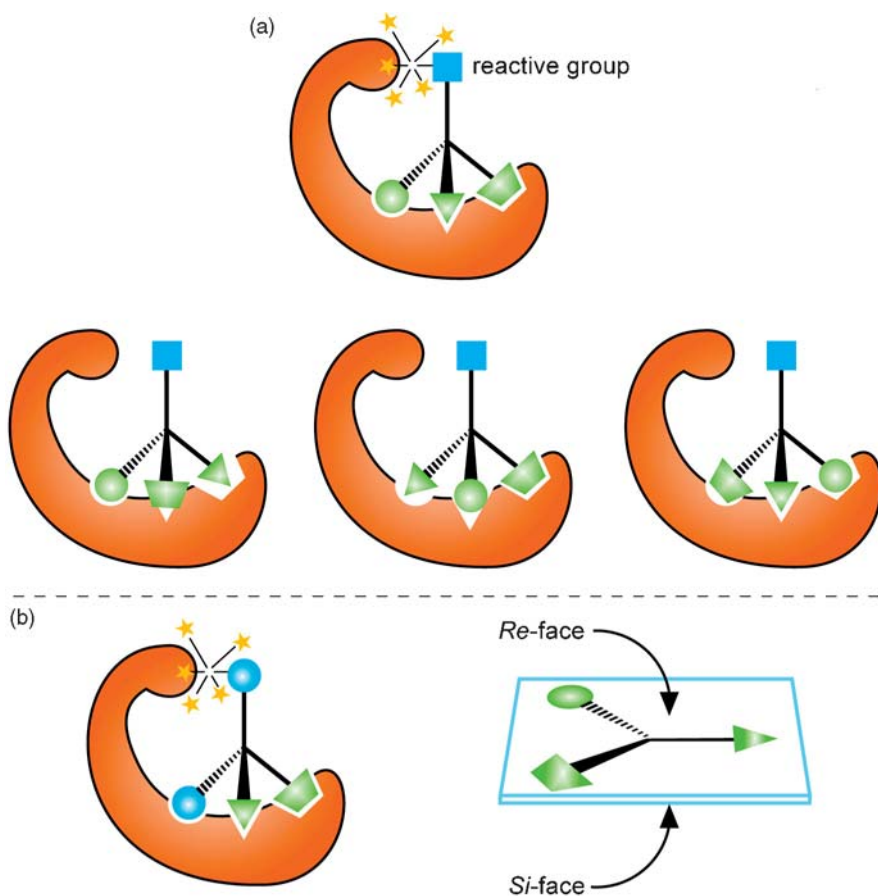


Figure 5.4 **a** The three-dimensional arrangement of binding residues at the active site enables selective binding of chiral substrates. The “wrong” substrate enantiomer (middle) does not match with the residues, resulting in a higher kinetic barrier for the formation of the enzyme–substrate complex. **b** The three-point binding also enables enzymes to differentiate between prochiral groups and *Re/Si* faces.

of reaction. The binding also gives the enzymatic reaction an entropic advantage, because it restricts the number of degrees of freedom available to the molecule. Note that this rate enhancement due to proximity effects and preferred orientation is not limited to enzymes. It holds for every chemical reaction, with or without a catalyst. Whenever the reactant is oriented in the “right” way, the reaction is faster. For example, in the thermal Diels–Alder cycloaddition of 1,3-butadiene to ethene, the diene must have a *cis* orientation. If the diene molecule is “locked” in the *cis* configuration, it is much more active – so active that 1,3-cyclopentadiene dimerizes readily at room temperature (Figure 5.5).

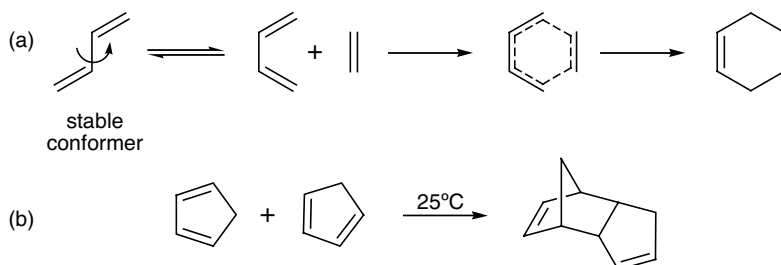


Figure 5.5 The thermal Diels–Alder reaction proceeds much faster with **b** 1,3-cyclopentadiene than with **a** 1,3-butadiene, because the double bonds in the cyclic diene are always *cis* to each other.

5.1.4

Common Mechanisms in Enzymatic Catalysis

Once the substrate is bound, other residues at the active site carry out the catalytic reaction. The elementary steps involved are similar to those we covered in Chapters 3 and 4. Broadly speaking, enzyme catalysis is divided into two common mechanisms: Brønsted acid/base catalysis; and nucleophilic catalysis [26].

Brønsted **acid/base catalysis** is the most common enzymatic mechanism, since nearly all enzymatic reactions involve a proton transfer. This means that nearly all enzymes have acidic and/or basic groups in their active site. In acid catalysis, the substrate is protonated by one of the amino acid residues at the active site (typically aspartic acid, glutamic acid, histidine, cysteine, lysine, or tyrosine). This residue itself must therefore be protonated at the reaction pH (typically between pH 5 and 9), with a pK_a just above this value. Conversely, in base catalysis, the pK_a of the deprotonating residue must be just below the physiological pH. Some enzymes can even carry out **bifunctional catalysis**, by protonating and deprotonating two different sites on the same substrate molecule simultaneously.

Note that the pK_a of a residue at the active site can vary substantially from the value observed for the free amino acid in water [27]. For example, the active site of the enzyme acetoacetate decarboxylase features a lysine residue with a very low pK_a of 5.9 (cf. $pK_a \sim 9$ for the free amino acid). In this case, the pK_a is influenced by an adjacent protonated lysine residue (Figure 5.6) [28,29]. A similar reduction, though less dramatic, is observed for aliphatic diamines (e.g., the two pK_a values for 1,4-diaminobutane are 10.80 and 9.35, respectively).

Metalloenzymes contain a bound metal ion as part of their structure. This ion can either participate directly in the catalysis, or stabilize the active conformation of the enzyme. In Lewis acid catalysis (typically with zinc, vanadium, and magnesium), the M^{n+} ion is used instead of H^+ . Many oxidoreductases use metal centers such as V, Mo, Co, and Fe in much the same way as homogeneous catalysis uses ligand–metal complexes. Figure 5.7 shows a simplified mechanism for the halide oxidation reaction catalyzed by vanadium chloroperoxidase. The vanadium atom acts as a Lewis acid, activating the bound peroxide [30].

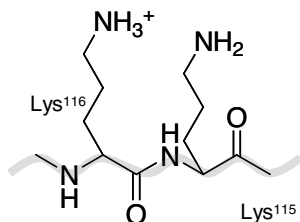


Figure 5.6 A protonated lysine residue at position 116 facilitates the low pK_a observed for the lysine residue 115 at the active site of acetoacetate decarboxylase [28]. This enzyme shows maximum activity at $pH = 5.95$.

In **nucleophilic catalysis** (sometimes called **covalent catalysis**), a nucleophilic group at the active site attacks the substrate, forming a covalently bonded intermediate. Enzymes are more efficient than “chemical” catalysts in this respect, because the enzyme’s active site is often water-free. In an aqueous solution, a charged nucleophile is solvated by layers of water molecules. This reduces its effectiveness. The same nucleophile at the active site of an enzyme is desolvated, or “naked,” with a much higher activity (a similar phenomenon occurs in some ionic liquids [32,33]). Amino acids that typically participate in such a mechanism are serine, cysteine, or lysine. Figure 5.8 shows an example of nucleophilic catalysis of amide hydrolysis by papain, a cysteine protease [34]. This enzyme features a catalytic triad at its active site,

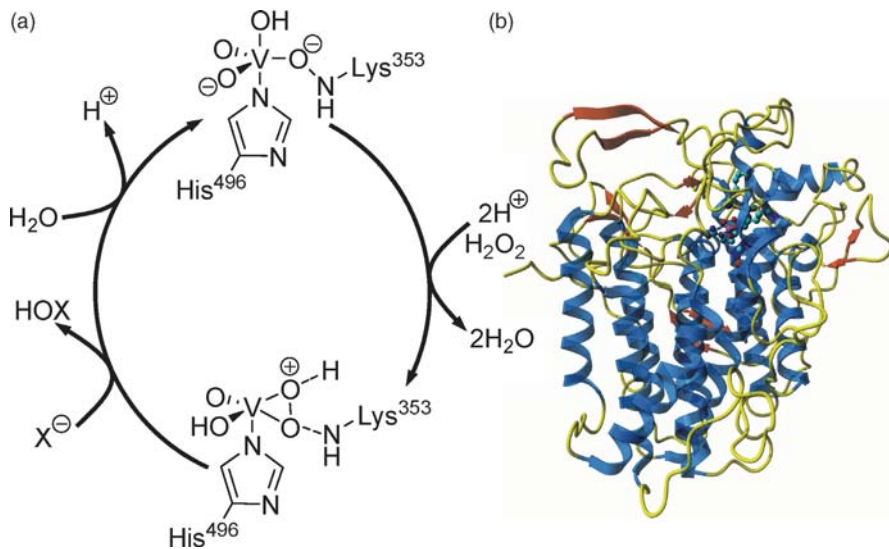


Figure 5.7 **a** Simplified catalytic cycle for vanadium chloroperoxidase, isolated from the fungus *Curvularia inaequalis* based on **b** crystal structures of the native enzyme and the peroxo intermediate [30,31]. Thanks to Dr. Teunie van Herk for the enzyme structure image.

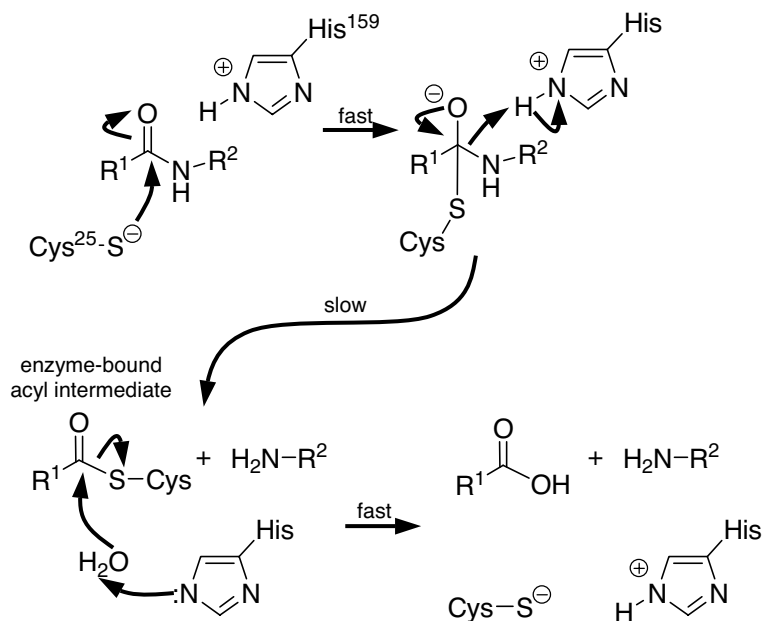


Figure 5.8 Amide hydrolysis in the presence of papain, an example of nucleophilic enzyme catalysis.

made up of Cys-25 (from which it gets its classification), His-159, and Asn-158. The catalytic cycle involves deprotonation of Cys-25 by His-159. The deprotonated thiol then attacks the peptide carbonyl carbon. This frees the amine product, giving a covalent acyl-enzyme intermediate. The enzyme is then deacylated by a water molecule, releasing the carboxylic acid product.

5.2

Applications of Enzyme Catalysis

Enzymes have been applied widely in the food, pulp and paper, and detergent sectors for decades, mostly as technical grade mixtures extracted from cells (**technical enzymes**). The applications range far and wide, from cheese ripening to leather manufacture. Table 5.3 gives some examples of the products and enzymes involved (for a comprehensive survey, see Uhlig's book [35]). Despite the large number of applications in the food industry, biocatalysis was only a curiosity in the chemical industry until recently, for several reasons. First, enzymes were relatively expensive, difficult to work with, and difficult to recycle. Second, chemicals were traditionally produced from petroleum, under high temperatures, high pressures, and extreme pH conditions. Third, chemicals production was seen as the domain of organic chemistry and organic chemists. The petroleum was inexpensive, environmental legislation was lax or nonexistent, and public awareness of environmental issues was

Table 5.3 Examples of enzyme applications in the food and detergent sectors [35].

Process	Enzyme(s) involved
Preparation of animal feed	proteases, amylases, hemicellulases
Cheese making	rennet, lysozyme
Dental hygiene	dextranase, glucanases, peroxidases
Fish curing	pancreatin
Flax processing	pectinases, macerases
Fructose production	glucose isomerase
Laundry detergents	proteases, cellulases, lipases, amylases
Lipid hydrolysis	lipases
Meat tenderizing	proteases
Winemaking	pectinases, proteases, β -glucanases

low. Thus, for most of the 20th century the chemical industry had little incentive to turn to biocatalysis.

All this is changing now. Chemical companies are hiring more life scientists, and increasing numbers of organic chemists are embracing biocatalysis solutions for complex synthetic problems. This is especially true for the production of chiral compounds [36]. Several major chemicals companies, including DSM, Rhodia, and BASF, have placed biocatalysis and biotechnology as a strategic factor in their current and future portfolio. Advanced process solutions, and most importantly the recent advances in genetic engineering and protein engineering technologies, are balancing the shortcomings of enzymes [37,38]. The annual turnover of the enzyme division of Novo Industri (now Novozymes), the world's largest enzyme manufacturer, gives an idea of the enzyme application market: In 1970 it was equivalent to \sim €26 M (\$35 M), growing to €350 M (\$470 M) in 1997, and \sim €660 M (\$900 M) in 2006 [39–41]. This nearly exponential growth promises a bright future for biocatalysis in the 21st century.

5.2.1

Whole-Cell Systems versus Isolated Enzymes

Enzymes can be used either as isolated compounds, or as part of a whole (living) cell. Each option has both advantages and disadvantages. Isolated enzymes often exhibit higher volumetric productivity and fewer side-reactions. Unlike with whole cells, there are no other enzymes present, so the products are not consumed. Another advantage is that isolated enzymes are less complicated than cells, and thus “closer” in concept to the traditional chemical catalysts. They are typically used for hydrolysis and isomerization reactions, which do not require cofactors. The main disadvantages are that you must isolate the enzyme and, if the reaction requires a cofactor, you must supply it. This complicates the situation, because the cofactor is often an expensive reagent, and must be regenerated. As shown in Figure 5.9, this regeneration can be achieved by another reaction catalyzed by an additional enzyme (known as the **coupled enzyme approach**) or by using a second substrate with the same enzyme (the

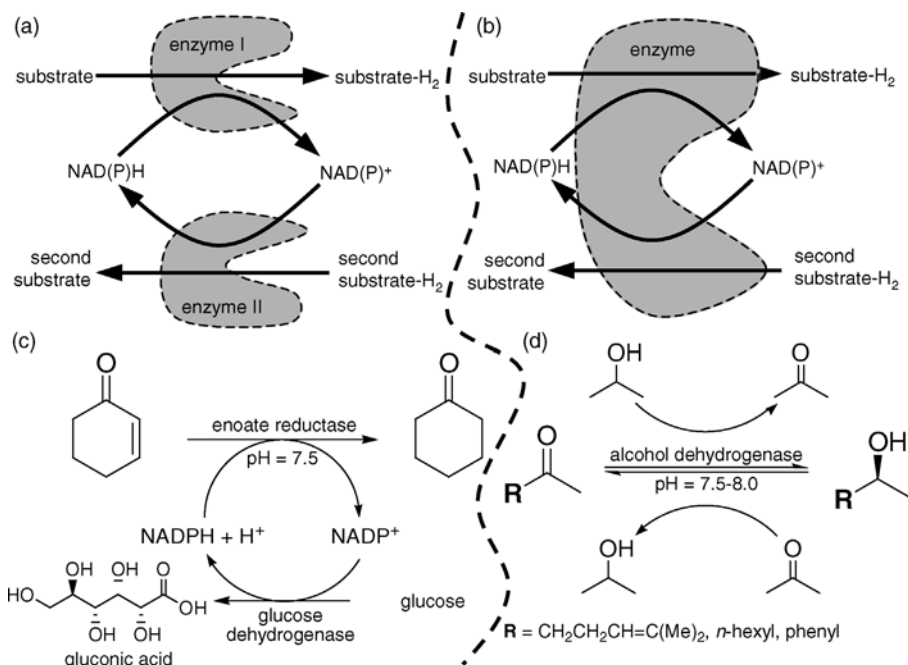


Figure 5.9 NAD⁺/NADH cofactor regeneration: **a** the coupled enzyme approach; **b** the coupled substrate approach; **c, d** examples [42,43] of the two approaches.

coupled substrate approach). For example, Bommarius and co-workers used the coupled enzyme approach for regenerating the cofactor NADPH consumed in the reduction of 2-cyclohexene-1-one catalyzed by various enoate reductases. The companion reaction in this case was the oxidation of glucose to gluconic acid, catalyzed by glucose dehydrogenase (Figure 5.9c) [42]. An elegant example of the coupled substrate approach is the alcohol/ketone redox cycle with asymmetric hydrogen transfer, described by Kroutil and co-workers [43]. They used a secondary alcohol dehydrogenase from *Rhodococcus ruber*, which is exceptionally stable in organic solvents (up to 20% v/v acetone and 50% v/v isopropanol). This stability allowed the regeneration of NAD/NADH through the isopropanol/acetone redox cycle (Figure 5.9d).

Conversely, if you are using whole cells, there is no need to isolate the enzyme, or to worry (provided you tend and feed them properly) about cofactor regeneration. Cells multiply and grow, making them suitable for large-scale applications. Furthermore, you can genetically engineer the cell to boost the desired reaction. The disadvantages are that product isolation is difficult, and that unless the organism is modified, the desired product is often broken down by another enzyme. This last problem can also be seen as an advantage: enzymes are designed by nature to function together in complex synthetic or degradative reaction cascades. Thus, genetically engineered

microorganisms can be used as “metabolic microreactors.” These cells are fed with simple carbohydrates or methane and carry out multiple cascade reactions. In principle, you can generate literally any organic product in this way. Recent examples of custom-made metabolic syntheses (usually referred to as **fermentation processes**) include the conversion of D-fructose to D-mannitol [39], the synthesis of various pharmaceuticals [44], the benzene-free routes to adipic acid [45] and hydroquinone [46] (see Chapter 1, Section 1.2.1), and the synthesis of indigo [47] discussed in Section 5.2.3 below.

5.2.2

Immobilized Enzymes: Bona Fide Heterogeneous Catalysis

As commercial catalysts, enzymes suffer from some disadvantages. Although they are very active and selective, they are far less stable than chemical catalysts, especially as far as temperature, pH, and organic solvents are concerned. Another problem is that enzymes are often more expensive than chemical catalysts, so recycling and reusing them is often a must for commercial viability. The presence of enzyme impurities in the product may also hamper subsequent steps in the process, stressing again the need for product separation and purification. All these problems can be solved to a large extent by immobilizing the enzyme (alternatively, enzymatic processes can be run without immobilization using semipermeable ultrafiltration membrane reactors [48,49]). An immobilized enzyme possesses many of the advantages of a conventional solid catalyst: It is easier to handle, it can be recovered from the product mixture by filtration, and, importantly, it is well suited to large-scale continuous processes. Moreover, immobilized enzymes are usually more stable with respect to temperature, pH ranges, and organic solvents [50] than their solution-phase analogues. The main disadvantage is that immobilization creates an extra diffusion barrier.

Immobilizing an enzyme is similar to immobilizing a homogeneous organometallic complex. The only difference is that enzymes have specific properties, which call for specific treatments. The three main enzyme immobilization approaches are: chemical or physical binding of the enzyme to a solid support; trapping the enzyme in a solid or gel matrix; and cross-linking of enzymes [51]. There are strong similarities between these methods and the preparation of heterogeneous catalysts discussed in Chapter 4, Section 4.1.4. The first approach is analogous to the support impregnation, while the second and third approaches have much in common with the preparation of bulk catalysts and supports.

5.2.2.1 Binding Enzymes to Solid Supports

Binding enzymes to solid supports can be achieved via covalent bonds, ionic interactions, or physical adsorption, although the last two options are prone to leaching. Enzymes are easily bound to several types of synthetic polymers, such as acrylic resins, as well as biopolymers, e.g., starch, cellulose [52], or chitosan [53,54]. Degussa's Eupergit resins, for example, are used as enzyme carriers in the production of semisynthetic antibiotics and chiral pharmaceuticals [55]. Typically, these copolymers contain an acrylamide/methacrylate backbone, with epoxide side groups

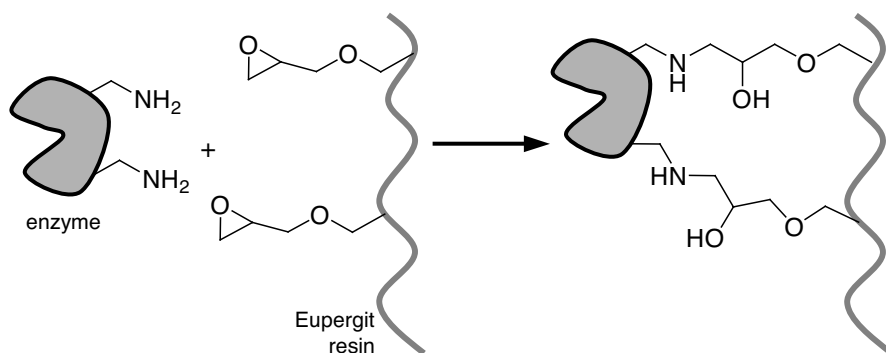


Figure 5.10 Immobilization of an enzyme on Eupergit resin by covalent bond formation [56].

that can react with the amine residues of lysine, arginine, asparagine, and glutamine (Figure 5.10). The result is a multipoint covalent attachment of the enzyme, and a corresponding high operational stability [56]. Immobilizing enzymes by physical adsorption on porous acrylic resins is also possible, and well suited to applications in a hydrophobic environment (the adsorbed enzyme may leach out under aqueous conditions).

An elegant variation on this theme is the covalent binding of enzymes to so-called **smart polymers** [57,58]. These polymers are sensitive to changes in the pH, ionic strength, and/or temperature of their environment. Small changes in the environment cause large conformational changes in the polymer chain. The thermoresponsive poly(*N*-isopropylacrylamide) (polyNIPAM), for example, has a critical solution temperature of 32 °C in water. This means that it dissolves easily in water below 32 °C, but it is insoluble in water above 32 °C. Thus, an enzyme that is covalently bound to a polyNIPAM support can be easily separated from the aqueous phase at the end of the reaction by simply heating the mixture [59]. The covalent binding of the enzyme to the polymer is usually attained either by introduction of vinyl groups on the enzyme and copolymerizing with the NIPAM monomer, or by reaction of amino residues on the enzyme with a NIPAM copolymer containing, for example, reactive ester groups.

Alternatively, enzymes can be immobilized on inorganic supports such as silica and alumina, following the same binding principles [60–62]. The lipases used in laundry detergents, for example, are immobilized first by their adsorption on silica and then by granulation of the silica particles [63]. The resulting granules break down during the washing cycle, releasing the enzymes into the water. This adsorption/granulation method can also be used in biocatalysis applications, provided of course that the reaction is carried out in nonaqueous solvents. Silica-bound enzymes can also be used in water, provided that the enzyme is covalently bound to the silica support [64].

5.2.2.2 Trapping Enzymes in Polymers or Sol/Gel Matrices

The most common method for enzyme entrapment is by polymerizing acrylamide in the presence of the enzyme. The result is a flexible porous polymeric gel, which traps the enzyme but allows the diffusion of substrates and products (Figure 5.11). Whole cells are also similarly entrapped in alginate, a natural polymer which occurs in

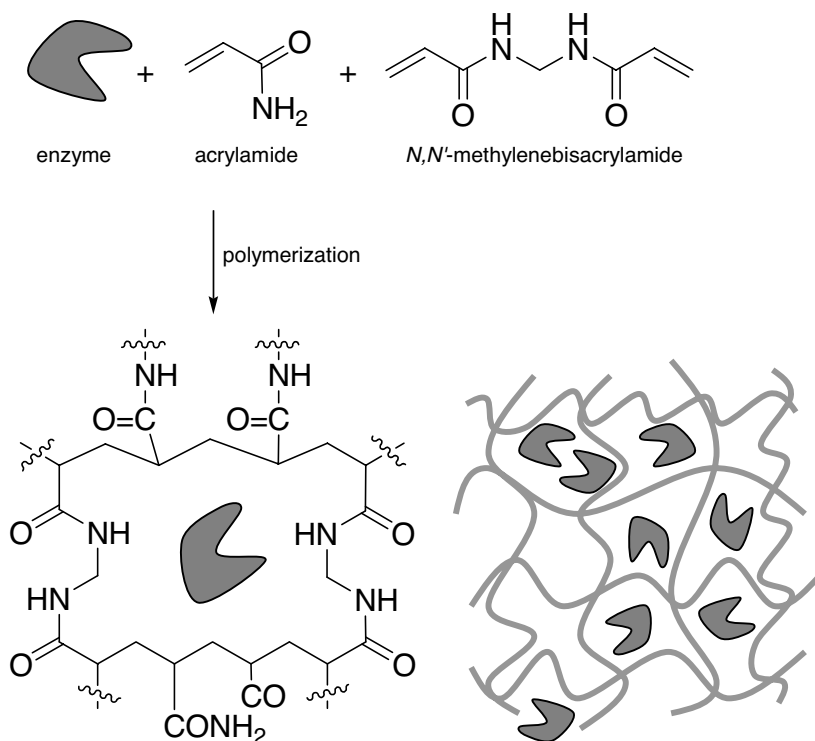


Figure 5.11 Entrapment of an enzyme in a polyacrylamide matrix.

several species of seaweed. The cells are mixed with the alginate solution and droplets are released into a solution containing a high concentration of calcium. The resulting calcium alginate is insoluble in water, so the droplets solidify and are easily separated by filtration.

Another option is to trap the enzyme in a ceramic composite matrix, using sol/gel technology. The first examples of enzymes trapped in sol/gel matrices, using a mixture of alkaline phosphatase and tetramethoxysilane (TMOS), were published by David Avnir in 1990 [65,66]. The resulting enzyme/silica composites showed a good thermal stability, but with lower activity than the free enzyme. Since then, the method has been refined by creating “tunable microenvironments” using various silica precursors and additives. Sol/gel lipase immobilizates, for example, catalyzed the kinetic resolution of chiral alcohols and amines, showing excellent enantioselectivity and good activity even after 20 recycles [67].

5.2.2.3 Cross-Linking of Enzymes

Like many other useful discoveries, enzyme immobilization by cross-linking was actually an unintended by-product of another research project. In 1964, Florante Quijoch and Frederic Richards at Yale university cross-linked crystals of carboxypeptidase-A with glutaraldehyde (pentane-1,5-dial), hoping to get stable crystals for X-ray diffraction studies. They noted that these cross-linked enzyme crystals (now

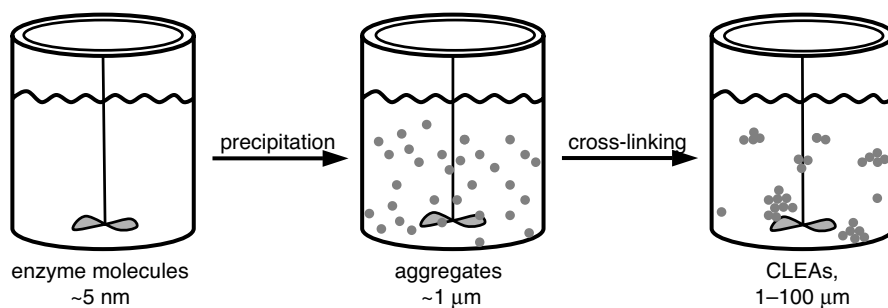


Figure 5.12 The formation of CLEAs is a two-stage process, which combines in essence enzyme separation and immobilization.

called CLECs) retained their catalytic activity, although it was somewhat lower than the free enzyme, due “either to the alteration of functional groups directly affecting the catalytic activity of the enzyme, or to an increase in the restriction to diffusion of the substrate caused by a decrease in the effective ‘pore’ size of the channels” [68]. It took almost 30 years, however, before the CLEC concept was patented and commercialized [69,70].

For most enzymes, the CLEC is much more robust than the simple isolated enzyme. CLECs can withstand higher temperatures, they denature more slowly in organic solvents, and they are less susceptible to proteolysis [71]. Moreover, since there is no external support involved, CLECs exhibit a high volumetric productivity. These advantages, together with the tunable particle size (typically 1–100 μm), make CLECs attractive for industrial biocatalysis applications.

An elegant alternative approach to enzyme cross-linking was developed recently by Roger Sheldon’s group at TU Delft [72,73]. Instead of cross-linking enzyme crystals, which can be difficult and costly, Sheldon simply precipitated the enzymes from aqueous solution as physical aggregates, by adding a precipitating agent such as poly (ethylene glycol) or $(\text{NH}_4)_2\text{SO}_4$. Cross-linking of these aggregates renders them permanently insoluble, while in principle maintaining their catalytic activity (Figure 5.12). These cross-linked enzyme aggregates, or CLEAs, are easily made, and do not require highly purified enzymes as starting materials [74]. CLEAs show similar advantages to CLECs, as demonstrated in several laboratory-scale studies [75,76].

5.2.3

Replacing “Conventional Routes” with Biocatalysis

The application of whole cells and isolated enzymes in the chemical industry is advancing rapidly, and many companies are investing in so-called **white biotechnology**. That said, most of the biocatalytic processes are aimed at new compounds which are difficult to synthesize by conventional chemical routes. Replacing an existing chemical process with a biocatalytic route is trickier, because the new process must deliver the same quality of product (or better), at a lower overall cost. The existing process has an advantage here, since its capital costs are already repaid. Thus, in order

to be profitable, the total costs of the new route must be lower than the production costs of the old one [77].

To illustrate this, let us consider the synthesis of indigo, the blue dye used for coloring jeans, with a worldwide demand of ~17 000 tpa (tons per annum). Originally, an indigo derivative was extracted from plants and animals, such as the *Hexaplex trunculus* sea snail (possibly the source for the blue and purple pigments mentioned in the Bible). Today, indigo is produced following the route developed by BASF in the early 1900s, starting from *N*-phenylglycine. The synthesis includes treatment with a KOH/NaOH melt containing NaNH_2 at 900°C , followed by air oxidation. In 2002, Genecor developed an alternative, eco-friendly indigo process (Figure 5.13), based on the fermentation of glucose in an engineered *E. coli* cell [47]. They modified the tryptophan pathway to achieve high-level indole production, and added genes that encoded naphthalene dioxygenase (NDO). This enzyme catalyzed the oxidation of indole to *cis*-indole-2,3-dihydrodiol, a key step in the process. The initial indigo produced by these cells had a red tint, which was caused by the presence

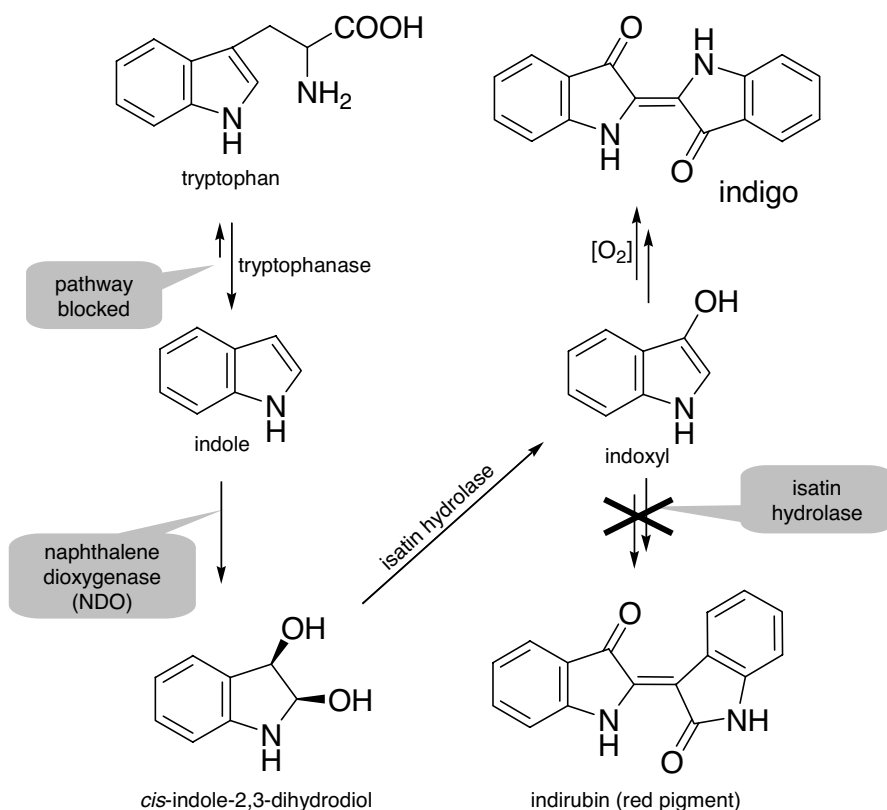


Figure 5.13 The Genecor metabolic route to indigo [47], starting from glucose and using a genetically modified *E. coli*, is a complex yet “clean” multistep process which delivers a product identical to that of the century-old traditional chemical route.

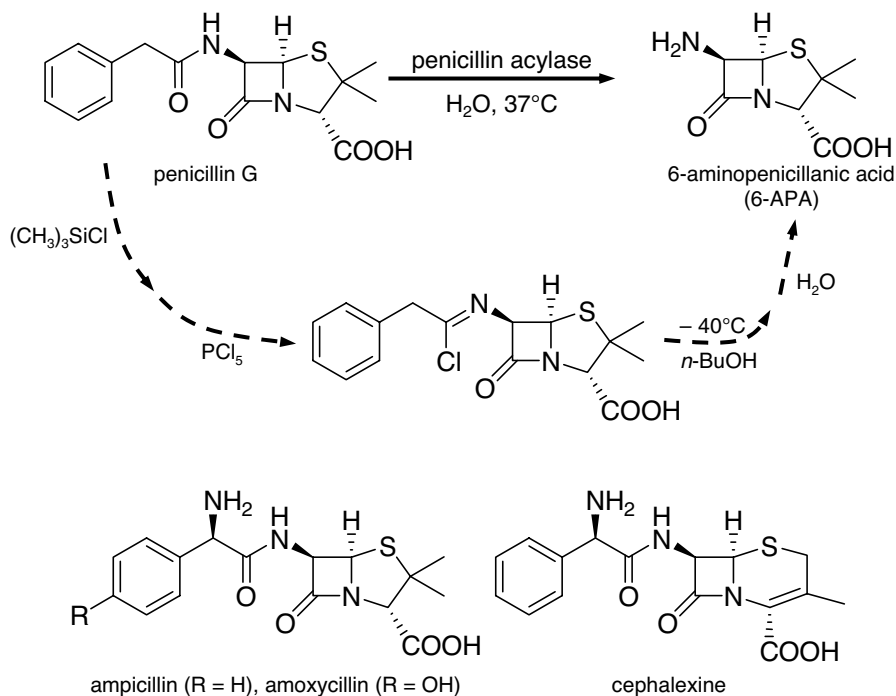


Figure 5.14 Chemical and biocatalytic conversion of penicillin G to 6-aminopenicillanic acid, the core structure of various antibiotics.

of the by-product indirubin, but this was eliminated by inserting another enzyme, isatin hydrolase. The process was successfully scaled up to 300 000 L, at production costs comparable to the existing chemical route. However, it was not commercialized, because its total costs (production + capital investment) were higher than the production costs of the existing route.

Two industrial process replacement success stories are the synthesis of acrylamide using nitrile hydratase (see Section 5.5.1 for details), and the synthesis of penicillin and cephalosporin antibiotics. DSM produces penicillin G by fermentation, using genetically engineered *Penicillium chrysogenum* strains. The penicillin is converted in the presence of penicillin acylase to 6-aminopenicillanic acid (6-APA; see Figure 5.14), which serves as a backbone for generating a variety of semisynthetic antibiotics. The process replaces complex solvent-based chemistry, typically conducted at temperatures as low as -40°C to preserve the labile β -lactam ring. Ampicillin, amoxycillin, and cephalaxin are all made via this route, with typical production volumes of 1000 tpa [78].

5.2.4

Combining “Bio” and “Conventional” Catalysis

Just as in the business world, chemical “joint ventures” are sometimes preferable to replacements. Since enzymes offer different advantages than “chemical catalysts,”

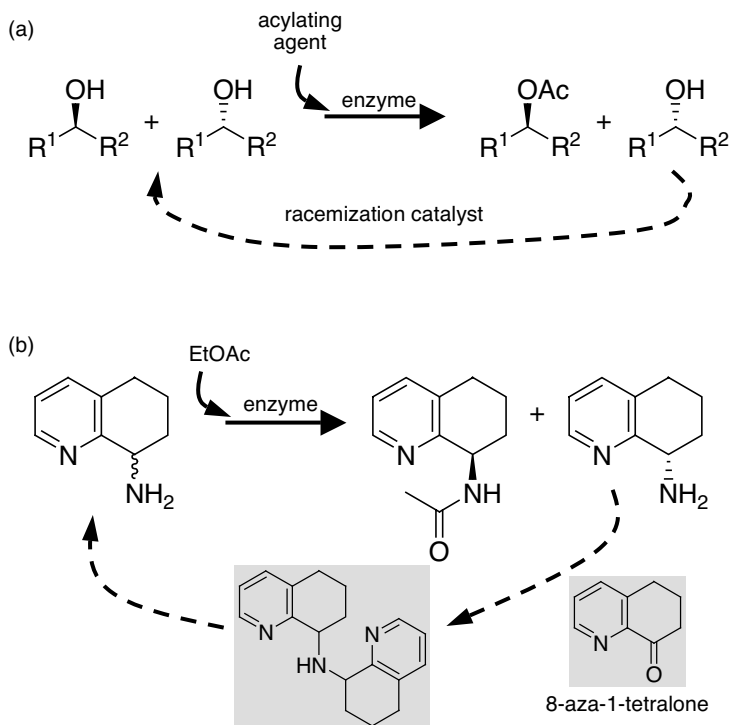


Figure 5.15 **a** Generic scheme of dynamic kinetic resolution of alcohols; **b** example of the resolution of a racemic 8-aminotetrahydroquinoline, where the racemization is catalyzed by the organic ketone 8-aza-1-tetralone (the racemization cycle is highlighted in gray).

combining the two in one process is often a good and pragmatic solution. The superb chiral recognition properties of enzymes, for example, make them ideal for resolving enantiomers, in a process called **kinetic resolution** [79]. Given a racemic alcohol mixture, for example, a lipase will catalyze the esterification of one enantiomer only (Figure 5.15a). The problem is that 50% of the substrate remains. However, in the presence of a (chemical) racemization catalyst, the unused enantiomer is continuously racemized, creating more of the reactive enantiomer and a higher overall yield [80]. In one example of this **dynamic kinetic resolution** [81,82], Jan-Erling Bäckvall and co-workers used organometallic Ru complexes as racemizing catalysts, obtaining 60–80% yield and more than 99% *ee* for a variety of alcohols [83]. Another interesting example is the lipase-catalyzed acetylation of the racemic 8-aminotetrahydroquinoline (Figure 5.15b). The enzyme converts only the (*R*)-enantiomer. However, catalytic amounts of 8-aza-1-tetralone racemize the remaining (*S*)-amine by forming a racemic enamine that is hydrolyzed back to the amine [84].

Another interesting example is the Du Pont chemoenzymatic synthesis of glycolic acid, $\text{CH}_2(\text{OH})\text{COOH}$, a compound used in skincare products and biopolymers. In this process (Figure 5.16), formaldehyde (methanal) and HCN are reacted, giving

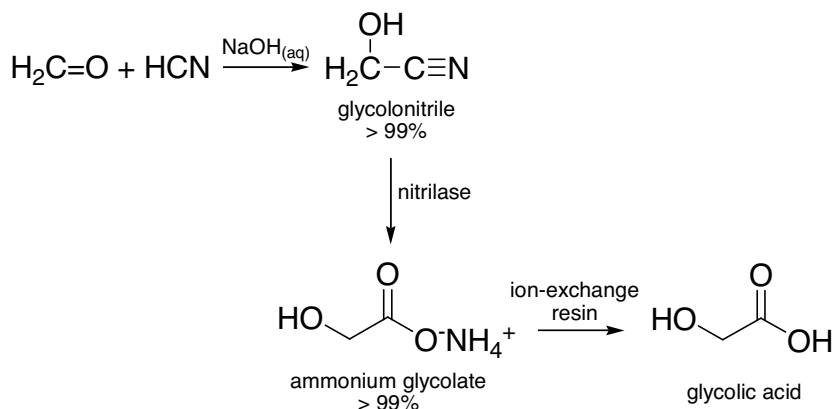


Figure 5.16 The Du Pont chemoenzymatic route to glycolic acid.

glycolonitrile (2-hydroxyacetonitrile) with >99% yield. This intermediate is then converted as is, in the presence of a nitrilase enzyme, to ammonium glycolate, which is converted to high-purity glycolic acid by ion exchange [85]. The process was run on a kilogram batch scale, in a continuous stirred-tank, or in a fixed-bed reactor where the enzyme was immobilized on alginate beads.

Combining whole-cell biocatalysis and radical polymerization, researchers at Imperial Chemical Industries (ICI) published a chemoenzymatic route to high-molecular-weight poly(phenylene) [86]. This polymer is used in the fibers and coatings industry. However, since it is practically insoluble, the challenge was to make a soluble polymer precursor that could first be coated or spun, and only then converted to poly(phenylene). The ICI process starts from benzene, which is oxidized by *Pseudomonas putida* cells to cyclohexa-3,5-diene-1,2-diol (see Figure 5.17). The

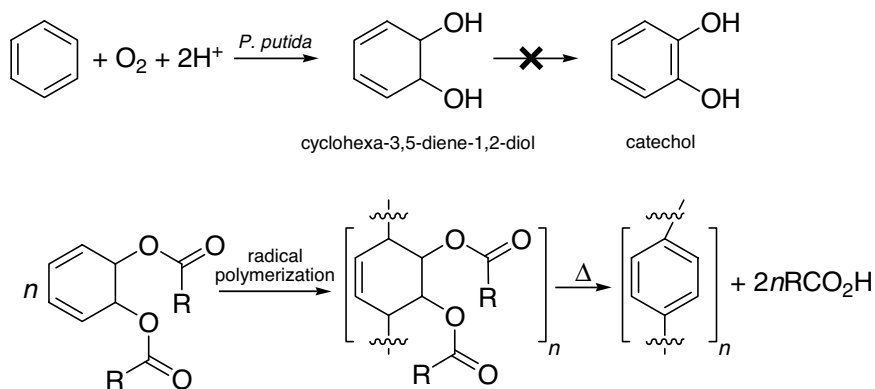


Figure 5.17 The ICI chemoenzymatic route to poly(phenylene) uses genetically altered *Pseudomonas putida* cells, which consume benzene and excrete the dihydrodiol monomer.

enzyme that catalyzes the key reaction is toluene dioxygenase. The wild-type cells convert this diol further to catechol, but this step was eliminated with genetic manipulation. Thus, the organism consumes the benzene and excretes the dihydrodiol, which is extracted and crystallized (interestingly, such benzene-eating bacteria were also found in areas that had been exposed to benzene for several decades). Ester derivatives of the dihydrodiol are readily polymerized, and the resulting polymers are easily decarboxylated to poly(phenylene).

5.3

Developing New Biocatalysts: Better than Nature's Best

Until recently, the chemical industry's main argument against using biocatalysis was that naturally occurring enzymes seldom meet the stringent requirements for a specific industrial setting, since they are optimized for homeostatic physiological conditions. However, since the early 1980s, three powerful molecular approaches have been developed to solve this problem. These are **bioprospecting**, **rational design**, and most recently and importantly, **directed evolution** [87,88]. This section gives an overview of the advantages and limitations of these techniques, which lie at the interface between chemistry, biology, and computer science [37].

5.3.1

Prospecting Natural Diversity

Traditionally, industrial enzymes come from a small number of well-classified microorganisms, clustered in taxonomic "hot spots," but the vast majority of microorganisms are unexplored [89]. Furthermore, most commercial enzyme-producing organisms come from only a few ecological niches, even though many habitats (e.g., soil, dung, or straw) could harbor good enzyme producers. Now, several companies are exploring different bacteria and different habitats, looking for enzymes that may be better suited to industrial process conditions [90]. Soda lakes and hot springs, for example, are favorite habitats for industrial microbiologists who seek **extremophiles** (enzymes capable of working under alkaline, high-temperature conditions) [91]. Techniques such as expression cloning and molecular screening enable the use of genes from "uncooperative" donor organisms which are much harder to cultivate.

There are two main microbial screening strategies:

- searching in specific ecological niches and screening of materials (e.g., soil samples) for organisms with specific activities in specific physicochemical conditions (high/low temperature, pH or presence of specific ions); and
- screening different taxonomic strains of previously identified microorganisms that have been recognized as enzyme producers.

Several new enzymes have been isolated from uncultivated microorganisms using these methods.

5.3.2

Rational Design

Rational design is a heuristic approach, based on a detailed understanding of the enzyme structure and mechanism. In this method, site-directed mutagenesis is used to introduce site-specific changes into the enzyme, often in combination with a computational structure modeling approach [92]. Although it has been widely used, this method has only resulted in limited success (especially considering the filtering effect of scientific publication, where successes get published while most failures do not). The two main problems in rational design are that

- resolving enzyme structures is difficult; and
- structure/activity relationships for enzymes are often elusive.

Even when an enzyme is studied exhaustively, identifying the amino acid residues that control the catalytic activity is a difficult task! In fact, site-specific single mutations rarely do their job, since single mutations far from the active site can change the protein's properties.

5.3.3

Directed Evolution

Directed evolution is an iterative process that mimics the natural evolution process *in vitro*, by generating a diverse library of enzymes and selecting those with the desired features. Natural evolution is very effective in the long term (bacteria adapt to every environment, living even in so-called “black smokers,” deep-ocean vents where temperatures can reach 350 °C and the pressure is 200 bar [93]). Unfortunately, it typically takes millions of years. Happily, directed evolution can be carried out within weeks or months and with an unlimited number of parents. Importantly, and unlike rational design, directed evolution is a stochastic method. It does not require any structural or mechanistic information on the enzyme of interest (although such information can help).

Evolving enzymes with specific properties (e.g., higher activity in organic solvents) is basically a search process in the enzyme space (see Chapter 6 for a more detailed discussion). One reason why directed evolution outperforms rational design is the sheer size of this space. Since enzymes are made of 20 amino acids, even the sequence of a “short enzyme” containing just 80 amino acids can already have 20^{80} permutations. This is far more than the number of atoms that make up the Earth. It is also the reason why directing the evolution of an existing enzyme is much likelier to succeed than searching for catalytically active amino acid sequences in random peptide libraries.

Figure 5.18 shows a schematic of a typical directed evolution workflow. First, a diverse library of genes is created, by **random mutagenesis** at the nucleotide level using **error-prone PCR**, or by using **gene recombination** methods, such as **DNA shuffling** [94]. Sex is an important issue in directed evolution. Random mutagenesis is akin to asexual reproduction. When you evolve an enzyme by sequential generations of random mutagenesis and screening, you use the best candidates in each generation to

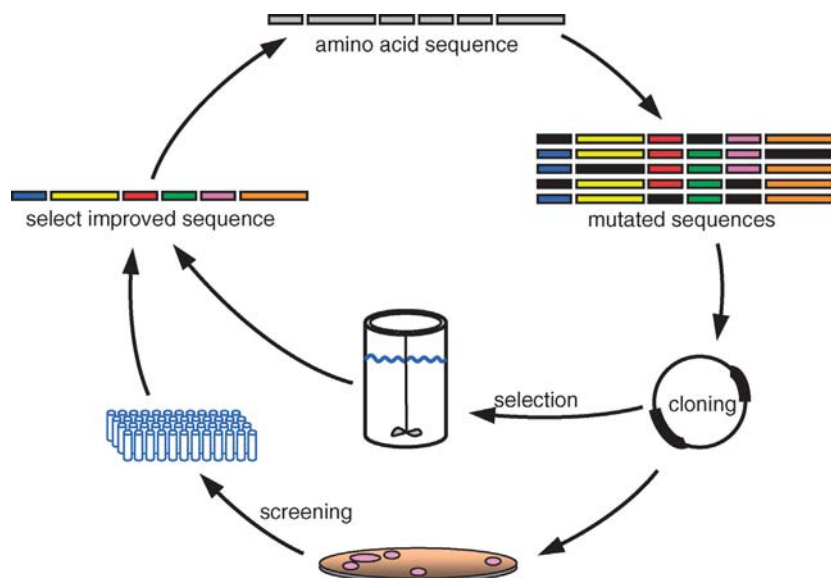


Figure 5.18 Schematic showing the main operations workflow in directed evolution.

parent the next generation, possibly losing other potentially useful candidates (this disadvantage of asexual evolution is known as Müller's ratchet [95]). Conversely, by recombining parental genes to produce libraries of different mutation combinations, you can quickly accumulate the beneficial mutations, while removing any deleterious ones [96]. The genes are then inserted into an **expression vector** and transformed into a laboratory microorganism, or **expression host**, which expresses the enzyme. The result is a large **library** of enzymes, some of which (hopefully) show improved properties compared to the starting compounds. These enzymes are sorted and the "good" genes are kept in the gene pool, and used as "parents" in the next generation.

Sorting out the "good enzymes" from the library is no mean task. There are two main sorting methods: **enzyme screening** and **enzyme selection**. In screening, every library member is assayed individually, usually using automated high-throughput colorimetric assays in microtiter plates. Although screening is a flexible and versatile technology, it limits the library size to $\sim 10^6$ candidates. This may seem like a lot, but it is a drop in the ocean compared to the total enzyme space. Alternatively, one can select "good enzymes" by linking the properties of the enzyme to the survival or growth of a host organism. This is done by genetic complementation, creating a host organism that is deficient in a certain pathway or activity. Selection has no problem with large libraries, since the library size is limited only by the cell transformation efficiency. Unfortunately, devising a selection method for a given enzyme is often difficult, since the desired enzyme feature is often non-natural, and cannot be coupled to the growth and survival of the host organism. Moreover, the host organism sometimes evolves survival pathways which are unrelated to the desired enzyme feature.

With the advances in genetic engineering technology, directed evolution is no longer "rocket science." It is a proven technology which opens a fast and relatively inexpensive pathway for developing new biocatalysts [97]. Successful synthetic

applications include the evolution of enzymes that can work in nonaqueous solvents [50], enhancement [98] and even inversion [99] of an enzyme's enantioselectivity, and creation of **thermophilic enzymes** [100] that are stable at higher temperatures (typically 60–90 °C). Another growing field of applications is bioremediation [101,102] using enzymes that are engineered specifically to break down xenobiotic compounds, such as organophosphate pesticide derivatives.

Current research efforts focus on applying the knowledge and understanding of protein structure and function to the design of focused directed evolution biocatalyst libraries. This approach is already delivering striking results compared to random mutagenesis and recombination of entire genes [103].

5.4

Nonenzymatic Biocatalysts

5.4.1

Catalytic Antibodies (Abzymes)

Antibodies are Y-shaped proteins which the immune system uses to identify and neutralize foreign molecules; they come from bacteria, viruses, and chemical toxins. Each antibody is made of four units: two large **heavy chains** and two small **light chains**, which are linked together by disulfide bridges. Unlike enzymes, the general structure of all antibodies is very similar. Each antibody has two unique binding sites, located at the top ends of its "Y" structure (Figure 5.19). These sites are responsible for binding the target molecule, or **antigen**. When a new foreign antigen is detected, the immune system produces a large and diverse "antibody library," with as many as 10^9 different antibodies, in the hope that some of these will be able to bind the new antigen. Each antibody recognizes the binding part, or **epitope**, of a specific antigen. The binding tags the antigen, singling it for the attacking T-cells of the immune system.

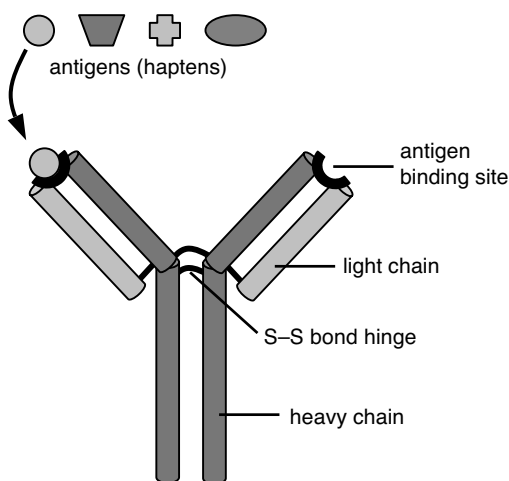


Figure 5.19 Schematic structure of an antibody protein binding to its specific antigen.

A natural antibody is not an enzyme. It shows selective substrate recognition, but it binds the antigens very tightly (typical $K_{\text{dissociation}}$ values are $\sim 10^{-6}$), and does not catalyze any reaction. Nevertheless, if one could weaken this binding, and design an antibody that would selectively recognize and bind the transition state of a specific reaction, this antibody should catalyze that reaction [104]. The problem is that in order to generate this antibody you need the antigen, i.e., you must isolate the activated complex that corresponds to the transition state, which is by definition impossible. In 1986, Peter Schultz and Richard Lerner solved this problem, by using transition-state “look-alikes” [105,106]. These small molecules, or **haptens**, were anchored on proteins, which were then injected into mice, triggering an immune response. The antibody-producing cells were isolated, immortalized by fusing them with cancer cells, and then cultured and screened for catalytic activity. These new catalytic antibodies, or **abzymes**, exhibit many enzyme-like mechanisms, including induced-fit binding and allosteric modulation [107]. The first examples of antibody catalysis were demonstrated for ester hydrolysis. Since then, the scope was extended to many other reactions [108], including proton transfer, decarboxylation, C–C coupling/scission [109], rearrangement [110], and cycloaddition. Just as with enzymes, abzyme design and development has also benefited from the recent advances in genetic engineering and protein design. A good overview of the recent developments in the field is given in the collection of essays edited by Ehud Keinan [111].

Abzyme design opens pathways to a variety of applications in chemistry, biology, and medicine [112,113]. For example, some abzymes can target and hydrolyze the benzoic ester fragment of cocaine, yielding inactive products [114]. In principle, this hydrolysis can eliminate the toxic effect of the drug while it is still in the bloodstream [115]. Figure 5.20 shows the hydrolysis reaction and the corresponding tetrahedral transition-state mimic used for generating the antibodies. This approach differs from the traditional medication strategies that target dopamine receptors (the brain cell molecules that are overstimulated during cocaine use), and may avoid the adverse side effects of the latter. The idea is that treating chronic cocaine abusers with such antibodies would deprive the abuser of the reinforcing effect of the drug, providing an opportunity for rehabilitation [116,117].

5.4.2

Catalytic RNA (Ribozymes)

In 1989, Sidney Altman and Thomas Cech were awarded the Nobel Prize in chemistry for a discovery that changed not only the field of biocatalysis, but also our perception of the molecular basis of life on Earth [118]. They showed that RNA, which until then was considered an innocent carrier of hereditary information, can actually catalyze reactions [119,120]. Two different RNA molecules were shown to catalyze site-specific phosphodiester bond cleavage, with rate enhancements of several orders of magnitude. This discovery of nonprotein biocatalysts came as a complete surprise, and laid open many questions and opportunities [121,122].

In a nutshell, RNA transcribes the genetic code of the DNA, and transfers it to the cell’s “protein factories.” This process also requires a shearing and splicing of the RNA molecules, because DNA strands contain regions which are not essential for

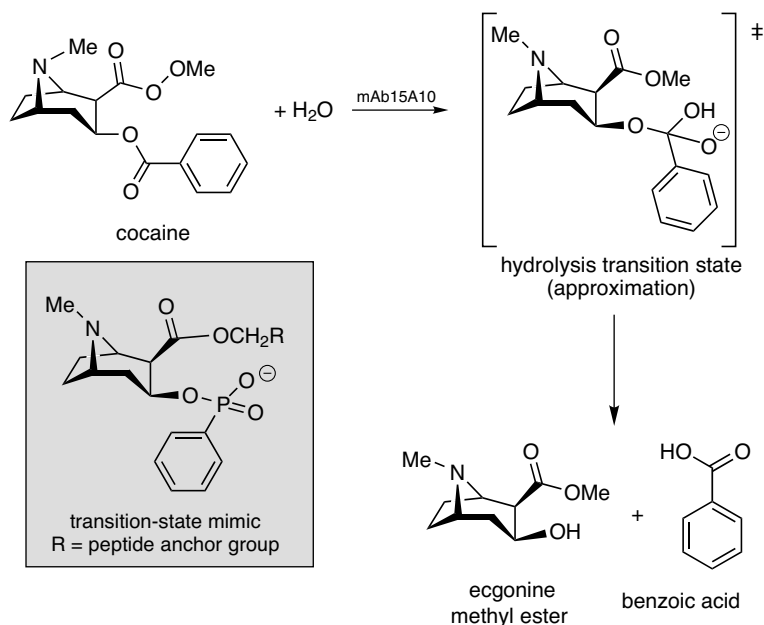


Figure 5.20 Hydrolysis of cocaine catalyzed by mAb 15A10. The abzyme was generated using a mimic of the tetrahedral activated complex, with a phosphate group replacing the carboxylic group (inset).

making proteins. These are also transcribed into the RNA molecules. Thus, these “extra pieces” of nucleic acid must be removed, and the useful pieces rejoined. As with all chemical reactions in a cell, this RNA shearing and splicing requires enzymes. Altman and Cech discovered that these “enzymes” were actually nucleic acids, or **ribozymes** [123].

Most naturally occurring ribozymes catalyze phosphoryl transfer reactions, where a sugar 2'-OH or 3'-OH attacks a phosphodiester linkage [121]. The two main classes are intramolecular ribozymes, where the sugar-OH nucleophile attacks its own 3'-phosphodiester (Figure 5.21a) and intermolecular ribozymes, where the nucleophile comes from a different RNA strand (Figure 5.21b). There is also evidence that the RNA catalyzes the peptide bond-forming aminoacyl transfer reaction in ribosomes [124,125].

5.5 Industrial Examples

5.5.1 High-Fructose Corn Syrup: 11 Million Tons per Year

The isomerization of glucose to fructose, catalyzed by the enzyme xylose isomerase, is by far the largest-scale biocatalytic process. Already known for several decades,

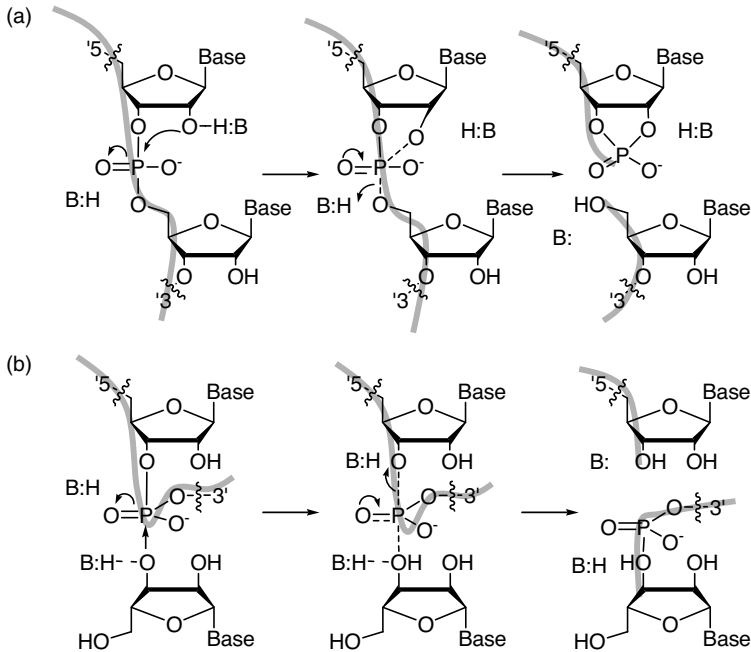


Figure 5.21 Splicing of RNA chains (gray lines) through a) intramolecular and b) intermolecular nucleophilic attack in the presence of a base [121].

this process was scaled up when fructose demand soared in the 1970s. The reason was a combined increase in sugar prices and a customer preference shift to low-calorie foods (fructose is three times as sweet as sucrose, giving consumers more sweetness for fewer calories). The process uses a 95% glucose syrup feed, which is highly viscous and requires relatively high temperatures (55–65 °C). The isomerization equilibrium gives roughly a 50:50 glucose/fructose ratio. To maximize the space-time yield, the actual product ratio produced is typically 58:42. The product is then concentrated to a 55:45 glucose/fructose ratio, which has the same sweetness weight equivalent (**dextrose equivalent**, or DE) as sucrose. This is the so-called high-fructose corn syrup (HFCS), which is ubiquitous in today's processed foods.

The key to the successful scale-up was the immobilization of the enzyme, which increased stability and reduced the enzyme costs to an acceptable level. The isomerization step is typically carried out in a parallel series of packed-bed reactors, where the enzyme is immobilized on silica or inert cellulose carriers (Figure 5.22). A ton of immobilized xylose isomerase can catalyze the production of ~5000 tons of HFCS [35]. Current research is concentrating on developing a more thermostable enzyme variant which would reach the 55:45 ratio directly in the reactor column.

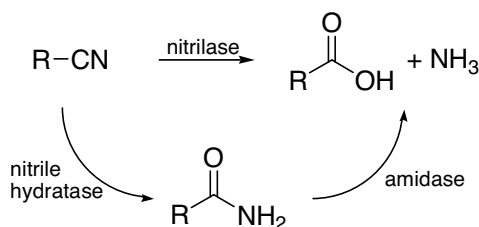
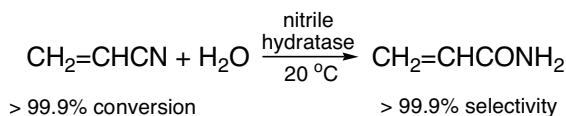


Figure 5.24 Unlike the chemical route, the biocatalytic hydrolysis of acrylonitrile to acrylamide is highly selective, owing to the specific function of the nitrile hydratase enzyme.

copper at 80–120 °C (Figure 5.23b; see Chapter 4 for a discussion on Raney metal catalysts). This process gave 60–80% conversion, with 96% selectivity. Although the catalytic route ran under relatively mild conditions, there was still room for improvement, since high degrees of polymerization can be achieved only when using a high-purity monomer feed.

In 1985, Nitto chemicals (now part of Mitsubishi Rayon) opened a 5000 tpa plant for hydrating acrylonitrile to acrylamide using *Rhodococcus rhodochrous* cells containing the enzyme nitrile hydratase (Figure 5.24). The biocatalytic route gives >99.9% yield, and one gram of cells can produce many kilograms of acrylamide [126]. Moreover, the product contains virtually no acrylic acid, because different enzymes are responsible for the hydrolysis of nitriles and amides (direct enzymatic hydrolysis of nitriles to carboxylic acids is also possible, with nitrilase enzymes). Today, all the acrylamide worldwide (~50 000 tpa) is produced via this route, by which the cells are conveniently immobilized in a polyacrylamide matrix. The reaction has since been extended to several other nitriles (Table 5.4), which are hydrolyzed to the amides with excellent space-time yields. The cells tolerate extremely high substrate concentrations, as high as 1000 g L⁻¹. Reactions of liquid nitriles can be run in the neat nitrile as solvent [127].

5.5.3

The BMS Paclitaxel Process

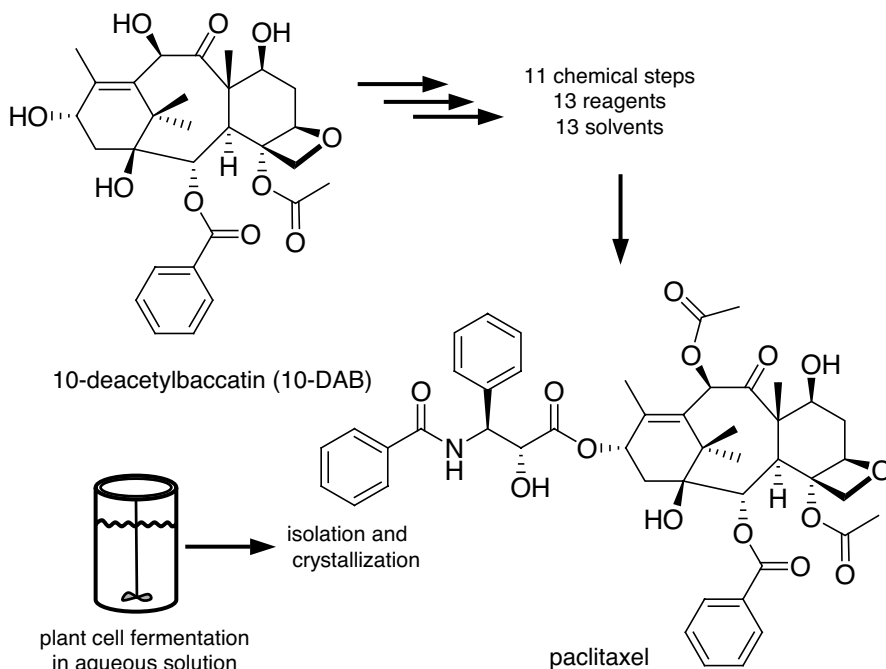
Paclitaxel, the active ingredient in the anticancer drug Taxol®, was discovered by Monroe Wall and Mansukh Wani, who isolated it from the bark of the Pacific yew tree in 1967. Clinical trials in the 1980s proved that Taxol could treat ovarian cancer. The problem was that the Pacific yew is one of the slowest growing trees in the world, and treating just one patient required the cutting down and processing of six 100-year old

Table 5.4 Examples of amide synthesis with *R. rhodochrous* nitrile hydratase [127].

Amide product	Concentration/g L ⁻¹
Nicotinamide	1460
γ-Picolylcarboxamide	1100
α-Picolylcarboxamide	980
Benzoylamide	850
Indole-3-carboxamide	700

trees (yew bark contains <5 ppm paclitaxel). Thus, another source of paclitaxel had to be found. In 1994, the groups of Robert Holton [128,129] and Kyriacos Nicolau [130], in a *tour de force* of total synthesis, published two total synthesis routes to paclitaxel. However, these included ~40 steps each, with an overall yield of <2%. Total synthesis was definitely not an economically viable option.

Instead, Bristol-Myers Squibb (BMS) together with Holton developed a semisynthetic route to paclitaxel, starting from the naturally occurring 10-deacetylbaccatin (10-DAB; see Figure 5.25). 10-DAB already contains the eight chiral centers of the paclitaxel molecule, and can be isolated easily from leaves and twigs of the

**Figure 5.25** Simplified schematic representation of the semisynthetic and biosynthetic pathways for producing paclitaxel.

European yew, without harming the trees. The supply of the starting material was thus ensured, and in 1998 Taxol became one of the world's most profitable drugs, with a yearly turnover of over 1.5 billion euros. However, the semisynthetic process was still complex and wasteful, including 11 chemical steps and 13 different solvents. BMS then switched from chemical synthesis to plant-cell fermentation technology. In the cell fermentation stage, calluses of a specific taxus cell line are propagated in water in large fermentation tanks, at ambient temperature and pressure. The cells are fed on sugars, amino acids, vitamins, and trace elements. The paclitaxel is extracted directly from the cell cultures, purified, and crystallized. Compared to the semisynthesis from 10-DAB, the fermentation process is done *in situ* in an aqueous "soup," thus eliminating ten solvents and six drying steps. In 2004, this process was awarded the US Presidential Green Chemistry Challenge Award.

5.5.4

The Tosoh/DSM Aspartame Process

Aspartyl phenylalanine-1-methyl ester, better known as aspartame, is an artificial sweetener with a worldwide production exceeding 15 000 tpa. It is marketed under the trade names Nutrasweet, Canderel, and Equal. This dipeptide, made of aspartic

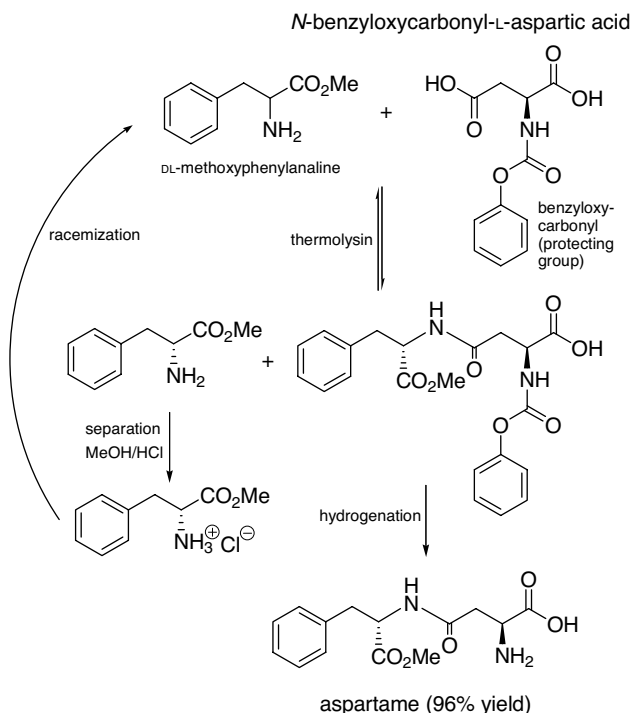


Figure 5.26 The Tosoh/DSM chemoenzymatic route to aspartame.

acid and phenylalanine, is ~ 200 times sweeter than sugar. The Holland Sweetener Company, a joint venture of Toya Soda and DSM, manufactures aspartame by a chemoenzymatic route [131], using a thermolysin enzyme [132] to couple the two amino acids, followed by precipitation and catalytic hydrogenation (Figure 5.26). Maintaining the stereospecificity is crucial, since the L configuration of the two amino acids is responsible for the sweet taste. This reaction, incidentally, can also be performed easily in a student laboratory on a smaller scale [133].

5.6 Exercises

1. Describe in your own words the advantages and disadvantages of using whole cells compared to isolated enzymes as biocatalysts, with respect to catalyst immobilization, catalyst recovery, ease of use, and product selectivity and purification.
2. Search the BRENDA database and find information on the enzymes EC 1.13.12.14, azobenzene reductase, and nitrogenase. What reactions do those enzymes catalyze? What are their optimum pH and temperature operating ranges? And what are their typical TOFs?
3. Propene oxide and C_4 epoxides are the key building blocks of the polymer industry. They are produced worldwide by alkene epoxidation. The problem is that the alkenes react with O_2 to give several side products, so good selectivities are attained only at low conversions ($<5\%$). Figure 5.27 shows an alternative pathway which

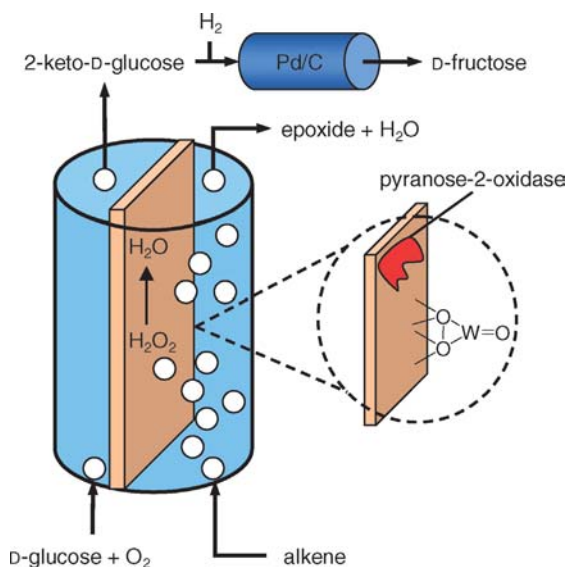


Figure 5.27 Simplified schematic of the dual epoxidation/glucose conversion process, with *in situ* H_2O_2 regeneration.

uses O_2 , alkene, and D-glucose as raw materials and produces epoxide and D-fructose as end-products. The process combines two catalytic cycles in a special membrane reactor. In the first cycle, H_2O_2 is generated *in situ* using the enzyme pyranose 2-oxidase. In the second, the alkene reacts with the H_2O_2 in the presence of a supported polyoxometallate epoxidation catalyst. The 2-keto-D-glucose is then hydrogenated to D-fructose in a separate reactor.

- Draw the two catalytic cycles, indicating the various elementary steps and catalytic intermediates.
 - Compare the advantages and disadvantages of this combined process to those of two separate processes for obtaining the two products. What are the main challenges in combining the enzymatic and nonenzymatic reactions in one reactor?
 - Search the Internet for information on pyranose 2-oxidase (E.C. 1.1.3.10). Is this enzyme commercially available? Would it function under the required reaction conditions? If not, how would you modify it?
4. Different enzymes often operate under similar conditions, enabling two or more enzymes to be combined in one pot. In the example shown in Figure 5.28, dihydroxyacetone is phosphorylated and then coupled to an aldehyde, resulting in a C–C coupled product with two new stereocenters. Wever and co-workers carried out this reaction by combining two isolated enzymes: an acid phosphatase and a

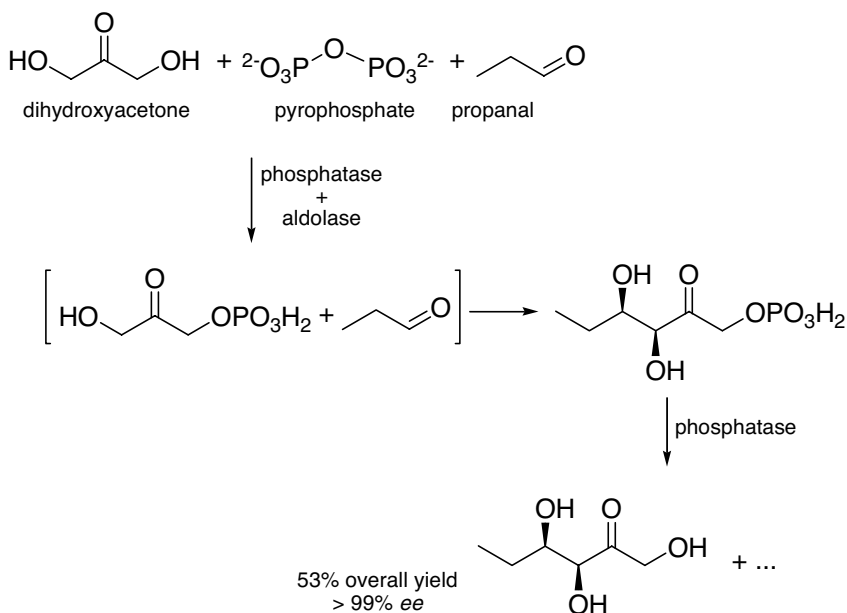


Figure 5.28 One-pot dual-enzyme cascade, starting from dihydroxyacetone and propionaldehyde (propanal), with *in situ* phosphorylation and dephosphorylation steps.

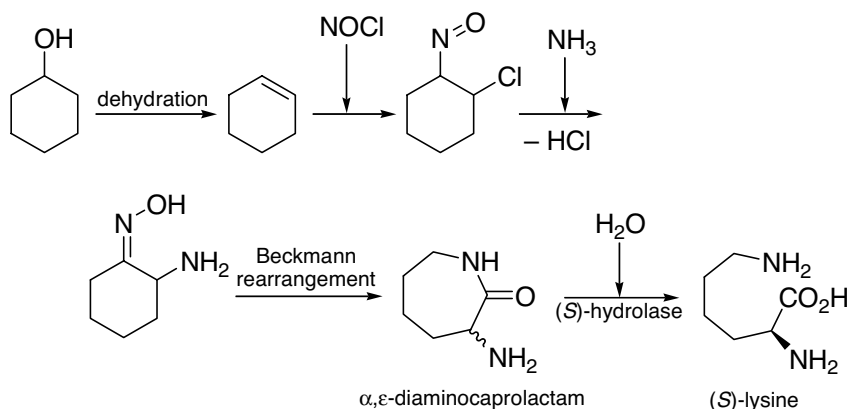


Figure 5.29 Chemoenzymatic route to (*S*)-lysine, starting from cyclohexanol.

rabbit muscle aldolase. Importantly, they used simple pyrophosphate, a cheap and readily available phosphate donor [134].

- (a) Complete the stoichiometry of the reaction shown in Figure 5.28 and calculate the atom economy, *E*-factor, and *Q*-value for the overall process.
 - (b) What are the pros and cons of using isolated enzymes in this case instead of whole cells? (List at least two advantages and two disadvantages.)
 - (c) Draw an alternative chemical (i.e., non-enzymatic) synthetic route from the starting materials to the product. What are the advantages and disadvantages of your route compared to the one-pot enzymatic procedure?
5. In the high-fructose corn syrup (HFCS) process, the enzyme glucose isomerase is typically immobilized by anchoring on silica. Suggest three other immobilization methods for this enzyme which may increase its thermal stability. Considering that the HFCS process already runs on a very large scale, what are the main conditions that your new catalyst must fulfill to replace the existing process?
 6. The four-step synthesis of α,ϵ -diaminocaprolactam shown in Figure 5.29 is part of a chemoenzymatic route to (*S*)-lysine, an essential amino acid in our diet [135]. The racemic caprolactam (azepan-2-one) product is then hydrolyzed selectively to (*S*)-lysine, using an immobilized (*S*)-hydrolase enzyme.
 - (a) What is the maximum yield of (*S*)-lysine that can be obtained by this hydrolysis route?
 - (b) Suggest a method using an additional enzyme (or another catalyst) for increasing the yield of (*S*)-lysine. What is the maximum yield using your new route?
 - (c) Today, (*S*)-lysine is produced by fermentation in mutant *Corynebacterium glutamicum* cells, starting from molasses, oxygen and ammonia. What are the advantages of the fermentation route over the chemoenzymatic one?

References

- 1 Truesdell, S. (2005) Biotransformations for a green future. *Chem. Eng. Prog.*, **101**, 44.
- 2 Hinnemann, B. and Nørskov, J.K. (2006) Catalysis by enzymes: the biological ammonia synthesis. *Top. Catal.*, **37**, 55.
- 3 Rothenberg, G. and Clark, J.H. (2000) Vanadium-catalyzed oxidative bromination using dilute mineral acids and hydrogen peroxide: an option for recycling waste acid streams. *Org. Process Res. Dev.*, **4**, 270.
- 4 Wandrey, C., Liese, A. and Kihumbu, D. (2000) Industrial biocatalysis: past, present, and future. *Org. Process Res. Dev.*, **4**, 286.
- 5 Straathof, A.J.J., Panke, S. and Schmid, A. (2002) The production of fine chemicals by biotransformations. *Curr. Opin. Biotechnol.*, **13**, 548.
- 6 Bugg, T. (1997) *An Introduction to Enzyme and Coenzyme Chemistry*, Blackwell Science, Oxford, ISBN 0-86542-793-3.
- 7 Berg, J.M., Tymoczko, J.L. and Stryer, L. (2002) *Biochemistry*, 5th edn. W.H. Freeman, New York, ISBN 0-7167-4684-0.
- 8 Voet, D., Voet, J.G. and Pratt, C.W. (2005) *Fundamentals of Biochemistry: Life at the Molecular Level*, Wiley, New York, ISBN 0-471-21495-3.
- 9 Bommarius, A.S. and Riebel, B. (2004) *Biocatalysis: Fundamentals and Applications*, Wiley-VCH, Weinheim, ISBN 3-527-30344-8.
- 10 Cohen, J. (1995) Getting all turned around over the origins of life on Earth. *Science*, **267**, 1265.
- 11 Bada, J.L. (1995) Origins of homochirality. *Nature*, **374**, 594.
- 12 Friedman, M. (1999) Chemistry, nutrition, and microbiology of D-amino acids. *J. Agric. Food Chem.*, **47**, 3457.
- 13 Fujii, N. (2002) D-Amino acids in living higher organisms. *Origins Life Evolution Bios.*, **32**, 103.
- 14 Weise C. (2003) BRENDA: everything you always wanted to know about enzymes. *Angew. Chem. Int. Ed.*, **42**, 5666.
- 15 Barthelmes, J., Ebeling, C., Chang, A., Schomburg, I. and Schomburg, D. (2007) BRENDA, AMENDA and FRENDA: The enzyme information system in 2007. *Nucl. Acids Res.*, **35**, D511.
- 16 Liu, W. and Wang, P. (2007) Cofactor regeneration for sustainable enzymatic biosynthesis. *Biotechnol. Adv.*, **25**, 369.
- 17 Lemieux, R.U. and Spohr, U. (1994) How Emil Fischer was led to the lock and key concept for enzyme specificity. *Adv. Carbohydr. Chem. Biochem.*, **50**, 1.
- 18 Thoma, J.A. and Koshland, D.E. Jr. (1960) Stereochemistry of enzyme, substrate, and products during β -amylase action. *J. Biol. Chem.*, **235**, 2511.
- 19 Koshland, D.E. Jr. (1994) The lock-and-key principle and the induced-fit theory. *Angew. Chem. Int. Ed. Engl.*, **33**, 2475.
- 20 Jencks, W.P. (1993) Destabilization is as important as binding. *Phil. Trans. Roy. Soc., Ser. A: Math., Phys. Eng.*, **345**, 3.
- 21 Simopoulos, T.T. and Jencks, W.P. (1994) Alkaline phosphatase is an almost perfect enzyme. *Biochemistry*, **33** (10), 375.
- 22 Jencks, W.P. (1975) Binding energy, specificity, and enzymic catalysis: the Circe effect. *Adv. Enzymol.*, **43**, 219.
- 23 Toney, M.D. and Kirsch, J.F. (1993) Lysine 258 in aspartate aminotransferase: enforcer of the Circe effect for amino acid substrates and the general-base catalyst for the 1,3-prototropic shift. *Biochemistry*, **32**, 1471.
- 24 Warshel, A., Florian, J., Strajbl, M. and Villa, J. (2001) Circe effect versus enzyme preorganization: what can be learned from the structure of the most proficient enzyme? *ChemBioChem*, **2**, 109.
- 25 Cannon, W.R. and Benkovic, S.J. (1998) Solvation, reorganization energy, and biological catalysis. *J. Biol. Chem.*, **273**, 26, 257.

- 26 Kraut Daniel, A., Carroll Kate, S. and Herschlag, D. (2003) Challenges in enzyme mechanism and energetics. *Annu. Rev. Biochem.*, **72**, 517.
- 27 Kokesh, F.C. and Westheimer, F.H. (1971) Reporter group at the active site of acetoacetate decarboxylase. II. Ionization constant of the amino group. *J. Am. Chem. Soc.*, **93**, 7270.
- 28 Highbarger, L.A., Gerlt, J.A. and Kenyon, G.L. (1996) Mechanism of the reaction catalyzed by acetoacetate decarboxylase. Importance of lysine 116 in determining the pK_a of active-site lysine 115. *Biochemistry*, **35**, 41.
- 29 Kresge, A.J. (1997) Electrostatic effects on acid dissociation constants. Importance of lysine 116 in determining the pK_a of lysine 115 in the active site of acetoacetate decarboxylase. *Chemtracts*, **10**, 27.
- 30 Hasan, Z., Renirie, R., Kerkman, R., Ruijssenaars, H.J., Hartog, A.F. and Wever, R. (2006) Laboratory-evolved vanadium chloroperoxidase Exhibits 100-fold higher halogenating activity at alkaline pH: catalytic effects from first and second coordination sphere mutations. *J. Biol. Chem.*, **281**, 9738.
- 31 Messerschmidt, A., Prade, L. and Wever, R. (1997) Implications for the catalytic mechanism of the vanadium-containing enzyme chloroperoxidase from the fungus *Curvularia inaequalis* by X-ray structures of the native and peroxide form. *Biol. Chem.*, **378**, 309.
- 32 Wasserscheid P. and Keim W. (2000) Ionic liquids – new “solutions” for transition metal catalysis. *Angew. Chem. Int. Ed.*, **39**, 3772.
- 33 Earle, M.J., Seddon, K.R., Adams, C.J. and Roberts, G. (1998) Friedel–Crafts reactions in room temperature ionic liquids. *Chem. Commun.*, 2097.
- 34 Storer, A.C. and Menard, R. (1994) Catalytic mechanism in papain family of cysteine peptidases. *Meth. Enzymol.*, **244**, 486.
- 35 Uhlig, H. (1998) *Industrial Enzymes and their Applications*, Wiley, New York, ISBN 0-471-19660-6.
- 36 Schmid, A., Dordick, J.S., Hauer, B., Kiener, A., Wubbolts, M. and Witholt, B. (2001) Industrial biocatalysis today and tomorrow. *Nature*, **409**, 258.
- 37 Coward-Kelly, G. and Chen, R.R. (2007) A window into biocatalysis and biotransformations. *Biotechnol. Prog.*, **23**, 52.
- 38 Kirk, O., Borchert, T.V. and Fuglsang, C.C. (2002) Industrial enzyme applications. *Curr. Opin. Biotechnol.*, **13**, 345.
- 39 Bornscheuer, U.T. and Buchholz, K. (2005) Highlights in biocatalysis – historical landmarks and current trends. *Eng. Life Sci.*, **5**, 309.
- 40 Anon. (2005) Novozymes 2004: industrial and technical enzymes. *Focus on Catalysts*, **2005** 3.
- 41 Values are based on the fixed Euro:DKR exchange rate, 2006 data taken from the Novozymes stock report.
- 42 Chaparro-Riggers, J.F., Rogers, T.A., Vazquez-Figueroa, E., Polizzi, K.M. and Bommaris, A.S. (2007) Comparison of three enoate reductases and their potential use for biotransformations. *Adv. Synth. Catal.*, **349**, 1521.
- 43 Stampfer W., Kosjek B., Moitzi C., Kroutil W. and Faber K. (2002) Biocatalytic asymmetric hydrogen transfer. *Angew. Chem. Int. Ed.*, **41**, 1014
- 44 Chartrain, M., Salmon, P.M., Robinson, D.K. and Buckland, B.C. (2000) Metabolic engineering and directed evolution for the production of pharmaceuticals. *Curr. Opin. Biotechnol.*, **11**, 209.
- 45 Niu, W., Draths, K.M. and Frost, J.W. (2002) Benzene-free synthesis of adipic acid. *Biotechnol. Prog.*, **18**, 201.
- 46 Ran, N.Q., Knop, D.R., Draths, K.M. and Frost, J.W. (2001) Benzene-free synthesis of hydroquinone. *J. Am. Chem. Soc.*, **123**, 10927.
- 47 Berry, A., Dodge, T.C., Pepsin, M. and Weyler, W. (2002) Application of metabolic engineering to improve both the production and use of biotech indigo. *J. Ind. Microbiol. Biotechnol.*, **28**, 127.
- 48 Rios, G.M., Belleville, M.P., Paolucci, D. and Sanchez, J. (2004) Progress in

- enzymatic membrane reactors – a review. *J. Membr. Sci.*, **242**, 189.
- 49 Giorno, L. and Drioli, E. (2000) Biocatalytic membrane reactors: applications and perspectives. *Trends Biotechnol.*, **18**, 339.
- 50 Castro, G.R. and Knubovets, T. (2003) Homogeneous biocatalysis in organic solvents and water–organic mixtures. *Crit. Rev. Biotechnol.*, **23**, 195.
- 51 Sheldon, R.A. (2007) Enzyme immobilization: the quest for optimum performance. *Adv. Synth. Catal.*, **349**, 1289.
- 52 Lilly, M.D. (1976) Enzymes immobilized to cellulose. *Meth. Enzymol.*, **44**, 46.
- 53 Muzzarelli, R.A.A. (1980) Immobilization of enzymes on chitin and chitosan. *Enz. Microb. Technol.*, **2**, 177.
- 54 Krajewska, B. (2004) Application of chitin- and chitosan-based materials for enzyme immobilizations: a review. *Enz. Microb. Technol.*, **35**, 126.
- 55 Kallenberg, A.I., van Rantwijk, F. and Sheldon, R.A. (2005) Immobilization of penicillin G acylase: the key to optimum performance. *Adv. Synth. Catal.*, **347**, 905.
- 56 Katchalski-Katzir, E., Kraemer, D.M. and Eupergit, C. (2000) a carrier for immobilization of enzymes of industrial potential. *J. Mol. Catal. B: Enzymatic*, **10**, 157.
- 57 Galaev, I.Y. and Mattiasson, B. (1999) “Smart” polymers and what they could do in biotechnology and medicine. *Trends Biotechnol.*, **17**, 335.
- 58 Jeong, B. and Gutowska, A. (2002) Lessons from nature: stimuli-responsive polymers and their biomedical applications. *Trends Biotechnol.*, **20**, 305.
- 59 Ivanov, A.E., Edink, E., Kumar, A., Galaev, I.Y., Arendsen, A.F., Bruggink, A. and Mattiasson, B. (2003) Conjugation of penicillin acylase with the reactive copolymer of *N*-isopropylacrylamide: a step toward a thermosensitive industrial biocatalyst. *Biotechnol. Prog.*, **19**, 1167.
- 60 Kirstein, D. (1996) Chelate mediated immobilization of proteins. *Adv. Mol. Cell Biol.*, **15A**, 247.
- 61 Svec, F. (2006) Less common applications of monoliths: I. Microscale protein mapping with proteolytic enzymes immobilized on monolithic supports. *Electrophoresis*, **27**, 947.
- 62 Kim, J., Grate, J.W., Wang, P. (2005) Nanostructures for enzyme stabilization. *Chem. Eng. Sci.*, **61**, 1017.
- 63 Kirk, O. and Christensen, M.W. (2002) Lipases from *Candida antarctica*: unique biocatalysts from a unique origin. *Org. Proc. Res. Dev.*, **6**, 446.
- 64 Petri, A., Marconcini, P. and Salvadori, P. (2005) Efficient immobilization of epoxide hydrolase onto silica gel and use in the enantioselective hydrolysis of racemic *para*-nitrostyrene oxide. *J. Mol. Catal. B: Enzymatic*, **32**, 219.
- 65 Braun, S., Rappoport, S., Zusman, R., Avnir, D. and Ottolenghi, M. (1990) Biochemically active sol–gel glasses: the trapping of enzymes. *Mater. Lett.*, **10**, 1.
- 66 Avnir, D. (1995) Organic chemistry within ceramic matrixes: doped sol-gel materials. *Acc. Chem. Res.*, **28**, 328.
- 67 Reetz, M.T., Tielmann, P., Wiesenhofer, W., Koenen, W. and Zonta, A. (2003) Second generation sol-gel encapsulated lipases: robust heterogeneous biocatalysts. *Adv. Synth. Catal.*, **345**, 717.
- 68 Quiocho, F.A. and Richards, F.M. (1964) Intermolecular cross linking of a protein in the crystalline state: carboxypeptidase A. *Proc. Natl. Acad. Sci. USA*, **52**, 833.
- 69 Navia, M.A. and Clair, N.L. (1993) US Patent 561,8710 (to Vertex Pharmaceuticals, Inc.).
- 70 Lalonde, J. (1997) Practical catalysis with enzyme crystals. *Chemtech*, **27**, 38.
- 71 Zelinski, T. and Waldmann, H. (1997) Crosslinked enzyme crystals (CLECs): efficient and stable biocatalysts for preparative organic chemistry. *Angew. Chem. Int. Ed. Engl.*, **36**, 722.
- 72 Cao, L., van Rantwijk, F. and Sheldon, R.A. (2000) Cross-linked enzyme aggregates: a simple and effective method for the immobilization of penicillin acylase. *Org. Lett.*, **2**, 1361.

- 73 Sheldon, R.A., Schoevaart, R. and van Langen, L.M. (2006) Cross-linked enzyme aggregates. *Meth. Biotechnol.*, **22**, 31.
- 74 Chmura, A., van der Kraan, G.M., Kielar, F., van Langen, L.M., van Rantwijk, F. and Sheldon, R.A. (2006) Cross-linked aggregates of the hydroxynitrile lyase from *Manihot esculenta*: highly active and robust biocatalysts. *Adv. Synth. Catal.*, **348**, 1655.
- 75 Toral, A.R., de los Rios, A.P., Hernandez, F.J., Janssen, M.H.A., Schoevaart, R., van Rantwijk, F. and Sheldon, R.A. (2007) Cross-linked *Candida antarctica* lipase B is active in denaturing ionic liquids. *Enz. Microb. Technol.*, **40**, 1095.
- 76 Sheldon, R.A., Sorgedragger, M.J. and Janssen, M.H.A. (2007) Use of cross-linked enzyme aggregates (CLEAs) for performing biotransformations. *Chim. Oggi — Chemistry Today*, **25**, 62.
- 77 Frost, J.W. and Draths, K.M. (1995) Biocatalytic syntheses of aromatics from D-glucose: renewable microbial sources of aromatic compounds. *Annu. Rev. Microbiol.*, **49**, 557.
- 78 van de Sandt, E.J.A.X. and de Vroom, E. (2000) Innovations in cephalosporin and penicillin production: painting the antibiotics industry green. *Chim. Oggi*, **18**, 72.
- 79 Kagan, H.B. and Fiaud, J.C. (1988) Kinetic resolution. *Top. Stereochem.*, **18**, 249.
- 80 Um, P.-J. and Drucekhammer, D.G. (1998) Dynamic enzymic resolution of thioesters. *J. Am. Chem. Soc.*, **120**, 5605.
- 81 Martin-Matute, B. and Bäckvall, J.-E. (2007) Dynamic kinetic resolution catalyzed by enzymes and metals. *Curr. Opin. Chem. Biol.*, **11**, 226.
- 82 Pellissier, H. (2003) Dynamic kinetic resolution. *Tetrahedron*, **59**, 8291.
- 83 Persson, B.A., Larsson, A.L.E., Le Ray, M. and Bäckvall, J.-E. (1999) Ruthenium- and enzyme-catalyzed dynamic kinetic resolution of secondary alcohols. *J. Am. Chem. Soc.*, **121**, 1645.
- 84 Crawford, J.B., Skerlj, R.T. and Bridger, G.J. (2007) Spontaneous enzymatically mediated dynamic kinetic resolution of 8-amino-5,6,7,8-tetrahydroquinoline. *J. Org. Chem.*, **72**, 669.
- 85 Panova, A., Mersinger, L.J., Liu, Q., Foo, T., Roe, D.C., Spillan, W.L., Sigmund, A.E., Ben-Bassat, A., Wagner, L.W., O'Keefe, D.P., Wu, S., Petrillo, K.L., Payne, M.S., Breske, S.T., Gallagher, F.G. and DiCosimo, R. (2007) Chemoenzymatic synthesis of glycolic acid. *Adv. Synth. Catal.*, **349**, 1462.
- 86 Ballard, D.G.H., Courtis, A., Shirley, I.M., Taylor, S.C. (1983) A biotech route to polyphenylene. *J. Chem. Soc., Chem. Commun.*, 954.
- 87 Sylvestre, J., Chautard, H., Cedrone, F. and Delcourt, M. (2006) Directed evolution of biocatalysts. *Org. Process Res. Dev.*, **10**, 562.
- 88 Woodyer, R., Chen, W. and Zhao, H. (2004) Outrunning nature: directed evolution of superior biocatalysts. *J. Chem. Educ.*, **81**, 126.
- 89 Dalboge, H. and Lange, L. (1998) Using molecular techniques to identify new microbial biocatalysts. *Trends Biotechnol.*, **16**, 265.
- 90 Gavaghan, H. (2000) Companies of all sizes are prospecting for proteins. *Nature*, **404**, 684.
- 91 Jones, B.E., Grant, W.D., Duckworth, A.W. and Owenson, G.G. (1998) Microbial diversity of soda lakes. *Extremophiles*, **2**, 191.
- 92 Watanabe, Y. (2002) Construction of heme enzymes: four approaches. *Curr. Opin. Chem. Biol.*, **6**, 208.
- 93 Prieur, D. (1997) Microbiology of deep-sea hydrothermal vents. *Trends Biotechnol.*, **15**, 242.
- 94 Harayama, S. (1998) Artificial evolution by DNA shuffling. *Trends Biotechnol.*, **16**, 76.
- 95 Muller, H.J. (1964) The relation of recombination to mutational advance. *Mutat. Res.*, **106**, 2.
- 96 Stemmer, W.P.C. (1994) Rapid evolution of a protein *in vitro* by DNA shuffling. *Nature*, **370**, 389.

- 97 Petrounia, I.P. and Arnold, F.H. (2000) Designed evolution of enzymatic properties. *Curr. Opin. Biotechnol.*, **11**, 325.
- 98 Liebeton, K., Zonta, A., Schimossek, K., Nardini, M., Lang, D., Dijkstra, B.W., Reetz, M.T. and Jaeger, K.-E. (2000) Directed evolution of an enantioselective lipase. *Chem. Biol.*, **7**, 709.
- 99 May, O., Nguyen, P.T., Arnold, F.H. (2000) Inverting enantioselectivity by directed evolution of hydantoinase for improved production of L-methionine. *Nature Biotechnol.*, **18**, 317.
- 100 Salazar, O., Cirino, P.C., Arnold, F.H. (2003) Thermostabilization of a cytochrome P450 peroxxygenase. *ChemBioChem*, **4**, 891.
- 101 Sakurai, A. and Sakakibara, M. (2005) Waste treatment using enzymes – a review. *Curr. Top. Biotechnol.*, **2**, 1.
- 102 Whiteley, C.G. and Lee, D.J. (2006) Enzyme technology and biological remediation. *Enz. Microb. Technol.*, **38**, 291.
- 103 Hibbert, E.G. and Dalby, P.A. (2005) Directed evolution strategies for improved enzymatic performance. *Microb. Cell Fact.*, **4**, 29.
- 104 Schultz, P.G. (1988) The interplay between chemistry and biology in the design of enzymatic catalysts. *Science*, **240**, 426.
- 105 Pollack, S.J., Jacobs, J.W. and Schultz, P.G. (1986) Selective chemical catalysis by an antibody. *Science*, **234**, 1570.
- 106 Tramontano, A., Janda, K.D. and Lerner, R.A. (1986) Catalytic antibodies. *Science*, **234**, 1566.
- 107 Stewart, J.D., Liotta, L.J. and Benkovic, S.J. (1993) Reaction mechanisms displayed by catalytic antibodies. *Acc. Chem. Res.*, **26**, 396.
- 108 Janda, K.D., Shevlin, C.G. and Lerner, R.A. (1993) Antibody catalysis of a disfavored chemical transformation. *Science*, **259**, 490.
- 109 Hilvert, D. (1993) Antibody catalysis of carbon–carbon bond formation and cleavage. *Acc. Chem. Res.*, **26**, 552.
- 110 Zhou, Z.S., Flohr, A. and Hilvert, D. (1999) An antibody-catalyzed allylic sulfoxide–sulfenate rearrangement. *J. Org. Chem.*, **64**, 8334.
- 111 Keinan E. (2005) *Catalytic Antibodies*, Wiley-VCH, Weinheim, ISBN 3-527-30688-9.
- 112 Hanson Carl, V., Nishiyama, Y. and Paul, S. (2005) Catalytic antibodies and their applications. *Curr. Opin. Biotechnol.*, **16**, 631.
- 113 Martin, M.T. (1996) Commercially valuable catalytic antibodies: The life to come. *Drug Discov. Today*, **1**, 239.
- 114 Landry, D.W., Zhao, K., Yang, G.X., Glickman, M. and Georgiadis, T.M. (1993) Antibody-catalyzed degradation of cocaine. *Science*, **259**, 1899.
- 115 Landry, D.W. (1997) Immunotherapy for cocaine addiction. *Sci. Am.*, **276**, 42.
- 116 Deng, S.X., de Prada, P. and Landry, D.W. (2002) Anticocaine catalytic antibodies. *J. Immunol. Meth.*, **269**, 299.
- 117 Mets, B., Winger, G., Cabrera, C., Seo, S., Jamdar, S., Yang, G., Zhao, K., Briscoe, R.J., Almonte, R., Woods, J.H. and Landry, D.W. (1998) A catalytic antibody against cocaine prevents cocaine's reinforcing and toxic effects in rats. *Proc. Natl. Acad. Sci. USA*, **95**, 10, 176.
- 118 Orgel, L.E. (1994) The origin of life on the earth. *Sci. Am.*, **271**, 76.
- 119 Guerrier-Takada, C., Gardiner, K., Marsh, T., Pace, N. and Altman, S. (1983) The RNA moiety of ribonuclease P is the catalytic subunit of the enzyme. *Cell*, **35**, 849.
- 120 Kruger, K., Grabowski, P.J., Zaug, A.J., Sands, J., Gottschling, D.E. and Cech, T.R. (1982) Self-splicing RNA: autoexcision and autocyclization of the ribosomal RNA intervening sequence of *Tetrahymena*. *Cell*, **31**, 147.
- 121 DeRose, V.J. (2002) Two decades of RNA catalysis. *Chem. Biol.*, **9**, 961.
- 122 Sun, L.Q., Cairns, M.J., Saravolac, E.G., Baker, A. and Gerlach, W.L. (2000)

- Catalytic nucleic acids: from lab to applications. *Pharmacol. Rev.*, **52**, 325.
- 123** Cech, T.R. (1993) Catalytic RNA: structure and mechanism. *Biochem. Soc. Trans.*, **21**, 229.
- 124** Nissen, P., Hansen, J., Ban, N., Moore, P.B. and Steitz, T.A. (2000) The structural basis of ribosome activity in peptide bond synthesis. *Science*, **289**, 920.
- 125** Muth, G.W., Ortoleva-Donnelly, L. and Strobel, S.A. (2000) A single adenosine with a neutral pK_a in the ribosomal peptidyl transferase center. *Science*, **289**, 947.
- 126** Yamada, H. and Kobayashi, M. (1996) Nitrile hydratase and its application to industrial production of acrylamide. *Biosci. Biotechnol. Biochem.*, **60**, 1391.
- 127** Yamada, H. and Nagasawa, T. (1990) Production of useful amides by enzymic hydration of nitriles. *Ann. N.Y. Acad. Sci.*, **613**, 142.
- 128** Holton, R.A., Somoza, C., Kim, H.B., Liang, F., Biediger, R.J., Boatman, P.D., Shindo, M., Smith, C.C., Kim, S., Nadizadeh, H., Suzuki, Y., Tao, C., Vu, P., Tang, S., Zhang, P., Murthi, K.K., Gentile, L.N. and Liu, J.H. (1994) First total synthesis of taxol. 1. Functionalization of the B ring. *J. Am. Chem. Soc.*, **116**, 1597.
- 129** Holton, R.A., Kim, H.B., Somoza, C., Liang, F., Biediger, R.J., Boatman, P.D., Shindo, M., Smith, C.C., Kim, S., Nadizadeh, H., Suzuki, Y., Tao, C., Vu, P., Tang, S., Zhang, P., Murthi, K.K., Gentile, L.N. and Liu, J.H. (1994) First total synthesis of taxol. 2. Completion of the C and D rings. *J. Am. Chem. Soc.*, **116**, 1599.
- 130** Nicolaou, K.C., Yang, Z., Liu, J.J., Ueno, H., Nantermet, P.G., Guy, R.K., Claiborne, C.F., Renaud, J., Couladouros, E.A., Paulvannan, K. and Sorensen, E.J. (1994) Total synthesis of taxol. *Nature*, **367**, 630.
- 131** Oyama, K., Irino, S., Harada, T. and Hagi, N. (1984) Enzymic production of aspartame. *Ann. N.Y. Acad. Sci.*, **434**, 95.
- 132** Oyama, K., Nishimura, S., Nonaka, Y., Kihara, K. and Hashimoto, T. (1981) Synthesis of an aspartame precursor by immobilized thermolysin in an organic solvent. *J. Org. Chem.*, **46**, 5241.
- 133** Lindeberg, G. (1987) A convenient synthesis of aspartame. *J. Chem. Educ.*, **64**, 1062.
- 134** van Herk, T., Hartog, A.F., Schoemaker, H.E. and Wever, R. (2006) Simple enzymatic *in situ* generation of dihydroxyacetone phosphate and its use in a cascade reaction for the production of carbohydrates: increased efficiency by phosphate cycling. *J. Org. Chem.*, **71**, 6244.
- 135** Ault, A. (2004) The monosodium glutamate story: The commercial production of MSG and other amino acids. *J. Chem. Educ.*, **81**, 347.

6

Computer Applications in Catalysis Research

Egyptian and Mayan hieroglyphs tell us that enzymes were applied in various manufacturing processes as early as 5000 years ago. Compared to this, the 50-odd years of computer simulations in catalysis research seem very short indeed. Nevertheless, computer modeling has changed our view of many catalytic processes. Initially developed as code-breaking machines during World War II, computers now play a key role in all types of scientific research, including all branches of catalysis. Computer models are used for testing hypotheses regarding catalytic cycles, visualizing catalysts and elementary steps, and optimizing catalytic processes in industry. The applications range wide, from solving ångström-scale bond lengths in catalyst crystal structures, all the way to predicting the performance of multi-cubic-meter reactive distillation columns. Note that some texts use the term “simulations” and some use “modeling”; depending on whom you ask, the two may or may not differ. In this book, both terms mean “work carried out using computers to help us solve problems in catalysis.”

- **CAUTION!** Books can have a hard time keeping up with advances in computer technology. For example, here is how the sixth edition of *Fundamentals of Analytical Chemistry* described Fourier-transform infrared spectrometers in 1992.

“Fourier-transform infrared spectrometers offer the advantages of unusually high sensitivity, resolution, and speed . . . offsetting these advantages is their high cost, because a moderately sophisticated dedicated computer is needed to decode the output data” [1]. (The “sophisticated computer” was a 33 MHz PC with 512 K of RAM, current market value ~\$2.)

6.1

Computers as Research Tools in Catalysis

Computer simulations are very much like experiments. Unless they are trivially simple, you cannot predict their results just from looking at the code. Moreover, if they are planned badly, or if they are programmed badly, they may either crash or yield meaningless numbers (the computer equivalent of brown goo). Just like

experiments, computer modeling is hardware-dependent, and yet, just as in experiments, you can sometimes obtain surprisingly nice results using relatively simple equipment. Importantly, computer models offer us no understanding, only numbers. We must examine the meaning and the worthiness of these numbers, always considering also the statistical errors involved. Too many scientists tend to accept the results of “successful” computer models at face value. The fact that a program did not crash does not mean that the results are meaningful!

That being said, computer models do feature several important advantages: First, you can simulate any experimental conditions, including reactions at extreme temperatures and pressures, which are difficult to set up in the laboratory. Fast reactions can be slowed down, and slow reactions can be speeded up. Moreover, you can easily change a single parameter in the model, thus observing the influence of this parameter on the reaction. Such simulations are essential in industrial process design, where any changes in the reactor configuration are very costly. Second, computer models can easily simulate the properties of new catalysts and materials, including ones that are difficult (or indeed impossible) to synthesize in the laboratory. Modeling the structure/activity relationships of such catalysts can save much synthetic effort. Simulations let us observe reactions and species that are inaccessible

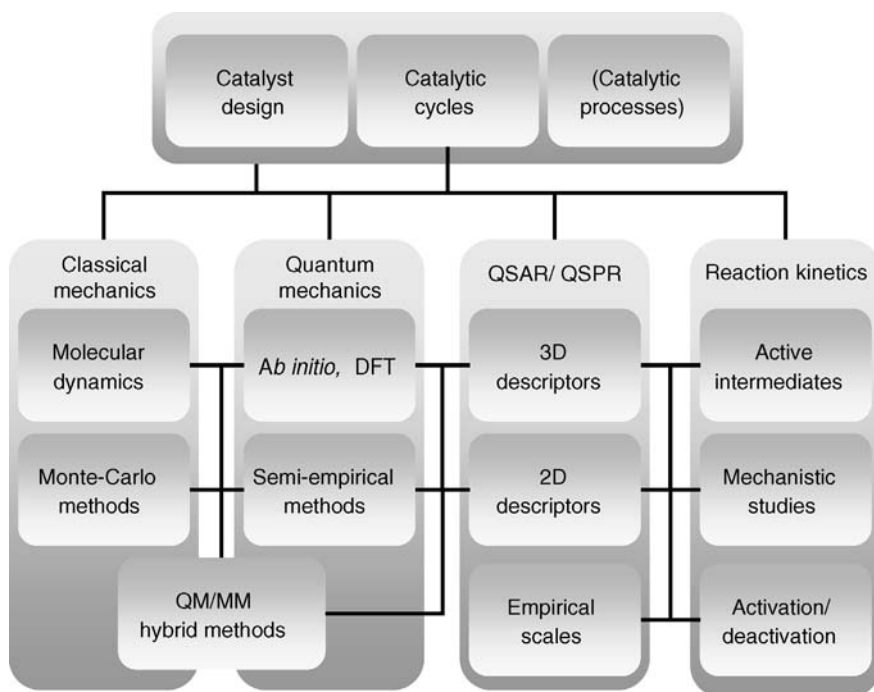


Figure 6.1 Computer applications in catalysis research range all the way from understanding the role of molecular active intermediates to large-scale process simulations.

by experiment, such as the transfer of single protons, and even the theoretical structures of the activated complexes that pertain to transition states. Finally, modeling is useful in interpreting results and testing theories, by fitting kinetic and thermodynamic equations to experimental (or indeed other computational) data.

Another important area where computers play an essential role is data analysis and **data mining**, particularly in analyzing large sets of reactions from combinatorial experiments. Statistical methods, such as principal component analysis (PCA), partial least squares (PLS), and artificial neural networks (ANNs), can highlight trends in large datasets. Knowing these trends, and the key parameters that govern them, often leads to a deeper understanding of the catalytic cycle. Data-mining models can even indicate regions in the “catalyst space” where “good catalysts” are likely to be found. This type of predictive modeling, coupled to the power of combinatorial synthesis and screening, puts us on the brink of true *in silico* catalyst design.

Figure 6.1 summarizes the key areas of computer applications in catalysis research. Note that this chapter does not cover reactor and process simulations, although of course these are performed using computers, and are essential for designing industrial catalytic processes. Textbooks on chemical engineering discuss these subjects in depth [2].

6.2 Modeling of Catalysts and Catalytic Cycles

6.2.1 A Short Overview of Modeling Methods

There are two main approaches to modeling chemical systems on the atom/molecule level: classical mechanics and quantum mechanics (QM) methods. As these subjects are covered in detail in many textbooks [3], I will give here only a short general overview. In classical mechanics simulations, the atoms or molecules are considered as particles, and the basic variables are the coordinates of the particles and their velocities. Parameterized potentials are then used for modeling the forces between these particles. Such models are often called **force field models**. Their main advantage is that the calculations are relatively simple and fast, allowing the modeling of very large systems (typically tens of thousands of particles). Force field methods are used in heterogeneous catalysis, for example, for calculating the structure and adsorption properties of porous supports [4] as well as the relative stability of oxide surfaces [5].

One classical mechanics simulation method is molecular dynamics (MD). Molecular dynamics solves the equations of motion. It models the system's evolution over time [6]. MD is deterministic: Starting from a given configuration at $t = \text{zero}$, and with a given model for the forces between the particles, the particles move according to Newton's equations. The computational cost of MD simulations depends on the system's size, the model's complexity, and the level of detail. For example, a propanol molecule can be treated on the atomic level (atomistic model) or as a chain of four spheres (coarse-grained model; see Figure 6.2).

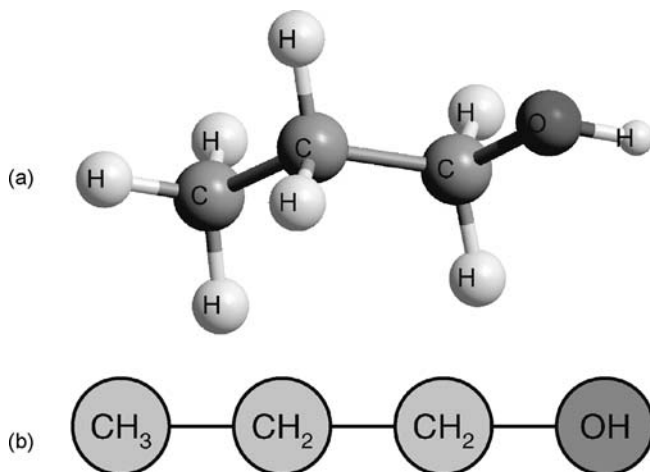


Figure 6.2 1-Propanol: **a** 3D atomistic representation; **b** simplified coarse-grained representation.

The Monte-Carlo (MC) method is an alternative approach. It generates an ensemble of particle configurations, with energies distributed according to the Boltzmann distribution, Eq. (6.1). In this equation, U is the potential energy of the system, $P(U)$ is the probability of finding a system with an energy U , k_B is Boltzmann's constant, and T is the absolute temperature. The configurations are generated by performing random particle **trial moves**, which are either accepted or rejected depending on their energy (the name “Monte-Carlo” reflects the stochastic nature of this method). Importantly, the configurations are not connected in time. This is the main difference between MC and MD. The advantage of MC is that, because time is not a factor, you can “speed up” or “slow down” the system. In this way, MC can simulate properties that are inaccessible with MD. However, lacking the concept of time, MC cannot give information on dynamic properties.

$$P(U) \propto e^{-\frac{U}{k_B T}} \quad (6.1)$$

The drawback of the classical mechanics approach is that it gives no information on the electronic structure of the system, and thus no information on chemical reactions. To simulate reactions, we must turn to quantum mechanics. Using QM we can obtain a full picture of the electronic and nuclear system, by solving the deceptively simple-looking Schrödinger equation (Eq. (6.2)), proposed by the Austrian physicist and 1933 Nobel laureate Erwin Schrödinger in 1926.

$$\mathbf{H}\Psi = E\Psi \quad (6.2)$$

In this equation, \mathbf{H} is the Hamiltonian operator, Ψ is the wavefunction that represents the state of the electrons and nuclei, and E is the system's energy. Although in theory it can be solved for any system, exact solutions are impracticable for anything more complicated than a hydrogen atom. Therefore we must find approximate

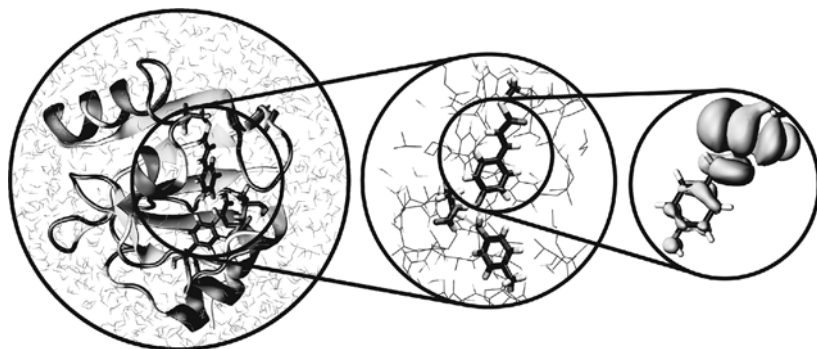


Figure 6.3 Three snapshots of MD and Car–Parrinello molecular dynamics simulations of the photoactive yellow protein, showing the entire protein (left), the “pocket” containing the chromophore (middle), and the chromophore itself (right). Thanks to Dr. Elske Leenders and Dr. Evert Jan Meijer for the simulation snapshots.

solutions, using for example the Born–Oppenheimer approximation, which decouples the energy contributions of the fast-moving electrons from those of the slow-moving nuclei. After the method has been chosen, the differential form of the Schrödinger equation is translated into matrix algebra form. This is done by rewriting the Hamiltonian as a matrix of basis functions (the so-called “basis set”), giving a set of equations that is suitable for solving by computer algorithms.

Two commonly used approximations are the **Hartree–Fock approach** and **density-functional theory** (DFT). The Hartree–Fock approach approximates the exact solution of the Schrödinger equation using a series of equations that describe the wavefunctions of each individual electron. If these equations are solved explicitly during the calculation, the method is known as *ab initio* Hartree–Fock. The less expensive (i.e., less time-consuming) semi-empirical methods use preselected parameters for some of the integrals. DFT, on the other hand, uses the electronic density as the basic quantity, instead of a many-body electronic wavefunction. The advantage of this is that the density is a function of only three variables (instead of $3N$ variables), and is simpler to deal with both in concept and in practice.

An interesting alternative that combines the advantages of both classical and quantum mechanics is to use hybrid QM/MM models, first introduced by Arieh Warshel for modeling enzymatic reactions [7]. Here, the chemical species at the active site are treated using high-level (and therefore expensive) QM models, which are coupled to a force field that describes the reaction environment. Hybrid models can thus take into account solvent effects in homogeneous catalysis, support structure and interface effects in heterogeneous catalysis, and enzyme structure effects in biocatalysis.

For example, Samuel French and co-workers used a combined QM/MM approach for modeling the catalyst/substrate interactions in the methanol synthesis process [8]. The annual worldwide production of methanol exceeds 32 M tons, most of which is

made from methane via syngas. A key step in this process is the catalytic hydrogenation of CO₂ and CO adsorbed on a Cu/ZnO/Al₂O₃ catalyst. Modeling the entire catalyst using *ab initio* QM methods is impractical. Instead, the researchers used a two-layer approach, based on embedded cluster methods. Short-range effects were modeled using (expensive) DFT calculations, while the long-range polarization effects of the surroundings were included using a classic potential shell.

Hybrid multiscale models enable us to focus on the relevant part of a system. For example, Leenders *et al.* studied the proton transfer process in the photoactive yellow protein (Figure 6.3) [9]. They used **Car–Parrinello molecular dynamics** [10], a QM method for dynamics simulations, to describe the chromophore and its hydrogen-bonded network in the protein pocket (middle and right-hand circles). This was combined with a traditional MD force field of 28 600 atoms, simulating the entire protein in water (left-hand circle).

6.2.2

Simplified Model Systems versus Real Reactions

A major challenge in designing computer experiments is choosing the model system. Liquid-phase catalytic reactions, for example, include catalyst precursors, solvents, various reagents, and substrates. Many of these reactions also involve heavy metals, which require special models for the d and f electron shells. Modeling such complex systems in detail is impractical. Instead, one must compromise and choose a smaller model system that (hopefully) mimics the real situation. One popular approach is studying the energetics of the reactants, catalyst, and products in the gas phase. Gas-phase systems are relatively simple, and can be modeled using high-level quantum mechanics. Such models can provide important information about the reaction, but there is a catch: catalytic performance often depends strongly on the reaction environment, and omitting this environment can lead to erroneous conclusions. Thus, the catalyst support plays a crucial role in heterogeneous catalysis, “innocent counterions” can make or break cycles in homogeneous catalysis [11], and enzymatic activity often depends on the entire protein, rather than on a few residues at the active site [12]. Simplified models are useful, but we should bear in mind their scope and limitations.

6.2.3

Modeling Large Catalyst Systems Using Classical Mechanics

Thanks to their speed and relatively low computational cost, MD and MC simulations can be used for studying the physical properties of large systems. This is extremely useful in heterogeneous catalysis, e.g., for modeling the structure and the properties of the bulk and the surface of a solid catalyst, or the properties of the bulk and interface of liquid/liquid biphasic systems. However, since the number of particles modeled is still very small compared to real materials, the models are susceptible to wall effects. One neat trick for avoiding this problem is to apply periodic boundary conditions: The volume containing the model is treated as the primitive cell of an

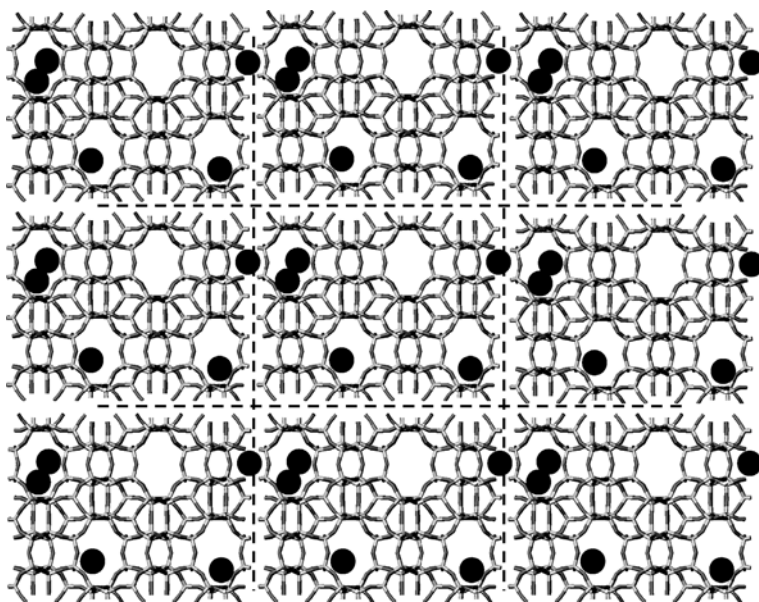


Figure 6.4 Simulated structure of the MFI-type zeolite Silicalite-1 (O atoms in dark gray and Si atoms light gray), projected on the bc plane and showing the zigzag channels. The broken lines indicate the periodic cell boundaries. Alkane molecules (not drawn to scale) are indicated by black circles. Thanks to Dr. Merijn Schenk for the zeolite picture.

infinite periodic lattice of identical cells. Particles that move “out” of their cell on one side are moved “back in” from the other side, just like in a Pac-Man game. Figure 6.4 shows the simulated structure of Silicalite-1, an MFI-type zeolite, with alkane molecules adsorbed in the zeolite channels. Such zeolites are widely used in the petrochemical industry for increasing the gasoline octane number by selective cracking of linear alkanes [13,14].

A good example where MC simulations have been used for understanding microscopic effects in heterogeneous catalysis is the so-called **window effect** – one of the most controversial phenomena in zeolite catalysis. Most zeolite-catalyzed hydrocracking processes result in a product distribution with a single maximum. However, in the late 1960s, Chen *et al.* discovered that some zeolites yield a bimodal product distribution: two maxima at n -C_{3–4} and n -C_{10–12}, but no product in the C_{7–9} “window” (Figure 6.5a) [15]. This is important, as it gives the possibility of obtaining tunable length-selective hydrocracking by choosing the right zeolite catalyst. However, although the window effect was neatly explained using the relative diffusion rates of alkanes in the zeolites [16], recent measurements failed to reproduce these diffusion parameters [17]. In 2003, Dubbeldam and co-workers, using molecular simulations, showed that the window effect indeed exists, and that diffusion rates can increase by orders of magnitude when the alkane is “too big” for the zeolite

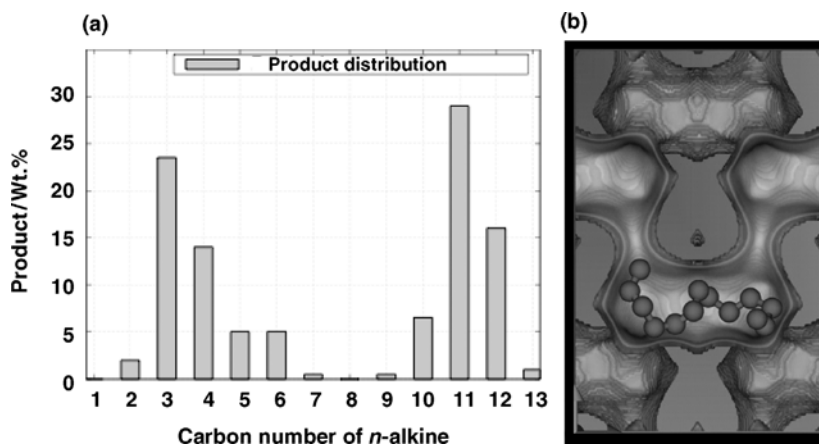


Figure 6.5 a Product distribution for hydrocracking catalyzed by an ERI-type zeolite, showing the “window effect” observed by Chen *et al.*; b simulation of *n*-C₁₃ in an ERI cage (window size = 0.36 nm × 0.51 nm). Thanks to Dr. David Dubbeldam for the zeolite simulation snapshot.

cage (Figure 6.5b) [18]. Moreover, the simulations revealed an alternative cracking mechanism, due to abnormally low adsorption for alkane chains similar in size or larger than the cages [19]. Long alkanes adsorb partially into a cage near the outer surface. After scission, the nonadsorbed part can diffuse out as product, or be adsorbed and undergo another scission. This mechanism is characteristic for cage/window-type zeolites with small windows close to the diameter of the adsorbate [20].

6.2.4

In-Depth Reaction Modeling Using Quantum Mechanics

QM algorithms can calculate the geometries and energies of reactants and products, as well as transition structures. This makes them useful tools for solving and visualizing energy/reaction coordinate diagrams in catalytic cycles. Olefin insertion into metal–alkyl bonds, for example, is a key elementary step in polymerization. Understanding how this insertion works is vital for making better catalysts for the multibillion-dollar polymer industry. According to the mechanism proposed by Cossee and Arlman in 1964 [21,22], the propagation step in olefin polymerization catalyzed by early transition metals occurs via a prior π -coordination to a vacant site on the complex. This is followed by olefin insertion through a four-center transition state in a $2\pi + 2\sigma$ reaction, involving the C–C π bond and the metal–alkyl σ bond (Figure 6.6a). In the case of ethene insertion, QM models also showed that agostic interactions are crucial in the polymer propagation step, as they provide extra stabilization and thereby lower the insertion barrier [23]. Examining the energy/reaction coordinate diagram (Figure 6.6b), we see that the models predict that the ethene association step is exothermic. The insertion of the ethene from the π complex into the agostic complex is also exothermic, but with a low barrier.

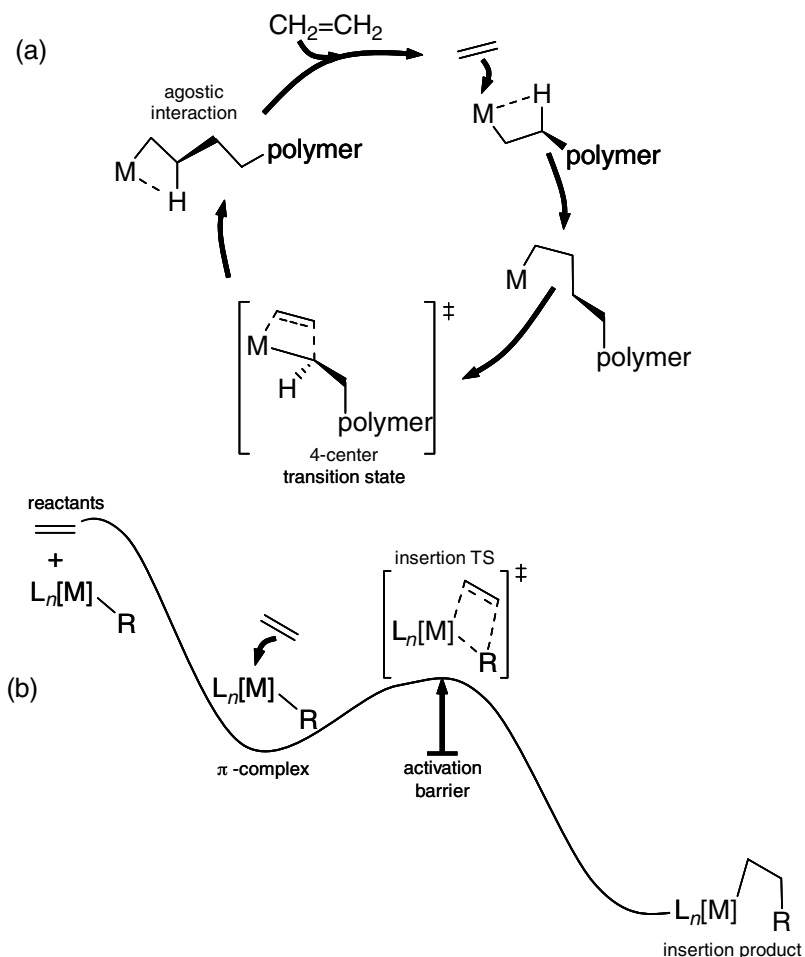


Figure 6.6 **a** Propagation cycle in the synthesis of polyethylene according to the Cossee mechanism; **b** calculated energy/reaction coordinate diagram for the ethene insertion step.

QM models of transition structures give the values of ΔH^\ddagger and ΔS^\ddagger , enabling a comparison between different reaction pathways. For example, homogeneous palladium chloride catalyzes the oxidation of alcohols to aldehydes/ketones in 1,2-dichloroethane (DCE). The active catalytic species is regenerated by dechlorination of DCE to ethene (Figure 6.7) [24]. The overall catalytic cycle is a useful one-pot oxidation and aliphatic dechlorination, with a new C–C bond thrown into the bargain. Using nonlocal density-functional theory, we studied two possible reaction pathways [25]. One was the insertion of HPdCl into the C–Cl bond, followed by HCl abstraction. The other was the abstraction of HCl from HPdCl, followed by oxidative insertion of a “naked Pd atom” into the C–Cl bond. Both paths converge on the same species, but the calculations showed that the former involves lower energy barriers,

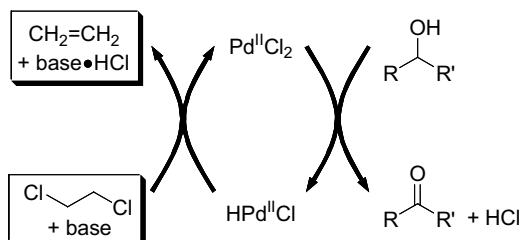


Figure 6.7 Catalytic oxidation of secondary alcohols to ketones, with a one-pot regeneration of the PdCl_2 catalyst by dechlorination of 1,2-dichloroethane to ethene.

and so is more likely. Based on these results, the oxidation cycle from methanol to formaldehyde (methanal) was calculated as a model reaction for the alcohol dehydrogenation in this system.

State-of-the-art QM and quantum dynamics calculations can even predict the intricate kinetics and thermodynamics of catalytic reactions at surfaces [26]. One of the most impressive examples is the detailed analysis of the synthesis of ammonia over ruthenium catalysts. In a large collaborative effort, scientists from ten institutions in six countries modeled the key elementary steps of this process, including a complete mapping of the adsorption energies, the dissociation of N_2 and H_2 at the catalyst surface, and the hydrogenation of the catalytic intermediates [27]. Importantly, the models predicted well the kinetics of ammonia production using actual industrial catalysts in industrial reactors. Interestingly, the calculations also showed that, under extreme conditions, ammonia can form in the gas phase via free-radical intermediates, which means that in principle ammonia can also form naturally in lightning storms. This demonstrates the utility of first-principles calculations in catalyst design, albeit with a currently high computational cost.

6.3 Predictive Modeling and Rational Catalyst Design

In silico catalyst optimization is the ultimate application of computers in catalysis. Imagine a computer program that is fed with data for a given reaction, and outputs the structure of the optimal catalyst for this reaction. Although this fantastic program does not exist (yet), much progress has been made in this direction since the mid-1990s, especially thanks to advances in laboratory automation (for model validation) and data analysis methods. Just like any other new idea, *in silico* catalyst optimization is accepted by some researchers and met with skepticism by others. Nevertheless, it is essential for realizing the potential of high-throughput screening and combinatorial chemistry in catalysis research [28,29]. Computers will not replace chemists, and data-mining methods will not replace mechanistic studies. These methods will simply be part of the chemist's toolbox in the 21st century.

Note that although the following discussion pertains equally to homogeneous, heterogeneous, and enzymatic catalysis, predictive modeling is much more difficult in the latter two cases. The reason is that finding good descriptors and good structure/activity relationships in heterogeneous and enzymatic systems is difficult [30]. Thus, the following examples are mainly from homogeneous catalysis. Sections 6.3.7 and 6.3.8 summarize the advances made in predictive modeling for heterogeneous catalysis and biocatalysis, respectively.

6.3.1

Catalysts, Descriptors, and Figures of Merit

Before making any predictions, we must first understand the problem of catalyst optimization, and especially define the space in which we want to optimize our data. To do this, we divide the system into three multidimensional spaces, **A**, **B**, and **C** (Figure 6.8). Space **A** is a grid containing all the catalyst structures (e.g., if the catalyst in question is a bidentate transition-metal complex, space **A** contains all the combinations of transition-metal atoms and bidentate ligands, with each point representing a different catalyst); space **B** contains the values of the catalyst descriptors and the reaction conditions (temperature, pressure, solvent type, backbone flexibility, cone angle, partial charge on the metal atom, lipophilicity, and so on); and space **C** contains the catalysts' figures of merit (i.e., the TON, TOF, e_e , price, and so forth). In this way, we have translated our abstract problem in catalysis to the (still abstract) problem of relating one multidimensional space to another. The advantage is that the relationship between spaces **B** and **C** can be quantified using quantitative structure/activity relationship (QSAR) and quantitative structure/property relationship (QSPR) models [31,32]. Note that linking spaces **B** and **C** using QSAR/QSPR models is precisely what we do when we optimize catalysts in the traditional way. The only difference here is that we will try and couple this process to an automated synthesis and screening of virtual and real catalyst candidates.

The key to the model lies in space **B**, the descriptors space. In Chapter 3, we have already discussed the definitions and applications of several important steric and

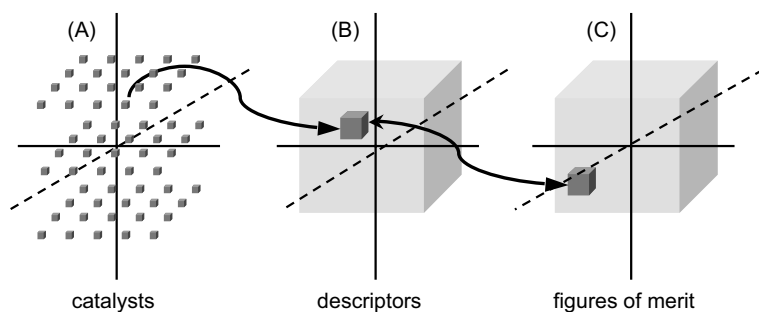


Figure 6.8 Three-dimensional simplified representation of the multidimensional spaces **A**, **B**, and **C**, containing the catalysts, the molecular descriptor values, and the figures of merit, respectively.

electronic descriptors in homogeneous catalysis. Choosing the right descriptors is critical for the model's success. In Section 6.3.2, I will explain the difference between the various descriptor types, with examples of current applications.

6.3.2

Three-Dimensional (3D) Descriptors

Every model is a compromise between cost (computational time) and performance. 3D descriptors are based on optimized molecular geometries, using either molecular mechanics force fields or quantum mechanics calculations. Tolman's cone angle [33], the bite angle [34], the percentage of approach sphere occupation [35], and the *trans*-CO stretching frequency discussed in Chapter 3 are all examples of 3D descriptors. Other examples include the partial charge at the ligating atoms, HOMO and LUMO energies, and molecular dipole moments. The advantage of using 3D descriptors is that they are chemically meaningful, i.e., they go hand-in-hand with

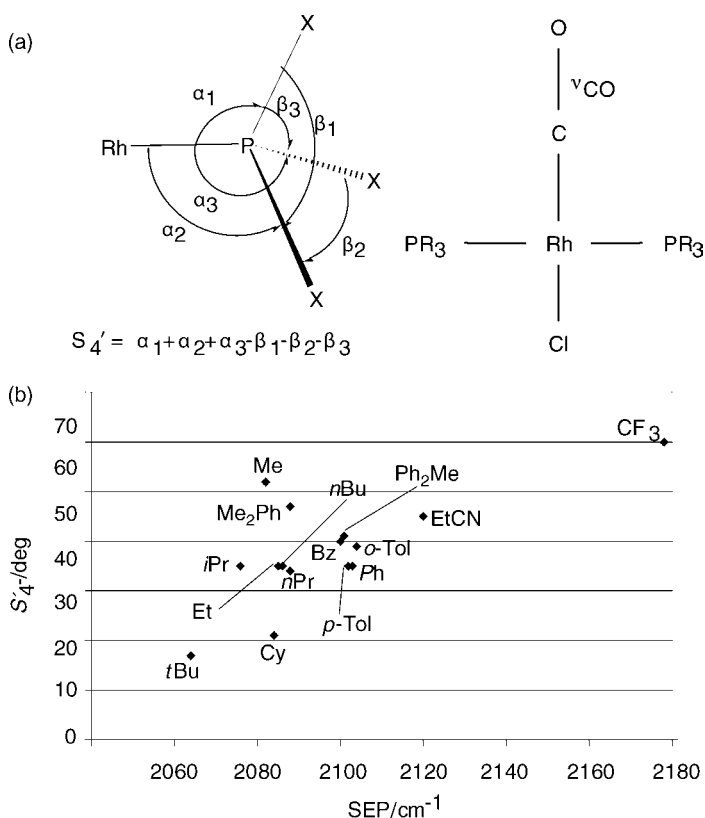


Figure 6.9 Descriptors calculated for phosphines in the *trans*-Rh(PR_3)₂(CO)Cl catalyst: **a** the deformation coordinate S_4' is employed as steric measure; **b** stereo-electronic map showing the distribution of the various PR_3 ligands.

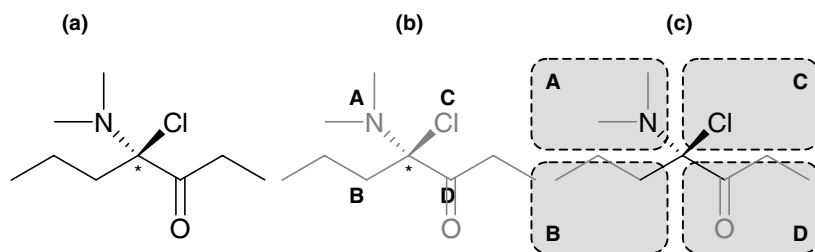


Figure 6.10 a Example of a chiral molecule, (*R*)-4-chloro-4-(dimethylamino)heptan-3-one, indicating **b** the four atoms directly bound to the chiral center and **c** their neighborhood (the neighborhood of atom **A** is defined as the set of atoms which are closer, i.e., on a shorter path, to **A** than to **B**, **C**, and **D**).

“chemical intuition.” The disadvantage is that the more accurate the description, the higher the cost.

Ideally, the descriptors should capture the structural and electronic variations responsible for catalytic activity. For example, Thomas Cundari and co-workers developed a simple and effective “stereo-electronic map” for characterizing phosphine and phosphate ligands, using semi-empirical calculations [32]. Thanks to their moderate cost, these models can be applied to libraries of 100–1000 compounds. The plot shown in Figure 6.9 is a representation of space **B** for this specific example. It includes just two descriptors: Orpen’s symmetric deformation coordinate, S'_4 , and the semi-empirical electronic parameter (SEP) [36]. Using this plot, one can fill the “empty holes” in the experimental design space with virtual ligands, and reduce “highly populated” areas by discarding duplicate molecules.

The modeling of chirality is an important application of 3D descriptors. Aires-de-Sousa and Gasteiger published an elegant numerical approach for modeling chirality in homogeneous catalysis [37,38]. Instead of representing chirality as a single value, they used a spectrum-like, fixed-length code. This code included information about the chiral centers’ geometry, properties of neighboring atoms, and bond lengths (Figure 6.10a–b). Using the addition of diethylzinc to benzaldehyde as a model reaction, the authors predicted each catalyst’s *ee*, as well as the preferred product enantiomer in each case.

6.3.2.1 Comparative Molecular Field Analysis (CoMFA)

Since its introduction in 1988, the CoMFA method has become one of the most powerful QSAR and drug design tools [39]. It has created a new paradigm of QSAR studies, where properties of molecules are related to their specific structural and electronic features, and their spatial arrangement. The groups of Kenny Lipkowitz and David Avnir used CoMFA for predicting the asymmetric induction of bisoxazolidine and phosphinoxazolidine ligands in the Diels–Alder reaction of *N*-2-alkenoyl-1,3-oxazolidin-2-one with cyclopentadiene (Figure 6.11a) [40–43]. Their basic assumption was that noncovalent interactions affect the catalytic activity, and therefore should correlate with the steric and electronic fields of the ligands. To obtain

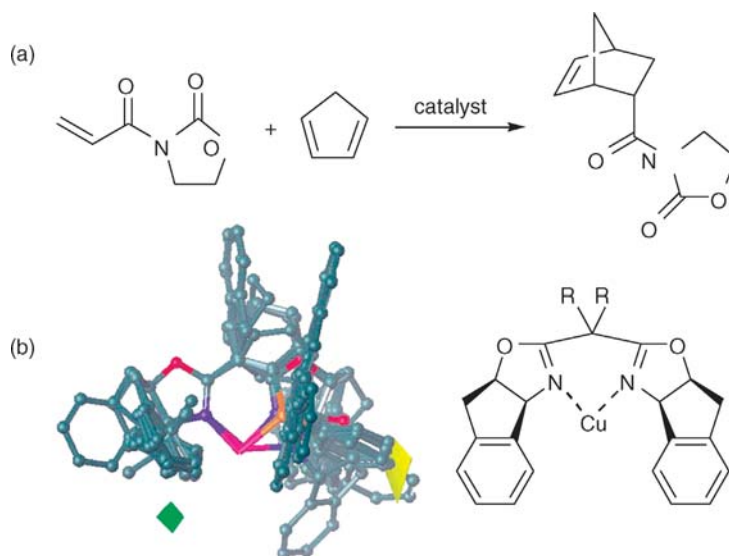


Figure 6.11 a Diels–Alder reaction of *N*-2-alkenyl-1, 3-oxazolidin-2-one with cyclopentadiene.; b alignment of all 23 bisoxazoline and phosphinoxazoline ligands used in the CoMFA study. Regions of space where steric bulk should enhance or decrease stereo-induction are plotted using iso-contour mapping.

these fields, the molecules are first aligned structurally, then the steric and electrostatic fields on a grid around them are sampled with probe atoms (Figure 6.11b). In most cases, the fields are based on atomic partial charges, calculated using quantum mechanics. The result is a table with thousands of columns which contain the field values at each grid point. These data are then analyzed using multivariate methods, such as partial least-squares regression (see Section 6.4.2). The model provides a linear relationship between the figure of merit (in this case the ee) and the intensity of the steric and electronic fields. This gives a picture of a “ligand stereotype”, which is analogous to the pharmacophore in drug design. Using this ligand stereotype, one can identify regions of the ligand where changing the steric bulk will result in a high ee value. Using the continuous chirality measure [44], Lipkowitz and Avnir showed that “more chiral” catalysts give higher ee values. They also demonstrated that one can increase the ee by increasing the ligand’s chirality.

6.3.2.2 The Ligand Repulsive Energy Method

Some ligands have several stable conformers with different steric properties, while others undergo structural changes when moving from free to metal-bound conformations. In these cases, one needs a descriptor that is related to the ligand’s energy. The ligand repulsive energy method quantifies the van der Waals repulsive energy variation (E_R) as a function of the ligand–metal complex distance (Eq. (6.3)) [45]. In this equation, $E_{vdw,R}$ is the repulsive part of the van der Waals potential, r is the actual ligand–metal complex distance, and r_c is the bond length between the metal

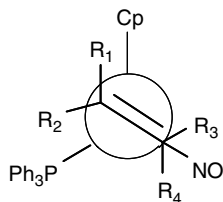


Figure 6.12 Newman projection of $[(\eta^5\text{-C}_5\text{H}_5)\text{Re}(\eta^2\text{-olefin})(\text{PPh}_3)(\text{NO})]^+$, viewed down the olefin centroid-Re axis.

and the ligating atom (the minus sign ensures that E_R will increase with the steric bulk of the ligand). As r changes, the nonbonded repulsion between the ligand and the environment also changes.

$$E_R = -r_e \left(\frac{\partial E_{\text{vdW},R}}{\partial r} \right) \quad (6.3)$$

Gillespie *et al.* used this concept for studying the binding selectivity of $[\eta^5\text{-C}_5\text{H}_5\text{-Re}(\text{NO})(\text{PPh}_3)]^+$ toward prochiral α -olefins (Figure 6.12). They examined the steric interplay between ligands on the Re atom and the substituent on the prochiral α -olefin (R_1 and R_2), ranking the relative importance of the size of ligands in terms of binding selectivities [46,47]. This study formed part of the so-called *de novo* ligand design pyramid, where the system's sterics and energetics are studied using different levels of computational theory [48,49]. Interestingly, although E_R values are based on computations involving energies, they correlate well with the cone angle and solid angle of the ligand, which are pure geometric constructs.

6.3.3

Two-Dimensional (2D) Descriptors

Although 3D descriptors offer a realistic representation of chemical systems, their calculation requires a geometry optimization step. This means that their computational cost depends on the system's size and number of degrees of freedom. If you plan to optimize large numbers of catalysts (e.g., virtual libraries for combinatorial optimization studies), 3D descriptors are simply too costly. In such cases, the simpler 2D descriptors (also called topological descriptors) provide a viable alternative. Topological descriptors are derived directly from molecular connectivity tables, without using any 3D atom coordinates. They are calculated using graph theory, which describes the atom connectivity in hydrogen-suppressed molecules. I will give here the basic method, plus some examples of applications in catalysis. A detailed treatment of graph theory is given elsewhere [50,51].

A molecular graph G is a structure formed by vertices (V) and edges (E), where $G = E + V$. The atoms and bonds of the molecules correspond to the vertices and edges of G . A standard representation of a graph is the adjacency matrix $A = (a_{ij})$, (Eq. (6.4)), where i and j are two generic nodes, and $E(G)$ represents the set of edges of G . Figure 6.13 shows an example of the molecular graph and the adjacency

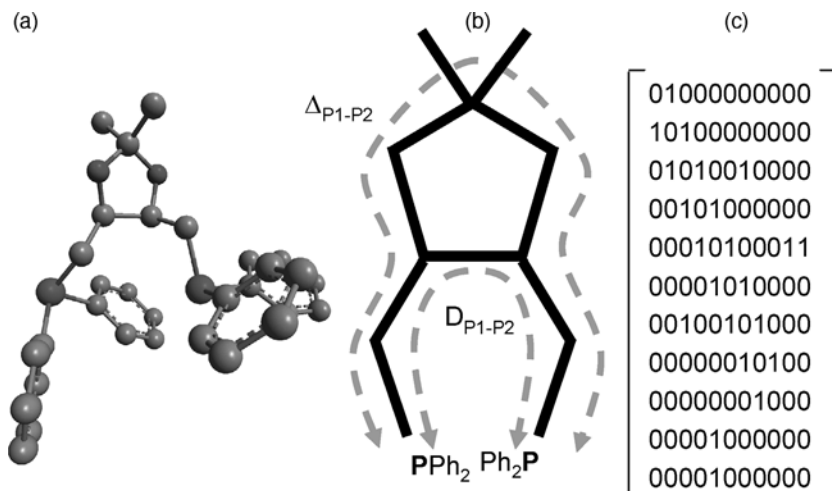


Figure 6.13 The DIOP ligand **a** structure; **b** molecular graph **c** adjacency matrix. The broken lines indicate the shortest and longest P–P connectivity paths, D_{P1-P2} and Δ_{P1-P2} , respectively. The adjacency matrix of a molecular graph is a matrix with rows and columns labeled by graph vertices v (i.e., the atoms), with a 1 or 0 in position (v_i, v_j) according to whether v_i or v_j are adjacent or not.

matrix for the DIOP ligand, (–)-2,2-dimethyl-4,5-bis(diphenylphosphinomethyl)-1,3-dioxolane-P,P'. The vertices and edges are labeled from 1 to 11 and from a to k, respectively.

$$a_{ij} = \begin{cases} 1 & \text{if } i \neq j \text{ and } (i,j) \in E(G) \\ 0 & \text{if } i = j \end{cases} \quad (6.4)$$

Two matrices are particularly important, both of them based on the topological distance between vertices within a graph: the **distance matrix** $D(G)$ and the **detour matrix** $\Delta(G)$. The first contains as values the smallest number of steps from vertex i to vertex j , and the second contains as values the longest paths. For example, Equation (6.5) shows the D and Δ matrices of the DIOP ligand.

$$D = \begin{bmatrix} 01234434555 \\ 10123323444 \\ 21012212333 \\ 32101223422 \\ 43210123411 \\ 43221012322 \\ 32122101233 \\ 43233210144 \\ 54344321055 \\ 54321234502 \\ 54321234520 \end{bmatrix} \quad \Delta = \begin{bmatrix} 01265567866 \\ 10154456755 \\ 21043345644 \\ 65404334555 \\ 54340434511 \\ 54334045655 \\ 65433401244 \\ 76544510155 \\ 87655621066 \\ 65451545602 \\ 65451545620 \end{bmatrix} \quad (6.5)$$

Based on the matrix expression of molecular graphs, we can calculate the length of paths connecting any pair of atoms, i.e., a series of consecutive edges that connect two

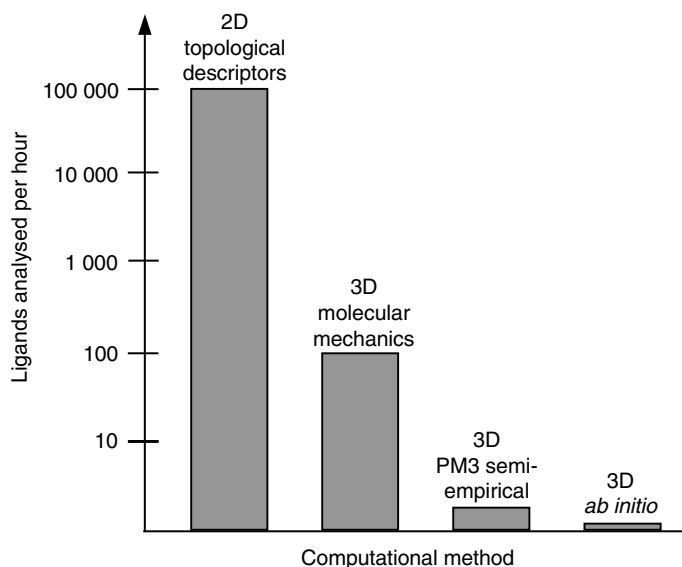


Figure 6.14 Bar graph comparing the analysis capacity, in number of ligands' bite angles and flexibility ranges calculated per hour, using topological descriptors (2D), and 3D descriptors based on MM force fields, semi-empirical QM calculations, and *ab initio* QM calculations.

All calculations were performed on a 2.5 GHz desktop computer (analysis capacity will improve with better computers and software, but the 2D/3D cost-effectiveness ratio will remain constant).

nodes and do not contain the same node more than once. In the case of bidentate phosphine ligands, for example, the connections of interest are those between the ligating phosphorus atoms, P_1 and P_2 . The minimum $D_{P_1-P_2}$ and maximum $\Delta_{P_1-P_2}$ connectivity paths are calculated from distance and detour matrixes, respectively. In the case of the DIOP ligand, $D_{P_1-P_2}$ is five bonds, and $\Delta_{P_1-P_2}$ is eight bonds.

Topological descriptors give information on the molecular size, flexibility, electron distribution, and various other physicochemical properties. They are, as Figure 6.14 shows, three to five orders of magnitude faster than 3D descriptors, depending on the geometry optimization method used for the latter. Unfortunately, this lower cost is offset by several limitations: First, although 2D descriptors account for specific physicochemical properties, they have no direct heuristic interpretation, because they are far from our “chemical intuition” (see also the discussion on data-mining methods in Section 6.4). Second, 2D descriptors neglect conformational information, and because they are two-dimensional they cannot be used for modeling chirality.

Strikingly, topological descriptors can account for molecular properties that may seem to demand geometry optimization. For example, we developed a simple set of topological descriptors for phosphine and phosphite bidentate ligands, focusing on P–P connectivity patterns [52]. These included all P–P connectivity paths, from the shortest ($D_{P_1-P_2}$) to the longest ($\Delta_{P_1-P_2}$), as well as their weighted versions (e.g., by molecular weight or electronegativity). Figure 6.15 shows some examples of these

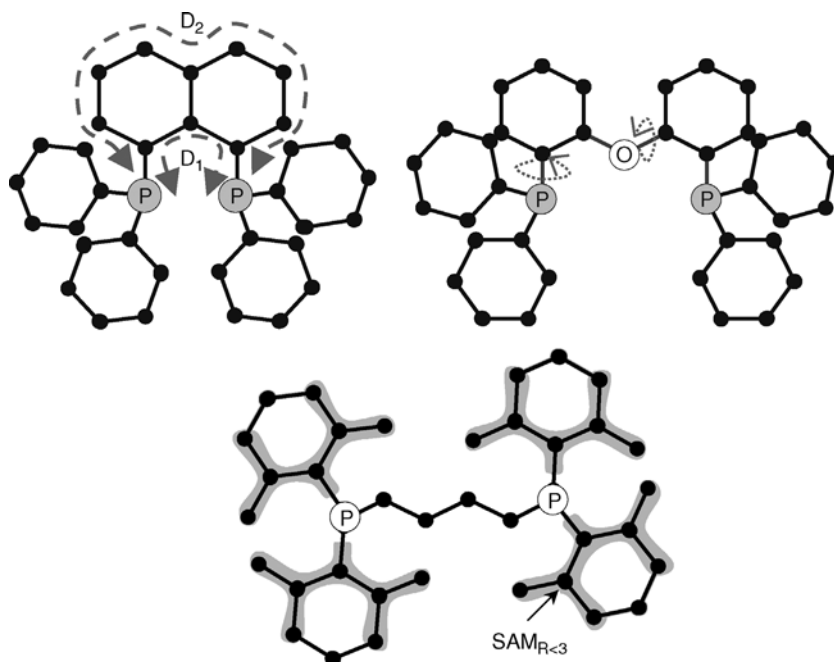


Figure 6.15 Examples of topological descriptors calculated on backbone and R groups of three bidentate ligands. The broken arrows on the left indicate the minimum P_1 – P_2 connectivity path (D_1) and the second P_1 – P_2 path (D_2). The dotted arrows indicate freely rotating bonds. The R group descriptor $SAM_{R<3}$ pertains to the sum of the mass units of atoms that are connected within three bonds of the ligating P atoms.

descriptors, and Figure 6.16 compares the performance of these 2D descriptors in predicting bite angle and flexibility values, with values obtained from X-ray diffraction experiments and PM3 semi-empirical QM calculations, respectively. The 2D and the 3D descriptors indicate the same trends, although the former give noisier results.

In another example, Chavali *et al.* demonstrated that 2D connectivity indices can give good structure/property correlations in molybdenum-catalyzed epoxidation [53,54]. They used the Computer Aided Molecular Design (CAMD) environment, a powerful computational tool used in product design. The method uses optimization techniques coupled with molecular design and property estimation methods, generating those molecular structures that match a desired set of properties.

6.3.4

Generating Virtual Catalyst Libraries in Space A

Now that we understand more about the various types of descriptors in space **B**, let us return to the problem of catalyst optimization. If we can generate a sufficiently large number of sufficiently diverse structures in space **A**, and link the spaces **A** and **B**, we

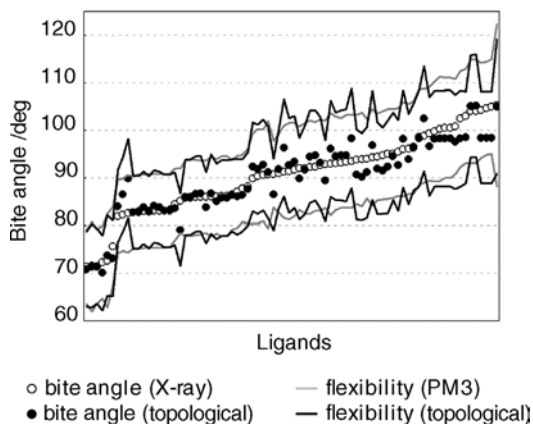


Figure 6.16 Observed and predicted bite angle and flexibility values for a set of biphosphine and biphosphite ligands. The empty dots and gray lines represent respectively the bite angle and flexibility values calculated on a set of 80 ligand–metal complexes retrieved from the Cambridge Crystallographic Database. Black dots and lines represent the same values predicted using a 2D descriptor QSAR model.

should be able to predict the relevant figures of merit in space **C** using QSAR/QSPR descriptor models. There are various ways of doing this. Here I will present a building-block assembly approach for generating space **A**. Using this approach, one easily obtains large numbers of structures. Following that, we will try and figure out what “catalyst diversity” means, and suggest ways for comparing the diversity of different catalyst libraries.

Let us assume that each catalyst contains one metal atom *M*, and one bidentate ligand which includes two ligating groups, L_1 and L_2 , a bridge group *B*, and three residue groups, R_1 , R_2 , and R_3 . To simplify things, we will limit the *R* groups to one per ligating or backbone group. There is no restriction on similarity between the groups, i.e., it is possible that $L_1 \equiv L_2$, and so forth. Each ligand has a unique identifier, in the form $L_1(R_1)-B(R_2)-L_2(R_3)$. Figure 6.17 shows a schematic representation of the catalyst parts and assembly possibilities, and Figure 6.18 shows a set of simple building blocks. The connection points for the *R* groups, and between the *L* and *B* groups, are predefined for each building block (for example, the pyridine ligating group 5 can connect to a backbone on positions 2, 3, or 4, and an *R* group can be subsequently attached to it on one of the remaining “free” positions). After the ligand has been assembled, any unused connection points are filled with H atoms.

Here one already faces an obstacle: The number of possible structures, using just 20 *L* groups, 10 *B* groups, 10 *R* groups, and this very simplified catalyst representation, is over 1.7 billion! Computing any parameters for such a large library is unrealistic. One way of overcoming this barrier is by sampling subsets of space **A** that are small enough for analysis (typically 500–100 000 catalyst structures, depending

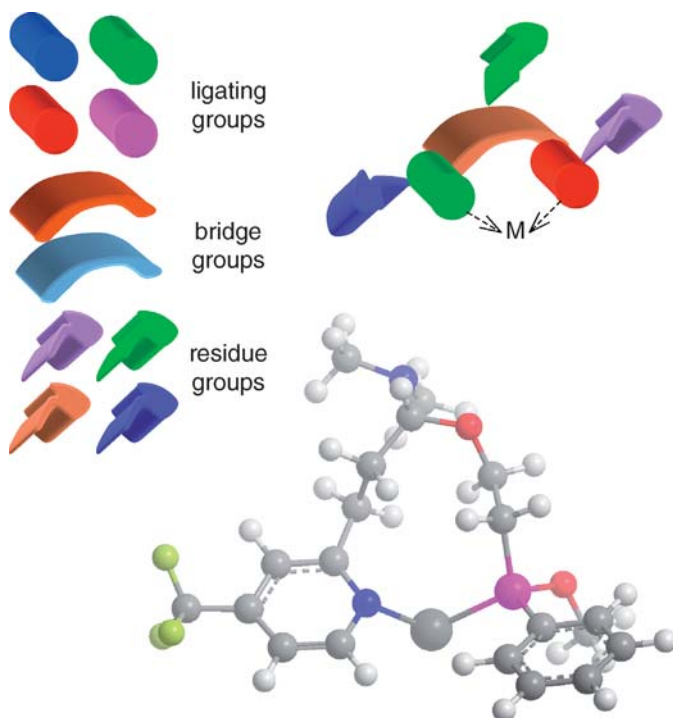


Figure 6.17 Structure and optimized geometry of a bidentate ligand–Rh complex of type $L_1(R_1)-B(R_2)-L_2(R_3)$, generated from the building blocks {5, 23, 18, 28, 12, 27} shown in Figure 6.18.

on the descriptor calculation method). These subsets, or virtual libraries, are assembled by generating sets of different $L_1(R_1)-B(R_2)-L_2(R_3)$ identifiers and subsequently optimizing the corresponding structures (one simple way of doing this is by assigning the different tasks to different software applications, and connecting the entire process by a batch code [55]). Selecting the subsets is not a trivial task, and should follow the principles of experimental design. The selection process can also incorporate prior knowledge about the reaction, applying an iterative approach using global optimization methods [56].

6.3.5

Understanding Catalyst Diversity

Although the term “diversity” is widely used in catalysis, it is ill defined. Diversity can be understood as a spread over a given catalyst space, or as a lack of similarity within a set of compounds [57–59]. Saying that “Library *a* is more diverse than library *b*” can mean that library *a* covers a wider range of the catalyst space. Alternatively, it can mean that the catalysts in library *a* are more uniformly spread in the same space. One thing is certain: library size alone does not guarantee diversity.

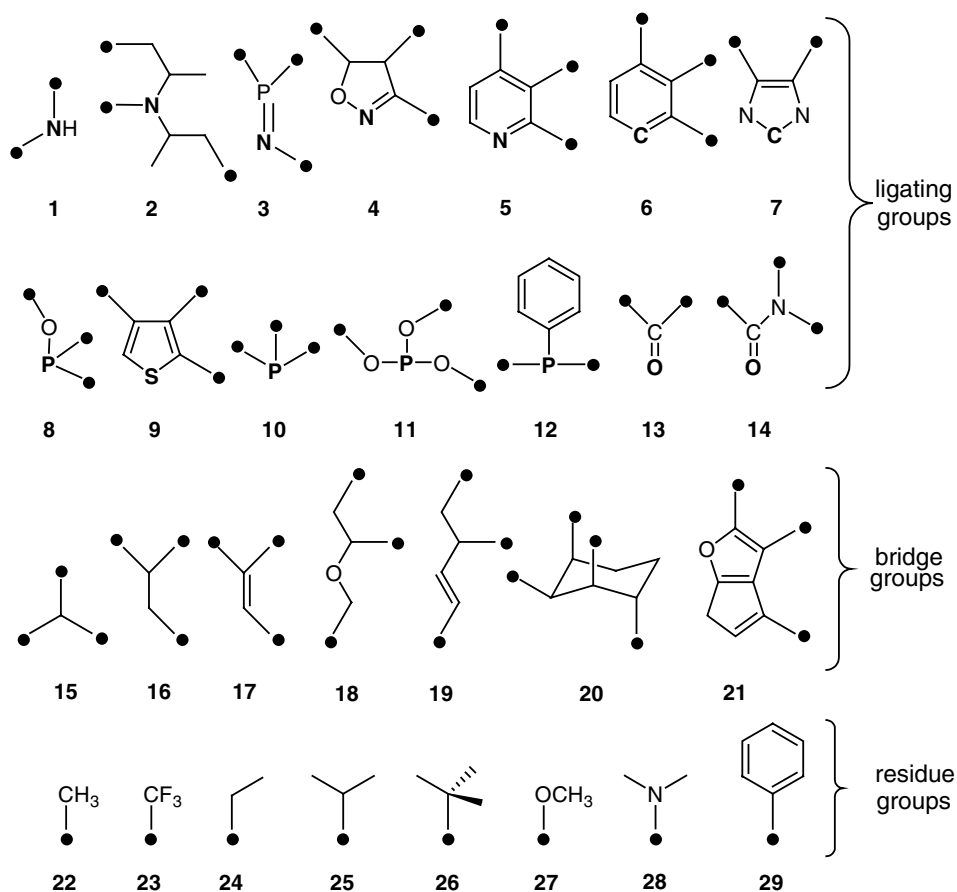


Figure 6.18 A set of building blocks, with black circles denoting the possible connection points.

Defining diversity is not trivial. A library of heterogeneous metal oxide catalysts, for example, can be synthesized from a diverse range of metal precursors, but the actual active catalyst may be very different from the precursor, because activity often depends on the process conditions and method of synthesis. Similarly, in homogeneous catalysis, you can define diversity in terms of functional groups or in terms of physico-chemical properties. Chemists traditionally define diversity in space **A**, by comparing molecular structures and especially functional groups. When using a building-block approach [55], the diversity can be defined by the number of different building blocks in a library. The problem is that this description ignores correlations and/or interactions between different sets of building blocks. This leads to the general complaint that small structural changes result in large activity changes, making diversity undefinable [60].

The solution to this problem lies in defining diversity in space **B**, the descriptor space [61]. Here the catalysts are quantified in terms of molecular and reaction

descriptors (e.g., polarizability, cone angle, flexibility). Thus, instead of evaluating molecules based on their “Chemdraw structures”, we compare them based on the values of specific descriptors. Note that choosing the right descriptors is a crucial step in determining catalyst diversity. This is because diversity is problem-related: For one reaction, the change in bite angle is crucial. For another, the reaction temperature and pressure are the key parameters.

Optimization Diversity versus Exploration Diversity After choosing the descriptors, we perform a principal component analysis (PCA) of the descriptor data (for an overview of PCA, see Section 6.4.1). The low-dimensional PCA model gives an ideal framework for catalyst optimization. By relating the scores of each catalyst to a figure of merit, optimization will yield a set of descriptors representing the best catalyst for the best specific reaction. Thus a diversity within the PCA scores is **optimization diversity**. It describes the size and coverage of the PCA score space of the catalysts. There are many different ways of measuring this. One measure is the determinant [62,63], which can be extended to a *D*-optimal onion design measure [64,65]. One simple ruler is the average distance of each catalyst to all the other catalysts in space **B**. This is the mean intercatalyst distance, δ_{average} , given by Equation (6.6), where d_{ij} is the distance between catalysts i and j in the score space. The value of δ_{average} tells us something about the *volume* that a library covers in space **B**. If δ_{average} is large for one library compared to another, the catalysts in the first library are further apart. This means that the library describes a larger volume of space **B**, and is therefore more diverse (see Figure 6.19). However, δ_{average} does not describe how well the catalysts are distributed. For this, we must also calculate the average distance from each catalyst to its nearest neighbour, δ_{min} , defined by Equation (6.7), in which $d_{\text{min},i}$ is the distance between catalyst i and its nearest neighbor in the scores space. δ_{min} gives an idea of the *clustering* of the catalysts in space **B**. If δ_{min} is small, each catalyst has at least one other catalyst close by. Conversely, if δ_{min} is large, the catalysts are far apart. A diverse library should be large, with the catalysts distributed well over the space. Both δ_{average} and δ_{min} should be large, so the product $\delta_{\text{average}} \times \delta_{\text{min}}$ is a good measure of library diversity.

$$\delta_{\text{average}} = \frac{1}{I} \sum_{i=1}^I \left(\frac{1}{I-1} \sum_{j=1}^I d_{ij} \right) \quad (6.6)$$

$$\delta_{\text{min}} = \frac{1}{I} \sum_{i=1}^I d_{\text{min},i} \quad (6.7)$$

Sometimes, however, one is not interested in optimization, but rather in finding a completely new catalyst. Catalysts with large residuals (high **E**-values, see Section 6.4.1) have, by definition, very different structures from the “average catalyst”. Therefore, as long as they have a high predicted figure of merit, they may provide entirely new reaction pathways. The PCA model residuals provide thus a measure of **exploration diversity**. The residuals of each catalyst in the PCA space reveal how different this catalyst is from the majority of the catalysts. Summing the squared

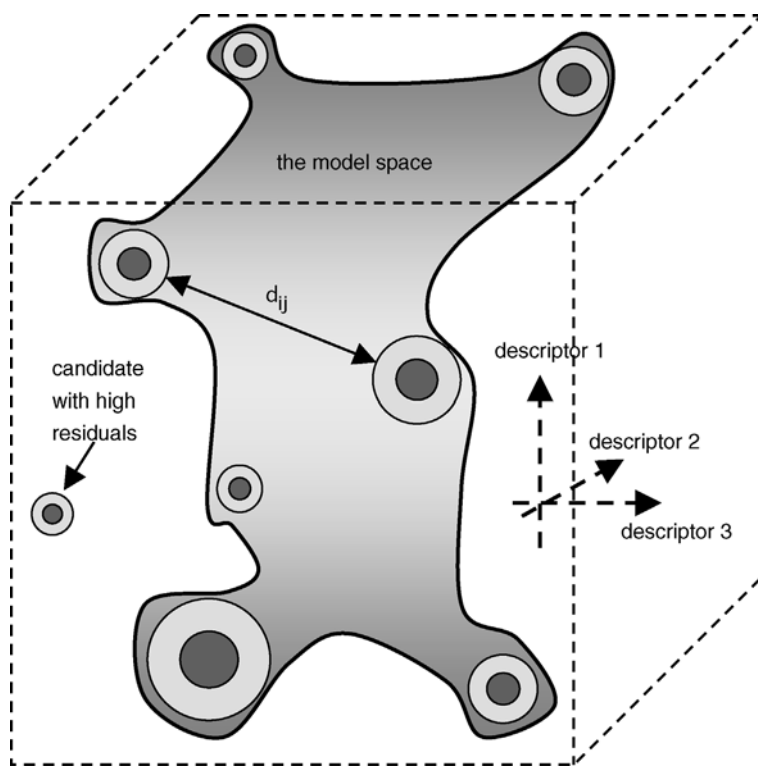


Figure 6.19 Graphic representation of the distances in a simplified three-dimensional descriptor space (space **B**). Catalysts with descriptor values “within” the model are good candidates for optimization. Those “outside” the model space may lead to new discoveries.

distances from each catalyst to the PCA model plane gives a measure for quantifying the library’s residuals. This is known as the Q -statistic (Eq. (6.8)), where M is the number of descriptors and e_{im} is an element of the residuals matrix **E**. The Q -statistic for a library equals the sum of the squared PCA residuals. A large Q -statistic indicates a library of catalysts that are very different from the “average catalyst.”

$$Q = \sum_{i=1}^I \sum_{m=1}^M e_{im}^2 \quad (6.8)$$

6.3.6

Virtual Catalyst Screening: Connecting Spaces A, B, and C

The final step is incorporating the library generation, model selection, descriptor calculation, and catalyst screening in one workflow [66]. One way of doing

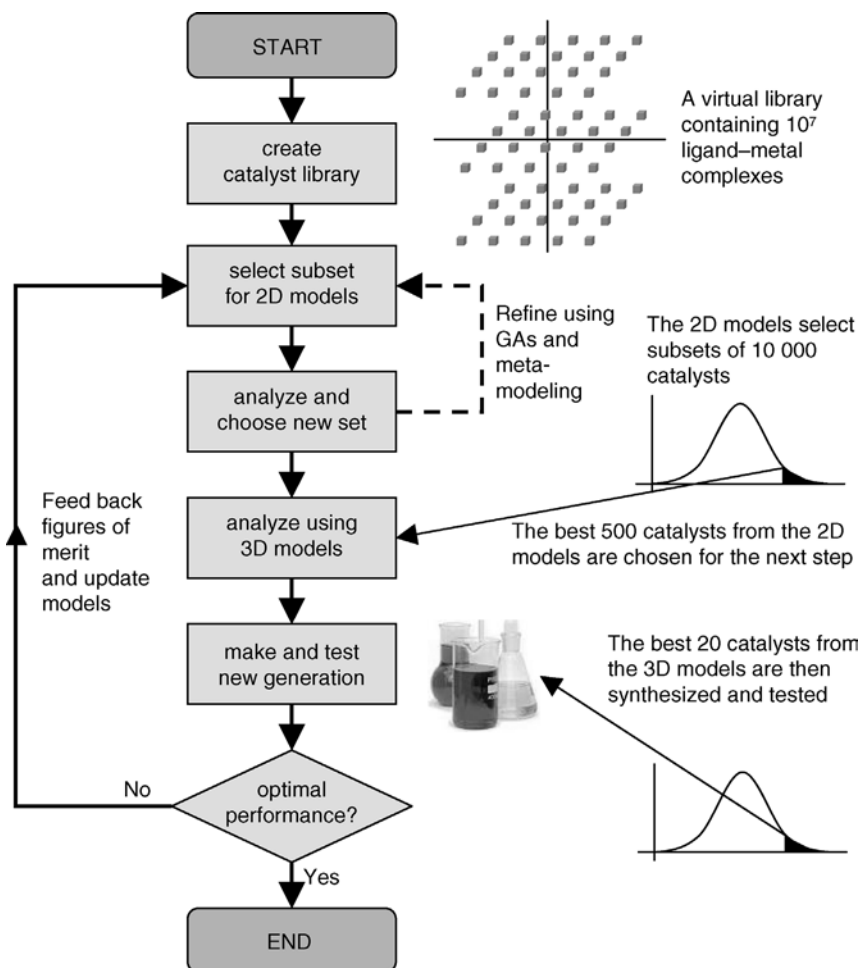


Figure 6.20 Iterative approach flowchart for homogeneous catalyst optimization.

this is by using an iterative approach, with consecutive modeling, synthesis, and analysis steps (Figure 6.20). First, we define and assemble the virtual catalyst libraries in space **A**, collect the initial data (from earlier experiments and the literature), and build a QSAR/QSPR regression model that connects the descriptors (space **B**) and the figures of merit (space **C**). I will discuss some modeling approaches in the next section. Subsequently, we perform a two-stage screening, using first 2D descriptors to examine relatively large areas of space **A** in a “rough screening.” The program selects random subsets from **A** (typically 10 000–50 000 catalysts), and calculates their 2D descriptor values. It then predicts their figures of merit using the above model. At this stage, you

can also use meta-modeling iterations for refining the results [67]. A subset of the best catalysts (typically 200–500 structures) is then selected for the “fine screening” stage.

The program then computes the 3D descriptors for this new subset, projects the results on the model, and predicts the figures of merit. The result is a small subset of 20–50 new catalysts which must be synthesized and tested experimentally. The dataset is updated and the cycle repeats. In theory this process can repeat indefinitely, but in practice the figures of merit usually converge after five or six cycles. This means that you can pinpoint “good regions” in a space of a million catalysts after testing fewer than 300 ligand–metal complexes!

Importantly, you can define the algorithm’s fitness function to reflect the actual requirements from the catalyst. An optimal catalyst exhibits high activity, high stability, and high selectivity. These three figures of merit are directly related to the product yield, the turnover number (TON) and the turnover frequency (TOF), but increasing one often comes at the expense of another. You can predefine the weight of each figure of merit, so that the computer will search for the optimal catalyst.

6.3.7

Predictive Modeling in Heterogeneous Catalysis

Much of the above discussion applies also to heterogeneous catalysis, with one important difference: Finding good descriptors for heterogeneous catalysts is much more difficult. Unlike molecular catalysts and organometallic complexes, the activity of solid catalysts depends on a multitude of parameters: different types of active sites, synthesis conditions, thermal treatments, and aging. Moreover, the properties of many solids can change discontinuously. New phases can form at different compositions, temperatures and pressures, and even the catalyst size can influence the reaction. Nano-sized gold particles, for example, are very different catalysts from “bulk gold”, and two supported gold catalysts can have different activities even when they contain identical amounts of gold and support, respectively [68]. As we already saw in Chapter 4, solid surfaces are anything but uniform, and solid catalysts have a variety of sites. To complicate things further, sometimes the real active sites are not those observed in characterization studies, but rather metastable defects which are difficult to characterize.

Because of this, relying solely on catalyst composition parameters is impractical (compositional descriptors are mainly applicable in cases where the catalyst is a crystalline material, and where the changes in composition do not lead to phase changes [69]). Instead, we need a descriptor toolbox that can account for the discontinuities and nonlinear dependencies. A few promising starts have been made in this direction [70–72]. Klanner *et al.* combined compositional descriptors and tabulated physico-chemical data, collecting a total of over 3000 descriptors for 467 catalysts, which were then tested in a high-throughput reactor in propene autoxidation. Naturally, such a dataset is over-determined (i.e., there are many more descriptors than data points, so that one can always find good correlations, but these

correlations are often meaningless). To obtain meaningful correlations, the researchers needed to discard some descriptors. Interestingly, feature selection algorithms could not select the relevant descriptors, and so a selection was made based on chemical intuition. This is a good example of how chemical knowledge can be integrated in data-mining models (see also Section 6.4 on data mining in catalysis). A subset of 75 “chemically relevant” descriptors was selected, and prediction models were constructed using artificial neural networks (ANNs) and classification trees (see Section 6.4 for an overview of these methods) [73]. Significantly, both methods could predict “good” or “bad” propene oxidation catalysts. The prediction accuracy of the ANNs was typically 0.5–0.7, much higher than that of random models (typically 0.2–0.3).

In another study, Corma and co-workers combined genetic algorithms (GAs) and ANNs for predicting the performance of virtual catalyst libraries for oxidative dehydrogenation of ethane, using the catalyst composition as input parameters [74,75]. The virtual screening was again combined with high-throughput experimentation, using the predictions of the ANNs as a theoretical prescreening, and thus avoiding the testing of poorly performing materials. Although the subsets tested were very small compared to the catalyst space, a significant improvement was obtained after seven generations, demonstrating the potential of this approach. The same group also used high-throughput X-ray diffraction studies to build descriptor datasets for epoxidation catalysts, combining the spectral data with catalyst composition data and creating an automated synthesis, testing, and modeling workflow [76].

The issue of catalyst diversity is just as important here as in homogeneous catalysis, and the discussion in Section 6.3.5 is just as pertinent. That being said, true diversity measures must be made in space **B**, the descriptor space, which brings us back to the challenge of finding good (and general) descriptor vectors for heterogeneous catalysts.

6.3.8

Predictive Modeling in Biocatalysis

Although enzymes are far too complex for a detailed descriptor modeling at the molecular level, predictive modeling plays an increasingly important role in the search for new biocatalysts [77]. The experimental techniques for designing enzymes that can operate under harsh process conditions (high temperatures, acidic/basic pH, and/or organic solvents) rely heavily on genetic engineering and combinatorial chemistry. These efforts are complemented by a variety of computational screening tools [78]. The main composition variable here is the primary structure (i.e., the amino acid sequence of the protein). Computer algorithms screen the sequence space, eliminating those sequences that are incompatible with the protein folding model, and thus reducing the number of garbage experiments [79]. Protein-modeling algorithms can even insert potentially active catalytic residues into “virtual proteins,” and search for candidates with an improved binding affinity to high-energy reaction intermediates [80,81]. Examples include

the redesign of active sites for improved catalytic activity [82], and the design of thermostable enzymes [83].

6.4

An Overview of Data-Mining Methods in Catalysis

In Chapter 1, I outlined some of the new advances in high-throughput experimentation (HTE) and their applications in catalysis research. Robotic systems can now perform thousands of experiments per day, yielding mind-boggling amounts of experimental results. HTE can help us screen larger regions of the catalyst space. However, the total space is much too large for exhaustive screening, even using robots, so we must choose which areas to search in. Moreover, although HTE gives overwhelming quantities of data, much of this is “garbage data” that must be sifted out [84]. In this section, I describe a few useful methods for filtering out garbage data, with some examples of their applications in catalysis research. For more details see the books by Massart [85] and Tranter [86].

As discussed above, one option is screening virtual catalyst libraries using QSAR and QSPR models, with the aim of pinpointing promising candidates for future experiments [87,88]. Such models can also indicate which chemical features regulate a process, and how these can be optimized. These models must be robust, and properly validated [89]. Figure 6.21 shows a simplified data analysis flowchart. First, the data are collected and treated in a preprocessing step. Depending on the situation and on the knowledge available, you may want to mean-center and/or scale the entire dataset, or perhaps divide it into subsets according to chemical restrictions. In many cases, inclusion of chemical knowledge and reaction restrictions will simplify the system. Then, dimension reduction methods such as PCA are used for highlighting the number of key variables, and linear/nonlinear regression models are built, tested, and validated. The model’s predictions can be fed back to the data collection stage, improving the figures of merit in an iterative fashion.

The simplest form of regression is multiple linear regression (MLR), $\mathbf{Y} = \mathbf{X}\mathbf{B} + \mathbf{E}$. Here, \mathbf{X} contains the descriptors, $[d_1 \dots d_n]$, \mathbf{B} contains the regression coefficients, \mathbf{Y} contains the figures of merit and \mathbf{E} contains the residuals. One well known example of MLR is the relationship shown in Equation (6.9). This model requires a few well-characterized parameters $d_1 \dots d_n$, which are usually derived from experimental measurements or from QM calculations. There are several applications of MLR in catalysis, e.g., the quantitative analysis of ligand effects (QALE) model developed by Fernandez *et al.* [90].

$$\ln k = \mathbf{a}d_1 + \mathbf{b}d_2 + \dots + \mathbf{z}d_n + \mathbf{E} \quad (6.9)$$

The trouble is that you often have too many descriptors, and/or insufficient information on the reaction mechanism. This creates two problems: building a regression model requires the calculation of the inverse of $\mathbf{X}^T\mathbf{X}$, which cannot be done for a matrix \mathbf{X} that contains more variables than experiments. Moreover, if you

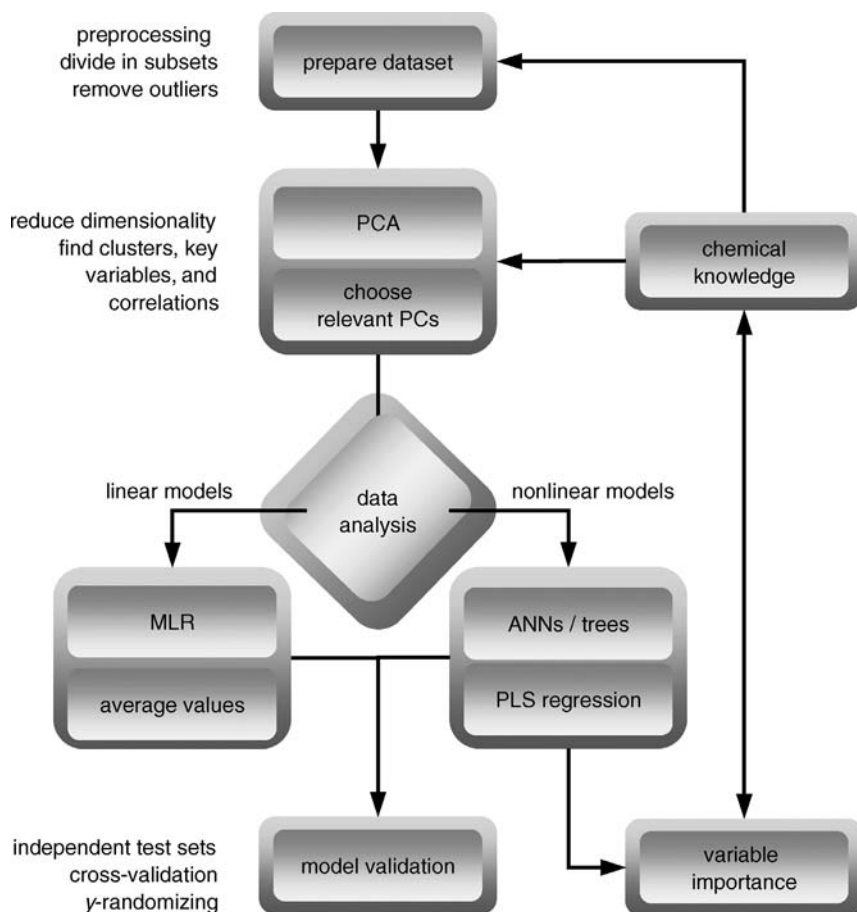


Figure 6.21 Flowchart showing a general approach to data mining.

have too many descriptors, you can always find a so-called chance model that fits your data perfectly, but has no statistical relevance. In such cases, you must find the right descriptors *and* the right way of correlating them to the figures of merit. One approach is first to reduce the number of parameters using PCA, and then choose the analysis method. You can use either linear or nonlinear models (Figure 6.21). Both approaches are equally valid. Linear models, such as partial least-squares regression, are more robust, and easier to interpret. Nonlinear methods, such as artificial neural networks, can handle more complicated systems, but they are often “black box” models.

Selecting the right variables often improves the models and makes interpretation easier. When there are too many descriptors, and especially when these descriptors do not have a clear physico-chemical meaning (e.g., connectivity indices and other 2D descriptors), stochastic methods such as genetic algorithms and evolutionary strategies can be used for finding an optimal subset of descriptors [91,92].

6.4.1

Principal Components Analysis (PCA)

Suppose that you have an experimental data matrix that contains the concentration profiles of 12 500 reactions, performed using 50 different catalysts tested with 50 different substrates under five different conditions, with each profile made of 10 points. This matrix contains $50 \times 50 \times 5 \times 10 = 125\,000$ data points. It merits some serious thinking about data mining, because it is unlikely that you will see anything useful just by looking at 125 000 numbers. PCA can reduce this large matrix into two smaller matrices which are easier to examine and interpret. Using PCA, you can extract the key factors. These are the **principal components**, or PCs (sometimes also called the **latent variables**). Each PC is a linear combination of the original variables, but unlike the original variables, which may be correlated with each other, the PCs are orthogonal (i.e., uncorrelated, independent of one another) [93].

Mathematically speaking, if \mathbf{X} is an $(I \times J)$ matrix that contains J variables for I reactions, PCA divides this matrix into a systematic part \mathbf{TP}^T (the PCA model), and a residuals part \mathbf{E} (Eq. (6.10)). \mathbf{T} ($I \times R$), and \mathbf{P} ($J \times R$) are two smaller matrices, the size of which depends on R , the number of significant PCs. \mathbf{T} is the **scores matrix**. It represents the spread of the reactions within the model space. \mathbf{P} is the **loadings matrix**. It describes the relationships between the variables.

$$\mathbf{X} = \mathbf{t}_1 \mathbf{p}_1^T + \mathbf{t}_2 \mathbf{p}_2^T + \dots + \mathbf{t}_n \mathbf{p}_n^T + \mathbf{E} = \mathbf{TP}^T + \mathbf{E} \quad (6.10)$$

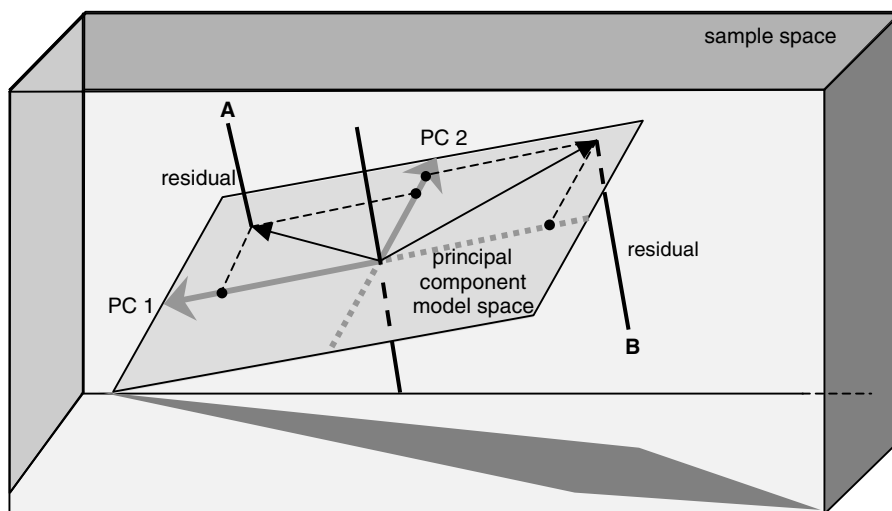


Figure 6.22 PCA reduces the dimensionality of the problem by projecting the original dataset onto a lower-dimension PC model, in which the new variables are orthogonal to each other. The distance from point A to the PCA model space equals the residual value for catalyst A.

What PCA actually does is project the data matrix \mathbf{X} onto a lower-dimensional space. You start with J variables, and end with R orthogonal PCs (where $R \ll J$). This projection gives a simplified view of the data, highlighting the important variables. Figure 6.22 shows an example where two points are projected from a three-dimensional space onto a two-dimensional surface.

PCs are ranked according to the fraction of variance of the dataset that they explain. The first PC is the most important (it explains the largest fraction of variance), and so forth. Selecting the correct number of PCs is crucial. Too few PCs will leave important information out of the model, but too many PCs will include noise, and decrease the model's robustness (if $R \sim J$, the PCA is pointless). Each time you make a new PCA model, you should examine the residuals matrix \mathbf{E} . If the residuals are structured, it means that some information is left out. You can also decide on the correct number of PCs by performing a cross-validation (see below), or by examining the percentage of the variance explained by the model.

Note that PCA is scale-dependent, so if the original variables differ by orders of magnitude (e.g., one variable is temperature, in the range 300–500 K, and the other is pressure, in the range 0.2–0.4 bar), the numerically large variables will dominate the first few PCs. You can remove this effect in the preprocessing stage, by scaling all variables to unit variance (also known as **autoscaling**). Starting from your original data matrix \mathbf{X} ($I \times J$), you subtract from each value the column average, and divide the result by the column standard deviation (Eq. (6.11)). In this way, the range of each variable is scaled so that ± 1 corresponds to one standard deviation.

$$a_{ij} = \frac{x_{ij} - \bar{x}_j}{s_j} \quad (6.11)$$

- **CAUTION!** Do not use autoscaling if the variables are all of the same type, because in this case variables with small values may simply describe noise. Autoscaling will inflate these variables, giving them the same weight as the important variables in your dataset.

6.4.2

Partial Least-Squares (PLS) Regression

PLS regression is a common method for modeling multivariate data [94]. It works with two matrices. The matrix \mathbf{X} contains the descriptors (the **independent variables**), and the matrix \mathbf{Y} contains the figures of merit (the **dependent variables**). The model approximates the relationship between \mathbf{X} and \mathbf{Y} according to Equation (6.12), where \mathbf{B}_{PLS} is the matrix of regression coefficients, and \mathbf{E} the matrix of residuals. The regression coefficients can be used for assessing which x variables mainly model a certain y variable. However, with correlated variables, these coefficients are not mathematically independent. To solve this problem, PLS estimates the correlation structure between \mathbf{X} and \mathbf{Y} in terms of projections onto a few latent variables, as in PCA. The resulting PLS x -weight vectors are used to combine the x variables with the scores, \mathbf{t} , which predict the y variables. The performance of a PLS model is measured using the

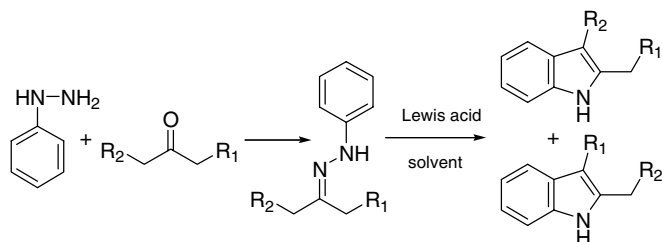


Figure 6.23 Formation of indoles from dissymmetric ketones by the Fischer indole synthesis.

explained y variation, R_y^2 , and the predicted y variation, q^2 (see also the discussion on model validation in Section 6.4.5). In general, PLS models are more robust than multiple linear regression and principal component regression methods.

$$\mathbf{Y} = \mathbf{B}_{\text{PLS}}\mathbf{X} + \mathbf{E} \quad (6.12)$$

For example, Carlson and Gautun developed an interesting PLS model for predicting the success/failure of regioselective indole synthesis (Figure 6.23) [95]. They tested 254 combinations of substrates, solvents, and Lewis acid catalysts, out of a possible 600. These were selected according to their principal property score values. In this way, the researchers maximized the spread in the property space, while minimizing the number of experiments. The score values, their squares, and their interaction terms were used as input variables for the PLS model. According to the model, the most important factor was the interaction term between nucleophilic/electrophilic properties of the ketones, and the size of one of the side chains, implying that large substituents and polarized ketones favor the reaction. The PCA scores plot showed clusters for the different ketones, indicating that the catalyst and solvent effects were valid for every ketone tested. A PLS analysis on reactions with the same ketone substrate revealed that catalyst hardness and solvent polarity/polarizability were positively correlated with “reaction success.”

The relative importance of each predictor variable in the PLS regression model is calculated using the **variable importance parameter (VIP)** [96], given by Eq. (6.13). In this equation, b_{ak} is the regression weight for variable k and factor a . SSQ_a is the percentage variance captured by latent variable a , n is the total number of variables, and lv is the number of latent variables used in the regression model. Since the VIP magnitude depends on the number of latent variables, the absolute VIP values are less meaningful than the relative values in a given dataset. Figure 6.24 shows an example of a VIP plot for a PLS regression model for 42 bidentate phosphine and phosphite ligands in the hydrocyanation of pentenenitrile, a key step in the production of the nylon 6.6 precursor hexamethylenediamine (hexane-1,6-diamine) [96].

$$\text{VIP}_k = \frac{\sum_{a=1}^{lv} b_{ak}^2 \cdot SSQ_a}{n \cdot \sum_{a=1}^{lv} SSQ_a} \quad (6.13)$$

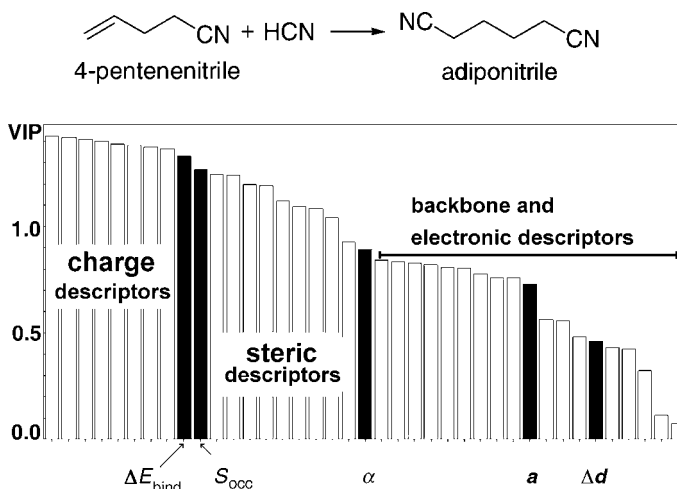


Figure 6.24 VIP plot for various descriptors in a PLS model for the hydrocyanation of pentenenitrile in the presence of Ni–biphosphine/biphosphite complexes. Charge descriptors refer to the Mulliken charge calculated at the ligating atoms. ΔE_{bind} is the energy difference between the free ligand and the metal complex, and can be related to the chelating effect and flexibility of the molecule. S_{occ} is the sphere occupation descriptor and measures the sterics around the metal center. α is the bite angle. α is the second derivative of the flexibility profile polynomial, and Δd is the difference in the interatomic distance between the ligating atoms between the free ligand and the complex.

6.4.3

Artificial Neural Networks (ANNs)

ANNs mimic the fault-tolerance and the learning capacity of biological neural systems, by simulating the low-level structure of the brain. They are applicable in every situation where there is a relationship between the independent variables (inputs) and predicted variables (outputs), but especially when this relationship is complex and difficult to explain in the usual terms of “correlations.” Many catalytic cycles show complex nonlinear behavior, and ANNs are excellent for modeling such data [97–100]. The disadvantage is that the network is opaque, a “black box” – it may give good results, but we cannot follow the “reasoning” behind the model. Furthermore, ANNs perform well when they are well trained, meaning that your training set must be representative of your test set. Another disadvantage of ANNs is that they tend to overfit, modeling noise as well as real data. This last problem can be avoided with proper model validation (see Section 6.4.5).

To capture the essence of biological neural systems, an artificial neuron receives a number of inputs, either from original data or from the output of other neurons in the network (Figure 6.25). This can be done in different ways, reflecting different **network topologies** or **architectures**. There is no golden rule that tells you which topology is most suited for a particular problem, so the best thing to do is simply to try

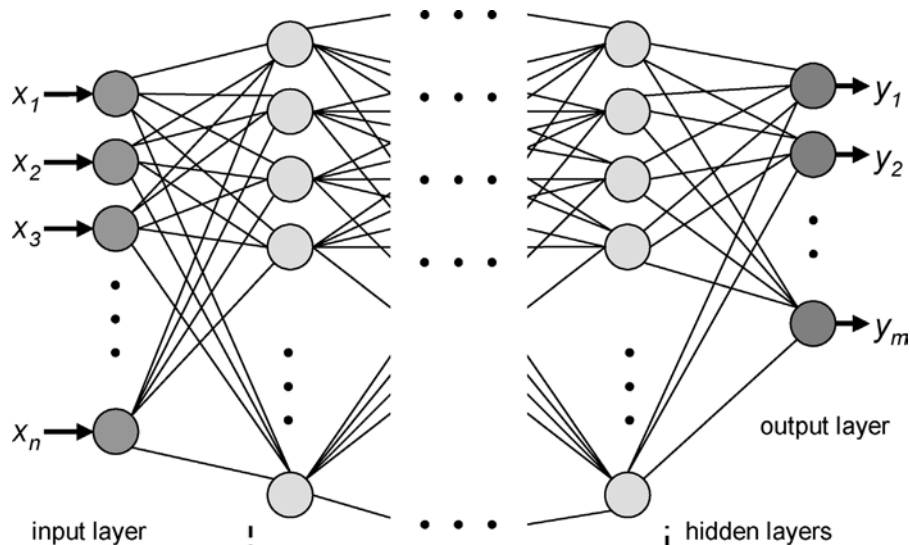


Figure 6.25 Schematic drawing of an artificial neural network with a multilayer perceptron topology, showing the pathways from the input x_i to the output y_i , and the “visible” and “hidden” node layers.

a few different options and compare the results. Equation (6.14) shows a general definition, where x is a neuron with n input dendrites x_i and one output axon $y(x)$, and w_i are the weights of these inputs. G is an activation function (usually a sigmoid function or a hyperbolic tangent), based on the sum of the n inputs, which determines each neuron’s output threshold.

$$y(x) = G \left(\sum_{i=0}^n w_i x_i \right) \quad (6.14)$$

ANNs have two different phases: a training phase and an execution phase. In the training phase, the weights w_i are determined, and the network is trained to return a specific output when given a specific input. In the execution phase the ANN is fed with new cases (e.g., descriptor values for new catalysts) and returns an output (e.g., a prediction of the figure of merit) on the basis of the network generated in the previous phase. When ANNs are used for regression analysis, confidence levels determine how the network will predict a quantitative value of performance (output value) for each input case. The network’s efficiency is evaluated using the standard deviation ratio, which is the ratio of the prediction error standard deviation to the original output data standard deviation. The lower the ratio, the better the prediction.

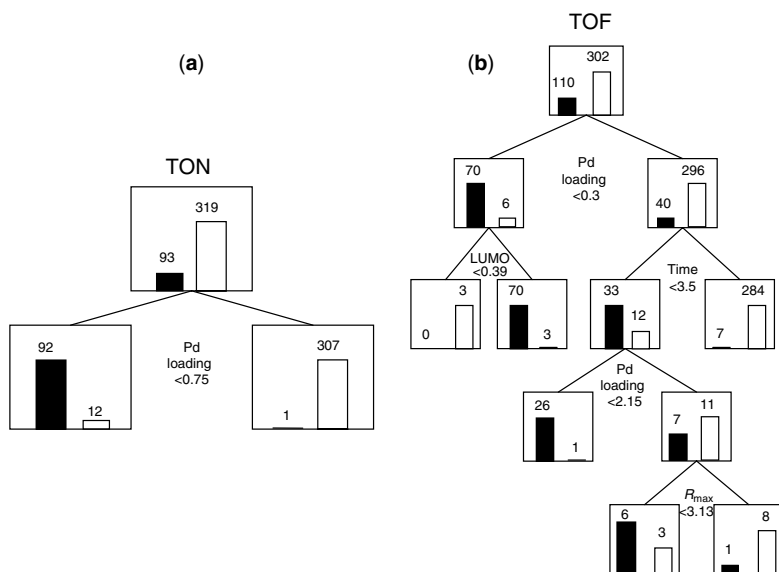


Figure 6.26 a TON and b TOF classification tree structures for a dataset of 412 Pd-catalyzed Heck reactions described by a total of 74 descriptors. The black and white bars represent positive and negative experiments, respectively. In the case of TON, the most relevant splitting condition is Pd loading < 0.75%. For the TOF, the first splitting condition is the reaction time, followed by the Pd loading, and the ligand's LUMO energy and R_{max} (the distance between the bulk of the ligand and the metal center).

6.4.4

Classification Trees

In **classification analysis** the variable selection procedure is similar to that of regression, but here the reactions are categorized into “positive” and “negative” cases according to their figure of merit values. This is done by selecting a threshold, e.g., “positive cases” can be defined as those with TON > 1000 and TOF > 500. In each stage, the model splits the data in two. Thus, the first node (also called the parental node) is divided into two child nodes according to the most relevant splitting condition, and so forth. The advantage of classification trees is that, unlike neural networks, one can follow the reasoning behind the model. Figure 6.26 shows an example of the TON and TOF classification tree structures for a dataset of 412 Pd-catalyzed Heck reactions described by a total of 74 descriptors [101].

6.4.5

Model Validation: Separating Knowledge from Garbage

One problem with computer models, or indeed with the scientists using them, is that when the models do not crash, the scientists tend to believe the results. Without proper validation, however, deducing anything from any model is a hazardous

business. The model may be overfitting (finding trends in noise), or predictions may be out of range (extrapolation), leading to ridiculous results. Model validation is like a control experiment in the laboratory. It may be tedious and time-consuming, but it is essential. This section gives the basics of four useful validation approaches. Readers wishing to explore this subject further should consult the work of Tropsha and co-workers [89].

Regardless of which model you use, the validation procedure depends on the amount and quality of the data. When there are enough data, the set should be divided into three parts: a training set, a test set, and a validation set (this is called **external validation**). The model is then constructed using the training set, tested with the test set, and (possibly) improved and retested. When you are happy about the model, you can test its performance on the validation set. After this, you cannot tinker with the model again (because it has already “seen” the validation set). If you have insufficient data for three subsets, you divide the data in two: a training set and a test set. You construct the model using the training set, validate it using cross-validation or bootstrapping (see below), and then test its performance with the test set.

6.4.5.1 Cross-Validation and Bootstrapping

Let us assume that we have measured the TON and TOF of 200 catalytic reactions, and calculated a QSAR/QSPR regression model, which connects the catalyst descriptors to the figures of merit. To validate this model, we divide our dataset into two parts: a **training set** (also known as the **calibration set**), used for developing the model, and a **test set** (also known as the **prediction set**) [94]. We know the figures of merit for the test set, but we do not use them when generating the model. Instead, we calculate the regression equation for the training set (say for $n = 150$ reactions), and using this equation, predict the TON and the TOF for the test set (the remaining 50 reactions). In this way we can compare the performance of different models, all trained on with the same training set. This is known as **cross-validation**. The model’s predictive performance is measured by the cross-validation correlation coefficient, q^2 (Eq. (6.15)), where y_i , \hat{y}_i , and \bar{y}_i are the measured, predicted, and average y -values, respectively. Note, however, that although a high q^2 value is a necessary condition for good predictions, it is not a sufficient condition [102]. Cross-validation should be complemented by other methods to ensure the model’s robustness and prediction accuracy.

$$q^2 = 1 - \frac{\sum_{i=1}^n (y_i - \hat{y}_i)^2}{\sum_{i=1}^n (y_i - \bar{y}_i)^2} \quad (6.15)$$

The choice of training and test sets may bias the results [103]. To avoid such problems, we can partition the original set in several different ways (i.e., choose different combinations of training sets and test sets) and compute an average score over the different partitions (**leave- n -out** cross-validation). The advantage here is that all the data are used for training, without holding any back in a separate test set. An extreme variant of this is splitting the 200 reactions into a training set of size 199 and a test of size 1. This is called **leave-one-out** cross-validation.

Resampling of the dataset in different ways, or **bootstrapping**, is similar to cross-validation [104]. The idea behind bootstrapping is that the dataset should be representative of the total population. Catalysts from the dataset are selected at random, and divided into subsets. Some catalysts may appear in several subsets, while others may not appear at all. Subsequently, some of the subsets are used for building a model. The results for the remaining catalysts are then predicted using this model. A high average q^2 value indicates the model's robustness.

6.4.5.2 Mixing the Dependent Variables (y -Randomizing)

Randomizing of the y variables (also known as a **permutation test**) is a common method of testing the model's robustness. Here, the vector containing the figures of merit is shuffled randomly, so that the figures of merit no longer match the original descriptor values. A new model is then generated using the original descriptor values, and the process is repeated several times. In principle, this should give models with very low R^2 and q^2 values. Models that fail this negative test should be discarded, because any random collection of values for the figures of merit would do just as well.

Another simple variant of this method is to test the model on completely random data. Generate a random series of numbers for your figure of merit y , and then run your model. You should get only noise – if you get meaningful results (i.e., high R^2 and q^2 values) out of random data, then there is something seriously wrong with your model.

6.4.5.3 Defining the Model Domain

Every model has limitations. Even the most robust and best-validated regression model will not predict the outcome for *all* catalysts. Therefore, you must define the application domain of the model. Usually, interpolation within the model space will yield acceptable results. Extrapolation is more dangerous, and should be done only in cases where the new catalysts or reaction conditions are sufficiently close to the model. There are several statistical parameters for measuring this “closeness,” such as the distance to the nearest neighbor within the model space (see the discussion on catalyst diversity in Section 6.3.5). Another approach uses the **effective prediction domain** (EPD), which defines the prediction boundaries of regression models with correlated variables [105].

6.5

Exercises

1. Diesel engines are “greener” than gasoline ones, because they are more efficient, and because diesel fuel requires less refining than gasoline. However, diesel engines emit soot particles, which should be filtered at the exhaust. The filters clog after one to two years, and must be regenerated. This regeneration can be done *in situ*, by coating the filter with a microwave-susceptible perovskite catalyst, and installing a small microwave source on the exhaust pipe [69,106]. Perovskites are crystalline mixed oxides with the formula ABO_3 , where **A** and **B** are cations of various metals (see Figure 6.27). The optimal catalyst should be sulfur-resistant,

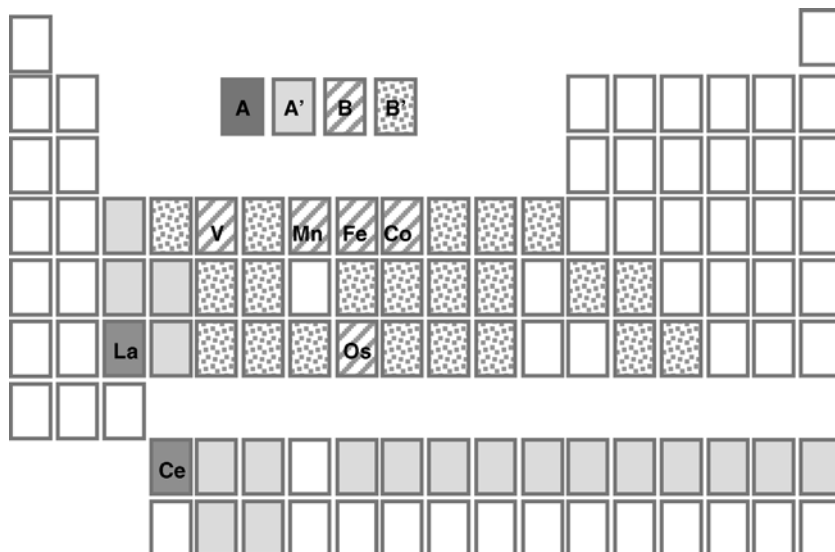


Figure 6.27 Possible metal precursors for making stable doped perovskite catalysts with the general formula $AA'BB'O_3$, for diesel-soot filter regeneration *in situ*.

microwave-susceptible, and cheap enough for installation on every diesel engine. You are the R&D manager of NewCat, Inc., and you have the experimental capacity for making and testing 400 different doped perovskites, where the main components are **A** and **B**, and the dopants are **A'** and **B'**, out of 200 000 possible combinations. How would you maximize your chance of finding the optimal catalyst?

2. Catalytic asymmetric hydrogenation is an extremely important industrial process, so designing new catalysts for this process using virtual screening is a worthy goal.

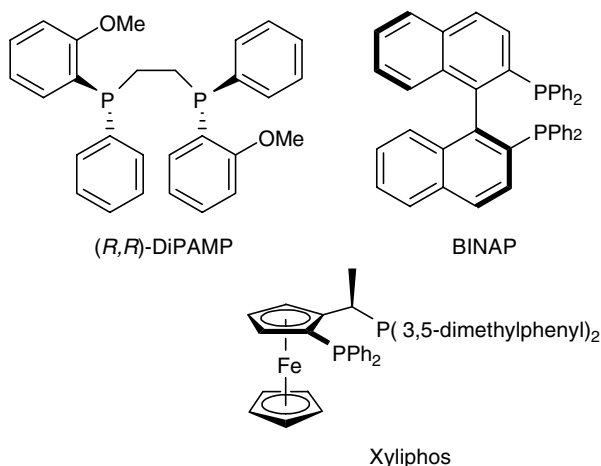


Figure 6.28 Structural formulas of the DiPAMP, BINAP, and Xyliphos ligands.

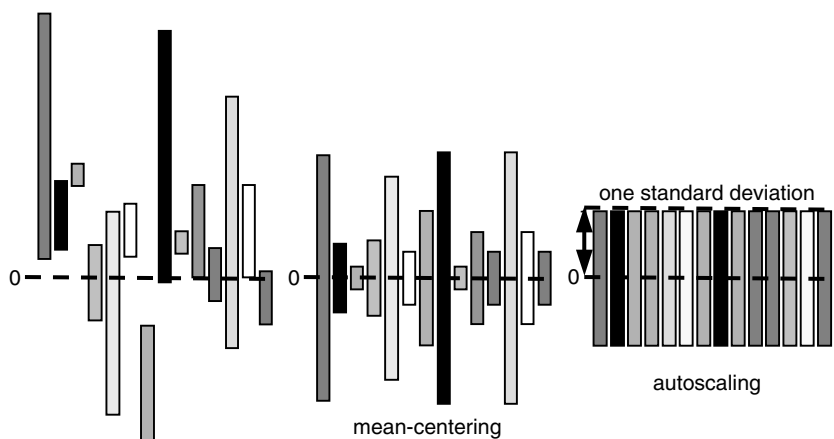


Figure 6.29 Schematic representation of mean-centering and autoscaling.

The problem is that chirality cannot be modeled using 2D descriptors (why is that?), which means that computationally expensive 3D descriptors and optimized geometries must be used. Figure 6.28 shows the structural formulas of three important ligands applied in large-scale industrial homogeneous asymmetric hydrogenation processes: Knowles' DiPAMP, Noyori's BINAP, and Blaser's Xyliphos. Compare the three structures, and point out the features which, in your opinion, may pertain to important descriptors for the respective hydrogenation reactions.

3. Explain in your own words the difference between mean-centering and autoscaling (see Figure 6.29). Why is the first generally useful, while the usefulness of the second depends on the variable composition? In many studies in catalysis, scientists report only the "good" results. Unsuccessful experiments are omitted – they are considered less interesting (several journals make a point of this in their instructions for authors). This seems reasonable, but it also creates a problem as far as data mining is concerned. Examine Figure 6.29 and explain why the results of "bad" catalysts are important for data-mining purposes.

References

- 1 Skoog, D.A., West, D.M. and Holler, F.J. (1992) *Fundamentals of Analytical Chemistry*, New York, ISBN 0-03-074922-0.
- 2 Dimian, A.C. (2003) *Integrated Design and Simulation of Chemical Processes*, Elsevier, ISBN 0444829962.
- 3 Atkins, P.W. (1994) *Physical Chemistry*, Oxford University Press, Oxford, ISBN 0-19-855730-2.
- 4 Vlugt, T.J.H., Krishna, R. and Smit, B. (1999) Molecular simulations of adsorption isotherms for linear and

- branched alkanes and their mixtures in silicalite. *J. Phys. Chem. B*, **103**, 1102.
- 5 Catlow, C.R.A., Gay, D.H., Nygren, M.A. and Sayle, D.C. (1997) Computer simulation of structural, defect and surface properties of solids. *NATO ASI Ser. E: Appl. Sci.*, **331**, 479.
 - 6 Binder, K., Horbach, J., Kob, W., Paul, W. and Varnik, F. (2004) Molecular dynamics simulations. *J. Phys. Condensed Matter*, **16**, S429.
 - 7 Warshel, A. and Levitt, M. (1976) Theoretical studies of enzymic reactions: dielectric, electrostatic and steric stabilization of the carbonium ion in the reaction of lysozyme. *J. Mol. Biol.*, **103**, 227.
 - 8 French, S.A., Sokol, A.A., Bromley, S.T., Catlow, C.R.A., Rogers, S.C., King, F. and Sherwood, P. (2001) From CO₂ to methanol by hybrid QM/MM embedding. *Angew. Chem. Int. Ed.*, **40**, 4437.
 - 9 Leenders, E.J.M., Guidoni, L., Roethlisberger, U., Vreede, J., Bolhuis, P.G. and Meijer, E.J. (2007) Protonation of the chromophore in the photoactive yellow protein. *J. Phys. Chem. B*, **111**, 3765.
 - 10 Carloni, P. and Rothlisberger, U. (2001) Simulations of enzymatic systems: perspectives from Car–Parrinello molecular dynamics simulations. *Theor. Comp. Chem.*, **9**, 215.
 - 11 Amatore, C. and Jutand, A. (2000) Anionic Pd(0) and Pd(II) intermediates in palladium-catalyzed Heck and cross-coupling reactions. *Acc. Chem. Res.*, **33**, 314.
 - 12 Warshel, A. (2003) Computer simulations of enzyme catalysis: methods, progress, and insights. *Annu. Rev. Biophys. Biomol. Struct.*, **32**, 425.
 - 13 Maxwell, I., Williams, C., Muller, F. and Krutzen, B. (1993) Zeolite catalysis – for the fuels of today and tomorrow. *Spec. Chem. Mag.*, **13**, 79.
 - 14 Corma, A. and Serra, J.M. (2005) Heterogeneous combinatorial catalysis applied to oil refining, petrochemistry and fine chemistry. *Catalysis Today*, **107-108**, 3.
 - 15 Chen, N.Y., Lucki, S.J. and Mower, E.B. (1969) Cage effect on product distribution from cracking over crystalline aluminosilicate zeolites. *J. Catal.*, **13**, 331.
 - 16 Gorrington, R.L. (1973) Diffusion of normal paraffins in zeolite T. Occurrence of window effect. *J. Catal.*, **31**, 13.
 - 17 Ruthven, D.M. (2006) The window effect in zeolitic diffusion. *Micropor. Mesopor. Mater.*, **96**, 262.
 - 18 Dubbeldam, D., Calero, S., Maesen, T.L.M. and Smit, B. (2003) Incommensurate diffusion in confined systems. *Phys. Rev. Lett.*, **90**, 245 901/1.
 - 19 Dubbeldam D., Calero S., Maesen, T.L.M., and Smit, B. (2003) Understanding the window effect in zeolite catalysis. *Angew. Chem. Int. Ed.*, **42**, 3624.
 - 20 Dubbeldam, D. and Snurr, R.Q. (2007) Recent developments in the molecular modeling of diffusion in nanoporous materials. *Molec. Sim.*, **33**, 305.
 - 21 Cossee, P. (1964) Ziegler–Natta catalysis. I. Mechanism of polymerization of α -olefins with Ziegler–Natta catalysts. *J. Catal.*, **3**, 80.
 - 22 Arlman, E.J. and Cossee, P. (1964) Ziegler–Natta catalysis. III. Stereospecific polymerization of propene with the catalyst system TiCl₃–AlEt₃. *J. Catal.*, **3**, 99.
 - 23 Yoshida, T., Koga, N. and Morokuma, K. (1995) *Ab initio* theoretical study on ethylene polymerization with homogeneous silylene-bridged group 4 metallocene catalysts. Ethylene insertion and elimination. *Organometallics*, **14**, 746.
 - 24 Aiet-Mohand, S., Henin, F. and Muzart, J. (1995) Palladium(II)-mediated oxidation of alcohols using 1,2-dichloroethane as Pd(0) reoxidant. *Tetrahedron Lett.*, **36**, 2473.
 - 25 Rothenberg, G., Humbel, S. and Muzart, J. (2001) Palladium-catalyzed oxidation of alcohols to carbonyl compounds with 1,2-dichloroethane as the primary oxidant: a theoretical study. *J. Chem. Soc., Perkin Trans.*, **2**, 1998.

- 26 Nørskov, J.K. and Christensen, C.H. (2006) Toward efficient hydrogen production at surfaces. *Science*, **312**, 1322.
- 27 Hellman, A., Baerends, E.J., Biczysko, M., Bligaard, T., Christensen, C.H., Clary, D.C., Dahl, S., van Harrevelt, R., Honkala, K., Jonsson, H., Kroes, G.J., Luppi, M., Manthe, U., Nørskov, J.K., Olsen, R.A., Rossmeisl, J., Skulason, E., Tautermann, C.S., Varandas, A.J.C. and Vincent, J.K. (2006) Predicting catalysis: understanding ammonia synthesis from first-principles calculations. *J. Phys. Chem. B*, **110**, 17 719.
- 28 Burello, E. and Rothenberg, G. (2006) *In silico* design in homogeneous catalysis using descriptor modelling. *Int. J. Mol. Sci.*, **7**, 375.
- 29 Rothenberg, G., Boelens, H.F.M., Iron, D. and Westerhuis, J.A. (2003) Monitoring the future of chemical reactions. *Chim. Oggi*, **21**, 80.
- 30 Klanner C., Farrusseng D., Baumes L., Lengliz M., Mirodatos C. and Schüth F. (2004) The development of descriptors for solids: teaching “catalytic intuition” to a computer. *Angew. Chem. Int. Ed.*, **43**, 5347.
- 31 Bönemann, H. (1985) Organocobalt compounds in pyridine syntheses – an example for structure–activity relations in homogeneous catalysis. *Angew. Chem. Int. Ed. Engl.*, **24**, 248.
- 32 Cooney, K.D., Cundari, T.R., Hoffman, N.W., Pittard, K.A., Temple, M.D. and Zhao, Y. (2003) *A priori* assessment of the stereoelectronic profile of phosphines and phosphites. *J. Am. Chem. Soc.*, **125**, 4318.
- 33 Tolman, C.A. (1977) Steric effects of phosphorus ligands in organometallic chemistry and homogeneous catalysis. *Chem. Rev.*, **77**, 313.
- 34 Dierkes, P. and van Leeuwen, P.W.N.M. (1999) The bite angle makes the difference: a practical ligand parameter for diphosphine ligands. *J. Chem. Soc., Dalton Trans.*, 1519.
- 35 White, D., Taverner, B.C., Leach, P.G.L. and Coville, N.J. (1993) Quantification of substituent and ligand size by the use of solid angles. *J. Comp. Chem.*, **14**, 1042.
- 36 Dunne, B.J., Morris, R.B. and Orpen, A.G. (1991) Structural systematics. Part 3. Geometry deformations in triphenylphosphine fragments: a test of bonding theories in phosphine complexes. *J. Chem. Soc., Dalton Trans.*, 653.
- 37 Aires-de-Sousa, J. and Gasteiger, J. (2005) Prediction of enantiomeric excess in a combinatorial library of catalytic enantioselective reactions. *J. Comb. Chem.*, **7**, 298.
- 38 Aires-de-Sousa, J. and Gasteiger, J. (2001) New description of molecular chirality and its application to the prediction of the preferred enantiomer in stereoselective reactions. *J. Chem. Inf. Comp. Sci.*, **41**, 369.
- 39 Cramer, R.D.I., Patterson, D.E. and Bunce, D.J. (1988) Comparative molecular field analysis (CoMFA). 1. Effect of shape on binding of steroids to carrier proteins. *J. Am. Chem. Soc.*, **110**, 5959.
- 40 Lipkowitz, K.B., Schefzick, S. and Avnir, D. (2001) Enhancement of enantiomeric excess by ligand distortion. *J. Am. Chem. Soc.*, **123**, 6710.
- 41 Lipkowitz, K.B. and Schefzick, S. (2002) Ligand distortion modes leading to increased chirality content of Katsuki–Jacobsen catalysts. *Chirality*, **14**, 677.
- 42 Lipkowitz, K.B. and Kozlowski, M.C. (2003) Understanding stereoinduction in catalysis via computer: new tools for asymmetric synthesis. *Synlett*, 1547.
- 43 Lipkowitz, K.B. and Pradhan, M. (2003) Computational studies of chiral catalysts: a comparative molecular field analysis of an asymmetric Diels–Alder reaction with catalysts containing bisoxazoline or phosphinooxazoline ligands. *J. Org. Chem.*, **68**, 4648.
- 44 Zabrodsky, H. and Avnir, D. (1995) Continuous symmetry measures. 4. Chirality. *J. Am. Chem. Soc.*, **117**, 462.
- 45 Bubel, R.J., Douglass, W. and White, D.P. (2000) Molecular mechanics-based measures of steric effects: customized

- code to compute ligand repulsive energies. *J. Comp. Chem.*, **21**, 239.
- 46 Gillespie, A.M. and White, D.P. (2001) Understanding the steric control of stereoselective olefin binding in cyclopentadienyl complexes of rhenium: an application of *de novo* ligand design. *Organometallics*, **20**, 5149.
- 47 Gillespie, A.M., Morello, G.R. and White, D.P. (2002) *De novo* ligand design: understanding stereoselective olefin binding to $(\eta^5\text{-C}_5\text{H}_5)\text{Re}(\text{NO})(\text{PPh}_3)^+$ with molecular mechanics, semiempirical quantum mechanics, and density functional theory. *Organometallics*, **21**, 3913.
- 48 Caffisch, A. and Karplus, M. (1995) Computational combinatorial chemistry for *de novo* ligand design: review and assessment. *Persp. Drug Disc. Design*, **3**, 51.
- 49 Boehm, H.-J. (1996) Fragment-based *de novo* ligand design. *Alfred Benzon Symp.*, **39**, 402.
- 50 Diestel, R. (2000) Graph theory, in *Graduate Texts in Mathematics*, vol. 173, Springer Verlag, New York, ISBN 3-540-26182-6.
- 51 Iedema, P.D. and Hoefsloot, H.C.J. (2001) Synthesis of branched polymer architectures from molecular weight and branching distributions for radical polymerisation with long-chain branching, accounting for topology-controlled random scission. *Macromol. Theor. Simul.*, **10**, 855.
- 52 Burello, E. and Rothenberg, G. (2005) Topological mapping of bidentate ligands: a fast approach for screening homogeneous catalysts. *Adv. Synth. Catal.*, **347**, 1969.
- 53 Chavali, S., Lin, B., Miller, D.C. and Camarda, K.V. (2004) Environmentally-benign transition metal catalyst design using optimization techniques. *Comp. Chem. Eng.*, **28**, 605.
- 54 Lin, B., Chavali, S., Camarda, K. and Miller, D.C. (2005) Computer-aided molecular design using Tabu search. *Comp. Chem. Eng.*, **29**, 337.
- 55 Hageman, J.A., Westerhuis, J.A., Frühauf, H.W. and Rothenberg, G. (2006) Design and assembly of virtual homogeneous catalyst libraries – towards *in silico* catalyst optimisation. *Adv. Synth. Catal.*, **348**, 361.
- 56 Hageman, J.A., Wehrens, R., Van Sprang, H.A. and Buydens, L.M.C. (2003) Hybrid genetic algorithm-tabu search approach for optimizing multilayer optical coatings. *Anal. Chim. Acta*, **490**, 211.
- 57 Willett, P. (2000) Chemoinformatics – similarity and diversity in chemical libraries. *Curr. Opin. Biotechnol.*, **11**, 85.
- 58 Fergus, S., Bender, A. and Spring, D.R. (2005) Assessment of structural diversity in combinatorial synthesis. *Curr. Opin. Chem. Biol.*, **9**, 304.
- 59 Maldonado, A.G., Doucet, J.P., Petitjean, M. and Fan, B.T. (2006) Molecular similarity and diversity in chemoinformatics: from theory to applications. *Mol. Divers.*, **10**, 39.
- 60 Gillet, V.J., Willett, P. and Bradshaw, J. (1997) The effectiveness of reactant pools for generating structurally-driven combinatorial libraries. *J. Chem. Inf. Comput. Sci.*, **37**, 731.
- 61 Westerhuis, J.A., Hageman, J.A., Frühauf, H.W. and Rothenberg, G. (2007) Understanding ligand diversity. *Chim. Oggi*, **25**, 28.
- 62 Aguiar, P.F.d., Bourguignon, B., Khots, M.S., Massart, D.L. and Phan-Thau-Luu, R. (1995) D-optimal designs. *Chemometr. Intell. Lab. Syst.*, **30**, 199.
- 63 Baroni, M., Clementi, S., Cruciani, G., Kettaneh-Wold, N. and Wold, S. (1993) D-optimal designs in QSAR. *QSAR*, **12**, 225.
- 64 Olsson, I.-M., Gottfries, J. and Wold, S. (2004) D-optimal onion designs in statistical molecular design. *Chemometr. Intell. Lab. Syst.*, **73**, 37.
- 65 Olsson, I.-M., Gottfries, J. and Wold, S. (2004) Controlling coverage of D-optimal onion designs and selections. *J. Chemometr.*, **18**, 548.
- 66 Rothenberg, G., Hageman, J.A., Clerc, F., Frühauf, H.-W. and Westerhuis, J.A.

- (2006) How to find the best homogeneous catalyst. *Chem. Ind. (CRC Press), Catal. Org. React.*, **115**, 261.
- 67** Jin, Y. (2005) A comprehensive survey of fitness approximation in evolutionary computation. *Soft Comput.*, **9**, 3.
- 68** Haruta, M., Yamada, N., Kobayashi, T. and Iijima, S. (1989) Gold catalysts prepared by coprecipitation for low-temperature oxidation of hydrogen and of carbon monoxide. *J. Catal.*, **115**, 301.
- 69** Beckers, J., van der Zande, L.M. and Rothenberg, G. (2006) Clean diesel power via microwave susceptible oxidation catalysts. *ChemPhysChem*, **7**, 747.
- 70** Klanner, C., Farrusseng, D., Baumes, L., Mirodatos, C. and Schueth, F. (2003) How to design diverse libraries of solid catalysts? *QSAR Comb. Sci.*, **22**, 729.
- 71** Farrusseng, D., Klanner, C., Baumes, L., Lengliz, M., Mirodatos, C. and Schueth, F. (2005) Design of discovery libraries for solids based on QSAR models. *QSAR Comb. Sci.*, **24**, 78.
- 72** Holena, M. and Baerns, M. (2003) Feedforward neural networks in catalysis. A tool for the approximation of the dependency of yield on catalyst composition, and for knowledge extraction. *Catal. Today*, **81**, 485.
- 73** Klanner C., Farrusseng D., Baumes L., Lengliz M., Mirodatos C. and Schueth F. (2004) The development of descriptors for solids: teaching “catalytic intuition” to a computer. *Angew. Chem. Int. Ed.*, **43**, 5347.
- 74** Corma, A., Serra, J.M., Argente, E., Botti, V. and Valero, S. (2002) Application of artificial neural networks to combinatorial catalysis: modeling and predicting ODHE catalysts. *ChemPhysChem*, **3**, 939.
- 75** Serra, J.M., Corma, A., Valero, S., Argente, E. and Botti, V. (2007) Soft computing techniques applied to combinatorial catalysis: a new approach for the discovery and optimization of catalytic materials. *QSAR Comb. Sci.*, **26**, 11.
- 76** Corma, A., Serra, J.M., Serna, P. and Moliner, M. 2005 Integrating high-throughput characterization into combinatorial heterogeneous catalysis: unsupervised construction of quantitative structure/property relationship models. *J. Catal.*, **232**, 335.
- 77** Arnold, H. (2001) Combinatorial and computational challenges for biocatalyst design. *Nature*, **409**, 253.
- 78** Hibbert, E.G. and Dalby, P.A. (2005) Directed evolution strategies for improved enzymatic performance. *Microb. Cell Fact.*, **4**, 29.
- 79** Hayes, R.J., Bentzien, J., Ary, M.L., Hwang, M.Y., Jacinto, J.M., Vielmetter, J., Kundu, A. and Dahiyat, B.I. (2002) Combining computational and experimental screening for rapid optimization of protein properties. *Proc. Nat. Acad. Sci. USA*, **99**, 926.
- 80** Bolon, D.N. and Mayo, S.L. (2001) Enzyme-like proteins by computational design. *Proc. Nat. Acad. Sci. USA*, **98**, 274.
- 81** Dwyer, M.A., Looger, L.L. and Hellinga, H.W. (2004) Computational design of a biologically active enzyme. *Science*, **304**, 1967.
- 82** Lassila, J.K., Keeffe, J.R., Oelschlaeger, P. and Mayo, S.L. (2005) Computationally designed variants of *Escherichia coli* chorismate mutase show altered catalytic activity. *PEDS*, **18**, 161.
- 83** Korkegian, A., Black, M.E., Baker, D. and Stoddard, B.L. (2005) Computational thermostabilization of an enzyme. *Science*, **308**, 857.
- 84** Caruthers, J.M., Lauterbach, J.A., Thomson, K.T., Venkatasubramanian, V., Snively, C.M., Bhan, A., Katare, S. and Oskarsdottir, G. (2003) Catalyst design: knowledge extraction from high-throughput experimentation. *J. Catal.*, **216**, 98.
- 85** Massart, D.L., Vandeginste, B.G.M., Buydens, L.M.C., de Jong, S., Lewi, P.J. and Smeyers-Verbeke, J. (1998) *Handbook of Chemometrics and Qualimetrics*, Elsevier, ISBN 0444828540.

- 86 Tranter, R.L. (2000) *Design and Analysis in Chemical Research*. CRC Press, Sheffield, ISBN 1-85075-994-4.
- 87 Eriksson, L. and Johansson, E. (1996) Multivariate design and modeling in QSAR. *Chemometr. Intell. Lab. Syst.*, **34**, 1.
- 88 Famini, G.R. and Wilson, L.Y. (1999) Using theoretical descriptors in linear free energy relationships: characterizing several polarity, acid and basicity scales. *J. Phys. Org. Chem.*, **12**, 645.
- 89 Tropsha, A., Gramatica, P. and Gombar, V.K. (2003) The importance of being earnest: validation is the absolute essential for successful application and interpretation of QSPR models. *QSAR Comb. Sci.*, **22**, 69.
- 90 Fernandez, A.L., Reyes, C., Prock, A. and Giering, W.P. (2000) The stereoelectronic parameters of phosphites. The quantitative analysis of ligand effects (QALE). *J. Chem. Soc., Perkin Trans. 2*, 1033.
- 91 Bocker, A., Schneider, G., Teekentrup, A. (2004) Status of HTS data mining approaches. *QSAR Comb. Sci.*, **23**, 207.
- 92 Walters, W.P. and Goldman, B.B. (2005) Feature selection in quantitative structure–activity relationships. *Curr. Opin. Drug Discov. Develop.*, **8**, 329.
- 93 Wold, S., Esbensen, K. and Geladi, P. (1987) Principal component analysis. *Chemometr. Intell. Lab. Syst.*, **2**, 37.
- 94 Geladi, P. and Kowalski, B.R. (1986) Partial least-squares regression: a tutorial. *Anal. Chim. Acta*, **185**, 1.
- 95 Carlson, R. and Gautun, H. (2005) Combinatorial libraries and the development of organic synthetic methods. PLS modelling to discriminate between successful and failed reaction systems. *Chemometr. Intell. Lab. Syst.*, **78**, 113.
- 96 Burello, E., Marion, P., Galland, J.-C., Chamard, A. and Rothenberg, G. (2005) Ligand descriptor analysis in nickel-catalysed hydrocyanation: a combined experimental and theoretical study. *Adv. Synth. Catal.*, **347**, 803.
- 97 Serra, J.M., Corma, A., Chica, A., Argente, E. and Botti, V. (2003) Can artificial neural networks help the experimentation in catalysis? *Catal Today*, **81**, 393.
- 98 Cundari, T.R., Deng, J., Pop, H.F. and Sarbu, C. (2000) Structural analysis of transition metal beta-X substituent interactions. Toward the use of soft computing methods for catalyst modelling. *J. Chem. Inf. Comp. Sci.*, **40**, 1052.
- 99 Cundari, T.R. and Russo, M. (2001) Database mining using soft computing techniques. An integrated neural network-fuzzy logic-genetic algorithm approach. *J. Chem. Inf. Comp. Sci.*, **41**, 281.
- 100 Cundari, T.R., Sarbu, C. and Pop, H.F. (2002) Robust fuzzy principal component analysis (FPCA). A comparative study concerning interaction of carbon–hydrogen bonds with molybdenum–oxo bonds. *J. Chem. Inf. Comp. Sci.*, **42**, 1363.
- 101 Burello, E., Farrusseng, D. and Rothenberg, G. (2004) Combinatorial explosion in homogeneous catalysis: screening 60 000 cross-coupling reactions. *Adv. Synth. Catal.*, **346**, 1844.
- 102 Golbraikh, A. and Tropsha, A. (2002) Beware of q^2 ! *J. Mol. Graph. Model.*, **20**, 269.
- 103 Golbraikh, A., Shen, M., Xiao, Z., Xiao, Y.-D., Lee, K.-H. and Tropsha, A. (2003) Rational selection of training and test sets for the development of validated QSAR models. *J. Computer-Aided Mol. Design*, **17**, 241.
- 104 Wehrens, R., Putter, H. and Buydens, L.M.C. (2000) The bootstrap: a tutorial. *Chemometr. Intell. Lab. Syst.*, **54**, 35.
- 105 Mandel, J. and Gerlach, R.W. (1986) The regression analysis of collinear data. *J. Res. Nat. Inst. Stand. Technol.*, **90**, 465.
- 106 van der Zande, L.M., Zhang-Steenwinkel, Y., Rothenberg, G. and Blik, A. (2004) Microwave regeneration of diesel soot filters. *NATO Sci. Ser. II: Math. Phys. Chem.*, **173**, 247.

Index

a

ABB Lummus/Albemarle AlkyClean process 168
 ABB Lummus/UOP SMART process 172
 α -abstraction 86, 87
 abzyme 213–214
 acrylamide 18, 217, 218
 activation energy 41, 45, 64
 active site 11, 27, 49, 51–52, 68, 79–80, 131, 144, 156, 194, 197–198, 211, 235, 255
 activity modifier 134
 adiponitrile 100
 adsorption isotherm 146, 147–148, 173, 176
 agostic interaction 93, 238
 allosteric site 68
 alloy leaching 137
 antigen 213
 apoenzyme 192
 aqueous biphasic catalysis 159, 160–161
 Arrhenius equation 41, 42, 45
 artificial neural network (ANN) 262
 aspartame 220
 associative mechanism 81
 atom economy 4–5, 6, 19, 22, 31, 111–112, 167
 autoscaling 260, 268

b

BHC Ibuprofen process 22
 bifunctional catalysis 197
 bimolecular reaction 43
 biocatalysis 12, 16, 17–18, 27, 40, 56, 79, 129, 189, 193, 199–200, 203, 205, 209–210, 214, 235, 256
 biodiesel 12, 108, 145, 168, 169–171
 bioprospecting 210
 bite angle 91, 102, 242, 248, 252

BMS Paclitaxel process 218
 σ -bond metathesis 87
 bootstrapping 265, 266
 BP AVADA ethyl acetate process 166
 BRENDA 192, 221

c

calcination 140, 141, 142–143, 149, 153
 calibration set 265
 Car–Parrinello molecular dynamics 236
 catalyst descriptors 29, 241, 265
 catalyst diversity 249, 250, 252, 256, 266
 catalyst precursor 25, 27, 58, 60, 62, 89, 98, 108, 139, 149, 236
 catalyst recovery and recycling 108
 catalyst reservoir 58
 catalyst stability 135, 145
 catalytic constant 56
 catalytic converter 66, 143, 154, 155–156
 catalytic cycle 4, 12, 13, 15, 19, 21, 27, 43, 44, 45–46, 51–52, 56, 58, 60, 62–64, 69, 78, 81, 83, 98–101, 113, 130, 133–134, 193, 199, 231, 233, 238–239, 262
 catalytic distillation 171
 catalytic intermediates 12, 27, 44, 52–53, 57–58, 63, 66, 78, 131, 160, 240
 catalytic RNA 214
 catalytic triad 194, 198
 chemisorption 134–135, 146, 176
 chemoselectivity 12
 Ciba–Geigy metolachlor process 102
 Circe effect 195
 classification analysis 264
 classification tree 264
 click chemistry 111
 click reaction 111, 112
 coenzyme 193, 194–195

cofactor 192, 193–195, 200–201
 common name 192
 comparative molecular field analysis (CoMFA) 243
 competitive adsorption 68
 competitive inhibition 68
 concentration effects 61, 62
 cone angle 88, 89, 116, 241, 242, 245
 conversion 4, 33, 35, 39, 40, 48, 66, 71
 coupled enzyme approach 200, 201
 coupled substrate approach 201
 covalent catalysis 198
 cross-linking of enzymes 202, 204
 cross-validation 260, 265
 cyclometallation 82

d

data mining 233, 247, 256, 257, 259, 268
 deactivation 66, 145, 167–168
 de-insertion 79, 85
 density-functional theory (DFT) 28, 235
 dependent variable 260, 266
 descriptor space 241, 251, 256
 detour matrix 246
 dextrose equivalent 216
 diastereoselectivity 12, 107
 directed evolution 17, 210, 211, 212–213
 dissociative mechanism 81
 distance matrix 246
 DNA shuffling 211
 drying 141, 142, 220
 Du Pont synthesis of adiponitrile 100
 dynamic kinetic resolution 208

e

Eadie–Hofstee plot 56
 E-factor 4, 5–6, 21, 189
 effective prediction domain (EPD) 266
 electron microscopy 151
 electronic promoter 134
 elementary reaction 15, 42, 43–44, 61, 101
 elementary steps 28, 29, 78, 92, 197, 231, 240
 Eley–Rideal mechanism 130
 β -elimination 79, 85, 98
 enantioselectivity 12, 92, 95, 213
 environmental quotient 6
 enzyme number 192
 enzyme screening 212
 enzyme selection 212
 epitope 213
 error-prone PCR 211
 exploration diversity 252
 expression host 212

expression vector 212
 external validation 265
 extraction mechanism 164
 extremophile 210
 extrusion 85, 143
 Eyring equation 41

f

fermentation processes 202
 figure of merit 241, 244, 249, 252, 255, 257, 265–266
 first-order kinetics 71
 Fischer–Tropsch synthesis 127
 fluorous biphasic catalysis 161
 forcefield models 233
 forming 141
 frequency factor 41

g

gene recombination 211
 general acid catalysis 105
 glycolic acid 208, 209
 green chemistry 1, 2, 3–4, 9–10, 14, 19–20, 23, 111, 129, 154, 161, 165, 220
 – principles 2, 4, 20, 111

h

Haber–Bosch ammonia synthesis 127
 Hapten 214
 Hartree–Fock approach 235
 heavy chain 213
 Heck reaction 12, 60, 161, 264
 Henry reaction 107
 heterogeneous catalysis 11, 12, 15, 16, 27, 40, 49, 51, 53, 66, 68, 77, 127, 129, 131, 133, 146–147, 154, 157, 159, 165, 202, 233, 236–237, 255
 high-fructose corn syrup (HFCS) 216, 223
 high-temperature fusion 137
 holoenzyme 192
 homogeneous catalysis 11, 12, 25, 27, 40, 50, 53, 58, 77, 78, 80, 88, 93, 96, 101, 104, 111, 113, 129, 157, 197, 251, 256
 hybrid catalyst 110
 α -hydride elimination 86
 hydroformylation reaction 77
 hydrothermal synthesis 136, 139, 140

i

ibuprofen 22, 23
 IFP biodiesel process 170
 immobilised enzyme 129, 202

- incipient wetness method 139
independent variable 260, 262
indigo 202, 206
induced fit model 194, 195
infrared (IR) spectroscopy 153
inhibition 66, 68–69
insertion 84, 238–239
interfacial mechanism 165
ionic liquids 163, 198
isolated enzyme 200, 205
- j**
Josiphos ligand 104
- k**
kinetic resolution 204, 208
kinetically perfect enzyme 56
- l**
Langmuir–Hinshelwood kinetics 49
Langmuir–Hinshelwood mechanism 130
latent variable 259, 260–261
L-DOPA 95, 96, 104
leave-one-out validation 265
life cycle assessment 9
ligand 13, 79–89, 91–93, 104, 156, 244–247
ligand bite angle 91
ligand bulk radius 89, 116
ligand exchange 79, 87
ligand flexibility 91
light chain 213
Lineweaver-Burk plot 56
lock-and-key model 194
- m**
macroporous 144, 147
macroscopic level 27, 129
magic angle spinning 153
maximum velocity 55
mean-centring 268
mercury porosimetry 148
mesoporous 144
metalloenzyme 193, 197
metolachlor 96, 102, 104
Michaelis–Menten kinetics 54, 195
microporous 140, 144, 147
microscopic level 27, 129, 131
microscopic reversibility
– principle 15, 83
migration 66, 68, 79, 84
migratory insertion 84
Mitsubishi Rayon acrylamide process 217
model catalyst systems 132, 133
model domain 266
modifier 134
molecular dynamics 233, 236
molecular graph 245
molecular shuttle bus 164
molecular sieve 140, 147
molecularity 43
monolayer capacity 148
Monte-Carlo 234
- n**
neoteric solvents 163
noncompetitive inhibitor 68, 69
nonelementary reaction 42, 61
nucleophilic catalysis 197, 198
- o**
optimisation diversity 252
organocatalysis 105, 106–107
orthometallation 87
oxidative addition 79, 81, 82–84, 86–87, 92
oxidative coupling 21, 82
- p**
paclitaxel 218, 219–220
parallel reactions 57
partial least-squares (PLS) 260
pelleting 143
peptide bond 112, 191
permutation test 266
perovskite 266, 267
phase-transfer catalysis 164
phase-transfer catalyst 159, 164
physisorption 146
poisoning 52, 65, 66, 69, 135, 145
pore size distribution 146, 148, 149
pore volume 139, 146, 148, 177
prediction set 265
predictive modeling 29, 233, 240, 255, 256, 265
pre-equilibrium 58, 60, 100
pre-exponential factor 41
primary structure 191, 192, 256
principal component 233, 252, 259, 261
principal components analysis (PCA) 259
product life cycle 9
product selectivity 4, 5, 12, 44, 57, 99, 102, 112, 135, 221
product yield 4, 5, 6, 91, 117, 255
promoter 134, 135
prosthetic group 193
proximity effect 195, 196
Pseudo-order conditions 62

r

random mutagenesis 211
 Raney nickel 138
 rate constant 41, 45–46, 49, 56–57, 61–62, 141
 rate equation 40, 41, 46, 48, 52, 57–58, 61–62, 80
 rate-determining step 40, 43, 45, 51–52, 57, 60, 62, 135
 rational catalyst design 240
 rational design 210, 211
 REACH 3
 reactant conversion 4
 reaction coordinate 44, 45–46, 238
 reaction efficiency 4
 reaction order 40, 42, 43, 45, 60–63
 reaction pocket 88, 89, 91
 reaction profile 44
 reactive distillation 171
 reductive elimination 79, 82, 83–84, 87, 92–93, 101
 regioselectivity 12
 residue
 ribozyme 214, 215

s

Sabatier's principle 65, 194
 saturation kinetics 55, 80
 scanning electron microscope 27, 152
 secondary structure 192
 second-order kinetics 46, 60
 selectivity 4–6, 12, 14, 22, 27, 57, 77, 102, 104, 108, 112, 130, 134–135, 159, 173, 255
 shell higher olefins process (SHOP) 97
 ship-in-a-bottle catalyst 110
 sintering 52, 66, 68, 131, 133, 135, 143, 145
 skeletal catalyst 138
 small-angle X-ray scattering 151
 smart polymer 203
 solid acid 16, 108, 140, 145, 168, 171, 173
 solid angle 89, 245
 solid state nuclear magnetic resonance 27, 150, 153
 Sonogashira reaction 113
 spectroscopy 25, 27–28, 44, 146, 149, 150–154
 specific acid catalysis 105
 specific surface area 144
 specificity constant 55
 sphere occupation 89, 242

spray drying 142
 steady-state approximation 52, 53–54
 steady-state concentration 52, 193
 steric crowding 91
 steric effect 88
 substrate 10, 12, 15, 17, 25, 33, 50, 54–56, 58, 65, 68, 77, 85, 92, 104, 111, 134–135, 192, 195, 197, 201, 235, 259, 261
 substrate accessibility 144
 substrate binding model 194
 surface organometallic chemistry 110, 156, 157
 sustainability 1, 2, 10
 sustainable development 1, 2, 154, 166
 Suzuki cross-coupling 105

t

tableting 143
 taxol 218, 220
 technical enzyme 199
 termolecular reaction 43
 tertiary structure 192
 test set 262, 265
 textural modifier 135
 thalidomide 94
 thermal degradation 66
 thermophilic enzyme 213
 3D descriptors 242, 243, 245, 248, 255
 three-way catalyst (TWC) 155
 Tolman's cone angle 88, 242
 Tosoh/DSM aspartame process 220
 training set 262, 265
 transmission electron microscope 151
 trial moves 234
 turnover frequency (TOF) 11, 40, 255
 turnover number (TON) 11, 40, 255
 2D descriptors 245, 247–248, 254, 268

u

Ullmann reaction 19, 20
 unimolecular reaction 43

v

vacuum pore impregnation 139, 177
 variable importance parameter (VIP) 261
 – plot 261, 262
 virtual library 254

w

Wacker oxidation process 99
 wet impregnation 139

white biotechnology 205
window effect 237

x

xerogel 141
X-ray diffraction 149, 150, 151, 204, 248,
256
X-ray photoelectron spectroscopy 149, 151

y

yield 4–6, 21–22, 39, 40, 44, 57, 87, 102, 208,
231, 255
Y-randomising 266

z

zeolites 16, 110, 131–132, 140, 237–238
zero-order kinetics 46

